Establishing a model of stress-induced senescence in zebrafish larvae

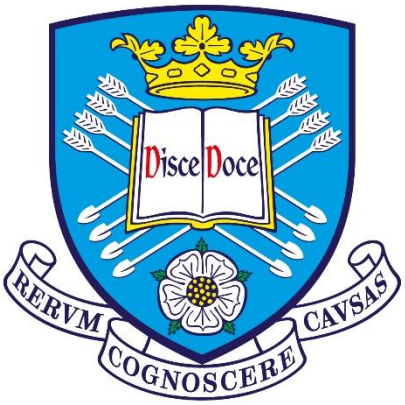

The University Of Sheffield.

Samir James Morsli

Department of Infection, Immunity and Cardiovascular Disease

A thesis submitted in partial fulfilment of the requirements for the degree of Doctor of Philosophy

September 2019

Abstract

Senescence has been associated with, and accumulates in, aged tissues and age-associated pathologies. Recent evidence suggests that targeting senescence could improve the health span of older individuals, which is the fastest growing demographic worldwide. Therefore, drugs that efficiently eliminate senescent cells, namely senolytics, are required. I proposed that a novel zebrafish-based model of senescence could provide a better method of identifying senolytics and understanding *in vivo* senescence. I hypothesised that zebrafish larvae undergo cellular senescence in response to irradiation, and that induced senescence in zebrafish larvae shares features with human ageing-induced senescence, allowing new insights into human ageing.

Here a non-lethal dose of irradiation was established in zebrafish larvae to develop a rapid accumulation of multiple senescence markers *in vivo*. Bacterial artificial chromosome (BAC) transgenesis was then used to develop a transgenic zebrafish that expresses GFP under promoter regulation of the senescence marker p21 [*TgBAC(p21:GFP)sh506*]. This transgenic reporter has allowed live *in vivo* imaging and prospective isolation of potentially senescent cells at the cellular level from a mixed population for the first time. Cell sorting of the GFP population showed an enrichment for multiple markers of senescence in the same cell, being positive for γH2AX and IL6, and negative for PCNA. For the first time, potentially senescent cells were able to be distinguished into a dim and bright population, whereby only the bright population expressed IL6. Irradiated zebrafish also show reduced mobility, a common predictor of age-associated mortality in humans. Now characterised, the system can provide a novel approach to compliment other established *in vivo* senescence models to further our understanding of the mechanisms underlying ageing, and allow the development of an *in vivo* compound screen for senolytics.

Acknowledgements

Firstly, I would like to thank my wonderful supervisors Stephen Renshaw & Ilaria Bellantuono for their support, guidance and advice throughout my PhD. To Ilaria for pushing me when I needed it and to Steve for providing moral support when I did not believe in myself enough. Extra thanks to Catarina Henriques, who provided hands on lab support and taught me vital techniques.

To all the brilliant post-docs and research assistants in Steve's, Ilaria's and Catarina's labs. Helping me troubleshoot experiments, providing reagents and advice, and for making me feel welcome in the workplace. Pam Ellis was a constant source of knowledge, expertise and guidance when it came to translating tools for assessing senescence into the context of my work. Cat Loynes for providing constant support in a non-judgemental manner, especially when I was trying to develop my transgenic zebrafish reporter. To Noémie Hamilton for pushing me to believe in myself, providing time and support when needed.

Special thanks to all of the students, past and present, including Sam Hassan, Kyle Buchan, Hannah Isles, Michael Nesbit and Piotr Szkuta who helped me in the lab and provided constant entertainment during coffee breaks, football matches and squash games.

To Greg, Sophia, Alex and Michael, for being great housemates and not groaning during the periods when I had nothing to say but complain.

To Dan and SFC, for providing constant entertainment in the form of gigs, as well as being a great source of support and friendship.

Finally to my family, for their unwavering love and patience. Especially to my mum who was always at the other end of the phone and provided constant support without fail. I am extremely grateful to your help in providing me with the support to get through these years; I do not know how I would have done it without you. To Tom, for being a perfect friend and source of inspiration, for a younger brother I do look up to you a lot! Karima, you have grown up massively during the last few years and I am immensely proud of you. To my Nan for being a constant source of wisdom and guidance, always steering me in the right direction. Finally, to my dad, your belief in me was a great source of support for me. You have all helped me believe in myself and I am eternally grateful for helping me get to this stage!

Abbreviations

AD – Alzheimer's disease

ANOVA – Analysis of variance

BAC – Bacterial artificial chromosome

CDKI – Cyclin-dependent kinase inhibitor

CSF – colony-stimulating factor

COPD – Chronic obstructive pulmonary disease

D&Q – Dasatinib & Quercetin

DDR – DNA damage response

dH2O – distilled water

DPF – days post fertilisation

DPIR – days post irradiation

DNA – Deoxyribonucleic acid

E3 – Embryo medium

EtOH - Ethanol

FLP - Flippase

FRT – Flippase recognition target

GFP – Green fluorescent protein

H3K27me3 – Histone 3 lysine 27 tri-methylation

IL – Interleukin

IPF – Idiopathic Pulmonary Fibrosis

MEF – Mouse embryonic fibroblast

MeOH - Methanol

mRNA – messenger ribonucleic acid

mTOR – Mammalian target of rapamycin

Ns – Not significant

OARSI - Osteoarthritis Research Society International

OIS – Oncogene-induced senescence

PBS – Phosphate buffer saline

PD – Parkinson's disease

PML - Promyelocytic leukemia

RIS – Replicative-induced senescence

ROI – Region of interest

ROS – Reactive Oxygen Species

SAHF – Senescence associated heterochromatin foci

SASP – Senescence associated secretory phenotype

SA-β-Gal – Senescence associated β galactosidase

SD – Standard Deviation

SEM – Standard error of the mean

SSc - Systemic Sclerosis

Tg – Transgenic

TUNEL - terminal deoxynucleotidyl transferase mediated dUTP Nick End Labelling assay

UK – United Kingdom

WISH – Whole mount *in situ* hybridisation

WOMAC - Western Ontario and McMaster Universities Osteoarthritis Index

ZFIN – Zebrafish Information Network

Table of Contents

1. Introduction 12
1.1. The ageing population 12
1.2.1 The rate at which we age is malleable: Lifespan 14
1.2.2 The rate at which we age is malleable: Healthspan 14
1.3. Mechanisms of ageing 15
1.4.1. Cellular senescence 18
1.4.2. Markers of senescence 18
1.4.3.1. Replicative senescence 20
1.4.3.2. Oncogene-induced senescence 21
1.4.3.3. Stress-induced senescence 22
1.5. Physiological senescence 23
1.6.1. Pathological senescence: accumulation with age 25
1.6.2. Senescence is causal to age-associated pathology 26
1.6.3. Pharmacological targeting of senescent cells to treat age-associated diseases. 27
1.6. The zebrafish as a model organism 34
1.7. Zebrafish as a model of senescence 36
1.7. Thesis aims 38
2 Materials and Methods 39
2.1. Reagents 39
2.2 Zebrafish work 39
2.2.1 Husbandry 39
2.2.2 Anaesthesia 39
2.2.3 Irradiation 40
2.2.4 Assessment of irradiation-induced toxicity in zebrafish 42
2.2.5. Fixation 43
2.2.6. Movement analysis 44
2.3. Molecular biology 45
2.3.1. Visualising & quantifying DNA & RNA: 45
2.3.2. Heat-shock Transformation 45
2.3.3. Plasmid DNA purification 45
2.3.4. PCR purification & Gel extraction 46
2.3.5. Restriction digests 46
2.3.6. Ligation 47
2.3.7. Developing specialised targeting constructs for BAC cloning 47
2.3.8. Tol2 RNA development 47
2.3.9. RNA extraction 48
2.3.10. cDNA synthesis 48

2.4 Whole-mount In situ Hybridisation (WISH) 48
2.4.1 Probe development 48
2.4.2 Whole-mount *In situ* hybridisation (WISH) protocol 52
2.5. Quantitative Polymerase Chain Reaction (qPCR) 53
MESA GREEN qPCR MasterMix Plus for SYBR® 53
2.6. Senescence-associated β-Galactosidase (SA-β-Gal) assay 55
2.7. Bacterial Artificial Chromosome (BAC) transgenesis 55
2.7.1 Making electro-competent EL250 cells 57
2.7.2 BAC electroporation into EL250s 57
2.7.3 Targeting BACs in EL250s with GFP targeting sequence 57
2.7.4 Injecting BACs into 1-cell stage zebrafish embryos 58
2.7.5. Development of transgenic line *TgBAC(p21:GFP)sh506* 58
2.7.6. Imaging *TgBAC(p21:GFP)sh506* larvae 58
2.8. Whole-mount immunofluorescence for γH2AX 60
2.9. Flow Cytometry of *TgBAC(p21:GFP)sh506* 61
2.9.1. Dissociation of zebrafish larvae 61
2.9.2. Flow cytometry of live cells from dissociated zebrafish larvae 61
2.10. Immunofluorescence of sorted cells for γH2AX, PCNA and IL6 62
2.10.1 Fluorescence Activated Cell Sorting 63
2.10.2. Fixing and cytospinning of sorted cells onto microscope slides 63
2.10.3. Immunofluorescence of sorted cells 63
2.11. Solutions 64
2.12. Software 65
2.13. Statistical Analysis 65
Chapter 3: Irradiation induces up-regulation of multiple senescence markers in zebrafish larvae 66
3.1.1. Introduction 66
3.1.2. Aims 68
3.2. Optimising dosage and timing of γ-irradiation in zebrafish larvae 69
3.2.2. Identifying an optimal stage of development for irradiation in zebrafish larvae 71
3.3. Irradiation activated senescence-associated cell-cycle inhibitors in zebrafish larvae 73
3.3.1. Primer optimisation for quantitatively assessing *p21* and *p16-like* mRNA expression 73
3.3.2. 3dpIR 12Gy irradiation significantly up-regulates *p21* and *p16-like* mRNA expression 75
3.3.3. Endogenous *p21* mRNA expression is regulated by the circadian rhythm, which is less pronounced following irradiation 77
3.4. Irradiation-induced *p21* mRNA expression is located spatially in head and intestinal regions of 3dpIR zebrafish larvae 81
3.4.1. Optimisation of proteinase K treatment to detect spatial *p21* mRNA expression 81
3.4.2. Optimising analysis methods for detecting whole mount *in situ* hybridisation *p21* mRNA expression 83

3.4.3. Dose-dependent increase in *p21* mRNA expression is predominantly located in pharangeal arches, intestine, and head regions of 3dpIR zebrafish larvae 85
3.4.4. An *in situ* hybridisation probe was unable to detect changes in *p16-like* expression in 3dpIR zebrafish larvae 87
3.5. Irradiated zebrafish larvae show increased senescence-associated β galactosidase activity in comparable regions to p21 mRNA expression 89
3.6. Irradiated zebrafish larvae have an activated DNA damage response pathway at 3dpIR 92
3.6.1. Detecting activation of γH2AX in whole mount zebrafish larvae 92
3.6.2. Irradiation activates the DNA-damage response marker γH2AX in *p21*-positive regions of 3dpIR zebrafish 96
3.7.2. RNA from whole irradiated zebrafish larvae shows up-regulation of some but not all SASP factors 98
3.8. Conclusion and chapter discussion 101
3.8.5 Future work and conclusions 106
3.9. Appendix 106
3.9.1. Table of SASP factors induced by irradiation 107
Chapter 4 – Development of transgenic larval zebrafish reporter for *p21* 115
4.1.1. Introduction 115
4.1.2. Aims 116
4.2. BAC transgenesis 117
4.2.1. BAC identification 117
4.2.2. Inserting GFP sequence after BAC *p21* start codon. 119
4.2.3. Modification of GFP-BAC for tol2-mediated transgenesis in single cell-stage zebrafish embryos 121
4.2.4. Identification of stable founders of the TgBAC(p21:GFP) zebrafish line 124
4.3. Characterisation of *TgBAC(p21:GFP)sh506* 126
4.3.1. Fluorescence imaging of *TgBAC(p21:GFP)sh506* after irradiation showed increased fluorescence that matches endogenous p21 mRNA patterns. 126
4.3.2. *TgBAC(p21:GFP)sh506* zebrafish show endogenous levels of *p21* mRNA expression 130
4.4. Conclusion and chapter discussion 132
4.4.1. Development of *TgBAC(p21:GFP)sh506* 132
4.4.2. *TgBAC(p21:GFP)sh506* faithfully reports *in vivo p21* promoter activation 132
4.4.5. Future work and conclusions 133
Chapter 5. Validation of zebrafish larval irradiation-induced senescence model. 134
5.1.1. Introduction 134
5.1.2. Aims 135
5.2.1. Optimisation of flow cytometry for assessment of cells from *TgBAC(p21:GFP)sh506* 136
5.2.2. Quantifying live GFP positive cells in *TgBAC(p21:GFP)sh506* fish after irradiation by flow cytometry 144
5.2.3. Optimisation of FACS for separating dissociated zebrafish cells based on GFP intensity in *TgBAC(p21:GFP)sh506* 148
5.2.4. Markers for DNA damage response and lack of proliferation associated with GFP intensity in cells sorted from irradiated *TgBAC(p21:GFP)sh506* 152

5.2.5. IL6 expression correlates with GFP intensity in 5dpf *TgBAC(p21:GFP)sh506* regardless of irradiation 154
5.3.1 - Irradiated zebrafish show no reduction in survival by 10dpIR 156
5.3.2 – GFP-dim and bright populations were persistent in 10dpIR *TgBAC(p21:GFP)sh506* zebrafish 158
5.3.3. GFP-bright cells from 10dpIR *TgBAC(p21:GFP)sh506* zebrafish show persistent DNA damage response and increased IL6 expression 160
5.4. Irradiated zebrafish show persistently reduced motility 163
5.5. Conclusion and chapter discussion 165
6. Final discussion and future work 170
6.1. Developing an assay for *in vivo* senescence accumulation with the potential for senolytic screens. 171
6.2. Prospective isolation of cells with p21 promoter activation could provide novel insight into the senescence phenotype 175
5.3. Final conclusions and closing remarks 177
References 178

List of figures

Figure 1.1. Mechanisms of ageing. 17
Table 1.1. List of senolytics that have shown in vivo efficacy in age-associated pathologies 33
Figure 2.1 Irradiation dose calculations. 41
Figure 2.2. Diagram depicting the optimised timing of irradiation assay. 42
Figure 2.3. Example images of signs of irradiation-induced toxicity. 43
Figure 2.4. Example tracking of locomotor activity. 44
Table 2.1. List of reagents used for transcription reactions. 49
Figure 2.5. Cloning of p16-like. 50
Figure 2.6. Development of p16-like dig-labelled *mRNA* probe for in situ hybridisation. 51
Table 2.2. List of reagents used for qpcr reactions. 53
Table 2.3. Table of primer sequences used for qpcr reactions. 54
Figure 2.7. Schematic diagram depicting the development of *TgBAC(p21:GFP*) using Bacterial Artificial Chromosome (BAC) transgenesis. 56
Table 2.4. List of reagents used for bac transgenesis. 59
Table 2.5. List of antibiotics used for bac transgenesis. 59
Table 2.6. Primer sequences used to insert GFP and itol2 targeting sequences into BACs. 60
Figure 2.8. Diagram depicting workflow to determine proportion of gfp positive cells from *TgBAC(p21:GFP)sh506* that are positive for multiple senescence markers in the same cell. 62
Figure 3.1. 20Gy irradiation at 1 day post-fertilisation causes loss in viability by 5 days post-fertilisation 70
Figure 3.2. Survival and health status of zebrafish following 12gy irradiation until 5dpf. 73
Figure 3.3. Technical qPCR reproducibility of 5dpf zebrafish. 74
Figure 3.4. Quantitative expression changes of p21 and p16-like mrna following irradiation. 76
Figure 3.5. Temporal regulation of senescence-associated genes p21 and p16-like following irradiation at 2dpf. 78
Figure 3.6. Temporal regulation of senescence-associated genes p21 and p16-like following irradiation at 3dpf. 80
Figure 3.7. Optimisation of enzymatic digestion of 5dpf zebrafish larvae for p21 in situ hybridisation. 82
Figure 3.8. Comparison of analysis techniques to assess the strength of p21 mrna signal by in situ hybridisation. 84
Figure 3.9. Whole-mount in situ hybridisation (WISH) of 5dpf zebrafish larvae shows dose-dependent p21 mRNA induction by irradiation. 86
Figure 3.10. Blind ranking of in situ hybridisation of p16-like did not show reliable changes in spatial expression following irradiation. 89
Figure 3.11. Senescence-associated beta-galactosidase activity in regions of p21-positivity. 90
Figure 3.12. Blind ranking of SA-β-gal staining correlates with pixel intensity. 91
Figure 3.13. Pilot experiment shows imaging & quantification of zebrafish tail regions allows for detection of γH2AX positive foci in 3dpIR zebrafish larvae. 94
Figure 3.14. Pilot experiment shows imaging & quantification of zebrafish head regions allows for detection of γH2AX foci in 3dpIR zebrafish larvae. 95

Figure 3.15. Upregulation of γH2AX DNA damage-associated foci in irradiated zebrafish larvae. 98
Figure 3.16. mRNA expression of alternative senescence-associated genes by qPCR. 99
Table 3.1. List of SASP factors induced following irradiation. 107
Figure 4.1. Identification of bac sequences at cdkn1a (p21) zebrafish locus. 118
Figure 4.2. Development of GFP targeting construct for *TgBAC(p21:GFP)* transgenic zebrafish. 121
Figure 4.3. Tol2 transposase mrna synthesis. 122
Figure 4.4. Example images of zebrafish injected with the p21:gfp bac at 4dpf. 123
Figure 4.5. Confirming germline transmission of *TgBAC(p21:GFP)sh506* 125
Figure 4.6. Representative images of *TgBAC(p21:GFP)sh506* zebrafish. 127
Figure 4.7. Quantification of head region fluorescence of 5dpf *TgBAC(p21:GFP)sh506*. 128
Figure 4.8. Comparison of p21 mRNA expression and *TgBAC(p21:GFP)sh506* fluorescence at 5dpf in zebrafish head region. 129
Figure 4.9. mRNA expression of p21 and gfp in *TgBAC(p21:GFP)sh506* zebrafish by qPCR. 131
Figure 5.1. Live cells dissociated from 5dpf *TgBAC(p21:GFP)sh506* zebrafish (example 1). 137
Figure 5.2. Live cells dissociated from 5dpf *TgBAC(p21:GFP)sh506* zebrafish (example 2). 139
Figure 5.3. Flow cytometry gating strategy to assess GFP intensity of live cells dissociated from 5dpf *TgBAC(p21:GFP)sh506* zebrafish 142
Figure 5.4. Quantification of live cells dissociated from 3dpIR *TgBAC(p21:GFP)sh506* 145
Figure 5.5. Assessment of cell size and granularity according to GFP intensity in 3dpIR *TgBAC(p21:GFP)sh506*. 147
Figure 5.6. FACS of *TgBAC(p21:GFP)sh506* zebrafish is between 86 and 99% efficient. 149
Figure 5.7. Cytospin at 500rpm of dissociated 5dpf zebrafish cells allowed single cells to be distinguished and maintain morphology. 150
Figure 5.8. GFP immunofluorescence on sorted cells from 3dpIR *TgBAC(p21:GFP)sh506* zebrafish. 151
Figure 5.9. GFP intensity positively correlates with γH2AX positive, PCNA negative cells following irradiation in 3dpIR *TgBAC(p21:GFP)sh506* zebrafish. 153
Figure 5.10. A portion of GFP positive cells are IL6 positive, PCNA negative irrespective of irradiation in 3dpIR *TgBAC(p21:GFP)sh506* zebrafish. 155
Table 5.1. Percentage survival of zebrafish from 5 to 12dpf following irradiation. 156
Figure 5.11. 10dpIR zebrafish are smaller than unirradiated counterparts. 157
Figure 5.12. GFP bright cells are still present in 10dpIR *TgBAC(p21:GFP)sh506* zebrafish 159
Figure 5.13. GFP positive cells following irradiation have a persistent proportion of γH2AX positive, PCNA negative cells in 10dpIR *TgBAC(p21:GFP)sh506* zebrafish 161
Figure 5.14. GFP bright cells from *TgBAC(p21:GFP)sh506* zebrafish 10 days after irradiation have a specific population of IL6 positive and PCNA negative cells. 162
Figure 5.15. Irradiated zebrafish show persistently reduced mobility. 164
Figure 6.1. An in vivo compound screen to identify modulators of senescence in irradiated *TgBAC(p21:GFP)sh506* zebrafish. 174

1. Introduction

1.1. The ageing population

Ageing of eukaryotic organisms can be defined as an almost universal decline in organ function leading to increased risk of mortality (Partridge, 2010; Leng, Chen and Mao, 2014). It is something that can be seen clearly, with features such as skin wrinkling, spine curvature and hair loss all becoming more prevalent over time, and it is something that occurs almost universally across all species (Chan & Duque, 2002.; HAMILTON, 1951; Katzman, Wanek, Shepherd, & Sellmeyer, 2010; Larsson et al., 2019; Makrantonaki & Zouboulis, 2007). What is fascinating about ageing is that the rate at which we age is extremely diverse (Fabian, D. & Flatt, 2011; Jones *et al.*, 2014). Dogs and humans are both mammals, and companion dogs share arguably the same environment, however the median lifespan of a dog is vastly shorter than that of a human at 14 years compared to 80 (Hoffman *et al.*, 2018). Even within humans from the same socioeconomic background and country can age differently and succumb to ageing in different ways (Huisman *et al.*, 2013; Public Health England, 2019). Ageing is a process that involves multiple organ tissues, environmental and genetic factors and occurs over an extremely long time in humans, making it arguably one of the most difficult areas to research as a whole (Studenski, 2008; Bellantuono and Potter, 2016). What is clear is that although we have made vast progress over the last few decades to understand how we age, with clear 'hallmarks of ageing' now being well characterised, we are yet to be able to effectively modulate the rate of ageing or reverse age-associated pathologies to keep people healthier for longer (López-Otín *et al.*, 2013).

Ageing is an important risk factor for most non-communicable diseases in almost all organ systems, including cancer, Alzheimer's, atherosclerosis, and osteoarthritis (Hebert *et al.*, 2001; Finkel, Serrano and Blasco, 2007; Colman *et al.*, 2009; Mantovani *et al.*, 2010; Shane Anderson and Loeser, 2010; Wang and Bennett, 2012). Even in the context of infectious diseases, an aged individual is much worse at fighting infections and less able to be vaccinated against them (Weinberger *et al.*, 2008). This leads to increased hospital admissions in older people, reduced quality of life and independence, and is costly to our health and social care services (Christensen *et al.*, 2009). However, this has only become an issue of great urgency over the last few decades with the onset of our ageing population.

In the UK, the predicted population increase between 2016 and 2036 is 36% for those aged between 65 and 79 years old, and 69% for those aged over 85 years old, whilst all other age groups remain relatively unchanged (Centre for Ageing Better, 2019). By 2037, one in four people in the UK will be 65 or older (Statistics, 2017). This means that our population is ageing, and this is the case in both developing and developed countries. One reason for this is that we are becoming better at treating individual diseases, with the invention of antibiotics for infectious disease, anti-cancer drugs and treatments such as Statins to treat heart disease (Wilmoth, 2000). However, this means that we are surviving with disease for longer, rather than increasing the proportion of our lives that are spent disease-free, otherwise known as our healthspan. This, alongside ageing being a key risk factor for non-communicable diseases, results in a greater proportion of our population that are retired and more likely to be suffering from age-associated frailty and multi-morbidity (Christensen *et al.*, 2009). On average in 2015, women, who typically have a longer lifespan than men, can expect to live 19 years of their life with age-associated diseases (Office for National Statistics, 2015). The amount of people requiring significant social care has doubled between 1991 and 2011 (Bulman, 2017). Additionally, 75% of over 65s suffer from more than one age-associated diseases, and 20% of over 65s have at least five age-related chronic conditions (Vogeli *et al.*, 2007; Goldman *et al.*, 2013). The prevalence of multi-morbidity means that an individualistic approach to treating age-associated diseases are becoming less effective, polypharmacy comes into play where drug interactions and multiple side effects limit the efficacy of drugs to treat individual pathologies used in combination. There must be a shift into the development of more multi-disciplinary, holistic approaches to limiting age-associated pathologies. In summary, there has never before been a greater and more urgent need to understand the underlying mechanisms of ageing that result in increased disease incidence and multimorbidity in older people. From an economic standpoint, reducing the pressure on our health and social services is essential, but also improved fitness in the elderly would allow a greater contribution to our workforce and strengthen individual independence (Silverstein, 2008; Marešová, Mohelská and Kuča, 2015). Further, 1 in 6 people in the UK over 65 live in relative poverty, therefore the financial pressure of requiring constant care can prove extremely debilitating for both the individual and the support networks that surround them (Pensions, 2018). This does not necessarily just mean developing new treatments to health span, but also improved social awareness of factors that contribute to healthy ageing through lifestyle changes such as diet, exercise and social interaction (Holmes and Joseph, 2011; McPhee *et al.*, 2016; Robinson, 2018).

1.2.1 The rate at which we age is malleable: Lifespan

Over the past few decades, the notion that it is possible to change the rate at which we age has become well evidenced. Rather counterintuitively, during the Great Depression in the early 20th Century, life expectancy increased and mortality rates decreased despite poor economic health and food rationing (Granados and Roux, 2009). Later, when mammals were calorie restricted they showed a strong improvement in life and health-span (McCay, Crowell and Maynard, 1935; Weindruch *et al.*, 1986; Mattison *et al.*, 2012). This provided vital evidence to support the idea that the rate of ageing is changeable. In *c.elegans* their median lifespan can be extended from three weeks to four months when there is limited availability of nutrition, in a state referred to as dauer diapause (Riddle, Swanson and Albert, 1981). Mutant screens in *c.elegans* showed that *daf* proteins, later shown to be orthologous to the human insulin/IGF pathways, can regulate lifespan and were involved in controlling the dauer state (Klass, 1983; Kenyon *et al.*, 1993; Gottlieb and Ruvkun, 1994). In humans, there are disorders such as Hutchinson-Guildford Progeria Syndrome (HGPS), and Werner Syndrome that present with rapid ageing phenotypes (Hutchinson, 1886; EPSTKIN *et al.*, 1966). Sequencing demonstrated that these were disorders of the *LMNA* and *WRN* genes, involved in DNA repair and nuclear membrane integrity, and further indicated mechanisms that modulate the ageing process (Chen *et al.*, 2003; Eriksson *et al.*, 2003). The Italian island of Sardinia has been of interest in understanding how people can live longer and healthier lives as it is a 'blue zone', which is a region where the lifespan is much higher than average (Salaris, 2015; Buettner and Skemp, 2016). Reasons for this include increased activity levels, improved diet, and high levels of societal interactions (Pes *et al.*, 2013; Buettner and Skemp, 2016). Indeed, when Frome, a small town in the south west of the UK introduced schemes to try and reduce isolation in older people, hospital admissions dropped by 14% between 2013 and 2017 whilst they increased by 28.5% in surrounding regions (Abel *et al.*, 2018). These examples demonstrate that the rate at which we age is malleable, and requires a multi-faceted and multi-disciplinary approach to help tackling the prevalence of age-associated disease in older people.

1.2.2 The rate at which we age is malleable: Healthspan

A pertinent question within the field of ageing research is whether it is possible to improve an individual's healthspan without further extending their lifespan, thereby compressing their morbidity (Fries, 1980). Without this 'compression of morbidity', there will be little net improvement on the number of people that are suffering from age-associated disease, it would instead delay the age at which they begin to suffer from them. There are notable cases whereby compression of morbidity has been described however. Centenarians, for example, have a much lower incidence of disease until later compared to those that live until decades earlier (Perls, 1997). They show a lower incidence of chronic illness, and are sick for a shorter period of time, reducing the medical costs for centenarians compared to those with a 70-year lifespan by two-thirds (Kheirbek *et al.*, 2017). This suggests, rather unsurprisingly, that if one can delay the initial onset of age-associated disease, then healthspan extension is possible. However, this is not so helpful for those that arrive at the clinic already presenting with symptoms, therefore, studying the underlying mechanisms that control maximum lifespan have been examined. For example, there is a strong correlation between rodents with a longer maximum lifespan and more efficient DNA repair mechanisms, which is the opposite phenotype to rapidly-

ageing patients with Werner syndrome (Tian *et al.*, 2019). Additionally, systemic improvements in multiple organ tissues was demonstrated upon modulating myostatin and activing signalling in a progeric mouse, without affecting lifespan (Alyodawi *et al.*, 2019). These evidence that compression of morbidity is possible in our ageing population, and that understanding the mechanisms linking ageing and increased disease incidence could provide new therapeutic avenues for extending healthspan.

1.3. Mechanisms of ageing

Research into the mechanisms underlying ageing are well underway. In a landmark review, nine processes were coined 'The Hallmarks of Ageing' (López-Otín *et al.*, 2013) (Figure 1.1). 'Genomic instability', 'stem cell exhaustion', 'telomere attrition', 'loss of proteostasis', 'deregulated protein sensing', 'mitochondrial dysfunction' 'epigenetic alterations', 'altered intercellular communication', and 'cellular senescence' are linked by stress and can be generally attributed to a loss in homeostasis. External stresses such as exposure to ultraviolet components of sunlight can increase oxidative stress, expose cells to DNA damage, and lead to genomic instability (Debacq-Chainiaux *et al.*, 2005). When the extent of stress reaches a critical level or the cell cannot handle the level of stress, they can go into a state of senescence (d'Adda di Fagagna *et al.*, 2003a; Parrinello *et al.*, 2003a). Senescence is a stress response that can alter intercellular communication and warn surrounding cells of a stress, even inducing senescence in nearby cells by a process called bystander or paracrine senescence (Nelson *et al.*, 2012a; Acosta *et al.*, 2013). When the protective caps on the end of chromosomes known as telomeres become critically short, this in turn can act as an internal stress and induce senescence (C B Harley, Futcher and Greider, 1990). The rate of telomere attrition is a strong predictor of median lifespan between species (Whittemore *et al.*, 2019). Additionally telomerase, an enzyme that can maintain telomere length, can be introduced to mice with pulmonary fibrosis to tackle telomere attrition and improve prognosis of this age-associated pathology (Povedano *et al.*, 2018). The methylation of genes can modulate gene expression, but alterations in epigenetic regulation are seen with age (Maures *et al.*, 2011). For example, H3K27me3 is generally known to decrease with age; it is also highlighted as a repressor of the senescence-inducing INK4A/ARF locus (Bracken *et al.*, 2007). Removing the demethylase that acts on H3K27me3 can extend the lifespan of *c.elegans* (Maures *et al.*, 2011). Another type of internal stress that can induce senescence is mitochondrial dysfunction (Wiley *et al.,* 2016). When the efficiency of cellular metabolism decreases over time, the amount of reactive oxygen species (ROS) that are produced increases and can damage DNA (Chance, Sies and Boveris, 1979; Bulua *et al.*, 2011). The ROS itself can further damage mitochondrial DNA and lead to a positive feedback loop and excessive oxidative stress. Mitochondrial dysfunction can further be aggravated by age-related loss of the protein quality control systems termed autophagy and mitophagy (Sun *et al.*, 2015). Modulation of autophagy and mitophagy can change the rate of ageing (Zhang and Cuervo, 2008). For example, mice with an extra copy of a lysosomal receptor required for chaperone-mediated autophagy experience a protective effect against the age-dependent increases in pathology that associated with reduced autophagy. The relationship between protein control and senescence is interesting in that effective autophagy can prevent senescence in stem cells, whilst increases in autophagy are seen in senescent cells and seems to control their inflammatory phenotype (Narita *et al.*, 2011; García-Prat *et al.*, 2016). Another way in which autophagy and senescence can be

regulated is through nutrient sensing (Herranz *et al.*, 2015). mTOR signalling, for example, can interpret nutrient and growth signals, and is required to induce the inflammatory nature of senescence (Herranz *et al.*, 2015; Laberge *et al.*, 2016). Modulation of this signalling pathway by rapamycin can extend lifespan of mice (Harrison *et al.*, 2009). The inflammatory nature of senescence, an example alteration of intercellular signalling, contributes to the age-dependent increase in chronic inflammation, which is causal to multiple age-associated diseases (Childs *et al.*, 2016; Jeon *et al.*, 2017a; Schafer *et al.*, 2017; Bussian *et al.*, 2018; Chinta, Woods, Demaria, Madden, *et al.*, 2018). Alongside this, with age the function of the immune system declines (Solana, Alonso and Peña, 1999; Solana and Mariani, 2000; Deng *et al.*, 2004a; Czesnikiewicz-Guzik *et al.*, 2008). We are less able to fight off infections and clear senescent cells, one reason being due to a reduced number of white blood cells in our blood with age. As well as reduced white blood cell numbers with age, those immune cells that that are present are less functional, T cells are less likely to be activated in response to a stimulus and increases in senescence markers are seen also (Deng *et al.*, 2004b; Liu *et al.*, 2009). Reduced immune cell number and function could be attributed to stem cell exhaustion in the hematopoietic stem cell niche. Stem cells are required to replenish the cell populations in damaged tissues and maintain tissue homeostasis, and there is an age-dependent decline in functional stem cells over time with increasing markers of senescence seen (Beerman *et al.*, 2010; Molofsky *et al.*, 2006; Fali *et al.*, 2018). Eventually over time, an organ's regenerative capacity will not be able to overcome the damage and our organ reserve, the ability for a tissue to return to physiologically functional state after a stress, would be depleted and lead to age-associated frailty (Neustadt and Pieczenik, 2008). Once one area starts to malfunction in this manner, it puts pressure on other regions, leading to a positive feedback loop and multimorbidity. At the DNA level, this is described as the 'Somatic Mutation Theory of Aging' (Szilard, 1959; Moskalev *et al.*, 2013). An added complexity to these hallmarks of ageing is that they are not mutually exclusive. This could be useful in the context of improving healthspan, in that one could propose that pharmacologically improving a central ageing hallmark like senescence may also help with other hallmarks of ageing, but conversely it may require targeting multiple hallmarks at once to have a functional improvement on whole organism health. The way in which our cells respond to various stressors seems central to many of these mechanisms, therefore I believe that targeting a stress response like senescence could be a promising approach and a good place to research to achieve the goal of systemic health-span extension.

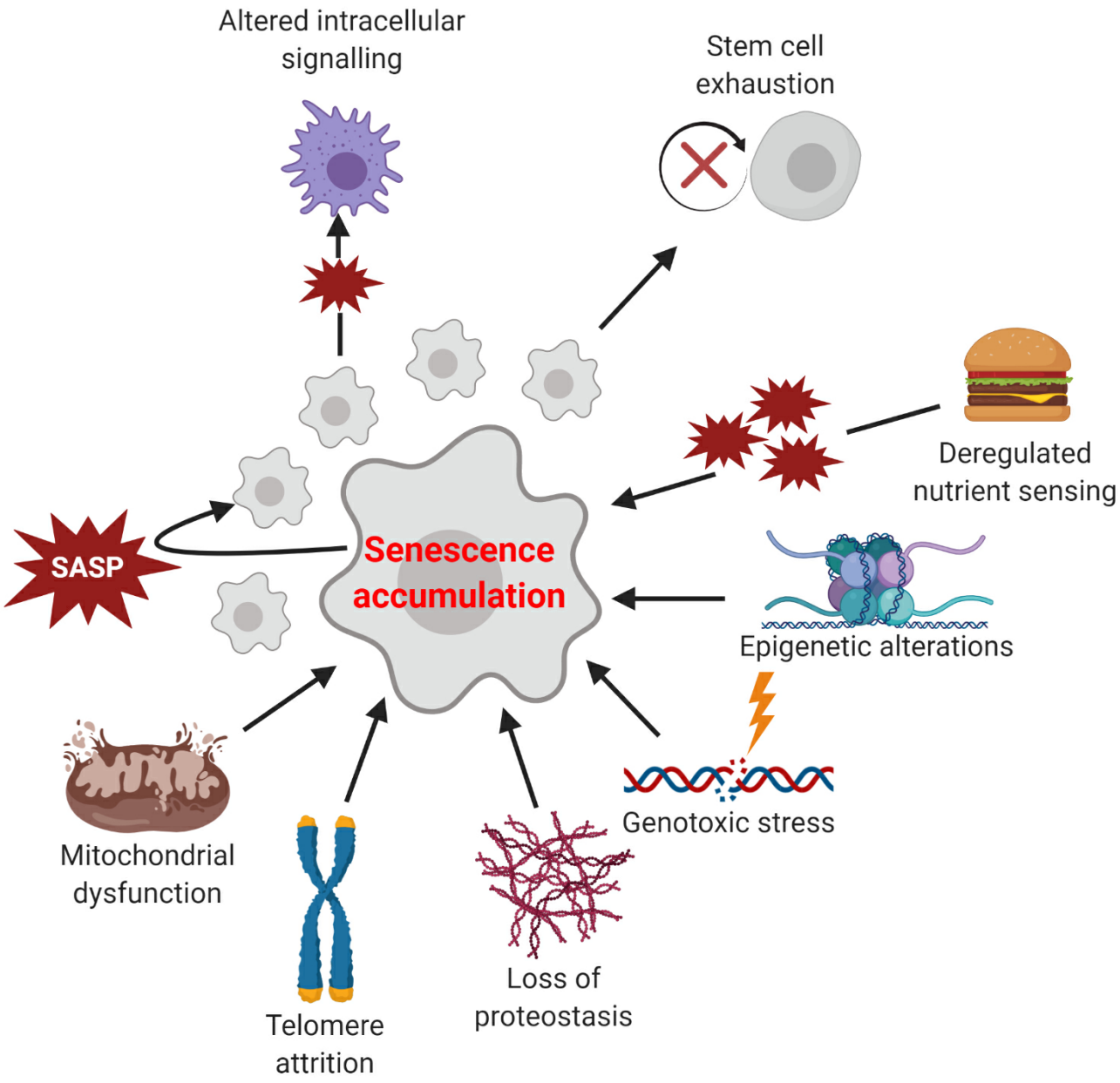

Figure 1.1. The mechanisms of ageing. Mitochondria dysfunction, telomere attrition, loss of proteostasis and genotoxic stress are all able to induce senescence. Senescent cells accumulate with age and can secrete warning signals known as the sensescence-associated secretory phenotype (SASP), which includes inflammatory factors. The SASP is able to induce senescence in nearby tissues in a process known as bystander senescence. It can also signal to immune cells and lead to chronic inflammation. This inflammatory microenvironment of accumulated senescent cells and chronic inflammation can damage stem cell niches and reduce function, further reducing organ reserve and leading to age-associated multimorbidity. Figure adapted from López-Otín *et al.* (2013). DIagram created with BioRender.com.

1.4.1. Cellular senescence

Cellular senescence is a hallmark of ageing, and the clearance of senescent cells has been highlighted as a potential mechanism by which age-associated pathologies could be treated (López-Otín *et al.*, 2013). Cellular senescence in most contexts can be defined as a stress-response (Sharpless and Sherr, 2015a; He and Sharpless, 2017). Senescence is a very dynamic and contextually dependent phenotype but generally, senescent cells have three main components in common (Shelton *et al.*, 1999). Stressed cells that become senescent undergo a seemingly permanent arrest of the cell cycle (Manuel Serrano *et al.*, 1997; Blais *et al.*, 2007). Though it is worth noting that this does not mean that only proliferating cells can become senescent, post-mitotic neurons are able to induce a senescence phenotype via p21 for example (Jurk *et al.*, 2012). Unlike with quiescence, the proliferative arrest is permanent, and these cells are no longer optimised to carry out their typical cellular functions, which is distinct from terminal differentiation (Buttitta and Edgar, 2007). A particularly important aspect of senescence, and one that sets it apart from alternative stress responses such as programmed cell death mechanisms, is the increases in metabolic activity and induction of a secretome deemed the Senescence Associated Secretory Phenotype (SASP) (Shelton *et al.*, 1999)**.** The SASP comprises of complex and dynamic signals, including pro-inflammatory cytokines, chemokines, growth factors, and proteases (Shelton *et al.*, 1999; Bavik, 2006; Coppé *et al.*, 2006; Acosta *et al.*, 2008; Kuilman and Peeper, 2009; Freund *et al.*, 2010; Krtolica *et al.*, 2011; Laberge *et al.*, 2016). This is thought to be the basis of their paracrine functions and interactions with the immune system (Gasser *et al.*, 2005a; Kang *et al.*, 2011b; Antonangeli *et al.*, 2016a). Additionally, the SASP is implicated in inducing senescence in surrounding tissues, termed bystander senescence (Nelson *et al.*, 2012b). Although senescent cells can be activated through comparable stressors that can also induce apoptosis, these cells actively develop methods for resisting cell death (Sasaki *et al.*, 2001). In fact, the length of time that senescent cells can survive for *in vivo* is unknown, though markers of senescence have been shown 12-months after chemotherapy treatment in breast cancer patients, which was the longest time-point examined in the study (Sanoff *et al.*, 2014). Understanding the three central components that define senescence are vital in being able to appreciate markers that can identify them, their functions and how they are linked with ageing.

1.4.2. Markers of senescence

Senescent cells can be difficult to identify and often requires multiple markers being used together. One of the first identified markers of senescence is senescence-associated β-Galactosidase activity (SA-β-Gal) (G P Dimri *et al.*, 1995). It correlated with cells from older humans and was absent in quiescent, terminally differentiated and cancer cells in that study. It was since shown that this activity is not actually required for senescence, where reducing the expression of the β-gal encoding gene *glb1* did not stop senescence induction (Lee *et al.*, 2006). As well as this, there are now multiple examples whereby non-senescent cells express SA-β-gal activity, putting into question the validity of it as a specific marker of senescence (Krishna *et al.*, 1999; Severino *et al.*, 2000; Going *et al.*, 2002; Untergasser *et al.*, 2003; Yang and Hu, 2005; Hall *et al.*, 2017).

As senescent cells are a stress response, markers of the DNA damage response such as γH2AX and p53 have been used to help identify senescence (d'Adda di Fagagna *et al.*, 2003; Herbig *et al.*, 2004). However, these alone cannot distinguish between other phenotypes that can occur following DNA damage response such as repair and apoptosis (Rogakou *et al.*, 2000; Haupt *et al.*, 2003). Additionally, senescent cells have been identified in p53-null mice (Muñoz-Espín *et al.*, 2013). In the context of senescence, the components of the DNA damage response, particularly p53, help signal to the cyclin-dependent kinase inhibitor P21 to help elicit the permanent cell cycle arrest that senescent cells are known for (Di Leonardo *et al.*, 1994). $P21^{WAF1}$ predominantly acts on CDK2 to arrest cell cycle at either G1 or G2 phase (Wade Harper *et al.*, 1993; Xiong *et al.*, 1993; Bunz *et al.*, 1998). Interestingly, mice lacking in the $P21^{WAF1}$ locus, *CDKN1A,* are defective in G1 and G2 cell cycle checkpoint control and have more tumours, a disease of uncontrolled proliferation, at 16months compared to wild-type siblings (Deng *et al.*, 1995; Martín-Caballero *et al.*, 2001). However, P21-mutant mice do not show sensitivity to senescent-inducing stressors such as radiation or telomerase-deficiency (Choudhury *et al.*, 2007). $P16^{INK4A}$ is another exemplar cyclin-dependent kinase inhibitor that helps to maintain the senescence cell cycle arrest by inhibiting the kinase activity of CDK4 and cyclin-D (Serrano, Hannon and Beach, 1993). The inhibition of CDK4 and cyclin-D by P16 is through activation of the tumour suppressor Rb, which in turn represses the E2F transcription factors associated with cell cycle progression (Narita *et al.*, 2003). Unlike P21, P16 is commonly mutated in tumours, and P16 mutant mice have increased susceptibility to tumour-inducing stressors (Serrano *et al.*, 1996). The current understanding of the relationship between the CDKIs is that $p21^{Waf1}$ seems to be an earlier marker of senescence, and helps induce the cell cycle arrest, whilst $P16^{Ink4a}$ further helps mediate the irreversible nature of senescence (Stein *et al.*, 1999). However, the exact kinetics of these genes are not entirely clear yet with relation to senescence induction and maintenance. Some evidence suggests that it takes 4 days of p21 expression to be indicative of senescence (Sang, Coller and Roberts, 2008). Others have shown that in replicative senescence of *in vitro* human fibroblasts, P21 is activated before P16 takes over for longer periods afterwards for senescence to be maintained (Alcorta *et al.*, 1996; Stein *et al.*, 1999). Conversely, more recent single-cell analysis of senescent cells 10 days after bleomycin treatment demonstrated that P21 is one of the highest predictors of senescence over quiescence, whilst P16 was not examined in this study (Wiley *et al.*, 2017). Additionally, $P16^{INK4A}$ expression has been identified in the context of macrophage polarization, independent of senescence (Hall *et al.*, 2017). In summary, P21 and P16 are clearly important in the induction of permanent cell cycle arrest in senescent cells and are therefore viable means for identifying these cells *in vivo*. However, as their involvement can alter according to context and there examples of expression of both genes independently of senescence, a combination of senescence markers would provide greater confidence of detecting the senescent phenotype reliably.

Similarly, though the SASP is a unifying feature of senescent cells, it is variable and temporally dynamic. For example, 10Gy IR on Mouse Embryonic Fibroblasts (MEFs) resulted in high IL6 expression, whereas senescent cells sorted from wounds show almost no change in IL6 expression (Demaria *et al.*, 2014). Furthermore, the SASP profile of primary lung mice fibroblasts was drastically different depending on whether they had underwent senescence through replicative senescence or stress-induced senescence, and the expression of SASP-related chemokines, cytokines, and growth factors such as IL-12, MIP-1α, and VEGF varied largely according the mode at which senescence was induced (L. A.

Maciel-Barón *et al.*, 2016). There were some common SASP features identified in senescent cells induced by five types of genotoxic stress and include the proteases MMP2, TIMP2, the growth factor binding protein IGFBP3, PAI1 amongst others (Özcan *et al.*, 2016). Interleukins such as IL1, IL6 and IL8 also seem to be quite common to the SASP phenotype (Coppé *et al.*, 2008; Acosta *et al.*, 2008; Kuilman and Peeper, 2009; Rodier *et al.*, 2009; Laberge *et al.*, 2016). Though the dynamic and complex nature of the SASP has plagued researchers in understanding the secretome of senescent cells, recent advancement in single-cell analysis has allowed the development of a proteomic database called the SASP atlas, which may help piece apart whether there are distinct and consistent components of the senescence secretome in different contexts (Basisty *et al.*, 2019).

Though senescent cells seem to last for a long time after stress *in vivo*, their mechanisms of cell death resistance are unclear (Sanoff *et al.*, 2014). Both of the aforementioned cell cycle inhibitors P21 and P16 have been identified as negative regulators of apoptosis (Bissonnette and Hunting, 1998; Sviderskaya *et al.*, 2003). Additionally, P53 can induce cytochrome c release from mitochondria for cell death mechanisms for example through its cytosolic subcellular localisation (Schuler *et al.*, 2000). In senescent cells, p53, though also up-regulated, can instead interact with FOXO4 and become localised to promyelocytic leukemia (PML) bodies in the nucleus that play a role in SASP regulation (Rodier *et al.*, 2011; Baar *et al.*, 2017). When this interaction is inhibited, senescent cells tend to become apoptotic more than non-senescent cells. Additionally, HSP90s are up regulated some senescent cells (Fuhrmann-Stroissnigg *et al.*, 2017; Basisty *et al.*, 2019). This heat shock protein interacts with Akt to inhibit apoptosis and promote cell survival (Fuhrmann-Stroissnigg *et al.*, 2017). Similarly, an siRNA against Bcl-xl, part of the bcl-2 family proteins involved in the same cell survival pathway, was able to reduce the viability of senescent cells (Zhu *et al.*, 2015). However, a contradictory study suggests that four different senescent fibroblast strains have low bcl2 activity, whilst still being more resistant to hydrogen peroxide-induced cell death than young cells (Sasaki *et al.*, 2001). This suggests the mechanisms for maintaining resistance to cell death in senescent cells can vary according to context.

Now there are multiple transcriptomic and proteomic changes identified with senescent cells, which helps to identify and research them. However, due to the many different contexts linked to senescence and the lack of reliable model organisms that can detect these cells at the cellular level *in vivo*, appreciating how they accumulate and are linked with ageing has proven challenging in the past (Calvin B Harley, Futcher and Greider, 1990; M Serrano *et al.*, 1997; Parrinello *et al.*, 2003b; Baker *et al.*, 2011; Demaria *et al.*, 2014; Liu *et al.*, 2019).

1.4.3.1. Replicative senescence

To understand how senescent cells are linked to ageing, an appreciation of the pathways for inducing senescence is essential. Replicative senescence was the first induction method identified (Hayflick and Moorhead, 1961; Hayflick, 1965; Calvin B Harley, Futcher and Greider, 1990; d'Adda di Fagagna *et al.*, 2003a). The term senescence was first coined in 1961 to describe the time-dependent decrease in proliferative ability of cells in culture after each round of cell division (Hayflick and Moorhead, 1961). When cells were unable to continue dividing, it was termed that the cells had reached their 'Hayflick Limit'. This was later attributed telomere attrition during cell division (Harley *et al.,* 1990). Telomeres are 'TTAGGG' repeat sequences of genomic DNA located at the end of chromosomes that get shorter with each round of DNA replication, due to the end-replication problem (Olovnikov, 1971; Watson, 1972). DNA polymerases

can only go in the five prime to three prime direction, therefore Okazaki fragments are required to make the lagging, reverse strand, of DNA. Once the last Okazaki template fragment has been removed, it leaves a short piece of single-stranded DNA at the three prime end, shortening the overall length of the chromosome with each round of DNA replication (Huffman *et al.*, 2000). Telomeres protect important intron and exon sequences by acting as a protective cap, and allow the recruitment of proteins that inhibit the response that would recognise this single-stranded piece of DNA as damaged (d'Adda di Fagagna *et al.*, 2003b; O'Sullivan and Karlseder, 2010). Eventually, these telomeres get too short and cannot provide room for these protective proteins to be recruited to them, the DNA damage response becomes activated and the cell enters replicative senescence where it will no longer undergo DNA replication or cell division. It was not known for some time whether this was an artefact of growing cells *in vitro*, or whether they actually had significance *in vivo.*

1.4.3.2. Oncogene-induced senescence

Cancer is a disease of uncontrolled proliferation, and therefore, it would be a logical place to assess whether the immortalisation of cells has something to do with overcoming the senescence phenotype and associated cell cycle arrest (Shay, Pereira-Smith and Wright, 1991). This was first shown through oncogenic activation of the G-protein RAS, which becomes hyperactive and causes excessive mitogenic signals, increasing p53 and $p16^{INK4A}$ levels and inducing senescence (M Serrano *et al.*, 1997). A concurrent induction mechanism following excess mitogenic signals from RAS is the resulting increase in metabolic activity, which in turn increases expression of DNA damaging reactive oxygen species (ROS), eventually inducing senescence (M Serrano *et al.*, 1997; Lin *et al.*, 1998; Halazonetis, Gorgoulis and Bartek, 2008). Importantly the DNA damage response is not always required for oncogene-induced senescence (Olsen *et al.*, 2002; Efeyan *et al.*, 2009). Certainly, immortalisation only occurred by an oncoprotein if key components of the senescence pathway, namely P53 and $P16^{INK4A}$, were inhibited. Additionally, tumours often contain mutations in senescence induction mechanisms, as well as activating telomerase to prevent telomere shortening (Kim *et al.*, 1994; Serrano *et al.*, 1996; Shay and Bacchetti, 1997). Experimentally altering the senescence machinery has a large effect on the onset of cancers *in vivo* (Lindsten *et al.*, 2000). Whereas modifying the machinery for programmed cell death, an alternative stress response, did not have much effect on *in vivo* cancer onset. The term oncogene-induced senescence (OIS) was used to describe senescent cells that were arrested in G1 phase following by oncogenic mutations in RAS (M Serrano *et al.*, 1997). Importantly, P53 and P16 were up regulated in these cells and the cell cycle arrest was abrogated when either of these proteins were mutated in the presence of RAS mutations. Interestingly, OIS is not universal across all cell types. Oncogenic mutations in BRAF will cause OIS, but this cannot be abrogated by P16 mutations, unlike in the case of RAS-mutant OIS (Michaloglou *et al.*, 2005). OIS was termed a unique type of senescence induction from replicative senescence as concurrent expression of telomerase did not overcome RAS-induced senescence (Wei, Wei and Sedivy, 1999). Senescent cells therefore play a key role in the prevention of cancer *in vivo*, and cancers must overcome the Hayflick limit to become immortalised.

1.4.3.3. Stress-induced senescence

Another type of senescence-induction is defined as stress-induced senescence. As DNA damage accumulates with age and stress induced senescence typically involves the P53/P21^{WAF1} DNA damage response pathway, this type of senescence is thought to have significance in the context of ageing (Toussaint *et al.*, 2002). ATM is a damage sensor proteins that recognise these shortened telomeres and recruits and activates proteins such as γH2AX and eventually the master regulator p53 (Burma *et al.*, 2001; Herbig *et al.*, 2004; Stiff *et al.*, 2004)**.** P53 will then induce cell cycle arrest through upregulation of Cyclin-dependent kinase inhibitors (CDKIs) such as p21^{Waf1}. If the damage is too severe or irreparable, the prolonged cell cycle arrest and p21^{Waf1} signalling induces further expression of other cell cycle regulators such as p16^{Ink4a} and pRb to strengthen the non-proliferative phenotype, modulate chromatin organisation, gene expression, and induce senescence (Collins and Sedivy, 2003; Narita *et al.*, 2003; Rodriguez and Meuth, 2006). Senescence can also be induced through autonomous production of stressors. ROS is also a side effect of mitochondrial metabolism for example, and with age mitochondria become dysfunctional and their reduced efficiency exacerbates the ROS production seen, also inducing senescence through the DDR (Chance, Sies and Boveris, 1979; Bulua *et al.*, 2011). Finally, exposure to exogenous sources of DNA-damaging agents such as doxorubicin, H_2O_2, bleomycin and exposure to ionising radiation (IR) have all been shown to activate this same pathway (Chen *et al.*, 1998; Suzuki *et al.*, 2001; Aoshiba, Tsuji and Nagai, 2003; Sliwinska *et al.*, 2009). An added complication is that both telomere shortening and oncogene activation can induce the DNA damage response, and as such the mechanisms of senescence induction are not necessarily mutually exclusive (d'Adda di Fagagna *et al.*, 2003a). Despite this, the phenotype that results from different induction methods can vary (L. A. Maciel-Barón *et al.*, 2016). An added layer of complexity is that senescence is not the only possible phenotype that can result from the DDR (Childs *et al.*, 2014). As well as senescence, the DDR can alternatively cause quiescence and repair DNA damage, as well as programmed cell death. Contributing factors to the cell fate choice include the type and extent of the DNA damage, as well as a specific cell type's DNA repair machinery. The addition of Doxorubicin to breast cancer cells for example can induce senescence or apoptosis depending on the applied dose, yet the addition of the DNA-damaging agent Bulsulfan to WI38 fibroblasts will only induce senescence regardless of dose (Song, Lee and Hwang, 2005; Probin *et al.*, 2006). P53 up-regulation can increase expression of pro-apoptotic genes, leading to cytochrome C release from mitochondria and the caspase cascade to trigger programmed cell death (Zou *et al.*, 1999; Vakifahmetoglu *et al.*, 2006). However, p53 can also interact with FOXO4, stay in the nucleus and instead cause senescence (Baar *et al.*, 2017). Normally, low dose gamma-irradiation (γ-IR) can induce a transient cell-cycle arrest via low activation of p53, but blocking p53 degradation through MDM2 inhibition via Nutlin-3 causes the same treatment in the same cell type to instead become senescent (Purvis *et al.*, 2012). Therefore, careful consideration into the context that one is examining senescence is an important consideration when studying these cells.

1.5. Physiological senescence

Though senescence is a hallmark of ageing, it clearly has evolved and been selected for to have physiological roles alongside other stress responses like apoptosis (Childs *et al.*, 2014). The first role identified for *in vivo* senescent cells, as already eluded to, is to prevent the onset of tumorigenesis. Senescent cells are non-proliferative, and the senescent program can be induced by oncogenic mutations like RAS and BRAF, as well as loss of function mutations in tumour suppressor genes like PTEN (M Serrano *et al.*, 1997; Chen *et al.*, 2005; Michaloglou *et al.*, 2005). Mice with mutated forms of key senescence proteins P16, P53, and P21 all are more susceptible to tumours than their wild type siblings, albeit to differing degrees (Jacks *et al.*, 1994; Serrano *et al.*, 1996; Martín-Caballero *et al.*, 2001). Additionally, mice with an extra copy of P53 or P16 were resistant to tumorigenesis (García-Cao *et al.*, 2002; Matheu *et al.*, 2004). Further, induction of senescence in tumour cells is thought to limit their pathology (Ventura *et al.*, 2007; Xue *et al.*, 2007). Though in lymphomas, the reintroduction of p53 led to apoptosis-based tumour regression, cellular senescence was identified in sarcomas by showing suppression of tumour growth and increases in P16 and SA-β-Gal activity (Ventura *et al.*, 2007). Murine liver tumours did not show increases in apoptotic markers such as TUNEL and caspase 3 upon p53 reactivation, but instead showed strong P16 expression and SA-β-Gal activity (Xue *et al.*, 2007). Further, increases in chemokine expression and leukocyte infiltration was seen, which could be attributed to a SASP from the induced senescent cells, but this was not directly shown in this study. This would demonstrate the unique advantages of senescence over apoptosis in tumour clearance, as senescent cells can lead to more prolonged paracrine signalling to phagocytes in a non-autonomous fashion (Kang *et al.*, 2011b). Only an oncogenic form of RAS able to signal downstream was able to induce senescence when injected into mouse liver tumours, and here there was rapid infiltration of multiple immune cell types and a decline in RAS-positive cells without detectable changes in TUNEL staining. Immuno-deficient mice also showed senescence induction following RAS injection, but were not able to clear the premalignant cells and tumour modules were later identified on the immune-deficient mouse livers. This effect was also seen in CD4 mutant mice, implicating CD4 positive T cells as central to the senescent cell-mediated immune surveillance. Both the removal of the senescence program increases *in vivo* tumour susceptibility and the reactivation of senescence reduces tumour progression, providing strong evidence that it is an anti-tumour mechanism.

The clear inflammatory nature of the SASP and evidence of immune surveillance of senescent cells prompted the idea that senescent cells may also play a role in other immune-mediated physiological functions such as wound healing and tissue regeneration (Demaria *et al.*, 2014). Cells expressing the senescence marker $P16^{INK4a}$ were identified at the site of cutaneous wounds in mice skin, and removal of these cells delayed the amount of time it took for the wound to heal and increased fibrotic collagen deposits were seen (Demaria *et al.*, 2014). PDGF-AA was secreted by senescent cells induced in response to tissue injury to promote myofibroblast differentiation and help with tissue remodelling required for effective tissue repair. In another study, when mice deficient in $P21^{Waf1}$ and $P16^{Ink4a}$ experienced acute liver injuries, additional fibrosis was observed, indicating incomplete tissue repair (Krizhanovsky *et al.*, 2008). Whereas, mice with unhindered senescence pathways exhibit cells that became senescent in response to injury, promote immune clearance, and showed improved tissue repair with less fibrosis. Likewise, in a cutaneous wound-healing model, myofibroblasts became senescent, which was thought to assist clearance of the extracellular matrix, and limit fibrosis (Jun and Lau, 2010). As it seemed that natural killer T cells (CD4+) were important in clearing senescent cells

in the context of cancer, studies explored whether there was a mechanism for this interaction in the context of wound healing (Kang *et al.*, 2011b). Though senescent cells were not directly examined, ligands for a natural killer T cell receptor, NKG2D, is expressed in cells with an activated DNA damage response pathway (Gasser *et al.*, 2005). More recently, fibroblasts induced into replicative senescence up-regulated ligands to the NKG2D receptor and was dependent on the DNA damage response (Sagiv *et al.*, 2016). In a liver fibrosis model, mice without the NKG2D receptor showed increased fibrosis and the accumulation of senescent cells was worsened.

Though it is less described, senescent markers seem to be present in the context of development (Muñoz-Espín *et al.*, 2013; Storer, Mas, Robert-moreno, *et al.*, 2013). There are periods of tissue remodelling during development that involve programmed cell death and immune clearance (Sulston *et al.*, 1983; Zou and Niswander, 1996; Kierdorf *et al.*, 2013). Macrophages are innate immune cells that are involved in surveying tissues during development to assist in tissue remodelling (McKercher *et al.*, 1996; Kierdorf *et al.*, 2013). There were fewer macrophages present during development in a $P21^{Waf1}$-null mice, these were lacking in senescent cells, suggesting a potential role in development also (Muñoz-Espín *et al.*, 2013). Interestingly, P53-null mice did not have this effect, p21 and SA-β-Gal activity was still detected and macrophages were present, suggesting that this type of senescence did not involve the central DNA damage response protein P53. Senescent cells were further identified during the development of the placenta (Rajagopalan and Long, 2012). Senescence activation in Natural Killer cells were identified nearby an explanted placenta, these cells was required to promote vascular remodelling during early pregnancy**.** Similarly, SASP expressing senescent cells were identified in mammalian embryos and seemed to be controlled by P21 and not P16 (Storer, Mas, Robert-moreno, *et al.*, 2013). Growth factor signalling through p-ERK induced senescence in this context and they were surrounded by infiltrating macrophages, suggesting a possible role in immune clearance here also. These examples are the first time that senescence has been implicated during normal development without the context of stress or disease.

The three seemingly diverse contexts involving senescence demonstrates the complexity of the phenotype. It is vital that one appreciates these physiological roles to understand the mechanism linking senescent cells with age-associated pathology. For example, in all three examples there is a strong association with the immune system and inflammation, a system known to have clear age-dependent loss in functions as mentioned (Solana *et al.*, 2012).

1.6.1. Pathological senescence: accumulation with age

Senescence is a clear and central hallmark of ageing (López-Otín *et al.,* 2013). The dominant theory about why these cells become pathological with age is the fact that they accumulate over time (van Deursen, 2014). The first evidence of this in humans was that increased SA-β-Gal activity was identified in older people (Goberdhan P. Dimri *et al.*, 1995). Further, in the skin and brain of aged primates there was an increase in multiple senescence markers such as SA-β-Gal activity, P16, P21, IL6 and γH2AX (Martin and Buckwalter, 2002; Herbig *et al.*, 2006a; Jeyapalan *et al.*, 2007; Bhat *et al.*, 2012; Kang *et al.*, 2015). Importantly, senescent cells also accumulate and correlate even further in the tissues of age-associated diseases such as Alzheimer's Disease (AD), Ideopathic Pulmonary Fibrosis (IPF) and Osteoarthritis (OA) in humans (Jeon *et al.*, 2017b; Schafer *et al.*, 2017; Bussian *et al.*, 2018). This compliments evidence from a whole host of other disease models in mice including Atherosclerosis and Parkinson's Disease (Childs *et al.*, 2016; Chinta, Woods, Demaria, Rane, *et al.*, 2018). The exact reasons as to why senescent cells accumulate with age are not completely understood, however several proposals have been established. One is that more senescent cells are produced in an aged context. If the 'somatic theory of ageing' holds true, then it would make sense that more senescent cells are seen with age due to increases in the amount of intrinsic and extrinsic genotoxic damage that cells are confronted with (Szilard, 1959; Moskalev *et al.*, 2013). Alongside this, over time cells will have gone through more rounds of cell division, increasing the likelihood for telomeres to be critically shortened and replicative senescence to be induced in an older individual (Calvin B Harley, Futcher and Greider, 1990; d'Adda di Fagagna *et al.*, 2003a). A complimentary age-dependent change that could contribute to senescence accumulation over time is alterations in the DNA damage response machinery. For example, the stability of P53 is lessened with age (Feng *et al.*, 2007). This could mean that the same genotoxic stress that would induce apoptosis in a younger cell can instead induce senescence in an aged context. DNA repair machinery itself changes with age, more DNA lesions are observed following H_2O_2 induced genotoxic stress of senescent fibroblasts compared to younger counterparts (Seluanov *et al.*, 2001). The ability for cells to repair UV-induced DNA damage decreased with donor age also (Wei *et al.*, 1993; Moriwaki *et al.*, 1996). Importantly, evidence has not directly shown that changes in DNA repair mechanisms or p53 stability are more likely to induce senescent cell accumulation. Alongside the idea that an older individual is more likely to be exposed to senescence-inducing stimuli and produce more senescent cells, there is an age-dependent decline in immune cell function that may be a driver for age-dependent senescent cell accumulation (Solana, Alonso and Peña, 1999; Solana and Mariani, 2000; Solana *et al.*, 2012; Antonangeli *et al.*, 2016b; Sagiv *et al.*, 2016). Although senescent cell markers remain for longer in the absence of immune cells, such as in the CD4 knockout mouse, direct interactions between these two cell types, such as real time phagocytosis of a senescent cell, have not yet been described (Kang *et al.*, 2011b). In reality, a combination of the aforementioned theories probably play a part in age-dependent senescent cell accumulation in a positive feedback loop. More senescent cells with age means more SASP, which could lead to a more chronic inflammatory microenvironment that further induces more genotoxic stress, inducing more senescence (Shelton *et al.*, 1999; Nelson *et al.*, 2012a). If they are not cleared well that could induce more bystander senescence in surrounding cells and tissues (da Silva *et al.*, 2019). Up until a few years ago, the evidence linking senescent cells and ageing was correlative, but now evidence suggests that these cells are causal to multiple age-associated pathologies.

1.6.2. Senescence is causal to age-associated pathology

The first causal link between senescence and ageing phenotypes surfaced through a transgenic mouse model that utilized the promoter of the senescence marker $p16^{Ink4a}$ as a driver for an inducible caspase 3 and 7-based cell death (Baker *et al.*, 2011). This allowed specific ablation of these cells in the presence of an inducer drug. These mice were bred with a progeric mouse, which displayed age-related disease much earlier in development due to BubR1-based DNA repair deficiency. Once $p16^{Ink4a}$ -expressing cells were ablated in these mice, a significant delay in age-related diseases such as sarcopenia and cataracts was demonstrated, though lifespan was unaffected. Effects were seen in mice treated with the drug from weaning, meaning life-long $p16^{Ink4a}$ ablation, as well as those treated from adulthood. As this was a progeric mouse with DNA repair deficiencies, it was not known whether this effect was translatable to a wild-type ageing context. To answer this, the $p16^{Ink4a}$ ablation system was then used in a wild-type strain mice (Baker *et al.*, 2016). These mice were treated from 12 months of age, and therefore already presented with some senescence, making the results more clinically relevant to the way in which patients are treated after symptom onset. The effect of this treatment was a 17-35% increased median lifespan, depending on the strain and sex of the animal. The onset of cancer and cataracts, which are both well-documented age-related disorders was reduced, and improvements in movement and exploratory behaviours were seen, suggesting healthspan improvements also. This research confirmed that senescent cell accumulation not only correlates with ageing, but that this phenomena is directly involved in the onset of age-associated pathologies that limit lifespan and healthspan.

Since then, causal evidence linking senescence and age-associated pathologies have been shown within the contexts of multiple different disease models in mice. Bleomycin-treated mice show lung injury and can be used to model lung damage seen in the age-associated disorder idiopathic pulmonary fibrosis in humans (Schafer *et al.*, 2017). Genetic ablation of senescent cells reduced inflammation and improved exercise capacity and running ability. Improvements in disease pathology and whole organism health are also seen in models of the age-associated bone diseases osteoporosis and osteoarthritis (Farr *et al.*, 2017; Jeon *et al.*, 2017). Reduced cartilage thickness and joint health are causal to osteoarthritis onset, an age-associated pathology common in older people with no treatment available (Loeser, 2017). The histopathology seen in the cartilage, detected by the commonly used OARSI scoring system was improved and markers of inflammation reduced in a spontaneous age-dependent mouse model of osteoarthritis. Joint-injury, alongside ageing, is another risk factor for osteoarthritis development, senescence removal in a model for post-traumatic osteoarthritis also showed clear improvements in bone health. Age-related bone loss is causal to osteoporosis development (Sozen, Ozisik and Calik Basaran, 2017). Removal of senescent cells in adult mice at 20-months old improved multiple measures of bone thickness, such as spinal bone volume over trabecular volume (BV/TV) (Farr *et al.,* 2017). Senescent cells are also causal to the pathology of the age-associated neurodegenerative disorders, Alzheimer's Disease and Parkinson's Disease (Bussian *et al.*, 2018; Chinta, Woods, Demaria, Rane, *et al.*, 2018). Paraquat is associated with increased risk of idiopathic Parkinson's Disease and Paraquat-treated mice show neuronal loss, loss of motor function and reduced neurogenesis, all features that are common with Parkinson's Disease (Chinta, Woods, Demaria, Rane, *et al.*, 2018). Paraquat treatment up-regulated markers of senescence, and when senescent cells were cleared from these mice via genetic ablation of p16-positive cells, improvements in all of these areas were seen. When assessing for a potential mechanism linking senescent cell accumulation and Parkinson's

pathology, conditioned media from senescent cells had detrimental effects on neurons suggesting the SASP as a driver for this pathology. Similarly, hippocampal expression of markers of inflammation and senescence were improved in a tau-dependent neurodegenerative mouse that models Alzheimer's (Bussian *et al.,* 2018). Importantly, this was associated with improvements in markers of cognition, such as their ability to discriminate between new objects and those that the mouse has already come across. These examples highlight where senescence is a common cause to a number of age-related phenotypes and disorders.

In the context of atherosclerosis and cancer, senescent cells have been shown to have both a causal and preventative role in their pathology. Low-density lipoprotein receptor–deficient (ldlr) mutant mice show atherosclerotic plaques in the aorta when fed on a high fat diet (Childs *et al.*, 2016). Senescent cells were identified in the atherosclerotic lesions in mice and their removal reduced inflammation, lipid accumulation and plaque numbers. Conversely however, loss-of function mutations in the senescence-associated P16 locus, *CDKN2A*, correlated with an increased risk of atherosclerosis development, this was suggested to act as a limiting factor on macrophage foam cell proliferation and as such, would limit the size of atherosclerotic plaques when functioning normally (Gizard *et al.*, 2005; Kuo *et al.*, 2011). As mentioned, senescent cells are non-proliferative and a clear anti-cancer mechanism (Serrano *et al.,* 1997). However, a more recent study showed that women with breast cancer that had higher markers of senescence in their blood were more likely to experience chemotherapy-induced side effects (Demaria *et al.*, 2017). Further, removing senescent cells actually abrogated the adverse effects of chemotherapy such as cardiac dysfunction, reduced the likelihood of cancer relapse, metastasis and improved physical functions of mice. A complimentary study also showed that the removal of senescent cells was able to reduce the amount of kidney damage seen in response to doxorubicin treatment (Baar *et al.*, 2017). These two examples show how senescent cells are an example of the antagonistic pleiotropy theory, where they are useful in one context but detrimental in another (Williams, 1957). This further emphasises the complexity of senescent cells and the care required to develop drugs that ideally only stop the detrimental effects seen from senescent cells and not cause side effects from removing the beneficial effects of these cells. Regardless, mounting evidence suggests that clearance of senescent cells is a viable therapeutic option for the treatment of multiple age-associated disorders and healthspan extension in humans.

1.6.3. Pharmacological targeting of senescent cells to treat age-associated diseases.

Now that there is causal evidence linking senescent cell accumulation and multiple age-associated pathologies, it is important to assess the theoretical potential of senescent cells to be a viable pharmacological target to treat age-associated multimorbidity (Scudellari, 2017). Firstly, having few senescent cells should not induce significant side effects because in the context of youth there are very few senescent cells without their being obvious consequences (Biran *et al.*, 2017a). In young mice for example there is only around 1% senescence, compared to up to 20% in older mice, and these are healthier than their older counterparts. Secondly, the pathology associated with senescent cells in the aged context could theoretically be reduced without having to clear all senescent cells. Unlike in the context of cancer or infection, a senescent cell remaining after treatment will not expand rapidly and become resistant to treatment, as they are non-proliferative (Kobayashi *et al.*, 2005; Shah *et al.*, 2007). It is thought that the accumulation of many senescent cells that is the issue rather than individual cells themselves, meaning lower compound doses may

be required and further improve the therapeutic index. Thirdly, senescent cells take time to accumulate, almost a whole lifetime, and so one would expect that once senescent cells are removed pharmacologically then it would take time for a patient to require treatment again (Herbig *et al.*, 2006a). Intermittent treatment would likely cause fewer off-target toxicities compared to constant treatment. Fourthly, senescent cells are linked with multiple hallmarks of ageing and have been identified in numerous age-associated diseases; if a treatment could effectively be used systemically without toxicity, it could potentially directly target age-associated multimorbidity and overcome issues of polypharmacy (Doan *et al.*, 2013). Of course, there are likely caveats to this, and huge amounts of research are required to test whether these theories are true, but initial data around pharmacologically altering senescent cells as a treatment against age-associated diseases are promising.

Whilst evidence continues to emerge causally linking senescent cells with age-associated disease, efforts to identify compounds that can phenocopy the positive effects seen from genetic-based senescent cell clearance are well under way (McHugh and Gil, 2018). One approach to reduce the negative effects of age-associated senescence is to reduce the inflammatory SASP, these types of compounds are called 'Senostatics'. A screen identified inhibition of PTBP1 as an approach to limit the SASP and block the tumour-promoting functions of senescence (Georgilis *et al.*, 2018). Additionally, the JAK/STAT pathway is important in cytokine production, and the JAK1/2 inhibitor ruxolitinib was able to reduce the age-related bone loss seen in mice that is associated with osteoporosis (Xu *et al.*, 2015; Farr *et al.*, 2017). Rapamycin has also been implicated as a potential senostatic through limiting mTOR signalling known to regulate the SASP (Laberge *et al.*, 2015; Wang *et al.*, 2017). Similarly, Metformin can inhibit the SASP by interfering with NF-κB signalling (Moiseeva *et al.*, 2013). Both Rapamycin and Metformin are known to extend lifespan and healthspan of model organisms, though whether these effects are directly due to SASP-inhibition is not known (Harrison *et al.*, 2009; Martin-Montalvo *et al.*, 2013; Bitto *et al.*, 2016; Correia-Melo *et al.*, 2019). Though this approach has some merit, a caveat is that in this context the senescent cells themselves will still be present, so it is possible that once the SASP-inhibiting drug has been metabolised then the SASP could be reactivated. If this were the case then patients would need to be on lifelong treatment, which is less favourable than acute treatment regimes. A further proposed method for targeting senescent cells is to boost their clearance by the immune system, in a comparable manner to the method described that won James Allison and Tasuko Honjo the 2018 Nobel Prize in Physiology and Medicine by reactivating T cell killing of cancer cells (Hodi *et al.*, 2013). For this to become a viable option, much more work into defining the mechanisms and characteristics of immune-mediated senescent cell clearance and deciphering whether reduced immune function is causal to senescent cell accumulation with age. One further proposed means of reducing senescent cell burden is promoting DNA repair to actually stop or reverse the senescent cell onset, which in theory would be less reliant on healthy progenitors to replenish the tissue like with senolytics (Bernardes De Jesus *et al.*, 2012). A concern with this approach is whether the cells who have reversed out of senescence are actually cancerous, or at least more susceptible to cancer than healthy counterparts. Indeed, re-activation of *tert* was shown to promote prostate cancer progression (Ding *et al.*, 2012). Conversely, a viral vector that reintroduces telomerase was given to adult mice and delayed ageing in multiple tissues, extending lifespan as a result without increasing the incidence of cancer (Bernardes

de Jesus *et al.*, 2012). One explanation for this contradiction is because the viral vector does not affect the genome and will be diluted out of cells as they proliferate, making them distinct from the telomerase activation seen in cancers. More recently, the same vector was used in a mouse model of lung fibrosis and showed reduced senescence, inflammation and lung fibrosis (Povedano *et al.*, 2018). This approach also shows promise but more evidence to ensure that the physiological role of senescence as an anti-cancer mechanism is not implicated. Particularly as this approach does not remove cells that were originally stressed enough to become senescent. Additionally, the evidence does not distinguish currently whether this approach can reverse cells that are already senescent, or prevent more from become senescent later, which has important implications in terms of translating to a therapy in humans.

The most popular approach is through targeting the mechanisms that senescent cells use to resist cell death to selectively kill them, in a process called senolysis (Kirkland *et al.*, 2017) (Table 1.1.). Theoretically, senescent cells should rely on these pathways more than non-stressed cells, in an analogous way that cancers with BRCA mutations are more susceptible to PARP inhibitors due to compromised DNA repair mechanisms (Bryant *et al.*, 2005). The main limitation of this approach is that the exact mechanisms for cell death resistance are not well understood and seem to be variable (Sasaki *et al.*, 2001; Zhu *et al.*, 2016). This means that their efficacy is contextually dependent and their therapeutic window, the dose that can kill senescent cells without damaging control cells, is small and can depend on the cell type and induction stimulus (Zhu *et al.,* 2016; Baar *et al.*, 2017). Despite this, senolytics have indeed shown significant *in vivo* efficacy in the context of multiple age-associated pathologies. Unlike the aforementioned approaches, direct removal of senescent cells should have long lasting effects as it takes a long time for senescence to be accumulated (Herbig *et al.,* 2006). Indeed, one dose of a senolytic had long lasting physical improvements in a mouse model of transplanted senescent cells (Xu *et al.*, 2018). Currently though, this theory has not been evidenced in a wild-type aged mouse.

The first identified and most successful senolytic currently is the combination of Dasatinib and Quercetin (Zhu *et al.*, 2015). Quercetin inhibits PI3K signalling and Dasatinib acts on the dependence receptor EFNB, both of which are involved in preventing apoptosis, in combination they are able to selectively reduce the viability of senescent cells induced by irradiation or serial passaging. The drug combination has since shown efficacy in models of multiple age-associated diseases including Atherosclerosis, Osteoporosis and Ideopathic Pulmonary Fibrosis (Roos *et al.*, 2016; Farr *et al.*, 2017; Schafer *et al.*, 2017). A phase one clinical trial has also been carried out testing the use of Dasatinib & Quercetin in the context of human Ideopathic Pulmonary Fibrosis (Justice *et al.*, 2019). Though this was only a three-week treatment regime tested in 16 patients, clinically relevant improvements in pulmonary and physical function were observed. For example, the distance walked in 6 minutes, improved from 447 (SD 83) to 468 (SD 81), a 4.5% improvement. This is the first time that a senolytic has shown efficacy in human disease. As it is only a phase one clinical trial, larger studies are required to determine their reliability. It would also be important to see whether the improvements in health status described in the IPF study such as 6-minute walking distance are classified relative to IPF severity and associated side effects from the treatment. Additionally, lung biopsies to show that in humans, oral Dasatinib and Quercetin treatment both reduces senescence and senescence-associated inflammation are vital to

determine the mechanism of action for these health improvements are truly due to senescence ablation. More recently, another clinical trial showed that Dasatinib was able to reduce the SASP in Systemic Sclerosis (SSc) patients (Martyanov, Whitfield and Varga, 2019). Interestingly, those who showed improvements in the modified Rodnan skin thickness score, a validated measure of SSc disease outcome, showed a much greater reduction in SASP factors compared to non-improvers (Clements *et al.*, 1995). This further implicates the SASP in human disease pathology. In the context of diabetic kidney disease, Dasatinib & Quercetin was able to reduce SASP markers such as IL1a, IL6, MMP9, MMP12 in peripheral blood, and markers of senescence such as P21, P16, and SA-β-Gal in skin and adipose tissue, as well as reduced macrophage infiltration (Hickson *et al.*, 2019). This directly evidenced that these drugs actually reduce senescence markers in humans. An important limitation to these clinical trials is that they were all one-armed studies, this means that differences were seen before and after treatment, but a placebo control was not used. This means that the placebo effect cannot be ruled out as a contributing factor to these trials, where patients get more time and attention from medical professionals that could contribute to better outcomes (Thompson, Ritenbaugh and Nichter, 2009). There are limitations to these drugs also; they are not effective in certain cell types such as endothelial cells (Zhu *et al.,* 2015; Hwang *et al.*, 2018). Further, Dasatinib & Quercetin are much less effective at treating senescent cells induced by doxorubicin compared to irradiation (Baar *et al.,* 2017). Dasatinib is used as a chemotherapeutic agent against leukaemia and has common side effects associated such as low blood counts and increased risk to infection (Futosi *et al.*, 2012; Zarbock, 2012).

Fisetin, like Quercetin, is a flavonoid that shows senolytic potential (Yousefzadeh *et al.*, 2018). Unlike Quercetin, its effects are seen without another drug in combination, it improved liver and pancreatic homeostasis and reduce markers of pathology in brain and kidney of progeric and wild type aged mice. Though no physiological improvements in healthspan were examined outside of histopathology, median and maximum lifespan were extended even when the treatment was given at later life. The senolytic mechanism of action for Fisetin is thought to involve caspase 3-mediated apoptosis of senescent cells, via the PI3K/AKT/NF-κB and ERK1/2 pathways (Kim *et al.*, 2015; Zhang and Jia, 2016). The effect on NF-κB would also potentially have a senostatic effect, though it has been proposed that senostatic treatment may have a net senolytic effect due to the limiting effects on bystander senescence (Chien *et al.*, 2011; da Silva *et al.*, 2019). Additionally, it is worth noting that flavonoids such as Quercetin and Fisetin are known to have multiple mechanisms of action that could contribute to *in vivo* healthspan extension outside of senescence, such as alterations in the gut microbiota (Kawabata *et al.*, 2013). An important limitation of both flavonoids in the context of age-associated multimorbidity is that they interact with the family of enzymes typically used to metabolise drugs in the liver, cytochrome p450, which limits their use in the elderly who are taking other common medications that also interact with the same enzyme (Doan *et al.*, 2013; Lee *et al.*, 2014; Elbarbry, Ung and Abdelkawy, 2017).

UNITY biotechnology is the first company with the sole focus of developing senolytics to target age-associated pathologies (UNITY Biotechnology, 2019). Their first drug being developed is a p53/MDM2 interaction inhibitor called UBX0101, which has shown efficacy in an osteoarthritis mouse model (Jeon *et al.,* 2017). In principle, inhibiting the negative regulator of p53 should cause cell death in senescent cells that are present in the joints of patients with osteoarthritis (Price *et al.*, 2002). Indeed, UNITY published initial results from a phase one clinical trial treating osteoarthritic knees with UBX0101 and showed some reduction in pain scoring at the highest dose, which was tolerated well (Spark, 2019; NCT03513016). However, in the second part of this study, the commonly used scoring for osteoarthritis severity, The Western Ontario and McMaster Universities Osteoarthritis Index (WOMAC), did not show large improvements, nor in the level of inflammation in the synovial fluid. A possible reason for this is that the trial only included patients between 40 and 85 years of age, and so could have included late-stage disease patients. Moreover, the effect of this drug on late-stage osteoarthritic mice was less pronounced than life-long treatment of the drug for post-traumatic osteoarthritis (Jeon *et al.,* 2017).

Navitoclax (ABT-263) is another senolytic that instead induces cell death by acting against anti-apoptotic proteins BCL-2, BCL-XL and BCL-W (Zhu *et al.,* 2016). Mutant mice with tau pathology and cognitive decline that is comparable with Alzheimer's disease showed senescence clearance and reduced tau phosphorylation in the presence of Navitoclax, but functional effects on cognitive function were not examined (Bussian *et al.,* 2018). Similarly, myocardial infarctions are known to accelerate the age-associated disease atherosclerosis (Dutta *et al.,* 2012). Removal of senescent cells were able to improve survival and recovery following a heart attack in mice (Walaszczyk *et al.*, 2019). ABT-263 was originally identified to have efficacy against cancer cells that overexpress BCL2 proteins (Tse *et al.*, 2008), but clinical trials using ABT-263 to treat leukaemia's and lymphomas (NCT00406809), and lung cancer (NCT00445198) showed limited efficacy and significant side effects such as thrombocytopenia. It is not clear whether the efficacy of this drug is due to directly targeting cancer cells expressing BCL2 or by removing tumour promoting senescent cells in the surrounding niche, as both cell types can be targeted by ABT-263 (Wang *et al.*, 2017). This does highlight ABT-263 as a potential adjuvant therapy option for chemotherapy drugs, as ABT-263 but interestingly not the combination of Dasatinib and Quercetin, were able to reduce cancer growth and metastasis induced by senescent cells produced from chemotherapy treatment (Wang *et al.*, 2017; Kovacovicova *et al.*, 2018). In other contexts, Dasatinib and Quercetin are more useful however; ABT-263 is not effective at targeting senescent human primary adipocytes for example (Zhu *et al.,* 2016).

An *in vitro* screening approach identified the HSP90 inhibitor 17-DMAG (Fuhrmann-Stroissnigg *et al.,* 2017). Phosphorylated Akt levels decreased in response to 17-DMAG, implicating a potential mechanism of action for the HSP90I on the cell-survival pathway. Progeric mice treated with 17-DMAG presented with reduced symptoms of age-associated pathology such as grip strength and tremor, but more clinically relevant models and assessment of pathology are required before testing in humans. A peptide with senolytic efficacy was also identified that, rather than directly inhibiting proteins, inhibited the interaction between FOXO4 and p53 (Barr *et al.,* 2017). This FOXO4-DRI peptide was able to reduce the amount of senescence seen in mice treated with doxorubicin, reducing inflammatory markers such as IL6 damage to the kidney and liver, implicating a potential role in combination with chemotoxic cancer therapies. Additionally, rapid-ageing mice treated with FOXO4-DRI showed multiple improvements in behaviour such as responsiveness and running distance on a wheel.

In summary, multiple methods for killing senescent cells are now in development with varying levels of *in vivo* efficacy, but senolytics seem to be the most promising currently. Much work is still required to ensure they are a safe and effective treatment option for patients with multimorbidity as a means to extend healthspan. Less toxic drugs would likely be required as higher doses would be required for systemic treatment to have an efficacious dose in all required organ systems, passing the blood brain barrier effectively for example (Serwer *et al.*, 2010).

The progress on identifying causal links between senescence and age-associated disease and developing drugs to treat them has been extensive, however there are still important limitations in the field that prevent the use of senolytics as an effective treatment against multi-morbidity in older people. There is almost no evidence of senolytics being useful in improving the healthspan of older patients suffering from multiple age-associated diseases at the same time. This is the most important aspect of developing drugs against the mechanisms of ageing, as it has the potential to tackle the problems of polypharmacy seen in the elderly population that limits the efficacy of treating individual disease (Doan *et al.,* 2013). UBX0101 treatment in humans presenting with osteoarthritis were only treated by local injection, and not systemic treatment for example (Spark, 2019). In comparison, Dasatinib and Quercetin were given by systemic oral treatment in patients with Ideopathic Pulmonary Fibrosis. (Justice *et al.,* 2019) In this context, a serious adverse event involving bacterial pneumonia and pulmonary oedema, as well as 37 mild and 31 moderate non-serious advents were described in the 16 patients treated over the short three-week period. However, the majority of these patients did also present with co-morbidities such as hypertension and depression, four of which had more than seven classified, and so the fact that a positive effect was seen in this context is indeed promising. Additionally, longer-term side effects related to senescent cell removal, such as increased cancer incidence and impaired recovery from a wound have not yet been examined in these trials. These data are an encouraging start, but do highlight that more work is to be done to make these drugs safe and effective as their efficacy is limited and contextually dependent.

Senolytic	Mechanism	Disease tested (species)	Reference
Dasatinib (D) & Quercetin (Q)	PI3K, AKT (Q); Dependence receptor (D) inhibitors	Cardiovascular disease (mouse)	Zhu et al., 2015
		Atherosclerosis (mouse)	Roos et al., 2016
		Idiopathic Pulmonary Fibrosis (mouse & human)	Schafer et al., 2017; Justice et al., 2019
		Systemic Sclerosis (human)	Martyanov et al., 2019
		Diabetic kidney disease (mouse & human)	Hickson et al., 2019
		Osteoporosis (mouse)	Farr et al., 2017
		Hepatic stenosis (mouse)	Ogrodnik et al., 2017
		Cachexia (mouse)	Zhu et al., 2015
UBX0101	MDM2/p53 interaction inhibitor	Osteoarthritis (mouse & human)	Jeon et al., 2017; Spark, 2019 (NCT03513016)
Navitoclax (ABT-263)	BCL2 inhibitor	Alzheimer's Disease (mouse)	Bussian et al., 2018
		Atherosclerosis (mouse)	Childs et al., 2016
		Myocardial infarction (mouse)	Dutta et al., 2012; Walaszczyk et al., 2019
		Sarcopenia (mouse)	Chang et al., 2016
Fisetin	PI3K, AKT, NFκB, ERK1/2 inhibitor	Lifespan & age-related pathology (mouse)	Yousefzadeh et al., 2018
FOXO4-DRI	FOXO4/p53 interaction inhibitor	Chemotherapy-induced toxicity (mouse)	Barr et al., 2017
17-DMAG	HSP90 inhibitor	Age-related pathology (progeric mouse)	Fuhrmann-Stroissnigg et al., 2017

Table 1.1. List of senolytics that have shown *in vivo* efficacy in age-associated pathologies.

It is clear that a deeper understanding of the senescence phenotype and the differences between senescent cells in different contexts is required to improve the therapeutic potential of this avenue of treatment. There is a need to accelerate the progress of senolytic development by screening for novel senolytic compounds in a whole organism context earlier in drug development. This allows for testing for changes in whole-organism health earlier. Long ageing mice experiments are inefficient and often show that previous *in vitro* work does not often translate as well into mammals, particularly in the context of an old animal with multiple age-associated diseases (Bellantuono & Potter, 2016). A more in-depth characterisation of senescent cells *in vivo* to determine individual cell variability; with a tool to prospectively identify potentially senescent cells from a mixed cell population *in vivo* would strengthen the understanding of the limitations of current markers of senescence and their reliability at predicting senolytic efficacy. Additionally, an understanding about whether there are distinguishable features *in vivo* between senescent cells that are present in a beneficial context, as an anti-tumour mechanism or to promote wound healing for example, and senescent cells that are present in a detrimental context and causal to age-associated pathology. An *in vivo* model that can assess the paracrine interactions between senescence, the SASP, and the immune system would likely assist in this regard. Novel tools to assist and compliment already established models will most likely lead to these important advances and develop viable treatment regimens for improving the quality of life of our ageing population.

1.7.1. The zebrafish as a model organism

The *danio rerio*, or zebrafish, are a useful model organism that are not highly utilised currently in the context of senescence research. The first zebrafish clones were used to understanding *in vivo* vertebrate developmental biology (Streisinger *et al.*, 1981). Zebrafish share 84% of known human disease-associated genes and 70% of human protein-encoding genes (Howe *et al.*, 2013). Their innate immune system for example, which is of clear importance in human ageing and senescence, show great conservation between the two species, despite diverging 450 million years ago during the Palaeozoic era (Kumar and Hedges, 1998). The model organism is advantageous due to rapid growth and development, optical transparency and the ability to genetically and pharmacologically manipulate zebrafish, making it a now extensively used system throughout a wide variety of disciplines, including those related to senescence and ageing (Murtha and Keller, 2003; Van houcke *et al.*, 2015).

Zebrafish have unique aspects as a model organism that make them useful to tackle current limitations in the senescence field. Firstly, unlike mammalian model systems, zebrafish are fertilised externally and translucent during early development (Poleo *et al.*, 2001; Renshaw and Loynes, 2006). This, alongside their genetic malleability and sequenced genome, means that methods for studying organismal processes at the cellular level, live and *in vivo* are plausible in zebrafish (Renshaw *et al.,* 2006). Developing transgenic fluorescent reporters for genes that are associated with certain cell types for example mean that those cell types can be visualised and imaged through fluorescent microscopy (Ellett *et al.*, 2011). For example, the discovery of neutrophil and macrophage-specific promoters in zebrafish enabled the development of stable transgenic lines to drive the expression of fluorescent proteins in these

innate immune cells (Renshaw et al., 2006; Ellet *et al.,* 2011). Live imaging of specific immune cell types was able to disseminate important evidence about the dynamics of the immune cell response and inflammation in response to tissue injury. This was able to be established by imaging transparent and transgenic fish, tracking individual cells within the same animal over time to elucidate novel components of immunity that were not feasible in mammalian systems (Mathias *et al.*, 2008; Yoo and Huttenlocher, 2011). Further, mechanisms about how the immune system interacts with other cells to fight infection or survey pre-neoplastic cells have been possible due to the unique advantages of the zebrafish as a model organism (Feng *et al.*, 2010; Prajsnar *et al.*, 2012; Santhakumar *et al.*, 2012; Elks *et al.*, 2013; Thompson *et al.*, 2014). These advantages could be translated into the context of senescence, whereby assessment of the temporal induction of senescent-associated genes, their reliability at detecting *in vivo* senescence, and whether immune cells directly interact with them could be possible in a more feasible manner than current mouse models (Baker *et al.,* 2006; Demaria *et al.,* 2014; Liu *et al.,* 2019).

Further, zebrafish are uniquely amenable to study the *in vivo* efficacy of drugs involved in complex multi-cellular processes because they are small, have high fecundity and develop rapidly (Meyers, 2018). For example, a drug for enhancing engraftment of blood transplants in leukemic patients was identified in a zebrafish-based screen, and has shown success in phase I and II clinical trials (North *et al.*, 2007; Cutler *et al.*, 2013). Novel compounds that regulate the resolution of inflammation have also been identified in zebrafish (Robertson *et al.*, 2014). Tanshinone IIA can reduce the number of neutrophils present at the site of injury, highlighting it as a potential treatment for diseases of failed inflammation resolution such as chronic obstructive pulmonary disorder of the lung. Additionally, zebrafish have been used to carry out a compound screen to find novel methods to reduce convulsions as a treatment against epilepsy (Baxendale *et al.*, 2012). Similarly, zebrafish mutants that phenocopied seizures seen in Dravet syndrome were screened to identify compounds that limited the convulsions (Griffin *et al.*, 2017). Locaserin showed improvements in zebrafish and patients, skipping pre-clinical murine testing entirely. These types of screens can be scaled up to an almost comparable manner with *in vitro* screening (Wang, Rajpurohit, Delaspre, Walker, White, Ceasrine, Kuruvilla, R.-J. Li, *et al.*, 2015). With automated quantitation, more than 500,000 zebrafish larvae were screened to identify novel compounds that increase the number of insulin-producing β cells in the pancreas, as a potential treatment for diabetes (Wang, Rajpurohit, Delaspre, Walker, White, Ceasrine, Kuruvilla, R.-J. Li, *et al.*, 2015). These together emphasise the unique potential of zebrafish to identify novel modulators of senescence in an *in vivo* context earlier in the drug development process. This should help overcome the toxicity issues seen in senolytics currently, whereby only those screened to show direct improvements in whole organism health and with limited off-target toxicity would be taken into preclinical trials. These types of assessment are not feasible in current *in vitro* screening approaches, and are timely and costly to do in aged mouse studies (Zhu *et al.,* 2015; Zhu *et al.,* 2016; Fuhrmann-Stroissnigg *et al.,* 2017). Currently though, there are no transgenic reporters for senescence that could identify senescent cells *in vivo*.

1.7.2. Zebrafish as a model of senescence

Though zebrafish senescence has not been as extensively studied as mammalian systems, almost all of the hallmarks of ageing that have strong associations with senescence are described in zebrafish (Figure 1.1) (López-Otín *et al.*, 2013; Van houcke *et al.*, 2015). As is seen in mammals, zebrafish cells exposed to an external genotoxic stressor will up-regulate markers of the DNA damage response and senescence including p53 and p21 (Sandrini *et al.*, 2009). In terms of epigenetic regulation, evidence of age-dependent decline in methylation with age in zebrafish has been described (Shimoda *et al.*, 2014). Though direct evidence for specific methylation marks identified as regulators of senescence-associated genes such as H3K27me3 were not studied, the hypomethylation described was located predominantly in CpG islands that are a common site of age-dependent hypomethylation in mammals. Further, older zebrafish demonstrate signs of reduced proteostasis, with increased protein oxidation in muscle with age and a decrease in the prevalence of heat shock protein 70 (Gerhard *et al.*, 2002; Kishi *et al.*, 2003; Murtha and Keller, 2003). Lipofuscin accumulation has been described as a potential marker of senescence, it accumulates with age and demonstrates a loss in protein quality control as it indicates aggregates of oxidised material (Georgakopoulou *et al.*, 2013). Lipofuscin accumulation has also been described with age in zebrafish (Ruhl *et al.*, 2015). Nutrient sensing can regulate senescence phenotypes in zebrafish also. For example deficiencies in the nutrient folate is associated with Alzheimer's disease in older humans, a disease causally linked with senescence (Kao *et al.*, 2014; Bussian *et al.*, 2018). When zebrafish are deficient in this nutrient, phosphorylated tau and β-amyloid protein deposits, a marker of Alzheimer's-like pathology, were also seen in their brains. Additionally, altered growth hormone signalling leads to accelerated ageing phenotypes such as spinal curvature and reduces anti-oxidative enzymes; it is plausible that this compromise could induce senescence via excess reactive oxygen species (ROS) availability (Rosa *et al.*, 2010). An important producer of ROS and senescence induction is through mitochondrial dysfunction, which is increased with age in zebrafish (Almaida-Pagán, Lucas-Sánchez and Tocher, 2014; Ruhl *et al.*, 2015). Zebrafish mitochondrial DNA shows a high similarity to that seen in humans, as seen on GenBank (Accession AC024175). Imbalanced mitochondrial fission and fusion, decreased autophagy and mitophagy and increased inflammation was described in the aged zebrafish retina, indicating abnormal intracellular signalling, protein regulation and mitochondrial dysfunction (Wang *et al.*, 2019). As is described in mammals, telomeres shorten and telomerase expression is decreased in zebrafish with age (Anchelin *et al.*, 2011; Carneiro, Castro and Ferreira, 2016). Further, when telomerase was mutated and non-functional in zebrafish, it caused earlier telomere attrition and as a result, earlier senescence accumulation and ageing phenotypes (Henriques *et al.*, 2013).

As well as the fact that many of the senescence-regulating pathways are common to zebrafish, senescent cells themselves have been described and are associated with ageing in this model organism. For example, the senescence marker SA-β-Galactosidase showed higher activity in aged zebrafish (Kishi *et al.*, 2003). Additionally, young zebrafish harbouring Lamin A (*LMNA)* mutations, which are known to cause human progeria, increased the expression of *p21* and SA-β-Gal (Koshimizu *et al.*, 2011). Random mutation of the zebrafish genome via retrovirus-insertion identified mutants that caused earlier senescence accumulation and ageing phenotypes (Kishi *et al.*, 2008). One of these mutants harboured a mutation in the homologue of the human telomeric repeat binding factor 2 (terf2) gene, known to regulate telomere length. Senescence plays a protective role against cancer in mammals and mutations in the

senescence pathway, particularly P53 and $P16^{INK4A}$ are known to induce tumour sensitivity (Jacks *et al.*, 1994; Serrano *et al.*, 1996). Similarly, zebrafish homozygous mutants for tp53 show increased tumorigenesis (Berghmans *et al.*, 2005). These mutants were unable to up-regulate p21; suggesting senescence is protective against immortalisation in zebrafish as is seen in humans. Additionally, a CRISPR against the zebrafish P16 orthologue was able to induce oncogenesis in zebrafish (Ablain *et al.*, 2018). With age zebrafish show declining ability to regenerate tissues (Anchelin *et al.*, 2011; Münzel *et al.*, 2014). In mammals this has been partially attributed to senescence-like phenotypes in immune and stem cell populations, so it may be that this is also contributing to the phenotype seen in aged zebrafish (Deng *et al.*, 2004; Molofsky *et al.*, 2006; Czesnikiewicz-Guzik *et al.*, 2008; Beerman *et al.*, 2010; Solana *et al.*, 2012; Fali *et al.*, 2018).

At the behavioural level, many of age-associated changes that are improved by senescence-removal in (Knights *et al.*, 2006)mammals are also demonstrated in zebrafish. For example, zebrafish show spine curvature and muscle wastage and reduced swimming ability with age, indicating a loss in structure and function of the musculoskeletal system (Gerhard *et al.*, 2002; Gilbert, Zerulla and Tierney, 2013). Sarcopenia is delayed in mice with genetically ablated senescence and preliminary evidence in humans suggests that senolytics can improve motor function in humans (Baker *et al.,* 2006; Justice *et al.,* 2019). The skeletal architecture in the spines of old zebrafish resembles osteoarthritic disease, the pathology of which can be improved in mice by the senolytic ABT-263 (Hayes *et al.*, 2013; Jeon *et al.*, 2017). Further, signs of cognitive decline correlate with age in wild-type zebrafish, measured by their ability to remember positive and negative cues associated with food and electric shock (Yu *et al.*, 2006). Irradiated zebrafish show earlier reductions in cognition. This is a common inducer of senescence in mammals, and removal of senescent cells was able to improve cognition in a mouse model of Alzheimer's Disease (Oanh N L Le *et al.*, 2010a; Demaria *et al.*, 2014; Bussian *et al.*, 2018). These together indicate that many vital hallmarks of senescence are conserved in zebrafish, making it a viable model organism for studying this age-associated phenotype. However, currently there is not a well-characterised assay for senescence induction in young zebrafish that would make them amenable to drug screening, nor a means to prospectively isolate senescent cells from a mixed population *in vivo.* Both of these are important for utilising zebrafish as a model organism to tackle current gaps in the senescence field.

1.8. Thesis aims

Senescence accumulation is a major driver associated with multiple age-associated pathologies in humans. The current therapies being developed, though promising, are not yet able to focus on systemic senolytic treatment to tackle multi-morbidity directly. Further understanding on the mechanisms underlying senescent cell accumulation and how they can directly cause disease, as well as tools to screen senolytics in the context of systemic treatment, would provide a more effective means to identify therapeutic targets to treat multiple age-associated pathologies at once.

I hypothesised that by irradiating zebrafish larvae, senescence accumulation could occur ectopically in a comparable manner to that which is described in mammalian systems. Further, that the stress-induced senescence seen in response to irradiation in zebrafish larvae shares features with human ageing-induced senescence, thereby allowing the unique advantages of the zebrafish to be used in this context. The thesis aims are:

- To optimise and characterise a method for ectopic induction of senescence in zebrafish larvae without causing significant off-target toxicities.
- To develop a novel transgenic reporter that can identify senescent cells in live zebrafish larvae.
- To investigate whether irradiated zebrafish larvae have phenotypes that are comparable with an aged context.

2 Materials and Methods

2.1. Reagents.

All reagents were purchased from Sigma (Poole, UK) unless stated otherwise

2.2 Zebrafish work

2.2.1 Husbandry

Zebrafish are housed in accordance to the UK Home Office Licence animal care protocols in the Bateson Centre at The University of Sheffield, UK under standard conditions (Nüsslein-Volhard, C. and Dahm, 2002). Adults reside in a 28°C closed aquarium system with 14 hours of light per day. Zebrafish between 5 and 13dpf were fed Tetra A-Z powdered fish food twice daily, whilst older fish were fed live artemia. Zebrafish were bred using either the marbling technique, or by individually pairing males and females. The former involves 10-40 adults laying eggs into marbles on top of a grid whereby the eggs will filter through for collection. Pairing involved placing a male and female adult fish into a small mating tank after feeding, separated by a divider. As the light cycle starts the following morning, the divider is removed and eggs are filtered through a plastic grid and collected within a few hours before returning adults to their respective tanks. This technique was used when it was necessary to be able to identify the parents that gave rise to the embryos, particularly for genotyping purposes. Collected embryos were sorted into petri dishes at a density of 30-60 embryos per dish and incubated in approximately 25-35mls of E3 media at 28°C. Experiments were performed up until 5.2dpf, before they became protected animals by The Animals (Scientific Procedures) Act 1986 set by the Home Office, where they were sacrificed through immersion in 0.017% 3-amino benzoic acid ethyl ester (tricaine) and either fixed for experimentation in 4% paraformaldehyde or immersed in bleach. When experiments were carried out on 12dpf larvae, all procedures were approved by the Home Office in the appropriate Project License (PPL: 70/8178) by a trained individual with an up-to-date personal license (163486AFC), and performed in compliance with animal welfare laws and guidelines. At the end of these experiments, animals were sacrificed by a schedule 1-approved method, which usually involved submersion in anaesthesia (1.33g/l 3-amino benzoic acid ethyl ester, MS222) and a secondary method of confirming rigor mortis.

2.2.2 Anaesthesia

Whenever zebrafish embryos were anaesthetised, 168mg/l of MS222 (Sigma, MO, USA) was added to a plate of up to 60 embryos, in approximately 25mls 1X E3. Adult zebrafish were anaesthetised by submerging them in a 4.2% MS322 solution, made up with aquarium system water. After experimentation, zebrafish were allowed to recover was completed through replacing medium with fresh E3 medium (for larvae) or aquarium system water (for adults) that did not contain tricaine.

2.2.3 Irradiation

To induce senescence, up to 200 zebrafish were removed from their chorions at 2 days post-fertilisation (dpf) using forceps prior to irradiation. The zebrafish were placed without anaesthetic in 10mls E3 media in a 25ml universal tube. An unirradiated control was always used and zebrafish were assigned randomly across irradiated and unirradiated groups. All fish would be moved into one petri dish and up to 20 fish would be assigned to one group then another 20 would be assigned to another, this process would be repeated until all fish were assigned to their respective groups. Zebrafish would be transported in universal tubes encased in gel packs heated to 28°C. Zebrafish are placed in a closed Cesium-137 source to receive the required dose of radiation. To be confident that our zebrafish larvae receive the expected dose of irradiation, we calculated the amount of time required to expose the correct dose of radiation, taking into account the age, half-life and radioactive decay of our source (Figure 2.1A). Further, dose mapping was carried out by Ashland (USA) to determine the actual dose that different areas of the canister received, to ensure the fish were located in the correct region (Figure 2.1B). A radiation-sensitive film was placed in the middle of the canister, between two water-equivalent phantoms. These films are then sent to the USA alongside an unirradiated film to remove any radiation incurred from the transport itself, the amount of light that flows through the film before and after radiation is measured to determine dose absorbed. The zebrafish placed in the centre of the canister to ensure the dose received is as expected, as depicted by the white regions on the dose mapping. After irradiation, zebrafish were returned to petri dishes at a maximum density of 60 zebrafish per dish in E3 media. These fish were returned to a 28°C incubator until assessment for the onset of senescence. Zebrafish were assessed for senescence at 5dpf (Figure 2.2.).

A

Cs^{137} Activity (30 year half-life)	Cs^{137} Dose calculations	
	From the date below	**Increase time by**
1Gy per 21s on 31/08/2000	1/09/2015	1.4141
	1/09/2016	1.4472
	1/09/2017	1.4810
	1/09/2018	1.5156

B

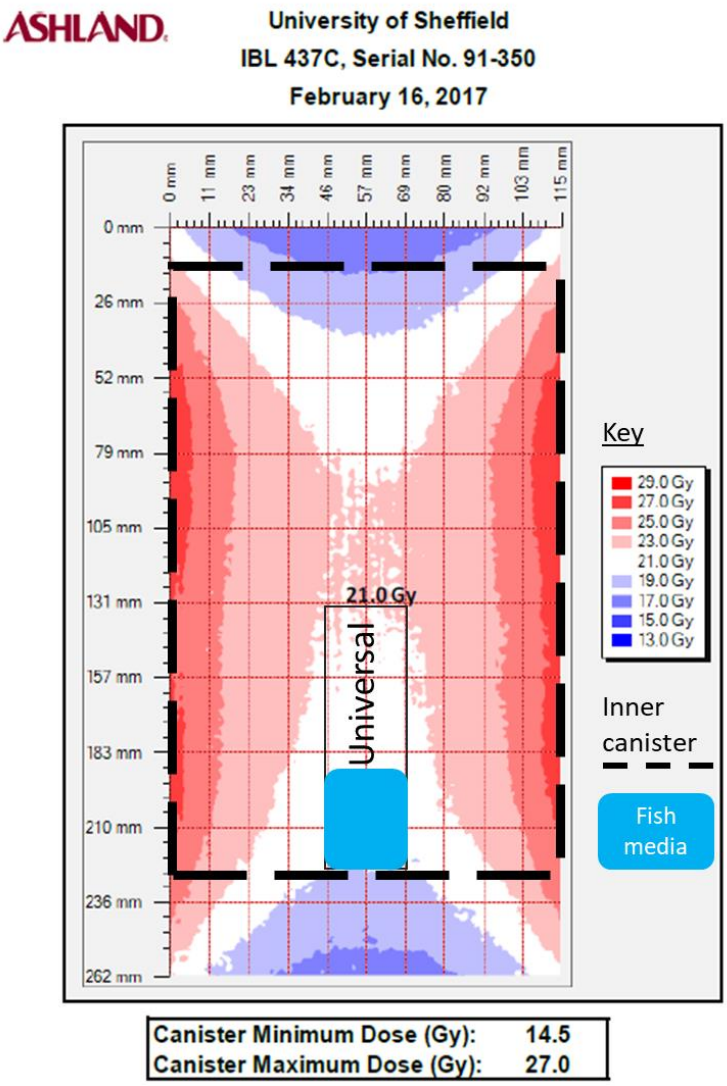

Figure 2.1. Irradiation dose calculations. A) Calcuations for determining the timings required for applying a dose of radiation from a Cs^{137} source, taking into account radioactive decay B) Dose mapping by Ashalnd (USA) describing actual dose received within the cannister following 21Gy of radiation. Fish are placed in the middle of the bottom of the inner canister to ensure dose received matches dose applied.

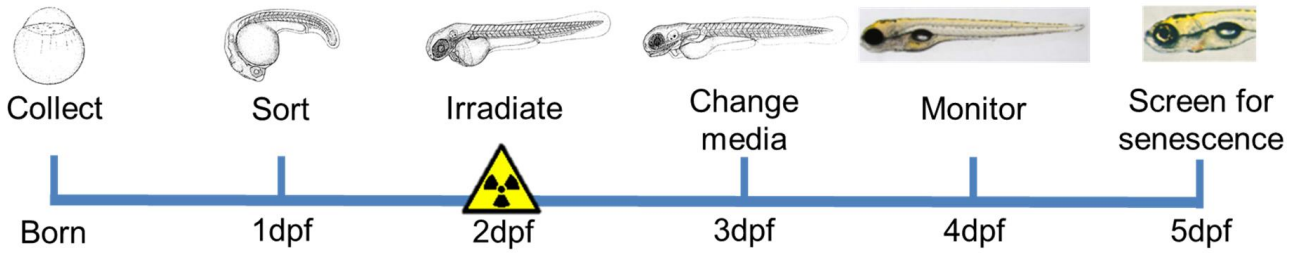

Figure 2.2. Diagram depicting the optimised timing of irradiation assay. Zebrafish are irradiated with 12Gy Cs^{137} closed source γ-irradiation at 2dpf, and senescence was assessed at 5dpf. Images of zebrafish stages adapted from ZFIN.

2.2.4 Assessment of irradiation-induced toxicity in zebrafish

To determine an effective dose of irradiation that did not induce off-target toxicities, zebrafish were examined for common signs of oxidative stress (Figure 2.3). Examples include pericardial oedema (Figure 2.3A), undeveloped or deflated swim bladder (Figure 2.3B), spine curvature, obviously stunted growth, or blue skin from the methylene blue in the E3, indicative of cell death (Davies *et al.*, 1980). Zebrafish with any of these signs of toxicity would be sacrificed through immersion in 0.017% 3-amino benzoic acid ethyl ester (tricaine) and immersed in bleach before 5.2dpf.

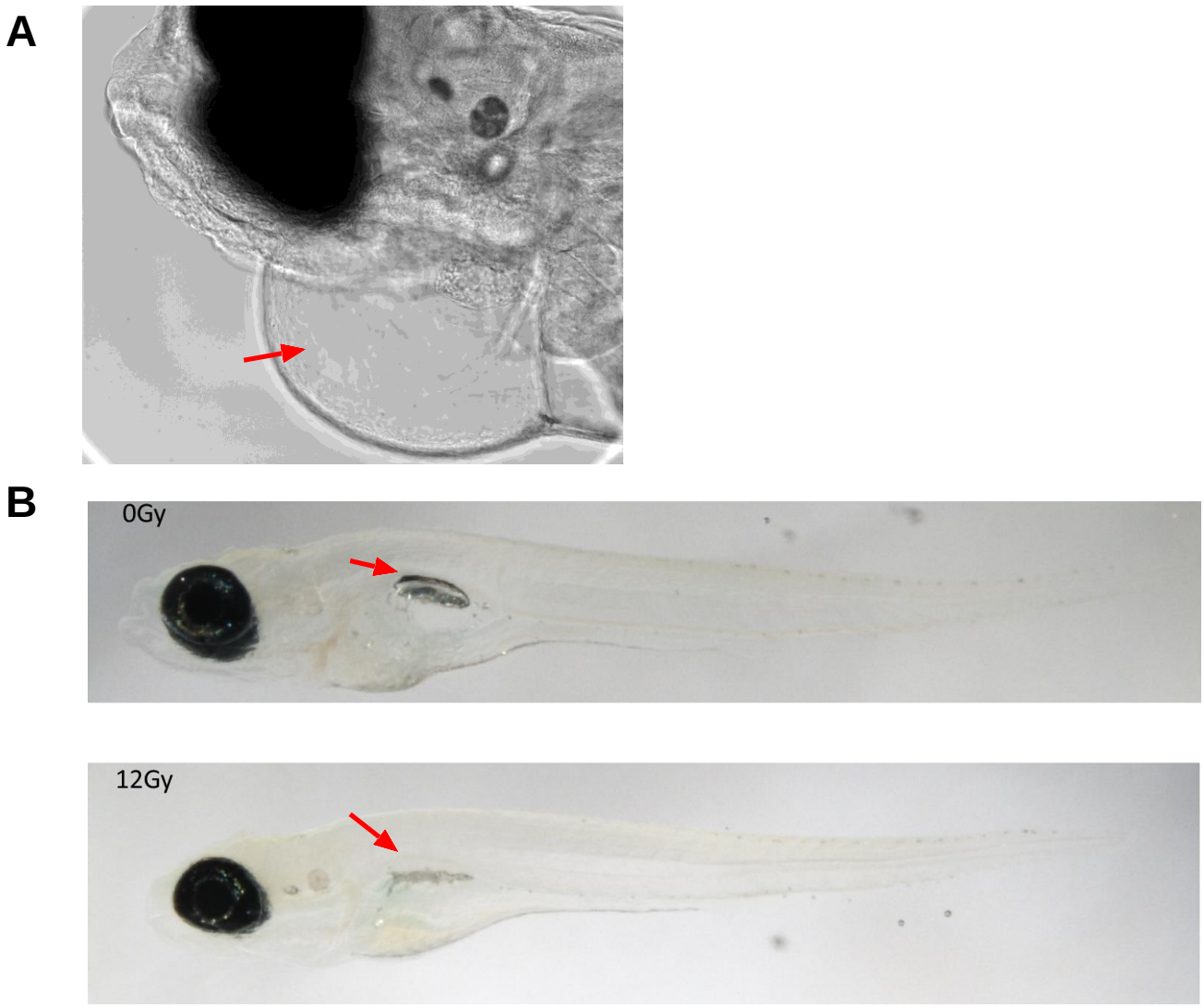

Figure 2.3. Example images of signs of irradiation-induced toxicity. Representative transmitted light photomicrographs of fish with signs of toxicity and as such removed from later analyses (10%, Figure 3.2.). A) Pericardial oedema B) Deflated swim bladder following 12Gy irraidation, with unirradiated zebrafish for comparison. Areas of oedema and swim bladder depicted with arrows.

2.2.5. Fixation

When fish reached the required stage of development for assessment of senescence markers by whole-mount *in situ* hybridisation, immunofluorescence, or the senescence-associated β-Galactosidase (SA-β-Gal) assay, they were fixed in 4% paraformaldehyde (PFA) overnight at 4°C. For *in situ* hybridisation, zebrafish were washed in PBS and dehydrated in a Methanol (MeOH) series of increasing concentration, until reaching 100% and being stored for at least 24 hours prior to use at -20°C. For SA-β-Gal and immunofluorescence experiments, the assay was carried out immediately after fixation.

2.2.6. Movement analysis

At 4, 5, and 12 days post-fertilisation (dpf), locomotor activity was recorded using the Zebrabox (ViewPoint Life Sciences, Lyon, France) tracking system and Zebralab software. The distance moved over a 30 minute period was recorded after zebrafish were transferred to a 24-well plate, one larvae per well in 1ml of E3 medium and acclimatised for 30-60 minutes (Figure 2.4.). Light and dark cycles of 5 minutes at 100% light and 5 minutes at 0% light were used to stimulate movement of the fish. The tracking was always carried out at the same time of day, between 2 and 4 hours of the changing of incubator light cycle where the zebrafish are stored.

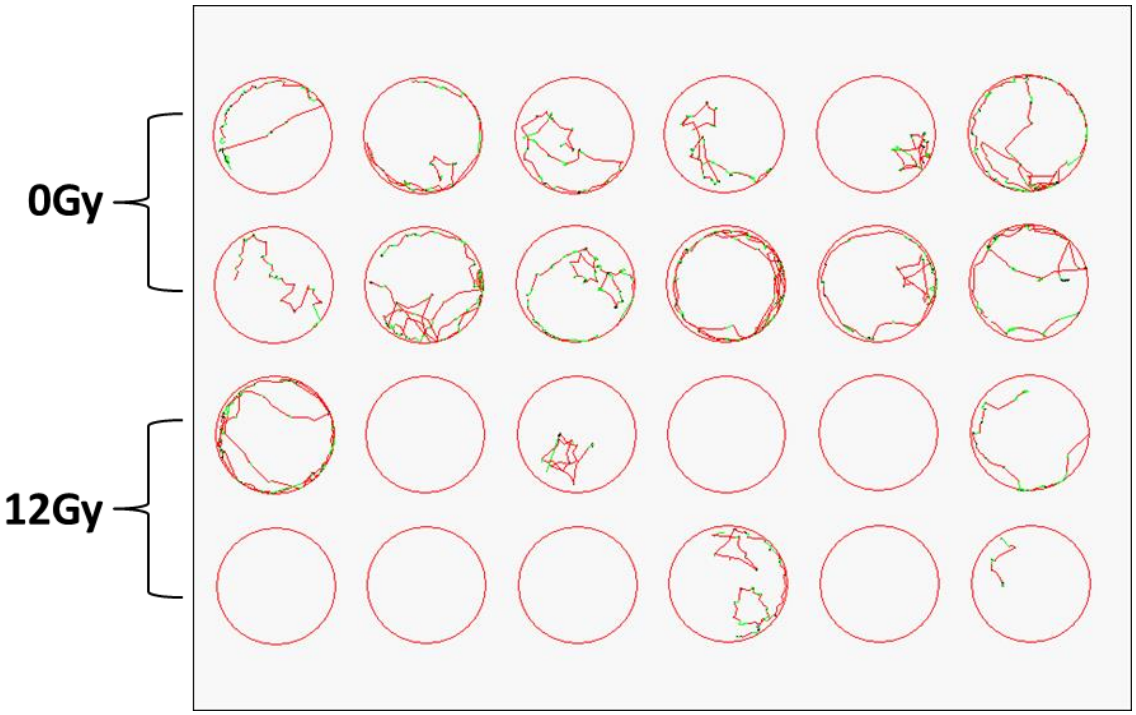

Figure 2.4. Example tracking of locomotor activity. Zebrafish are placed on a 24-well plate, acclimitised for 30-60 mintes, and their movement recorded. Red tracks depict slower movement and green tracks depict fast movement (further than 3 lengths of the fish, 12mm at 5dpf within a second). This is example tracks over a 30 second period. Data was quantified over a 30 minute period.

2.3. Molecular biology

2.3.1. Visualising & quantifying DNA & RNA:

The ApE plasmid editor (Biology Labs Utah, 2013) was used to plan and visualise DNA plasmids, targeting constructs, primer sequences, and sequencing data. DNA & RNA were quantified using agarose gel electrophoresis. Next, 1% agarose (Bioline Reagents Ltd, London, United Kingdom) was dissolved in 1x TAE buffer and heated until the agarose is in solution. Ethidium Bromide was added to the gel (0.8µg/ml, ThermoFisher Scientific Inc., USA) and once set, the sample was loaded with 6x loading buffer (NEB, Ipswich, USA), alongside a 1kbp normalised DNA hyperladder (Bioline Reagents Ltd, United Kingdom) for reference and quantification.

2.3.2. Heat-shock Transformation

Competent E.coli cells (ThermoFisher Scientific Inc., USA) were defrosted on ice alongside SOC media (Sigma, MO, USA) & DNA (100ng). DNA was added to cells and incubated on ice for 30 minutes, before being added to a 42°C water bath for 30 seconds, and returned to ice for 2 minutes. 200µl SOC media was added to cells and placed on a 37°C rocker for 90 minutes, and then cultured overnight at 37°C on dry, pre-warmed agar plates containing appropriate antibiotic at 50µg/ml.

2.3.3. Plasmid DNA purification

Following transformation, DNA was purified using a plasmid DNA Midiprep Kit (Qiagen, Venlo, Netherlands). Bacteria were grown at 37°C in LB containing appropriate antibiotics before 4°C centrifugation at 6,000g for 15 minutes pelleted the bacteria containing plasmid DNA, where they can then be stored at -20°C. The bacterial pellet was thawed when required and re-suspended in 6mls of Buffer P1 containing RNase A and Lyse Blue. 6mls of Buffer P2 was then added before 6 vigorous inversions and 5 minutes incubation. 6mls of chilled Buffer P3 are added to the suspension, mixed, and immediately transported to a QIA filter cartridge for 10 minutes. 4mls Buffer QBT was added to the HiSpeed Midi tip and the column emptied by gravity flow. A plunger was gently inserted to the QIA filter to transfer the solution into the equilibrated HiSpeed Midi tip. 20mls of Buffer QC was added to the HiSpeed Midi tip, and the DNA eluted by addition of 5mls Buffer QF. 3.5mls of room temperature isopropanol (Sigma, MO, USA) precipitate the elute and incubated for 5 minutes. DNA was then transferred into reaction vials, and centrifuged at 13,000rpm at 4°C for 30 minutes. DNA pellets were washed with 200µl 70% RNase-free EtOH (Fisher Scientific UK, Loughborough, UK) and again centrifuged at 13,000rpm at 4°C for 10 minutes. The pellets were air dried, and resuspended in 1ml DEPC water, before being stored at -20°C until required. Plasmid DNA Miniprep purification kits (Qiagen, Netherlands) were also used to purify smaller plasmid volumes (1-5mls) as required.

BACs were purified through a Nucleobond pc100 midiprep kit (Machery-Nagel, Düren, Deutschland) as per manufacturer's instructions. BAC-containing bacteria are centrifuged 6,000g at 4°C for 15 minutes before removing supernatant and adding 8mls pre-chilled Buffer S1 containing RNAse. 8mls Buffer S2 was added and mixed through gentle inversion, before 8mls pre-chilled Buffer S3 was added and mixed through inversion. Buffer N2 was added to a Nucleobond AX100 column before the bacterial lysate is filtered through into the column. The column was washed with 12mls Buffer N3, before the DNA was eluted with 5mls of preheated (50°C) buffer N5 and precipitated with 3.5mls

room temperature isopropanol (Sigma, USA). Precipitate DNA is added to reaction vials and centrifuged at 15,000g, 4°C for 15 minutes and supernatant discarded. A total of 2mls 70% EtOH (Fisher Scientific UK, UK) is split between reaction vials, before mixing by vortex and centrifugation at 15,000g, room temperature for 10 minutes. Supernatant is removed, and the DNA pellet dried for 10 minutes, before being dissolved in 10% TE buffer before quantification. The protocol was modified to improve the yield by splitting the precipitated DNA in fewer reaction vials and carrying out successive 4°C centrifugations at 15,000g for 15 minutes, and adding DNA to the same two reaction vials. Additionally, dissolving the DNA pellet overnight, rather than the 20 minutes suggested, at 4°C in 10% TE buffer improved the yield. DNA concentration was determined by a Nanodrop™ spectrophotometer (ND1000, Thermo-Scientific, Hemel Hempstead, UK).

2.3.4. PCR purification & Gel extraction

For DNA products <4kbp in size, a PCR purification kit (Qiagen, Netherlands) was used as per manufacturer's instructions. Five volumes of buffer PB was added to the solution and placed into a pre-chilled QIAquick MinElute® column. The sample is centrifuged for 60 seconds, 13,000rpm at room temperature and the supernatant removed. This was repeated where the PCR & buffer PB solution had a greater volume than 750µl. Buffer PE (750µl) was added to the column and centrifuged for 60 seconds, 13,000rpm at room temperature. A repeat centrifugation 60 seconds, 13,000rpm at room temperature was carried out to remove residual buffer, and then the column was placed into a reaction vial. The DNA was eluted with 10µl of buffer EB and a repeat centrifugation, before being quantified through agarose gel electrophoresis. For DNA products larger than 4kbp, a QIAquick column was instead used and the DNA eluted in 30-50µl. Alternatively, when a DNA product of a known size required purification, it was first visualised in a low-level UV lamp and excised using a MinElute® Gel Extraction kit (Qiagen, Netherlands) according to manufacturer's instructions. Once excised, the gel fragment is weighed and 3 volumes of Buffer QG added, before being incubated at 50°C for 10 minutes, or until the gel had completely dissolved. One volume of room temperature Isopropanol (Sigma, USA) was added and the sample placed in a pre-chilled MinElute® spin column, before 60 seconds centrifugation, 13,000rpm, at room temperature. This centrifugation was repeated where the dissolved agarose gel & buffer QG solution had a greater volume than 750µl. Buffer QG (500µl) was added and centrifugation repeated, then 750µl buffer PE was added and centrifugation repeated again. The column is centrifuged again to remove residual buffers, and the column placed in a reaction vial. Buffer EB (10µl) was added to the column membrane, and centrifugation was repeated, before quantification by agarose gel electrophoresis.

2.3.5. Restriction digests

Each digestion was incubated for at least 2 hours at 37°C. All restriction enzymes used were obtained from New England Biolabs (NEB, Ipswich, USA), and the relevant digestion buffer was chosen according to their instructions.

2.3.6. Ligation

Ligations of two DNA constructs were carried out using T4 DNA ligase at 16°C overnight. The amount of vector and insert used was calculated using the following equation:

$$V + I = 100ng$$

$$I = \frac{3(100 - I) \times size\ insert\ bp}{size\ vector\ bp}$$

Ligated DNA was then transformed using the aforementioned protocol, and between six and ten bacterial colonies were grown up in 5mls Lysogeny Broth (LB) and purified using the plasmid purification MiniPrep kit (Qiagen, Netherlands). Restriction digests were used to confirm whether the ligation was successful.

2.3.7. Developing specialised targeting constructs for BAC cloning

Once a plasmid of interest was purified, a test PCR would be carried out to ascertain the optimised conditions for the specific reaction. Once optimised, a 300µl PCR was carried out using Q5 polymerase (NEB, USA) with specially designed primers (Integrated DNA Technologies, Iowa, USA). 5µl of dpn1 (NEB, USA) was then added and incubated at 37°C for an hour. The product was purified with a PCR purification kit (Qiagen, Netherlands), and then added to a 1% agarose gel for electrophoresis, before the correct size DNA fragment is extracted through the Gel Extraction kit (Qiagen, Netherlands). The product was then quantified and stored in -20°C until required.

2.3.8. Tol2 RNA development

To make tol2 transposase RNA, 20µg of a tol2-containing plasmid was linearised with 1µl of Not1 restriction enzyme (NEB, USA) for 2 hours at 37°C in a 200µl reaction volume. The linearised DNA was then purified using a PCR purification kit (Qiagen, Netherlands) and quantified using gel electrophoresis. 1µg of linearised DNA was used in a mMessage mMachine transcription reaction kit (ThermoFisher Scientific Inc., USA) to make RNA according to manufacturer's instructions. The linearised DNA was incubated at 37°C for 2 hours with the SP6 polymerase in a final volume of 20µl before 1µl of Turbo DNase is added and incubated for a further 15 minutes at 37°C. The resulting RNA was phenol:chloroform extracted, first 115µl dH_2O and 15µl Ammonium Acetate Stop Solution was added, then an equal volume of phenol:chloroform (Sigma, USA) was added and the solution vortexed for 3 minutes, and centrifuged at 4°C for 7 minutes, 13,000rpm. The top aqueous layer that resulted was transferred into a new reaction vial, and equal volume of chloroform (Sigma, USA) added before vortexing for 1 minute and centrifuged at 4°C for 5 minutes, 13,000rpm. The resulting aqueous layer was again transferred to a new reaction vial, and equal volume of room temperature isopropanol was added (Sigma, USA). The solution was chilled at -20°C for 15 minutes, before being centrifuged at 4°C for 15 minutes, 13,000rpm. Supernatant was removed and the pellet washed in 500µl 70% EtOH

and centrifuged twice further at 4°C for 10 minutes each, 13,000rpm. The supernatant was again removed and resuspended in 20µls dH_2O, before a sample was quantified by gel electrophoresis and the rest stored in -80°C until required.

2.3.9. RNA extraction

Zebrafish embryos were homogenised by addition of Trizol reagent (Sigma, USA) and mixing with a pellet pestle on ice. Samples were added into a QIAshredder shredder column (Qiagen, Netherlands) to further homogenise the tissue, before centrifugation at 13,000rpm for two minutes a room temperature. The RNA is then purified through addition of 100µl chloroform (Sigma, USA), vortexing for 3 minutes, and centrifuging at 13,000rpm for 5 minutes. The aqueous phase was transferred into a new reaction vial and 250µl of isopropanol (Sigma, USA) was then added before vortexing again and incubating at room temperature for 10 minutes. The sample was then centrifuged at 4°C for 15 minutes and then the pellet is washed with 70% EtOH, resuspended in H_2O, and quantified by a Nanodrop™ spectrophotometer (ND1000, Thermo Scientific, Hemel Hempstead, UK) and stored in -80°C until required.

2.3.10. cDNA synthesis

cDNA was made from purified 2µg zebrafish RNA using First-Strand cDNA Synthesis using SuperScript™ II Reverse Transcription kit (Invitrogen, UK) as per manufacturer's instructions. RNA was added to a reaction vial alongside 1µl OligoDT (500µg/ml), 1µl nucleotide mix (10mM each nucleotide), and made up to 12µl with dH_2O. The mixture was heated to 65°C for 5 minutes and quick chilled on ice before adding 4µl 5X First-Strand Buffer, and 2µl 0.1M DTT. The solutions was mixed and incubated at 42°C for 2 minutes, before 1µl of SuperScript™ II Reverse Transcriptase (200 units) was added and incubated at 42°C for 50 minutes. The reaction was inactivated by heating to 70°C for 15 minutes.

2.4 Whole-mount In situ Hybridisation (WISH)

2.4.1 Probe development

WISH antisense RNA probe for *p21* was synthesised from linearised plasmid DNA made from a plasmid vector containing the *p21* coding sequence, provided by David Whitmore (University College London) (Laranjeiro *et al.*, 2013). 2µg of linearised DNA was used to transcribe RNA with the T7/SP6 DIG RNA labelling kit in a final volume of 20µl, the list of reagents are described in table 2.1 and were incubated for 2 hours at 37°C (Sigma, USA). Either SP6 or T7 polymerase was used to make the RNA according to the orientation of the gene of interest in the plasmid. Following the reaction, 4µl of DNase was added and incubated for 20 minutes at 37°C, before precipitation with 1µl EDTA 0.5M pH 8, 2.5µl LiCl 4M, and 75µl 100% EtOH, the solution was then incubated at -80°C for up to 24 hours. The precipitate was centrifuged at 4°C, 14,000rpm, for 30 minutes. The pellet was then washed in 70% EtOH and centrifuged at 4°C, 13,000rpm, 10 minutes, before being air dried for 10 minutes. The RNA was then resuspended in 20µl sterile water, and quantitated on an agarose gel. Finally, 80µl formamide was added and the probes were stored immediately at -80°C until required.

Reagent	Volume (µl)
Linearised DNA	2µg
Transcription buffer	2µl
NTP-DIG-RNA labelling mix	2µl
RNAse inhibitor	1µl
SP6 or T7 Polymerase	1µl
dH2O	13µl

Table 2.1. List of reagents used for transcription reactions

To make DIG-labelled RNA probes for whole mount zebrafish *in situ* hybridisations for *p16-like,* where no plasmid was available; a PCR on cDNA made from RNA extracted from homogenized zebrafish embryos with primers for the gene of interest was carried out (Figure 2.5.). This was then purified through gel extraction (Qiagen, Netherlands), and ligated into an pCR-Blunt ii- TOPO vector (ThermoFisher Scientific Inc., USA), before being transformed into competent cells and grown overnight at 37°C on agar containing appropriate antibiotic. Between 6 and 10 bacterial colonies that resulted would then be grown up in 5mls of LB with antibiotic for purification using the plasmid purification MiniPrep kit (Qiagen, Netherlands), the elutes were then sent for sequencing to confirm whether the ligation worked and contained the TOPO vector with *p16-like*, as well as the orientation of the gene (Figure 2.6A). The sequence was aligned against the known *p16-like* mRNA sequence and confirmed 100% sequence identity (Figure 2.6B). Once the correct bacterial colonies were identified, a larger plasmid purification using a Midiprep kit (Qiagen, Netherlands) was carried out. 20µg of purified plasmid was then used for linearisation with the appropriate restriction enzyme at 37°C for 2 hours in a final volume of 200µl. Equal volume of phenol:chloroform was added and the mixture vortexed for 3 minutes, before centrifugation at 14,000rpm for 7 minutes. The aqueous layer is transferred to a new tube, and an equal volume of chloroform was then added. The mixture was then vortexed for 1 minute, and centrifuged at 14,000rpm for 5 minutes. Again the aqueous layer was transferred into a new reaction vial, before precipitating the linearised plasmid with 10% Na acetate 3M, and 1 volume isopropanol at -20°C for up to 24 hours. The solution was then centrifuged at 14,000rpm at 4°C for 20 minutes, the supernatant removed and the pellet washed with 70% EtOH. Room temperature centrifugation at 5 minutes was repeated to re-pellet the linearised DNA, before air drying for 10 minutes, and resuspending in 20µl dH_2O. Quantification through gel electrophoresis confirmed both concentration of linearised DNA and that the restriction enzyme reaction was carried out to completion. The linearised DNA was then used to make a DIG-labelled mRNA probe as described above (Figure 2.6C).

A

B

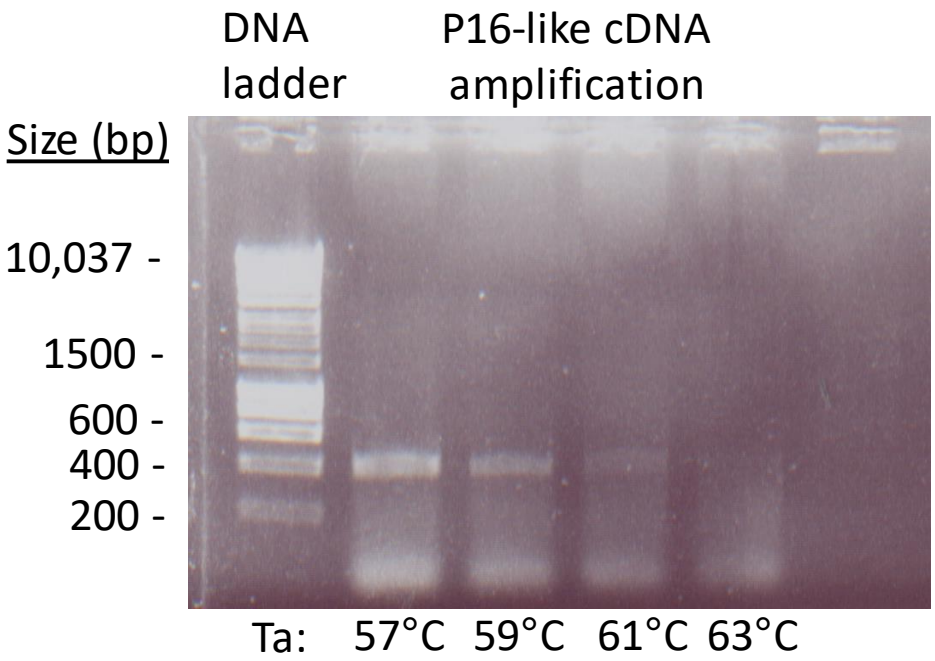

Figure 2.5. Cloning of *p16-like*. A) ApE map of whole p16-like zebrafish mRNA (uppercase letters). Forward (purple) and reverse (green) primers described where PCR amplification took place. B) Optimisation of PCR annealing temperature to extract p16-like sequence from whole zebrafish cDNA with size of 400bp.

A

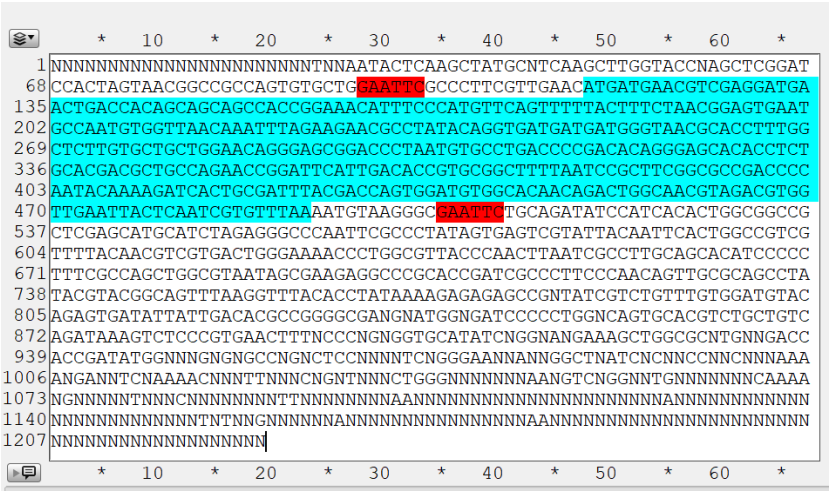
95 EcoRI (2)
EcoR1 digestion site
p16-like zeroblunt-Topo-M13R
1225 bp
p16-like cDNA sequence
504 EcoRI (2)
EcoR1 digestion site

B

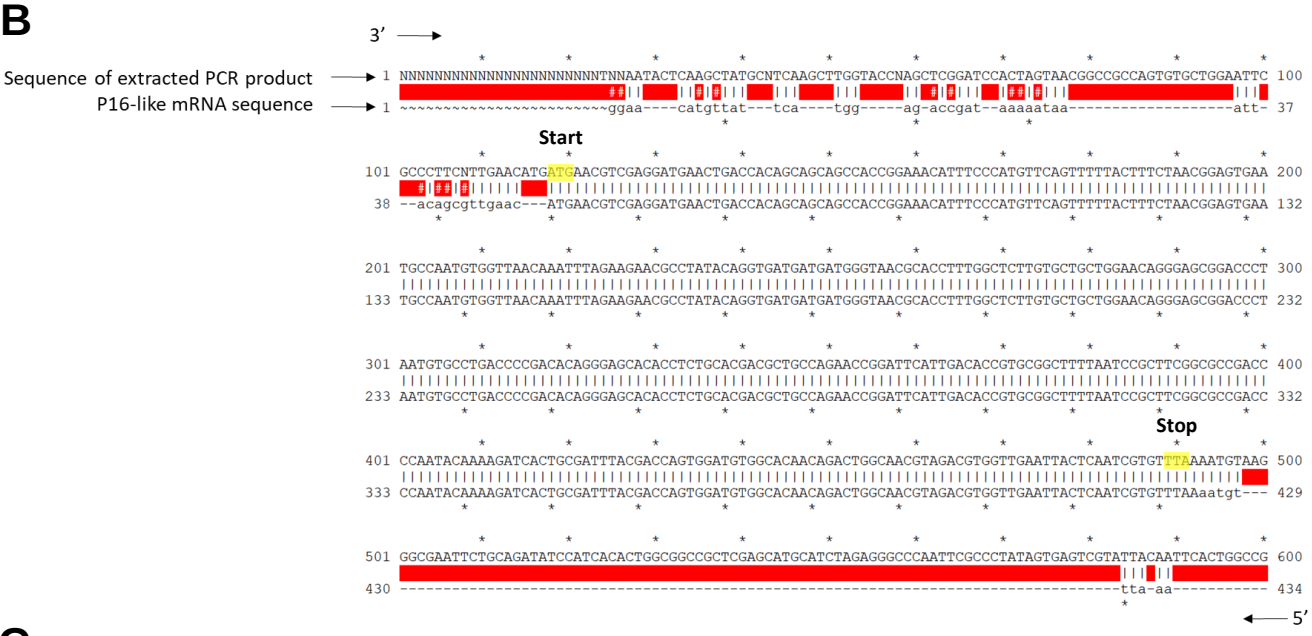
3'
Sequence of extracted PCR product
P16-like mRNA sequence
Start
Stop
5'

C

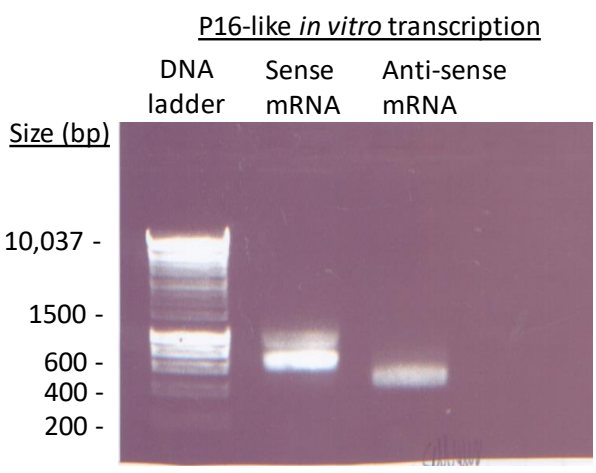
P16-like *in vitro* transcription
DNA ladder
Sense mRNA
Anti-sense mRNA
Size (bp)
10,037 -
1500 -
600 -
400 -
200 -

Figure 2.6. Development of *p16-like* DIG-labelled mRNA probe for *in situ* hybridisation. A) ApE map of sequencing for *p16-like* cDNA that was ligated into pCR-Blunt ii- TOPO vector, with EcoR1 restriction sites highlighted to make linearised DNA for *in sit* probe synthesis. B) Sequence alignment of PCR product ligated into pCR-Blunt II-TOPO against known p16 mRNA sequence. C) Visualisation of DIG-labelled mRNA probes for *p16-like* by gel electrophoresis.

2.4.2 Whole-mount *In situ* hybridisation (WISH) protocol

WISH was carried out to determine spatial expression of *p21* and *p16-like* mRNA following irradiation. Fixed and dehydrated zebrafish were rehydrated through a series of 5-minute washes in decreasing concentrations of MeOH, made up in PBS, before 4 further 5 minute washes in 100% PBT (PBS plus tween 20) (Sigma-Aldrich, UK). The fish were then digested in Proteinase K, where the length of incubation and concentration used required optimisation. Following optimisation, 10µg/µl for 75 minutes at 22°C (room temperature) was used for 5dpf larvae. Embryos were then fixed in 4% PFA-PBS for 20 minutes at room temperature and then washed 5 times for 5 minutes in PBT. The embryos were incubated in preheated 1ml PreHyb for 2-5hours at 70°C, before incubating in preheated ProbeHyb overnight at 70°C. The following day, the ProbeHyb was removed and embryos washed briefly in pre-heated HybWash, before washing in a series of 4 HybWash:2XSSC dilutions for 15 minutes each at 70°C. The embryos were then washed in 2X SSC for 15 minutes, and twice in 0.2X SSC for 30 minutes at 70°C. Then they were returned to room temperature and incubated in a series of 0.2X SSC: PBT dilutions for 10 minutes until incubating in PBT alone for a further 10 minutes. The embryos are then incubated in Blocking Solution at room temperature for several hours, and then incubated in a 1:5000 dilution of the anti-DIG-AP antibody (Roche, UK) overnight at 4°C. The following day, the embryos were washed for 15 minutes in PBT 6 times at room temperature and transferred to a 24-well plate. The zebrafish were then washed in Staining Wash 3 times for 5 minutes, and then the staining solution is added, containing BCIP (175µg/ml) and NBT (225µg/ml). Once the satisfactory amount of staining had developed, the staining solution is removed and stop solution added (PBS, 1mM EDTA) for 5 minutes, before washing in 4% PFA for 30 minutes at room temperature. The embryos were then placed through a MeOH series and stored in 100% MeOH overnight. The embryos can be stored at -20°C until required, where they then are placed through a reverse methanol series containing increasing concentrations of glycerol. Imaging was performed by placing larvae in 80-100% glycerol solution on a glass cover slip (Scientific Laboratory Supplies, UK) and orientating them with a human hair. Transmitted light imaging was performed using a Nikon SMZ1500 stereomicroscope with a Prior Z-drive and a Nikon DS-Fi1 colour camera with NIS elements software (Version 4.3). For quantitation, colorimetric analysis was chosen by selection of the zebrafish head, excluding the eye and extending as far as the otic vesicle. Blink ranking was carried out by randomly assigning codes to images from irradiated and non-irradiated groups, before ordering them by eye according to staining intensity whereby the strongest staining had the highest rank. The code was then used to determine which group each image and rank

corresponded to and then data were examined by a Kruskal-Wallice (for *p21,* 3 groups examined) or Mann-Whitney test of ranks (for *p16-like*, 2 groups examined).

2.5. Quantitative Polymerase Chain Reaction (qPCR)

To assess quantitative changes in mRNA expression of senescence-associated genes, quantitative PCRs were carried out. RNA extraction and cDNA synthesis were carried out as described above (2.3.9, 2.3.10). Quantitative PCR (qPCR) was performed using MESA GREEN qPCR MasterMix Plus for SYBR® (Eurogentec, UK) and an ABI 7900HT Sequence Detection System (Applied Biosystems, CA, USA). qPCRs were carried out in triplicate for each cDNA sample and mRNA expression was normalised to βactin, which acted as a reference gene. Reaction vials, dH2O, pipettes, pipette tips were all UV-treated for 20-40 minutes prior to use, and surfaces cleaned with RNAseZAP® (Sigma-Aldrich, UK) to prevent nuclease contamination. Wells containing only water, and wells containing cDNA made from reactions without the reverse transcriptase were used to confirm there were no sources of contamination. Quantification was carried out by relative mRNA expression (2^-ΔCt, relative to βactin) or fold expression change following irradiation (2^-ΔΔCt, relative to βactin and unirradiated control) (Livak and Schmittgen, 2001). Reactions are described in Table 2.2, primer sequences are listed in Table 2.3.

Reagent	**Volume per reaction (µl)**
MESA GREEN qPCR MasterMix Plus for SYBR®	5
10µM forward primer	0.2
10µM reverse primer	0.2
dH2O	2.6
cDNA (diluted 1:10)	2
Total:	**10**

Table 2.2. List of reagents used for qPCR reactions

Gene	Sequence
β*actin*	Forward – 5’ TTCACCACCACAGCCGAAAGA 3’
	Reverse – 5’ TACCGCAAGATTCCATACCCA 3’
P21 (cdkn1a)	Forward – 5’ AGGAAAAGCAGCAGAAACG 3’
	Reverse – 5’ TGTTGGTCTGTTTGCGCTT 3’
P16-like (cdkn2a/b)	Forward - 5’ ATGATGAACGTCGAGGATGAACTG 3’
	Reverse – 5’ ATTGGCATTCACTCCGTTAGAAAGT 3’
Il1b	Forward – 5’ TGGACTTCGCAGCACAAAATG 3’
	Reverse – 5’ GTTCACTCCACGCTCTTGGATG 3’
Il6	Forward – 5’ GCTCATCCAGCAGGGTCCG 3’
	Reverse – 5’ CGACACACACTGTTTGGCCTTG 3’
Il8a	Forward – 5’ GAAAGCCGACGCATTGGAAA 3’
	Reverse – 5’ TTAACCCATGGAGCAGAGGG 3’
Mmp2	Forward – 5’ AGCTTTGACGATGACCGCAAATGG 3’
	Reverse – 5’ GCCAATGGCTTGTCTGTTGGTTCT 3’
Mmp9	Forward – 5’ AACCACCGCAGACTATGACAAGGA 3’
	Reverse – 5’ GTGCAAGGCTATCCCAAGAGT 3’
Mmp13	Forward – 5’ ATGGTGCAAGGCTATCCCAAGAGT 3’
	Reverse – 5’ GCCTGTTGTTGGAGCCAAACTCAA 3’
Cyclin-g1	Forward – 5’ GTGATGAAGATTCAGCCCAAGC 3’
	Reverse – 5’ CACTGGCCAGAGGGACATTTTTCT 3’
P53	Forward – 5’ GCTTGTCACAGGGGTCATTT 3’
	Reverse – 5’ ACAAAGGTCCCAGTGGAGTG 3’

Table 2.3. Table of primer sequences used for qPCR reactions

2.6. Senescence-associated β-Galactosidase (SA-β-Gal) assay

After overnight fixation in 4% paraformaldehyde (PFA) in PBS, larvae were washed 3 times for 1 hour in PBS (pH 7.0). Larvae were then washed for 1 hour in PBS (pH 6.0) at 4°C. The enzymatic reaction was then performed overnight at 37°C in 5mM potassium ferrocyanide, 2mM $MgCl_2$, and 1 mg/ml X-gal in PBS (pH 6.0). Afterwards, zebrafish were washed 3 times in PBS (pH 7.0) and fixed in 4% PFA for 4 hours. Zebrafish were washed 3 times in PBS (pH 7.0) and prepared for imaging by placed through a series of washes containing increasing concentrations of glycerol. Imaging was performed by placing larvae in 80% glycerol solution on a glass cover slip (Scientific Laboratory Supplies, UK) and orientating them with a human hair. Transmitted light imaging was performed using a Nikon SMZ1500 stereomicroscope with a Prior Z-drive and a Nikon DS-Fi1 colour camera with NIS elements software (Version 4.3). For quantitation, colorimetric analysis was chosen by selection of the zebrafish head, excluding the eye and extending as far as the otic vesicle. Blink ranking was carried out by randomly assigning codes to images from irradiated and non-irradiated groups, before ordering them by eye according to staining intensity whereby the strongest staining had the highest rank. The code was then used to determine which group each image and rank corresponded to and then data were examined by a Mann-Whitney test of ranks.

2.7. Bacterial Artificial Chromosome (BAC) transgenesis

Firstly, a pipeline for the development of TgBAC(*p21:GFP*) was established (Figure 2.7) (Suster *et al.,* 2011). A BACs was to be identified that encompassed the *cdkn1a* zebrafish locus (p21) (Table 2.4.). Once identified, the BACs were cloned into competent cells with the appropriate antibiotic resistance (Lee *et al.*, 2001) (Table 2.5.). A plasmid containing the gene sequence for GFP was identified, and a restriction digest was carried out on the identified BACs and a plasmid containing the GFP-encoding sequence, such that the GFP sequence could then be ligated into the BAC directly after the start codon of the p21 coding sequence. Primers were designed such that the first 50 base pairs overlapped with the BAC, the last 3 bases being the ATG (p21 start codon), followed by 24 more bases that overlap with the target sequence (Table 2.6.). This should result in a plasmid that expresses GFP under p21 promoter activation, but the p21 coding-sequence itself is disrupted, such that endogenous levels of p21 are not affected in zebrafish with BAC insertion into their genome. As the BAC is a large plasmid, and therefore prone to breakage and partial insertions (Suster *et al.*, 2011), a tol2-transposon mediated system to improve transgenesis efficiency was incorporated. This involves modifying the GFP-BAC plasmid such with tol2-recognition sites that the tol2 transposase can recognise and insert randomly into the zebrafish genome as a whole. Finally, the modified plasmids were injected into single-cell stage nacre-strain zebrafish embryos, and screened prior to independent feeding for GFP expression. The next generation of GFP-positive fish were assessed using the established irradiation assay for germline-transmission of the plasmid and irradiation-induced fluorescence up-regulation that matches p21-mRNA expression spatially predominantly in the head and intestinal regions.

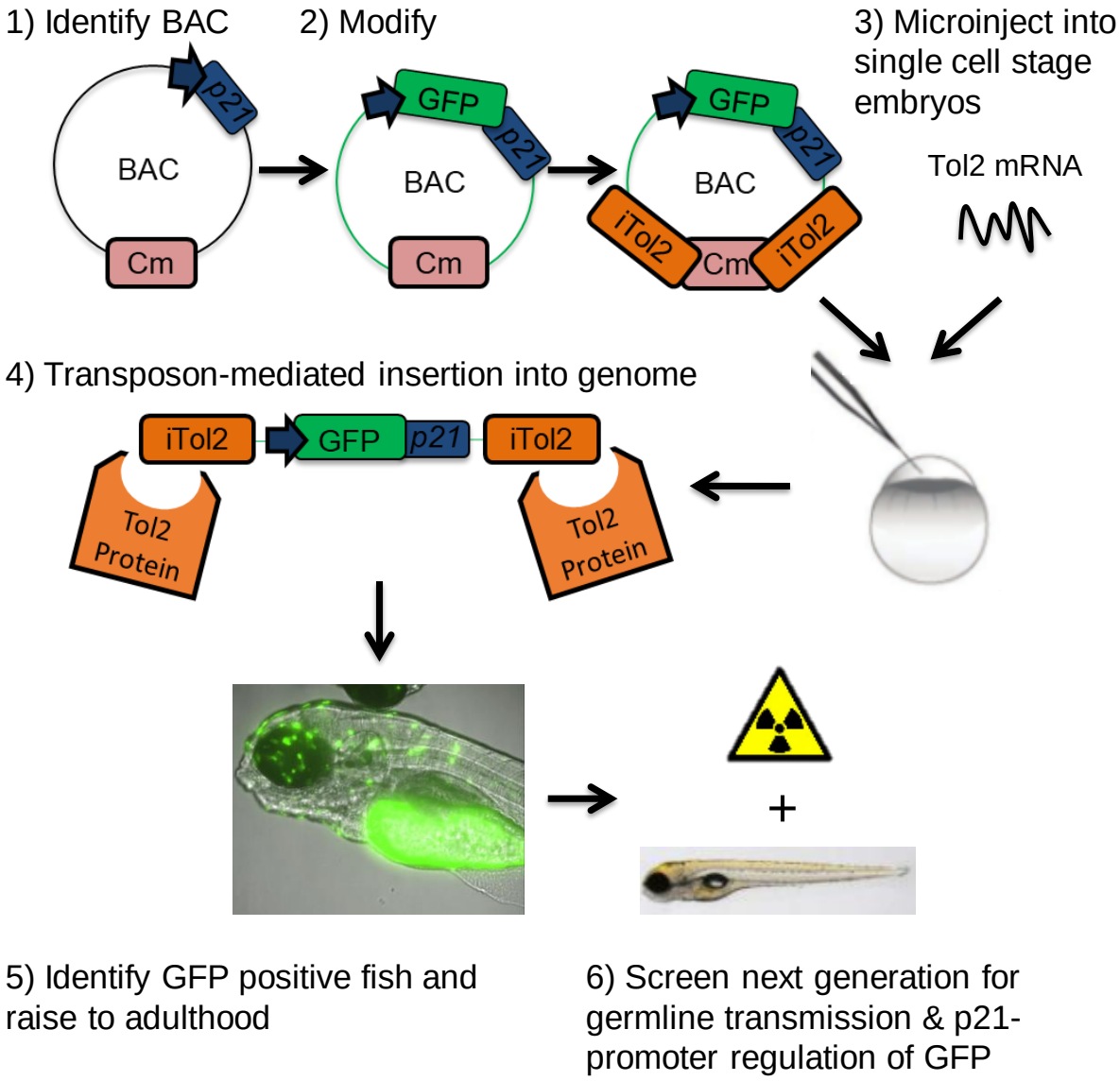

Figure 2.7. Schematic diagram depicting the development of TgBAC(p21:GFP) using Bacterial Artificial Chromosome (BAC) transgenesis. The BAC chosen (DKEY192-O24) included the zebrafish p21 gene sequence and surrounding promoter regions. The GFP sequence was targeting into the BAC and inserted after the first p21 start codon. Once created, the BAC was injected alongside tol2 mRNA in single-cell stage zebrafish embryos. Tol2 is a transposase that aids in incorporation of the BAC into the genome, through the addition of tol2 recognition sites onto the BAC itself. The injected embryos were then screened for fluorescence at 5dpf. Once adults, their progeny were examined for p21-regulated fluorescence to determine successful incorporation of the BAC into the germline, creating the stable transgenic reporter zebrafish. Image of single cell-stage embryo and 5dpf non-fluorescent zebrafish larvae adapted from ZFIN.

2.7.1 Making electro-competent EL250 cells

A stock of EL250 bacteria (gift of Dr Neal Copeland, National Cancer Institute) was incubated overnight in 2mls LB at 32°C. 1ml was then transferred into a fresh 50ml LB culture and incubated at 32°C until the Jenway 6100 spectrophotometer determined optimal density, with Abs at 0.5 (600nm, OD_{600}). The bacteria were then centrifuged at 3,000rpm for 15 minutes at 4°C, before removing the supernatant and resuspended in 50mls ice-cold dH_2O. Centrifugation was repeated and the bacteria re-suspended in 5mls ice-cold dH_2O. The bacteria were then split into 5 reaction vials and washed 3 further times in ice-cold dH_2O in a 4°C microfuge at 13.3krpm, for 20 seconds per wash. 100µl of dH_2O was used to re-suspend the pellet in each reaction vial, and then further split into 50µl aliquots for electroporation. The bacteria were electroporated (25µF, 1.3kv, 200Ω) and 12% Glycerin was added before the competent cells were stored at -80°C until required.

2.7.2 BAC electroporation into EL250s

Purified BACs (100ng) were added to a 40µl aliquot of electrically competent EL250s and then placed on ice for 60 seconds. The EL250s were added to a cuvette (Bio-Rad, California, USA) before being electroporated (25µF, 1.3kv, 200Ω). 1ml SOC media (Sigma, USA) was added, and the cells were incubated on a shaker at 32°C for 90 minutes, before being added to agar plates with Chloramphenicol (12.5µg/µl) and incubated overnight at 32°C.

2.7.3 Targeting BACs in EL250s with GFP targeting sequence

BAC-containing EL250 bacterial colonies were picked from the agar plate and added to 1ml of liquid broth (LB) with antibiotic (12.5µg/µl Chloramphenicol, Cm) at 32°C overnight. 0.4ml of culture was then added to 20mls LB Cm in a baffled flask at 32°C until the spectrophotometer determined optimum density at Abs0.5 (600nm). Half of the culture was transferred into a pre-heated conical flask and incubated in a shaking 42°C water bath for 15 minutes. The flask was then transferred to a shaking ice slurry bath for 20 minutes at 4°C. From this point, everything was carried out at 4°C, the culture was transferred to reaction vials and centrifuged at 13,000rpm, the supernatant was removed and the bacterial pellet washed in ice-cold dH_2O. The pellet was centrifuged again at 13,000rpm and resuspended in dH_2O such that all pellets were pooled into one reaction vial, before another centrifugation at 13,000rpm. The target construct (300ng) was added to the cells with a final volume of 50µl made up with ice-cold dH_2O. The cells were then electroporated at 1.8kV, shaken at 32°C for 90 minutes in 1ml LB containing no antibiotics, and then added to agar plates with antibiotics. To confirm whether targeting was successful, at least 6 bacterial colonies were spread out onto three agar plates with low-dose Kanamycin, Carbenacillin, or Chloramphenicol present. Successful targeting will result in Kanamycin resistance as the targeting sequence contained a resistance sequence, whilst also being chloramphenicol resistant with resistance coming from the BAC itself. The bacteria should also be Carbenacillin sensitive, bacteria resistant to this antibiotic indicates there is plasmid contamination, as the plasmids used to develop the targeting constructs contain a resistance sequence that was outside the targeting construct region. The kanamycin resistance was removed from BACs through treatment with L-arabinose (Santa Cruz Biotechnology, Texas, USA). EL250s were grown until the spectrophotometer confirmed bacterial density at Abs0.5. Then the cells were incubated in 0.1% L-arabinose for an hour at 32°C. The cells were then grown up in LB without antibiotics for an hour at 32°C and then overnight on agar plates containing antibiotics. To confirmation that arabinose treatment worked, the resulting

bacterial colonies are again spread out onto three further agar plates containing Kanamycin, Carbenacillin, and Chloramphenicol respectively. In this case, the EL250s should become sensitive to Kanamycin once more.

2.7.4 Injecting BACs into 1-cell stage zebrafish embryos

Purified BAC containing the GFP and tol2 targeting sequences were purified by the Nucleobond PC100 kit (Machery-Nagel, Deutschland) as per manufacturers instructions and quantified. PhenolRed (Sigma, USA), Tol2 RNA (25-30ng/µl), and the purified BAC (50ng/µl) were made up to 5µl in dH_2O. Injections were performed using glass capillary needles (Kwik-FilTM Borosilicate Glass Capillaries, World Precision Instruments (WPI), Herts, UK), made using a Flaming Brown micropipette puller (Sutter Instrument Co., Novato, USA). A Pneumatic PicoPump PV 820 was used to inject approximately 2-4nl, determined by a graticule, of the BAC solution into single-cell stage zebrafish embryos. A control group was injected with a BAC solution not containing tol2 RNA, to assess whether the transposase RNA is functional. Following microinjection, embryos were transferred to E3 media and left to recover at 28°C.

2.7.5. Development of transgenic line *TgBAC(p21:GFP)sh506*

Following 1-cell stage injection of zebrafish embryos, larvae were selected for GFP fluorescence at 4dpf when endogenous expression has been described (Laranjeiro *et al.,* 2013). Those positive for GFP and showed no signs of toxicity were raised to adulthood. As adults, the zebrafish were crossed to wild-type adult zebrafish and these offspring were assessed for GFP fluorescence with and without irradiation and their pattern of expression compared to known *p21* mRNA expression as determined by WISH. Two adults were identified as able to pass on fluorescence to their offspring in a pattern that resembled *p21* mRNA expression were deemed founders for the *TgBAC(p21:GFP)sh506* and *TgBAC(p21:GFP)sh507*. Expression from both alleles were identical by eye, but because the founder for *TgBAC(p21:GFP)sh506* had higher fecundity, subsequent experiments and the next generation used this allele alone.

2.7.6. Imaging *TgBAC(p21:GFP)sh506* larvae

TgBAC(p21:GFP)sh506 were mounted at 4 or 5dpf in 1% low melting point agarose solution (Sigma-Aldrich) containing 4.2% 3-amino benzoic acid ethyl ester. Larvae were then transferred to an Eclipse TE2000-U inverted compound fluorescence microscope with 10x NA objective lens to acquire images using an andor zyla 5 camera (Nikon). Zebrafish were excited with a 488nm laser and GFP fluorescence detected by a GFP-specific filter. Maximum intensity projections were generated by NIS elements and mean fluorescence intensity of regions of interest were quantified by FIJI (ImageJ2).

Name	Description	Reference
DKEY-192O24	pIndigo BAC-536 vector containing zebrafish p21 gene sequence	ZFIN, 2019
DKEY-254C20	pIndigo BAC-536 vector containing zebrafish p21 gene sequence	ZFIN, 2019
CH211-228E15	pTARBAC2.1 cloning vector containing zebrafish p21 gene sequence	Children's Hospital Oakland Research Institute (2016). [Online] Available from: http://bacpac.chori.org/zebrafish211.htm [Accessed 28/07/16]
K11	Plasmid containing GFP & kanamycin resistance sequence flanked by FRT sites	Generated by Dr. Stone Elworthy, The University of Sheffield
Itol2kan	Plasmid containing inverted tol2 recognition sequences and a kanamycin resistance sequence, used to make eye marker targeting sequence	Generated by Renshaw lab, The University of Sheffield

Table 2.4. List of reagents used for BAC transgenesis

Antibiotic	Working concentration
Carbenicillin (Carb)	50µg/ml
Kanamycin (Kan)	50µg/ml OR 10mg/L
Chloramphenicol (Cm)	12.5µg/ml

Table 2.5. List of antibiotics used for BAC transgenesis

Name	Primer sequences
GFP targeting construct	Forward 5'ATATTTAATGTGATTTTTACTGTGGTTTGTGTTTGXAGAATTACCGCCATGGTGAGCAAGG GCGAGCTGTTC 3'
	Reverse 5'GCCTAGTCGGCCCATTACCGAGTGAACGTAGGATCCGCTTGTGCGCCGCGATATCTGCAG AATTCGCCCTTGA 3'
Tol2 targeting construct	Forward 5' AAGCTTAAGTGATCTCCAAAAAATAA 3'
	Reverse 5' GAATTCAATACTCAAGTACAATTTTA 3'

Table 2.6. Primer sequences used to insert GFP and itol2 targeting sequences into BACs

2.8. Whole-mount immunofluorescence for γH2AX

To assess the amount of DNA damage response activation seen following irradiation of zebrafish larvae, whole-mount immunofluorescence for γH2AX was carried out. Fixation of larvae <5.2dpf was carried out as described above, using 4% paraformaldehyde (PFA) in PBS overnight at 4°C. After fixation, embryos were washed 3 times in PBS (1ml total volume, with a maximum of 20 fish per reaction vial). Zebrafish were then transferred to glass reaction vials and incubated with Acetone for 7 minutes at -20°C. Fish were then washed twice with PBS-T (PBS, 0.1% Tween-20, Sigma-Aldrich, UK). Zebrafish were blocked for 60 minutes in PBST with 2% blocking reagent (Roche, UK), 5% foetal calf serum (Sigma-Aldrich, UK) and 1% DMSO (Sigma-Aldrich, UK). Zebrafish were then incubated with Histone H2A.XS139ph (phospho Ser139) antibody (Genetex, CA, USA, 1:1000 dilution in blocking solution) and then washed 4 times for 15 minutes each in PBS-T before being incubated with Alexa Fluor 568 goat anti-rabbit (Invitrogen, UK, 1:500 dilution in blocking solution) for two hours at room temperature in the dark. From now on, all reaction vials are wrapped in foil to limit light exposure. Zebrafish are washed 4 times for 15 minutes each in PBS-T before adding DAPI (Sigma-Aldrich, UK, 1:2000 dilution in PBS) for 15 minutes at room temperature. Larvae were washed once more with PBS and liquid was aspirated before the fish were mounted with Vectashield (Vector laboratories, UK). The UltraVIEWVoX spinning disc confocal laser imaging system (Perkin Elmer) was used to image the tails or heads of these fish, using 1µM z-stacks with the Prior 200µm z-piezo. Fluorescence for DAPI was acquired using an excitation wavelength of 405nm and emission was detected with a DAPI emission filter. Fluorescence for γH2AX was acquired using an excitation wavelength of 561nm and emission was detected with a TxRed emission filter. Images were analysed on Volocity™ software (version 6.3) to determine number of cells positive for γH2AX. Multiple analysis techniques were utilized, either by counting number of cells with 5 or more foci, or counting the number of very positive (bright red) cells, or by determining mean fluorescence intensity on FIJI (ImageJ2), through drawing a region of interest around nuclei and determining mean fluorescence intensity of each region. At least 300 cells were quantified for each technique.

2.9. Flow Cytometry of *TgBAC(p21:GFP)sh506*

2.9.1. Dissociation of zebrafish larvae

Zebrafish are sacrificed by immersion in 1.33g/l 3-amino benzoic acid ethyl ester (in E3 media) and up to 100 are placed on the lid of an ice-cold petri dish. Excess E3 media is removed and zebrafish are chopped up finely with a scalpel blade before being recovered in 1-3mls PBS, depending how many fish were pooled (approximately 1ml PBS per 30 larvae was used). Liberase TL (Roche, UK) is added to reaction vials containing zebrafish at 40µg/ml and incubated at 37°C for 35 minutes. Every 10 minutes during this incubation, zebrafish are disturbed by mixing to prevent clumping, no visible features of the zebrafish remain after this period. The reaction is stopped by addition of Fetal Bovine Serum (FBS) (Sigma-Aldrich, UK) to a final concentration of 10% and the suspension is filtered through a 40µm filter. The suspension is then centrifuged at 1,500rpm for 5 minutes, before cells are re-suspended in media for flow cytometry (L15 media, 20% FBS, 5mM EDTA).

2.9.2. Flow cytometry of live cells from dissociated zebrafish larvae

To assess *TgBAC(p21:GFP)sh506* suspensions following dissociation, cells were incubated with 7-Aminoactinomycin D (7AAD, ThermoFisher Scientific Inc., USA) at a concentration of 5µl per million cells for 5 minutes before being examined by a LSRII (BD) flow cytometer (BD Biosciences, San Jose, CA, USA). Gating was used to ensure only live cells were assessed. Debris was removed from analysis by gating out regions that were too small to be cells and were present in a control sample of live cell media alone. Secondly, a gate was used to remove non-spherical objects, which were usually clumped cells, by removing objects that did not have a 1:1 ratio of forward scatter height to area. The viability dye 7AAD allowed removal of dead cells from later analyses; it was excited by a 488 laser and detected by a 695/40nm filter. A 7AAD negative sample determined the amount of fluorescence required for a cell to be deemed live or dead in this system. The same was then carried out for GFP fluorescence, using both irradiated and unirradiated wild-type siblings to remove any background fluorescence from analysis. GFP fluorescence was excited by a 488 laser and detected by a 530/30nm filter. Though the detectors used for both fluorophores are spectrally separate, assessment for compensation was carried out because the same laser was exciting them. Detection of 7AAD and GFP fluorescence were plotted together and showed no overlapping signal the detectors. Data were analysed using FlowJo software (TreeStar).

2.10. Immunofluorescence of sorted cells for γH2AX, PCNA and IL6

A strategy was devised to be able to assess multiple markers of senescence in individual cells from *TgBAC(p21:GFP)sh506* (Figure 2.8).

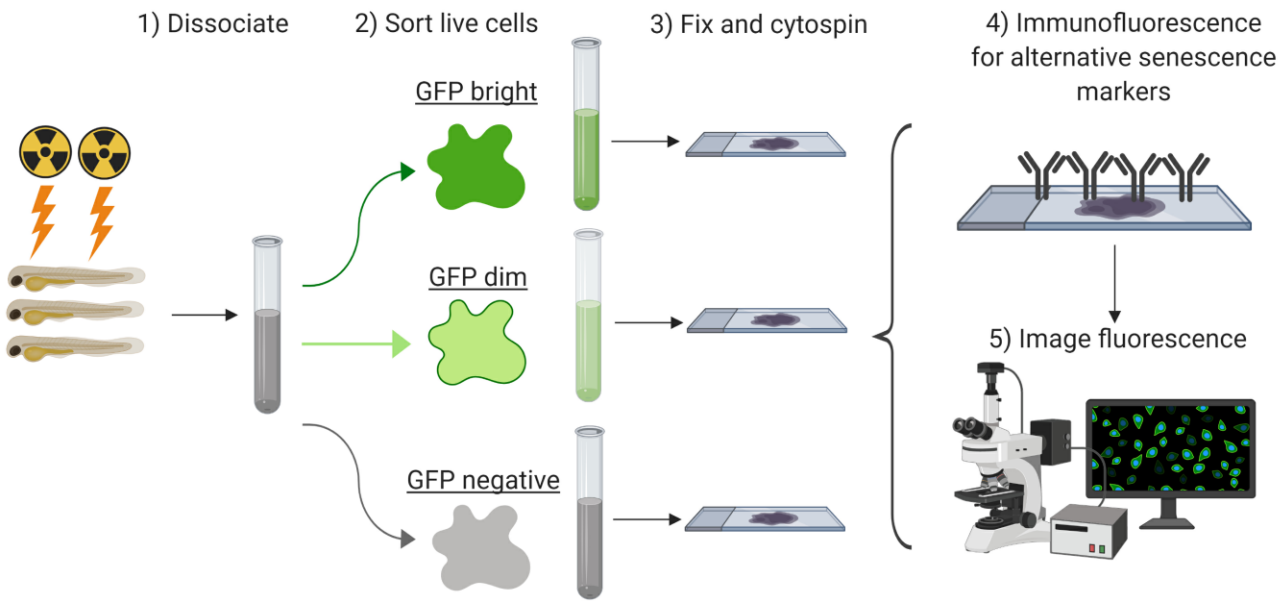

Figure 2.8. Diagram depicting workflow to determine proportion of GFP positive cells from *TgBAC(p21:GFP)sh506* that are positive for multiple senescence markers in the same cell. Zebrafish were irradiated at 2 days post fertilisation (dpf) before being dissociated into cell suspension at 5dpf. The suspension was then gated such that only live cells were sorted according to GFP intensity. GFP negative populations were defined as cells with a GFP intensity seen in wild-type zebrafish, GFP dim populations were defined as cells with a GFP intensity above what was seen in wild-type fish and the maximum intensity seen in unirradiated TgBAC(p21:GFP)sh506 zebrafish. GFP bright populations were defined as those with an intensity that is only seen in irradiated TgBAC(p21:GFP)sh506 zebrafish. Cells were fixed and cytospun onto microscope slides, before immunofluorescence was carried out to assess protein expression of pγH2AX, IL6 and PCNA in the sorted populations. Diagram created with BioRender.com.

2.10.1 Fluorescence Activated Cell Sorting

To sort cells of differing GFP intensities, *TgBAC(p21:GFP)sh506* zebrafish were dissociated as described above. Cells were incubated with 7-Aminoactinomycin D (7AAD, ThermoFisher Scientific Inc., USA) at a concentration of 5µl per million cells for 5 minutes before being examined by a FACSAria IIu flow cytometer (BD Biosciences, San Jose, CA, USA). The gating strategy described above was used and cells were sorted at 4°C using the slowest flow rate and largest nozzle available to minimise further stressing the cells. GFP negative populations were defined as cells with a GFP intensity seen in wild-type zebrafish, GFP dim populations were defined as cells with a GFP intensity above wild-type fish and the maximum intensity seen in unirradiated *TgBAC(p21:GFP)sh506* zebrafish. GFP bright populations were defined as those with an intensity that is only seen in irradiated *TgBAC(p21:GFP)sh506* zebrafish. Between 50,000 (GFP bright) and 500,000 (GFP dim and negative) cells would be sorted per group from pools of up to 100 fish. Post-sort efficiency was determined by placing sorted cells back through the FACSAria IIu flow cytometer and examining the proportion of cells that were specific to their originally sorted group, GFP negative, GFP dim or GFP bright.

2.10.2. Fixing and cytospinning of sorted cells onto microscope slides

Sorted cell populations from *TgBAC(p21:GFP)sh506* were kept on ice and centrifuged at 4000rpm (4°C) and washed with 1ml ice-cold PBS. Cells were centrifuged (4000rpm, 4°C) and fixed with 500µl 4% paraformaldehyde (PDA) for 20 minutes on ice. Cells were centrifuged (4000rpm, 4°C), PFA was removed and cells were washed with 1ml PBS, before another centrifugation (4000rpm, 4°C) and resuspension in 200µl PBS for cytospinning onto microscope slides. Cytospin receptacles were assembled and the suspension of fixed cells were added to the cytospin slide centrifuge (Cytospin 3, Shandon Southern Instruments, Inc, Sewickley, PA, USA). Cells were centrifuged at 500rpm for 5 minutes with medium acceleration onto SuperFrost Ultra Plus™ adhesion slides (ThermoFisher Scientific Inc., USA) before being dried face up in the dark overnight at room temperature (22°C).

2.10.3. Immunofluorescence of sorted cells

Following overnight drying, cytospun cells from *TgBAC(p21:GFP)sh506* were then permeabilised with 0.5% Triton X-100 (Sigma-Aldrich) in PBS for 10 minutes at room temperature. The area around cells on the slide were defined with a hydrophobic pen (ThermoFisher Scientific Inc., USA) and then blocked for 1-2 hours at room temperature (PBS with 3% Bovine Serum Albumin, 5% Goat Serum, 0.3% Tween-20). Adhesion slides were then incubated with primary antibodies overnight in the dark at 4°C in a humid incubating chamber. Combination of antibodies against Proliferating Cell Nuclear Antigen (PCNA, Santa Cruz, CA, USA, 1:200 dilution) and Histone H2A.XS139ph (phospho Ser139) antibody (Genetex, CA, USA, 1:300 dilution) or Proliferating Cell Nuclear Antigen (PCNA, Santa Cruz, CA, USA, 1:200 dilution) and Interleukin 6 (Abcam, MA, USA, 1 in 500 dilution) or Green Fluorescent Protein (GFP, Sigma-Aldrich, UK, 1:500

dilution) were used. The next day, antibodies were washed 3 times for 10 minutes each at room temperature in 0.1% Tween-20 (Sigma-Aldrich, UK) in PBS. A hydrophobic pen was used to re-define area of cells on the adhesion slides, before overnight incubation in secondary antibodies were carried out at 4°C. Combinations of antibodies against Alexa Fluor 488 goat anti-chicken (Abcam, MA, USA, 1 in 500 dilution), Alexa Fluor 568 goat anti-rabbit (Invitrogen, UK, 1:500 dilution) and Alexa Fluor 647 goat anti-mouse (Invitrogen, UK, 1:500 dilution) were used. The next day, antibodies were washed 3 times for 10 minutes each at room temperature in 0.1% Tween-20 (Sigma-Aldrich, UK) in PBS, before being stained with DAPI (Sigma-Aldrich, UK, 1:2000 dilution in PBS) for 10 minutes at room temperature. Slides were then washed with PBS for 10 minutes and then mounted in Vectashield (Vector laboratories, UK) and sealed with a 22x22mm No. 0 coverslip (Scientific Laboratory Supplies, UK) using nail varnish. Slides were imaged on a Deltavision microscope using an UplanSApo 40x oil objective (NA 1.3) and Photometrics CoolsnapHQ CCD camera. Z stacks were imaged at 1µm and deconvolution software was used for the γH2AX staining to make the foci more visible. Excitation by a 100W Hg lamp was used. DAPI fluorescence was detected by a 360/457nm filter, GFP was detected by a 490/528nm filter, γH2AX and IL6 fluorescence was detected by a 555/617nm filter, PCNA fluorescence was detected by a 640/700nm filter. Quantification was carried out with maximum intensity projections of 15 z-stacks (15µm thickness). Negative control slides without primary antibody incubation was used to determine background fluorescence and settings were determined by using an example image from each group, before all other images are given an automatic and random code for quantification. Cells positive for γH2AX were deemed to have 5 or more foci in a single nucleus (stained with DAPI), cells positive for IL6 had clear red fluorescence in the regions around the nucleus, whilst cells positive for PCNA had clear nuclear staining. At least 300 cells were quantified per group.

2.11. Solutions

ISH solutions

- PreHyb: 50% formamide, 5X SSC, 0.1% Tween 20, Citric acid to pH6, 50ug/ml heparin, 500ug/ml tRNA
- ProbeHyb: 50% formamide, 5X SSC, 0.1% Tween 20, Citric acid to pH6, 50ug/ml heparin, 500ug/ml tRNA, 1:200 dilution of probe in formamide
- WashHyb: 50% formamide, 5X SSC, 0.1% Tween 20, Citric acid to pH6
- 20X SSC: 35.06g NaCl, 17.64g NaCitrate, pH7 using citric acid, dH_2O to 200mls

E3 (10X) – diluted to 1x using dH_2O, and three drops of methylene blue per litre to avoid fungal contamination

- 50mM NaCl
- 1.7mM KCl
- 3.3mM $CaCl_2$
- 3.3mM $MgSO_4$

PBS

- NaCl 8g/l
- Na_2HPO_4 1.4g/l
- KCl 0.2g/l
- KH_2PO_4 0.2g/l

2.12. Software

1- Graph pad & Prism (version 8.1) was used for all data entry and statistical analysis.

2- NIS elements (version 4.3) was used where described for experiments performed using the Nikon wide field fluorescence microscope.

3- Velocity™ Software (version 6.3) was used where described to image experiments performed using the UltraVIEW VoX spinning disk confocal microscope (Perkin Elmer, Cambridge, UK).

4- FIJI (ImageJ2) was used where described to analyse experiments for mean pixel intensity, mean fluorescence intensity, or counting positive cells from immunofluorescence.

2.13. Statistical Analysis

Prism software (version 8.1) was used for the generation of all survival curves, column and grouped graphs, as well as all statistical analyses used. The statistical test used was dependent on the number of groups analysed, whether the data was parametric or non-parametric (for example in the context of ranked data), whether the data had Gaussian distribution or not. Analysis and post-hoc tests carried out for individual data sets are specified in their respective figure legends. The Dunnett's posthoc test was used for comparing means to a control mean, whereas the Sidak's test was used for making a selected set of comparisons, and Tukey's test was used for comparing all mean values with one another. The following identifies the significance values: *P < 0.05, **P < 0.01, ***P < 0.001, ****P < 0.0001. All error bars represent standard deviation unless stated otherwise.

Chapter 3: Irradiation induces up-regulation of multiple senescence markers in zebrafish larvae

3.1.1. Introduction

Removing senescent cells from older people is a viable option for tackling age-associated multi-morbidity and extending healthspan. This is due to senescent cells being causally linked to multiple age-associated disorders, including Alzheimer's Disease, Parkinson's Disease, Osteoarthritis, Osteoporosis, Ideopathic Pulmonary Fibrosis and cancer to name a few (Bussian et al., 2018; Schafer et al., 2017; Jeon et al., 2017; Childs et al., 2016; Chinta et al., 2018). Currently the treatment regime for older people, many of whom suffer from multiple diseases at once, is to treat diseases individually. However, this has led to the issue of polypharmacy, where multiple drugs being taken together exacerbate side effects and reduce their therapeutic efficacy, by interacting with Cytochrome P450 (Doan *et al.,* 2013). However, as ageing is a risk factor that is common to these diseases, then targeting a mechanism underlying ageing that leads to increased susceptibility to these diseases, such as the accumulation of senescent cells, could overcome these issues as only one treatment option theoretically would be required to tackle multimorbidity directly (Bellantuono, 2018). As our population is ageing and multimorbidity is becoming more prevalent, we have an urgent need to understand senescence and improve the efficacy of senolytic compounds (Centre for Ageing Better, 2019).

Currently, studying senescent cells in a whole organism context is difficult because there is no clear marker to study them easily *in vivo*, rather combinations of markers are required (Sharpless and Sherr, 2015). Further, mouse models of senescence accumulation do not permit live tracking of *in vivo* senescence at the cellular level in real time, thereby limiting their ability to study senescent cell interactions with immune cells for example (Baker *et al.,* 2006; Demaria *et al.,* 2014; Liu *et al.,* 2019). The p16-3MR transgenic mouse model for example uses luciferase to detect p16 positive cells, however this signal is diffuse making them only detectable at the population level, and p16 positive cells cannot be sorted by luciferase signal to study them at greater resolution (Demaria *et al.,* 2014). This reporter also expresses RFP in p16-positive cells but this cannot be detected well without first culling the animal and fixing the tissue, and therefore you cannot track senescent cells within the same animal over time easily. Though one could sort fluorescent p16-positive cells, which allows for more in-depth assessment other senescence markers, this loses spatial information (Baker *et al.,* 2011, Liu *et al.,* 2019). To be able to study these cells live and *in vivo*, a transgenic zebrafish reporter could instead be utilised as they are, unlike mice, fertilised externally and transparent at early developmental stages (Meyers, 2018).

To be able to use the transparency of young zebrafish to study *in vivo* senescence, a means to induce senescent cell accumulation during these early stages is required. A rapid assay for *in vivo* senescence accumulation would also make

the system compatible with *in vivo* compound screens, where off target toxicities and changes in organism health could be identified earlier in the drug development process (Vaz, Outeiro and Ferreira, 2018). This would improve the efficiency of identifying new senolytics, as efforts would not be wasted in translating compounds with *in vitro* efficacy into a more translatable *in vivo* context (Fuhrmann-Stroissnigg *et al.,* 2017). There is only limited evidence of early senescence accumulation in zebrafish larvae outside of assessing SA-β-Gal activity, which is not specifically required for senescence (Lee *et al.,* 2006; Kishi *et al.,* 2008; Koshimizu *et al.,* 2011). As such, a more in-depth characterisation of ectopic senescence induction in zebrafish larvae is required. To induce senescence accumulation in young zebrafish, I propose using total body irradiation. Irradiation has been used as a rapid inducer of *in vivo* senescence accumulation in mice and evidence suggests that zebrafish respond similarly to this senescence inducer (Le *et al.,* 2010; Demaria *et al.,* 2014). For example, increased activity of SA-β-Gal in adult zebrafish skin was described following irradiation (Tsai *et al.*, 2007). Although this is not a specific senescence marker alone, irradiation in mice also increased SA-β-Gal activity, as well as other more specific markers of senescence including P16 (Demaria *et al.,* 2014). At larval stages, an alternative oxidative stressors such as H_2O_2 can increase SA-β-Gal activity in zebrafish larvae also (Driessens *et al.*, 2009; Koshimizu *et al.*, 2011). Though different senescence inducers can lead to different senescence phenotypes, one could propose that irradiation could induce senescence in a comparable manner in early development (L A Maciel-Barón *et al.*, 2016)

To develop a panel of markers for identifying and characterising irradiation-induced senescence in zebrafish larvae, one must compare which genes are associated with irradiation-induced senescence in mammals. For example, key components of the DNA damage response, such as p53, p21, γH2AX that are important in irradiation-induced mammalian senescence, have also been implicated in replicative senescence in zebrafish, and so will be assessed following irradiation (Suzuki *et al.*, 2001; Henriques *et al.*, 2013; Demaria *et al.*, 2014). Although the locus for zebrafish p16 (*cdkn2a/b*) is not well characterised, mammalian P16 is up-regulated in response to irradiation and is also involved in the anti-cancer role of senescence (Serrano *et al.,* 1996; Demaria *et al.,* 2014). Inactivation of *cdkn2a/b* by CRISPR correlated with melanoma formation in adult zebrafish, implying that there may be a conserved role and therefore should be examined in the context of irradiation of zebrafish larvae also (Ablain *et al.,* 2018). Finally, markers for the senescence-associated secretory phenotype (SASP) such as interleukins 1, 6, 8 and matrix metalloproteinases 2, 3, 9, 13 are implicated in both in irradiation-induced senescence in mammals and senescence, and have zebrafish orthologues (Appendix table 3.1; Chen *et al.*, 2002; Lieschke and Currie, 2007; Coppé *et al.*, 2008; Varela *et al.*, 2012; Özcan *et al.*, 2016). Examining a combination of these factors, alongside SA-β-Gal activity, would provide evidence to support the proposal that irradiation of zebrafish larvae can cause senescence accumulation, as is seen in mammals.

3.1.2. Aims

To be able to use zebrafish as a novel tool for screening modifiers of senescence, a clear and rapid assay for senescence induction is required. Senescence accumulation can occur in response to irradiation in multiple mammalian systems. Zebrafish have a competent DNA damage response pathway, and irradiation of zebrafish larvae shows earlier accumulation of ageing-phenotypes associated to senescence such as cognitive decline. However, an irradiation assay to ectopically induce senescence accumulation in zebrafish during early development has not yet been established. I hypothesise that irradiation of zebrafish larvae will induce accumulation of senescence as is described in mammalian *in vivo* and *in vitro* systems. The aims of this chapter are:

- To characterise an assay for irradiating zebrafish larvae that causes up-regulation of senescence markers without affecting survival
- To develop methods for identifying induction of multiple senescence markers following irradiation of zebrafish larvae
- To establish whether there are particular regions of the zebrafish that are more sensitive to senescence induction by irradiation
- To determine whether there are any signs of irradiation-independent senescence in developing zebrafish larvae

3.2. Optimising dosage and timing of γ-irradiation in zebrafish larvae

No reports currently exist on the optimal dose and timing required for irradiation to induce senescence in zebrafish larvae, although senescence has been up regulated by other means in this model organism. I hypothesised that irradiation, at the appropriate dose and timing, can activate senescence-associated genes without causing significant loss in survival and viability.

To establish an appropriate irradiation dose in 1dpf zebrafish, a dose response based on previous evidence of zebrafish survival following irradiation was carried out (Daróczi, 2006; Daroczi *et al.*, 2006, 2009). 1dpf zebrafish were treated with 5, 12 or 20Gy irradiation before their survival and viability was assessed until before the onset of independent feeding, 5dpf (Figure 3.1). By 5dpf, only 20Gy irradiation caused a significant reduction in viability compared to unirradiated controls, where only 20% of fish were deemed viable. There was a 20% loss in viability in the other groups, but this was not an irradiation-specific effect as unirradiated controls showed comparable levels of viability by 5dpf. 12Gy was deemed an appropriate dose to treat zebrafish larvae, with it being the highest dose that did not cause significant loss in viability.

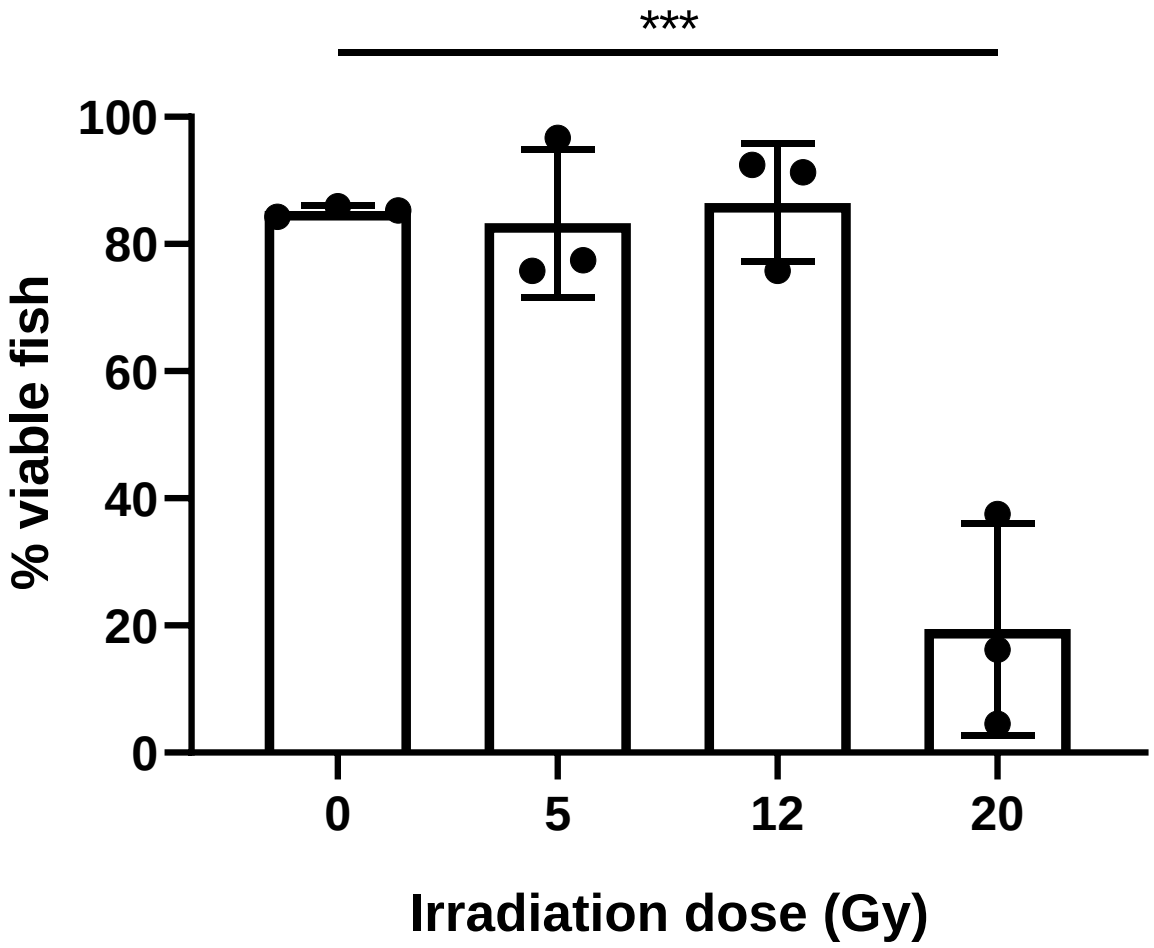

Figure 3.1: 20Gy irradiation at 1 day post-fertilisation causes loss in viability by 5 days post-fertilisation. Zebrafish were removed from chorions and irradiated at 1dpf with a range of doses of Cs^{137} γ-Irradiation. Survival was assessed daily until 5dpf, where the proportion of viable and healthy fish was assessed. Data are shown as Mean +/- SD and examined by one-way ANOVA with Dunnet's test for multipe comparisons with the control group (0Gy), at least 50 fish were examined across three independent repeats, *** p>0.001.

3.2.2. Identifying an optimal stage of development for irradiation in zebrafish larvae

To establish an optimal time at which zebrafish can be treated with irradiation, 12Gy irradiation was given at 1, 2, or 3dpf (Figure 3.2). 12Gy did not give a loss in survival by 5dpf when given at 1, 2 or 3dpf. A more in-depth assessment of 1dpf irradiated zebrafish showed signs of toxicity such as oedema and deflated swim bladder by 5dpf. A third of fish (n = 100) had under-developed swim bladders, and though not statistically significant there were some cases of more severe toxicities such as spinal curvature and stunted growth. 12.5% of fish had a blueish colouring to their skin, which looked like the methylene blue in the media was being absorbed, a possible indication of dead or damaged tissue (Davies *et al.*, 1980). 12Gy irradiation of zebrafish at 2dpf showed much lower signs in toxicity, where only 10% of irradiated fish presented with underdeveloped swim bladders. Irradiation at 3dpf showed even less signs of toxicity. Importantly, enough time is required for senescence to be induced before the zebrafish are protected by ASPA such that it remains a high throughput assay. Therefore, 12Gy irradiation at 2dpf was deemed most appropriate for our senescence induction assay with the caveat that fish showing signs of ill health, such as deflated swim bladders, are removed from later analyses.

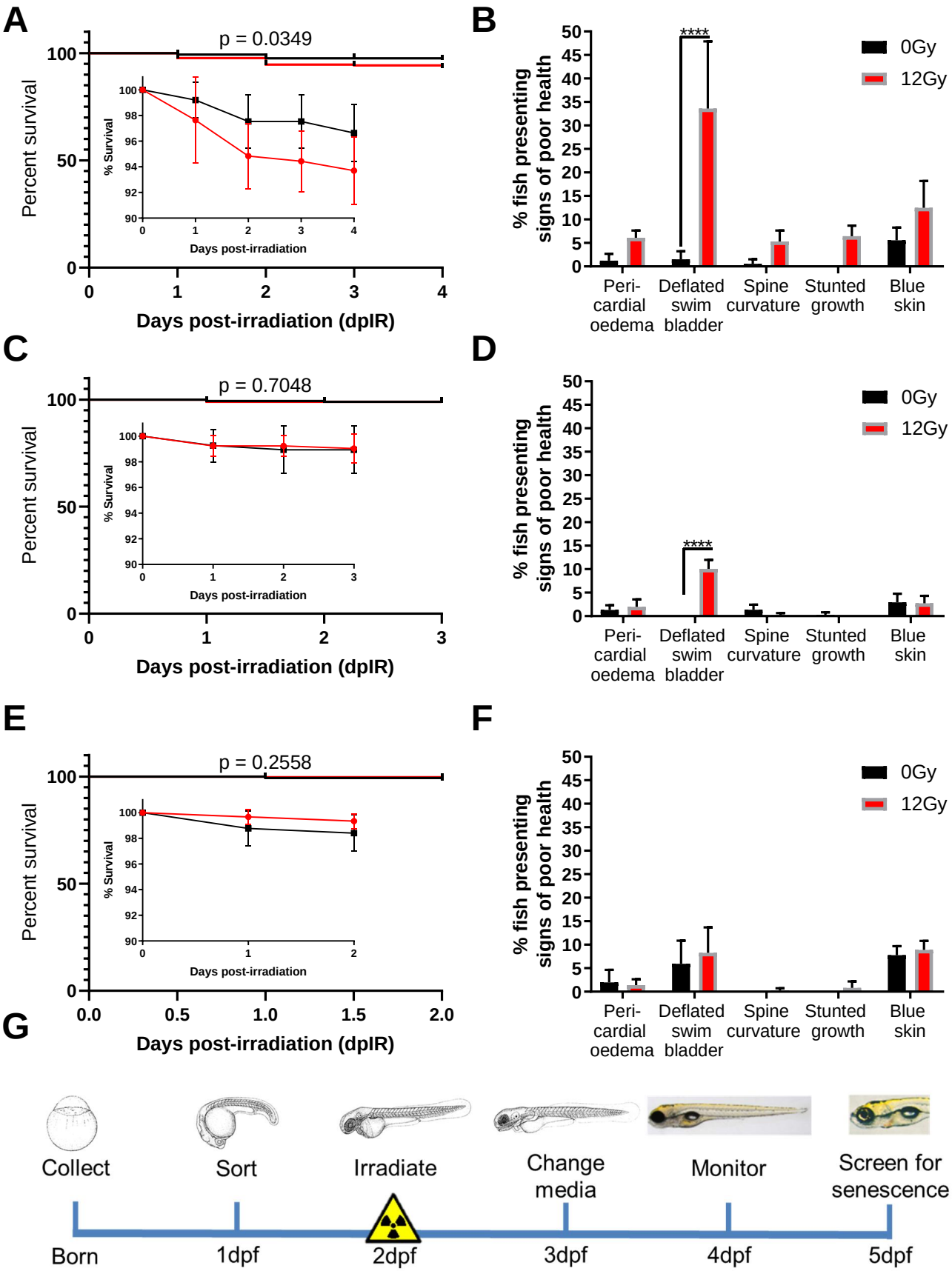
A
p = 0.0349
Percent survival
Days post-irradiation (dpIR)
% Survival
Days post-irradiation
B
% fish presenting signs of poor health
****
0Gy
12Gy
Peri-cardial oedema
Deflated swim bladder
Spine curvature
Stunted growth
Blue skin
C
p = 0.7048
Percent survival
Days post-irradiation (dpIR)
% Survival
Days post-irradiation
D
% fish presenting signs of poor health
****
0Gy
12Gy
Peri-cardial oedema
Deflated swim bladder
Spine curvature
Stunted growth
Blue skin
E
p = 0.2558
Percent survival
Days post-irradiation (dpIR)
% Survival
Days post-irradiation
F
% fish presenting signs of poor health
0Gy
12Gy
Peri-cardial oedema
Deflated swim bladder
Spine curvature
Stunted growth
Blue skin
G
Collect
Sort
Irradiate
Change media
Monitor
Screen for senescence
Born
1dpf
2dpf
3dpf
4dpf
5dpf

Figure 3.2. Survival and health status of zebrafish following 12Gy irradiation until 5dpf. A) Zebrafish were irradiated at either A,B) 1dpf, C,D) 2dpf or E,F) 3dpf. A,C,E) Survival was assessed daily until zebrafish reached 5dpf. Kaplan Meier curves displayed with % survival inserted. B,D,F) Viable zebrafish at 5dpf were assessed for signs of poor health that are commonly associated with irradiation. G) Diagram depicting the optimal timing for an irradiation assay that doesn't induce excess toxicity whilst still allowing time for senescence to be induced by 5dpf. Images of zebrafish from different stages adapted from ZFIN. B,D,F) Data was examined by 2way ANOVA with Bonferroni's test for multiple comparisons. n=300 over three independent experiments **** $p < 0.0001$.Error bars are standard deviation.

3.3. Irradiation activated senescence-associated cell-cycle inhibitors in zebrafish larvae

Once a non-toxic dose of irradiation had been determined, I sought to assess whether there were signs of stress-induced senescence in irradiated zebrafish 3 days after irradiation (3dIR). The senescence-associated genes *cdkn1a* (*p21*) and *cdkn2ab* (*p16-like*) are commonly used as markers of senescence, and so I used quantitative PCR (qPCR) to study their transcriptional activation following irradiation.

3.3.1. Primer optimisation for quantitatively assessing *p21* and *p16-like* mRNA expression

To verify whether the selected primers for were amplifying the desired cDNA efficiently, serial dilutions of irradiated zebrafish cDNA was performed followed by PCR amplification (Figure 3.3). A reaction is considered efficient with a coefficient between -3.3 and -3.9. The efficiency of *p21* was 85% (coefficient =-3.758), and 95% efficient for *p16-like* (coefficient -3.448) (Figure 3.3A, B). βactin was chosen as a reference gene to work out fold expression changes of *p21* and *p16-like* as there was no difference in expression between cDNA from irradiated and unirradiated controls, the primers for this gene was 95% efficient also (-3.514) (Figure 3.3C). These data suggest the primers amplify the specific gene of interest efficiently within the cDNA concentrations analysed. To assess technical reproducibility, PCRs of the same cDNA were repeated over different days, and Ct values were assessed, these showed very little variability with R^2 values of at least 0.95, suggesting proficiency of both the experimental protocol and handler (Figure 3.3A-C).

A

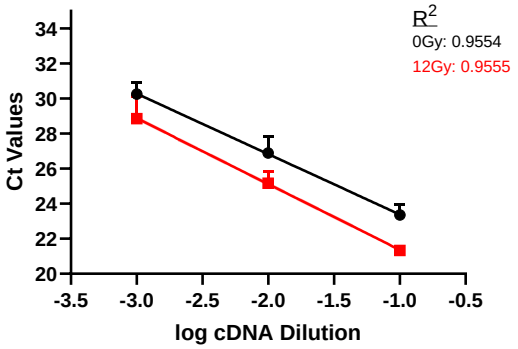

0	12
Y = -3.448*X + 19.93	Y = -3.758*X + 17.60

B

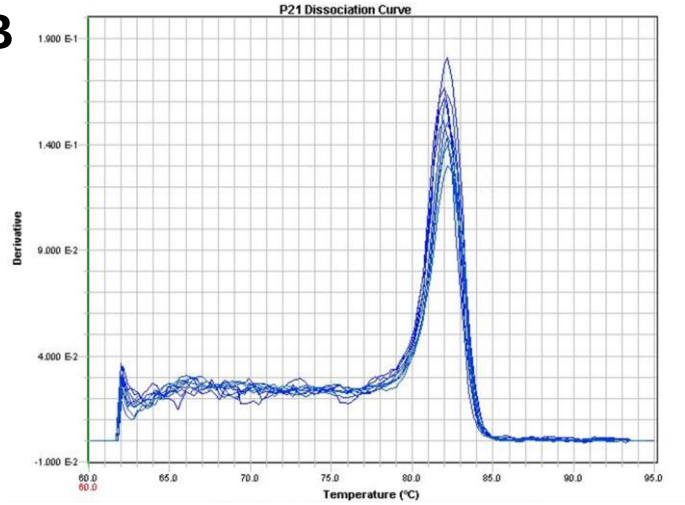

C

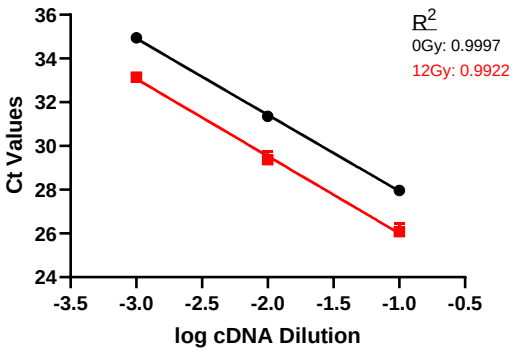

0	12
Y = -3.488*X + 24.45	Y = -3.530*X + 22.48

D

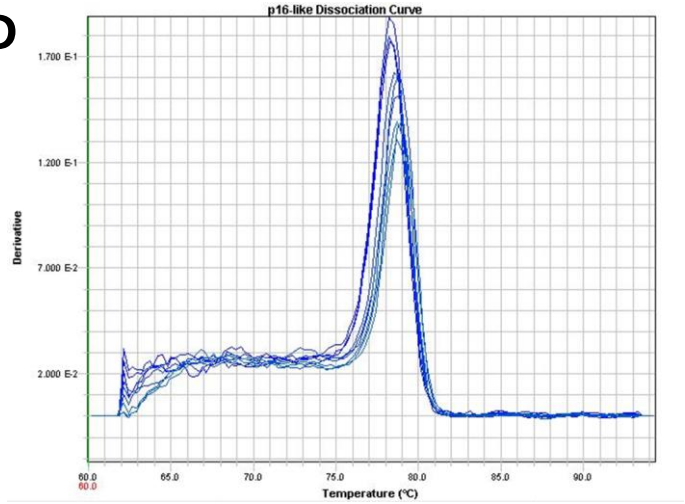

E

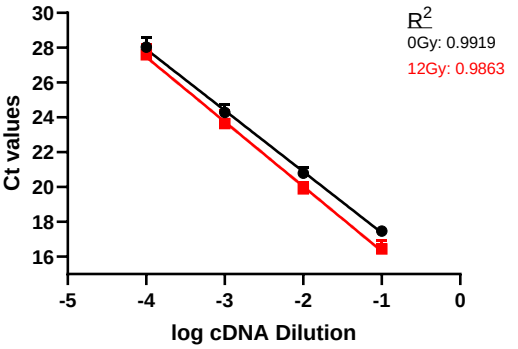

0	12
Y = -3.514*X + 13.86	Y = -3.718*X + 12.60

F

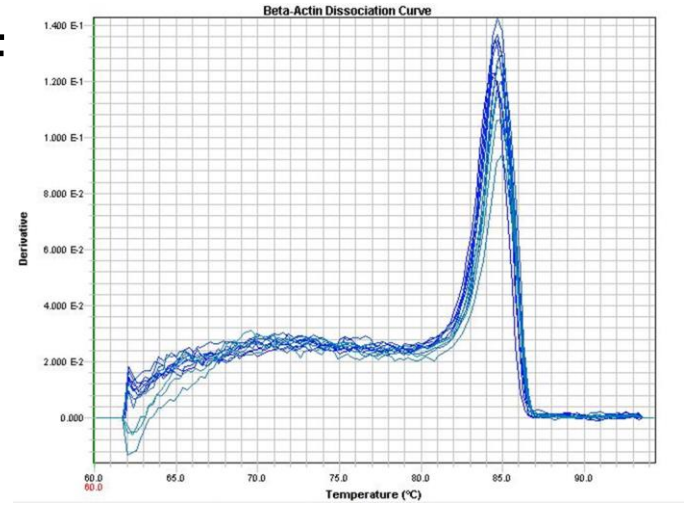

Figure 3.3. Technical qPCR reproducibility of 5dpf zebrafish. qPCR was carried out to determine primer efficiency (A,C,E) and specificity (B,D,F) to assess expression the senescence markers *p21* (A,B), *p16-like* (C,D). The housekeeping gene βactin was also assessed to act as a reference gene mRNA from pools of 50 irradiated 5dpf zebrafish were used to make cDNA for PCR amplification unirradiated zebrafish were used for comparison. A,C,E) The same cDNA was used at differen dilutions (1:10, 1:100, 1:1000, 1:10,000) to determine whether the primers can amplify efficiently B,D,F) A melting reaction was performed to determine whether primer-cDNA binding was specific. A least 50 fish were pooled for each of the three independent repeats..

3.3.2. 3dpIR 12Gy irradiation significantly up-regulates *p21* and *p16-like* mRNA expression

To determine the expression of the senescence-associated genes *p21* and *p16-like* in 3dpIR zebrafish, quantitative PCR was carried out (Figure 3.4). A dose response for *p21* expression was assessed following 3, 5 or 12Gy irradiation compared to unirradiated controls and the reference gene βactin. A dose-dependent increase in *p21* mRNA expression was detected in AB(wt) strain larvae, with the largest mRNA expression seen at 12Gy (Figure 3.4A).

To assess whether there are spatial differences in irradiation induced *p21* expression, I examined RNA extracted from zebrafish tails only (Figure 3.4B). Again, a dose-dependent increase of *p21* mRNA was seen, and 12Gy irradiation gave the highest induction. mRNA expression from the zebrafish tail was 0.066 (SD 0.004) increase following 12Gy irradiation, which is comparable to changes from whole zebrafish mRNA (0.066, SD 0.009) indicating there isn't much difference in this area of the fish compared to the whole organism. An optimal location to optimised imaging-based senescence detection techniques would be the tail as it is the thinnest region of the organism. To ensure this induction of *p21* mRNA wasn't a strain-specific effect of AB(wt) zebrafish, I also examined changes in expression in nacre-strain zebrafish, and found a comparable mRNA expression patterns for *p21* (Figure 3.4C). *p16-like* mRNA was also assed in nacre-strain zebrafish, and the mRNA expression was again highest in the 12Gy groups (0.003, SD 0.001) compared to unirradiated controls (0.0009, SD 0.0003) (Figure 3.4D). Interestingly, the expression of *p16-like* was around 20 fold lower than that of *p21.* Together, this evidence suggests that 12Gy irradiation at 2dpf can induce expression of central senescence markers by 5dpf.

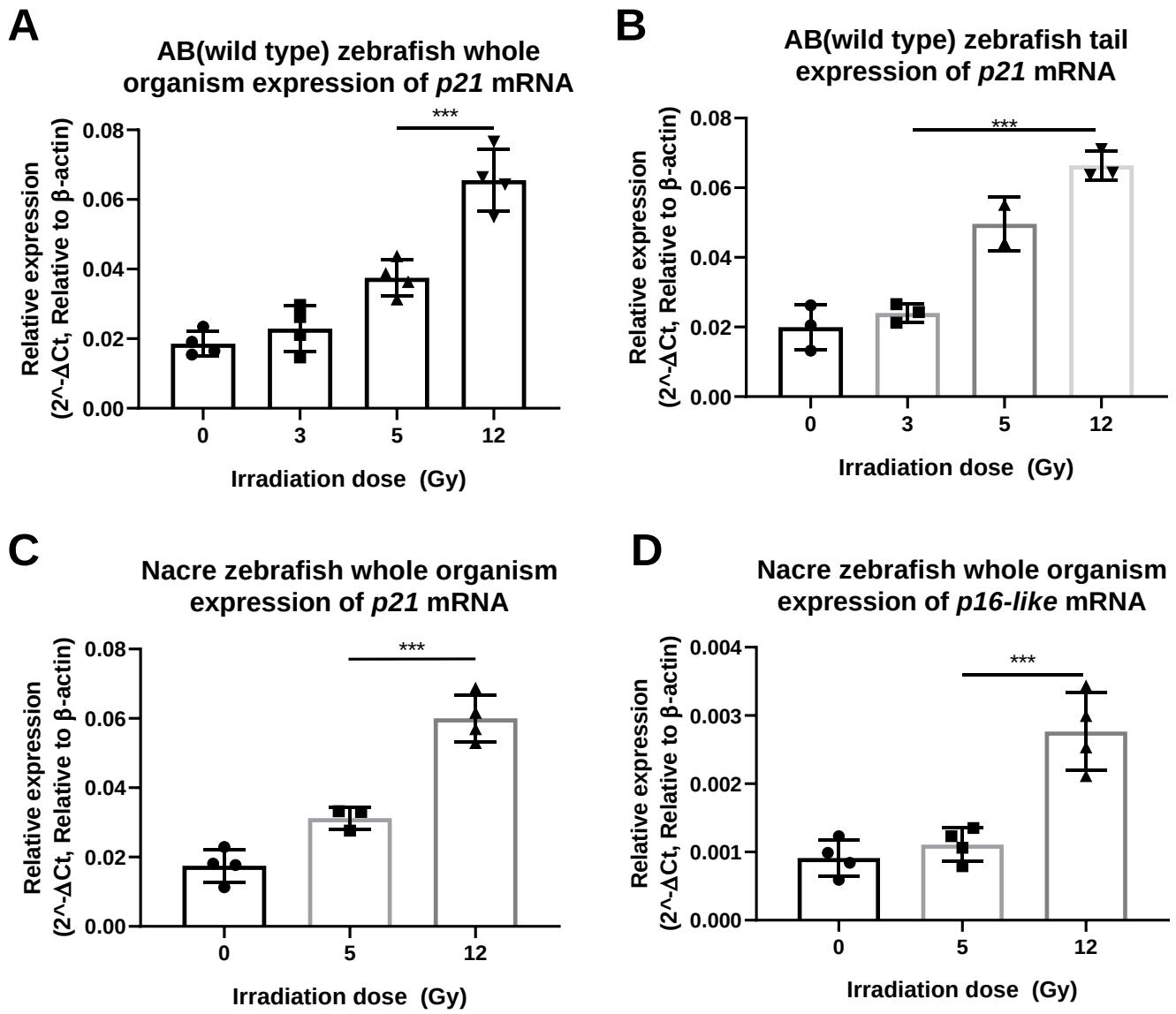

Figure 3.4. Quantitative expression changes of *p21* and *p16-like* mRNA following irradiation. Zebrafish were irradiated at 2 days post-fertilisation (2dpf) and assessed for the senescence markers *p21* (A-C) and *p16-like* (D). Changes in expression are relative to the reference gene βactin. Expression was assessed in two different zebrafish strains, AB(wild-type) (A,B) and Nacre (C,D). mRNA from pools of 50 whole zebrafish (A,C,D) and zebrafish tails (B) were used for each independent replicate. Relative expression was calculated by 2^-ΔCt, relative to β-actin expression and unirradiated controls. Data was examined by one-way ANOVA with Sidak's multiple comparisons test. At least 50 fish were pooled for each of the three-four independent repeats. Error bars represent standard deviation.

3.3.3. Endogenous *p21* mRNA expression is regulated by the circadian rhythm, which is less pronounced following irradiation

There is evidence that suggests that p21 expression is influenced by the circadian rhythm, independently of senescence (Laranjeiro *et al.,* 2013). To determine the best time of day to assess irradiation-induced expression of senescence-associated genes, a time-course for *p21* and *p16-like* mRNA expression following irradiation was carried out. Following irradiation at 2 or 3dpf, RNA was extracted every morning and evening until the zebrafish reached 5dpf. 24 hours following 12Gy irradiation at 2dpf, both *p21* and *p16-like* mRNA expression is increased 6 fold, which decreases by 72 (3 days) post irradiation (Figure 3.5A, B). Fold expression change of *p21* did seem to fluctuate according to the time of day (Figure 3.5A), which was not seen with *p16-like* (Figure 3.5B). Fold expression change tended to increase during the evening time-points (30 and 54hpIR), at its peak being up to 7x higher than during morning time-points (24, 48, 72hpIR). With *p16-like*, it seemed that fold expression only decreased between 54 and 72hpIR indicating potentially different regulatory mechanisms between the two senescence-associated genes. Examining fold expression of *p21* in unirradiated and irradiated fish independently showed that there is oscillating expression according to the time of day in both groups (Figure 3.5C), though expression in the irradiated fish remained higher throughout. *P16-like* again did not show this oscillation (Figure 3.5D), however interestingly it did seem to show an up-regulation at 5dpf in unirradiated fish which would explain the effect seen in Figure 3.5B. Although the fold change in expression of *p21* and *p16-like* mRNA being comparable at 72hpIR (3dpIR), the actual expression levels of *p16-like* following irradiation (0.002, Figure 3.5D) was around 35 times lower than that of *p21* mRNA (0.07, Figure 3.5C). When comparing fold expression change of *p21* and *p16-like* mRNA expression relative to the 24hpIR time-point, I was able to compare the magnitude of this change in expression during the day in irradiated and non-irradiated zebrafish. With *p21* expression, the oscillations over time was less pronounced in irradiated zebrafish and no longer significantly different between morning and evening time-points (Figure 3.5E). Again, this effect was not seen with *p16-like* expression, which seemed consistent up until 70hpIR where unirradiated fish showed an increase in expression (Figure 3.5F). I also assessed whether irradiation at 3dpf had the same effect on cyclic *p21* mRNA expression, as this would allow an extra day for irradiation-independent cyclic *p21* regulation to be established before irradiation-induced *p21* transcription. Irradiation at 3dpf showed comparable results to irradiation at 2dpf, with oscillating irradiation-independent *p21*, but not *p16-like* mRNA expression (Figure 3.6). Interestingly, unirradiated controls in these zebrafish did not show an increase in *p16-mRNA* between the final two time-points as was seen in Figure 3.5B. Therefore, as is evidenced in the literature, *p21* seems to be regulated by the time of day but expression induced by irradiation is always greater.

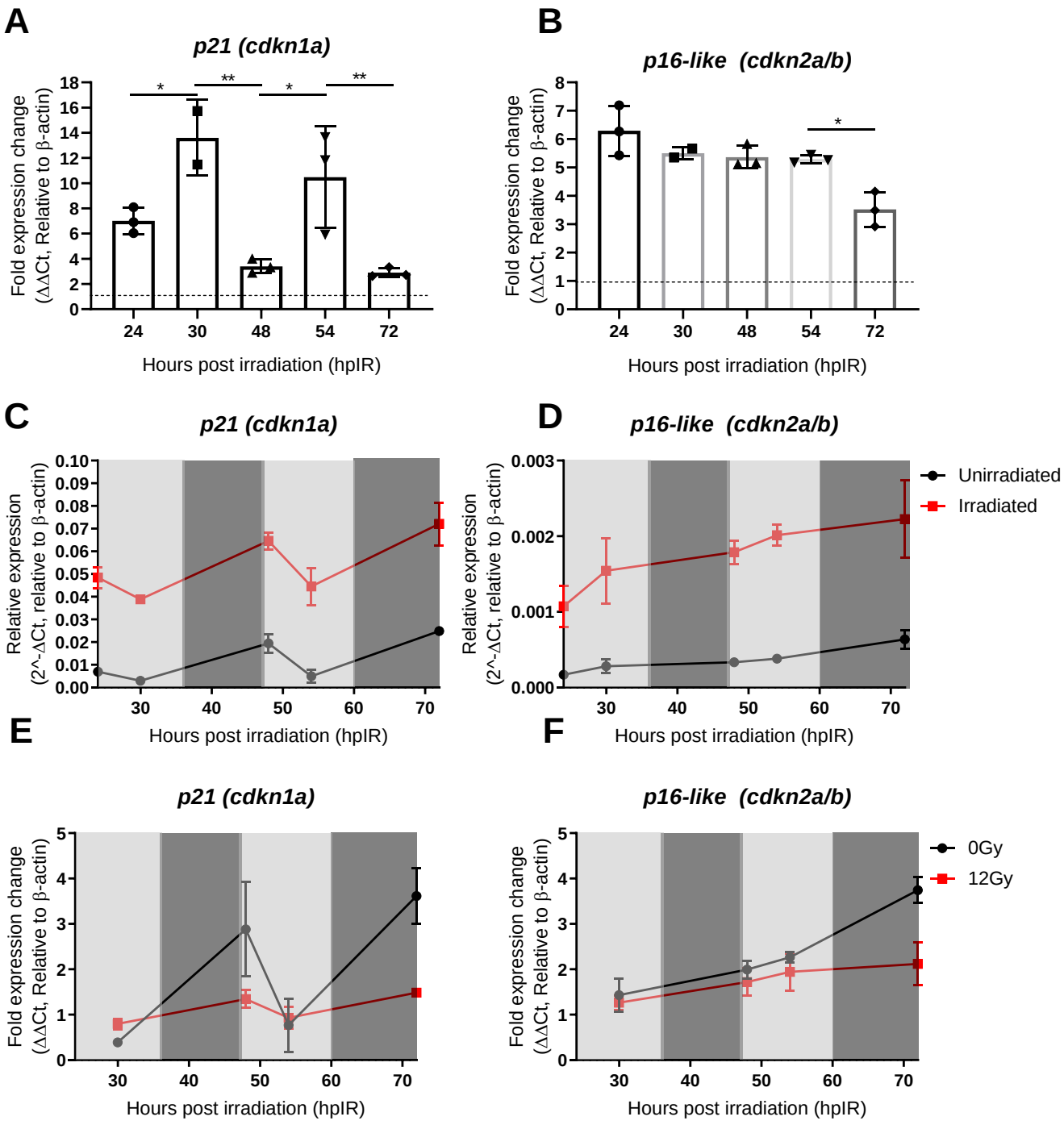
A
p21 (cdkn1a)
Fold expression change (ΔΔCt, Relative to β-actin)
Hours post irradiation (hpIR)
B
p16-like (cdkn2a/b)
Fold expression change (ΔΔCt, Relative to β-actin)
Hours post irradiation (hpIR)
C
p21 (cdkn1a)
Relative expression (2^-ΔCt, relative to β-actin)
Hours post irradiation (hpIR)
D
p16-like (cdkn2a/b)
Relative expression (2^-ΔCt, relative to β-actin)
Hours post irradiation (hpIR)
Unirradiated
Irradiated
E
p21 (cdkn1a)
Fold expression change (ΔΔCt, Relative to β-actin)
Hours post irradiation (hpIR)
F
p16-like (cdkn2a/b)
Fold expression change (ΔΔCt, Relative to β-actin)
Hours post irradiation (hpIR)
0Gy
12Gy

Figure 3.5. Temporal regulation of senescence-assocaited genes *p21* and *p16-like* following irradiation at 2dpf. Zebrafish were irradiated at 2 days post-fertilisation and assessed for *p21* and *p16-like* expression every morning (10am-12pm) and afternoon (4-6pmuntil they 5 days post-fertilisation. A) Fold expression change in p21, relative to 0Gy control and β-actin reference gene (ΔΔCt). B) Fold expression change in p16-like, relative to 0Gy control and β-actin reference gene (ΔΔCt). C) p21 fold induction, relative to β-actin (2^-ΔCt). D) p16-like fold induction, relative to β-actin (2^-ΔCt). E) Fold change in p21 expression, relative to intial 24hpIR timepoint. F) Fold change in p16-like expression, relative to intial 24hpIR timepoint. Data were examined by one-way ANOVA with Sidak's test for multipe comparisons. At least 50 fish were pooled for each of the three independent experiments, * p>0.05; ** p>0.01; *** p>0.001. Error bars represent standard deviation.

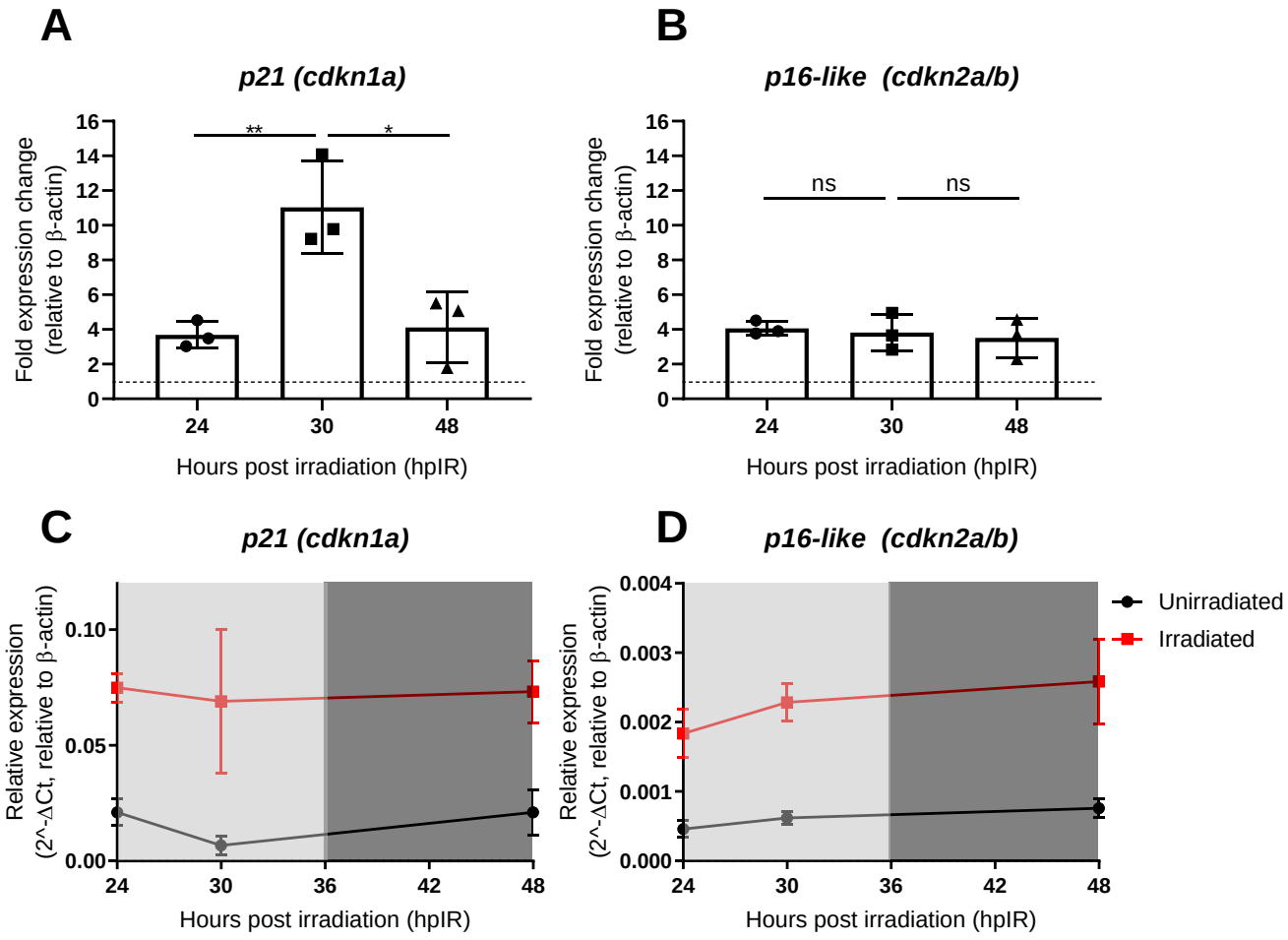

Figure 3.6. Temporal regulation of senescence-assocaited genes *p21* and *p16-like* following irradiation at 3dpf. Zebrafish were irradiated at 3 days post-fertilisation and assessed for *p21* and *p16-like* expression every morning (10am-12pm) and afternoon (4-6pm) until they 5 days post-fertilisation. A) Fold expression change in p21, relative to 0Gy control and β-actin reference gene (ΔΔCt). B) Fold expression change in p16-like, relative to 0Gy control and β-actin reference gene (ΔΔCt). C) p21 fold induction, relative to β-actin (2^-ΔCt). D) p16-like fold induction, relative to β-actin (2^-ΔCt). Data were examined by one-way ANOVA with Sidak's test for multipe comparisons. At least 50 fish were pooled for each of the three independent experiments. * p>0.05; ** p>0.01. Error bars represent standard deviation.

3.4. Irradiation-induced *p21* mRNA expression is located spatially in head and intestinal regions of 3dpIR zebrafish larvae

3.4.1. Optimisation of proteinase K treatment to detect spatial *p21* mRNA expression

To determine whether there were particular tissues or spatial regions of irradiation-induced expression of senescence-associated genes, I optimised whole-mount *in situ* hybridisation of 3dpIR zebrafish larvae. I used a published probe for *p21* (Laranjeiro *et al.,* 2013), and first optimised the correct incubation protocol for proteinase K digestion, an important step that determines mRNA accessibility for probe binding and can cause background staining if suboptimal (Figure 3.7). 4 treatment regimens were examined, using two different concentrations (10 or 15µg/µl) and temperatures (22 or 37°C) across 55 to 90 minute incubation length. These conditions were chosen based on evidence from colleagues using this technique at 5dpf for alternative genes of interest. A treatment of 10µg/µl for 75 minutes at 22°C (room temperature) provided the most specific staining in irradiated fish, compared to the sense probe, which should have no specific binding (Figure 3.7). Now, an optimal method for digesting fixed zebrafish larvae has been established for detecting specific *p21* mRNA expression at 5 days post-fertilisation.

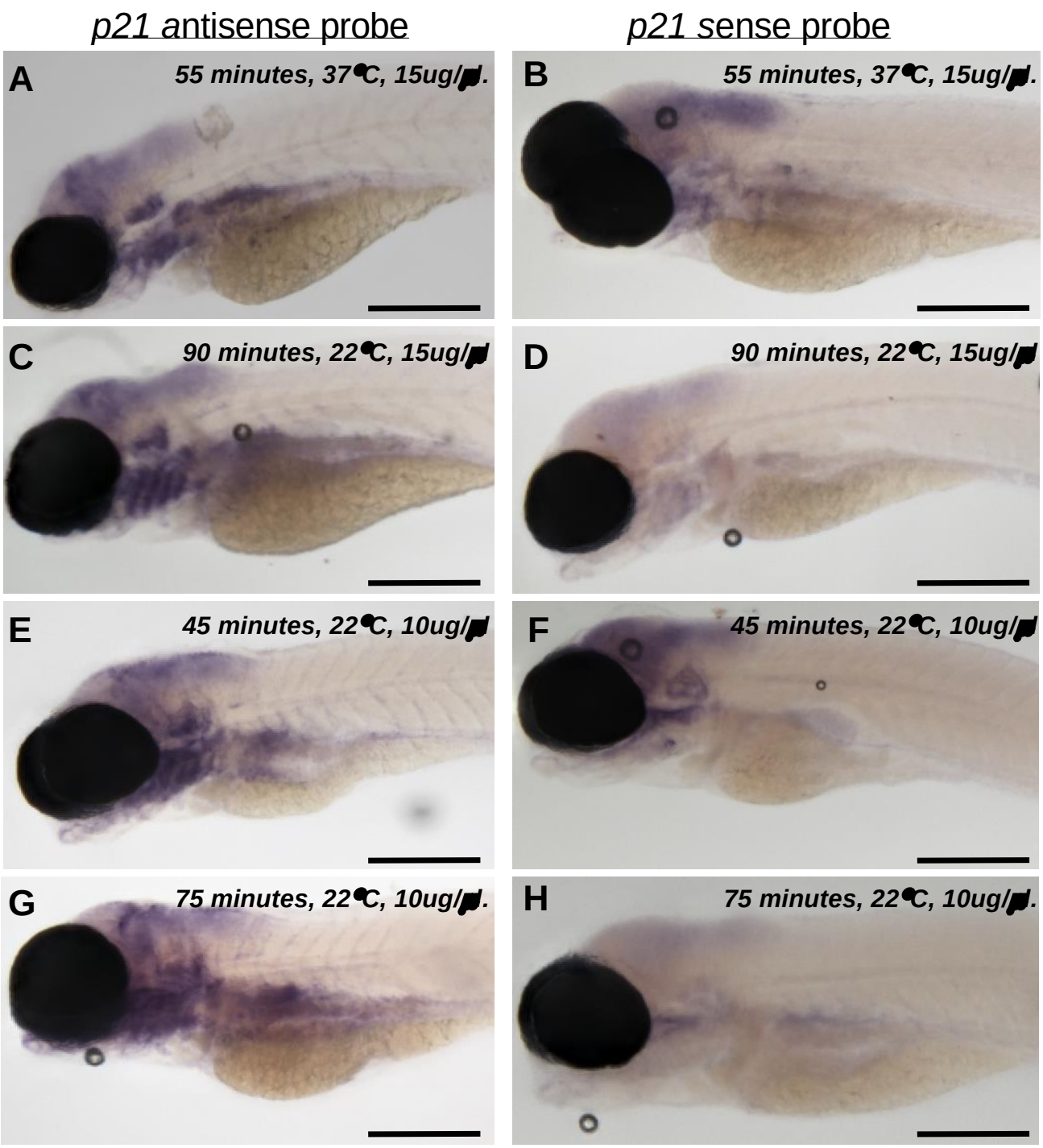

Figure 3.7. Optimisation of enzymatic digestion of 5dpf zebrafish larvae for *p21 in situ* hybridisation. Transmitted light photomicropraphs of an *in situ* hybridisation for *p21* mRNA in 12Gy-irradiated zebrafish following different proteinase k treatment conditions, representative images shown. Expression of *p21* mRNA (left panels) and a negative control sense probe that has no binding parter (right panels) 3 days after 12Gy irradiation. A,B) 55 minutes 37 degrees 15ug/μl. C,D) 90 minutes 22 degrees 15ug/μl. E,F) 45 minutes 22 degrees 10ug/μl. G,H) 75 minutes 22 degrees 10ug/μl. 15-20 fish used per treatment group. Scale 250μm.

3.4.2. Optimising analysis methods for detecting whole mount *in situ* hybridisation *p21* mRNA expression

To determine the best method for analysing changes in *in situ* hybridisation staining for *p21* mRNA expression, two alternative analysis techniques were used in a pilot experiment to assess strength of staining after 5 or 12Gy irradiation (Figure 3.8). Firstly, I measured mean grey value of images around the head and intestinal regions whilst blinded, where there was a clear visual increase in purple staining (Figure 3.8A, B). This technique showed a statistically significant dose-dependent decrease in mean grey value following irradiation. To corroborate this technique, I blindly ranked these images according to strength of staining, so that the higher the rank, the stronger the staining (Figure 3.8D). Like with mean grey value, ranking showed a significant dose-dependent increase in irradiation-induced *p21* expression at 3dIR. Out of the two techniques, I employed the ranking technique for final analyses, as it was the more discriminatory of the two (Figure 3.8A, B).

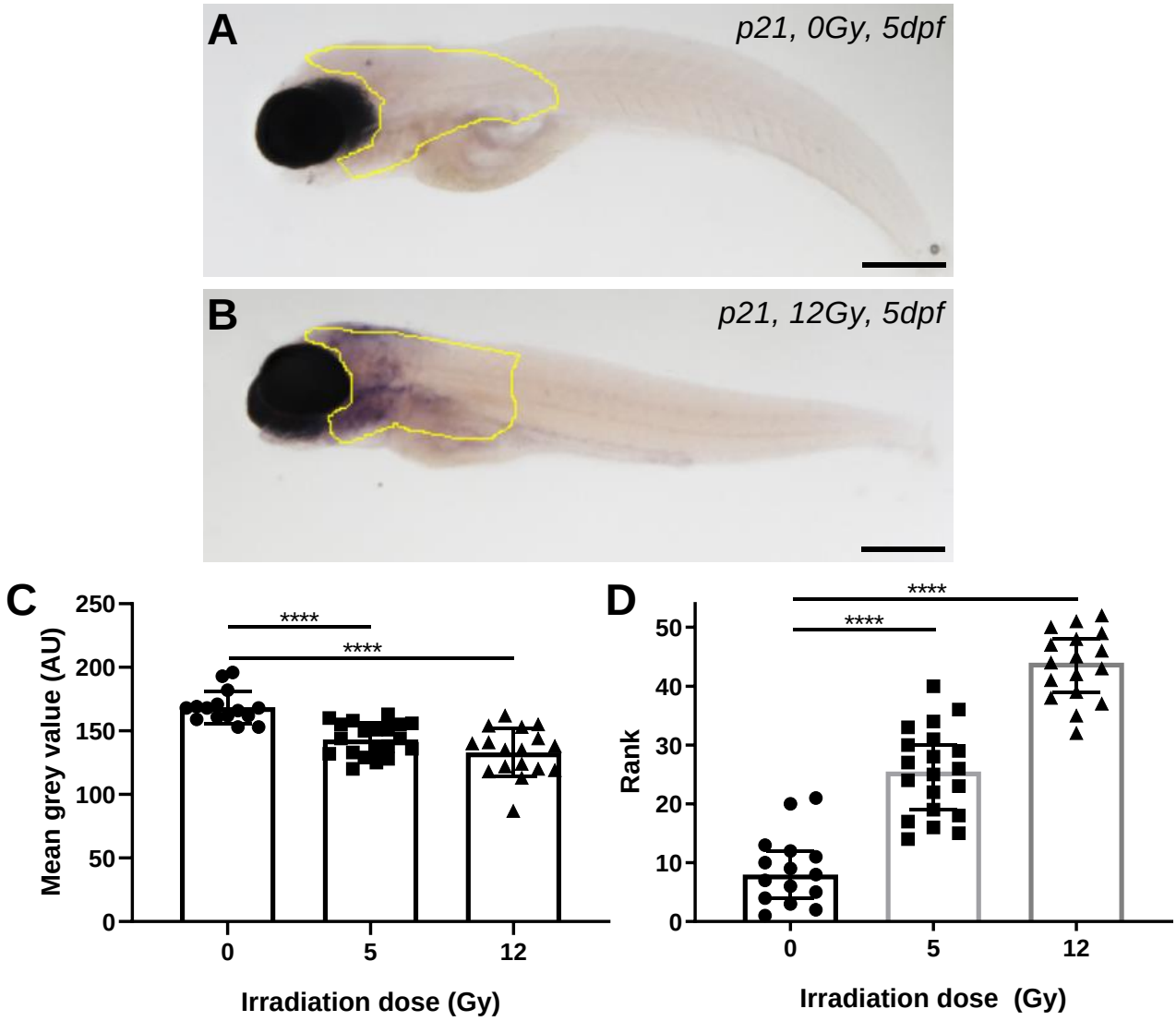

Figure 3.8. Comparison of analysis techniques to assess the strength of p21 mRNA signal by *in situ* hybridsation. A,B) Transmitted light photomicrographs of an *in situ* hybridisation for *p21,* example images where region of interest (highlighted in yellow) was quantified for mean grey value, where the stronger the staining, the lower the value will be. Regions were defined as the head region excluding the eyes to the end of the main protrusion of the yolk sac. A) Example image of 0Gy fish, 3dpIR. B) Example image of 12Gy fish, 3dpIR. C) Quantification of mean grey value. D) Corresponding values of blind ranking in the same fish. 15 fish were used per treatment group. Data were examined by one-way ANOVA. **** $p<0.0001$. Scale 250μm. Error bars standard deviation.

3.4.3. Dose-dependent increase in *p21* mRNA expression is predominantly located in pharyngeal arches, intestine, and head regions of 3dpIR zebrafish larvae

To determine whether *p21* induction is different across regions of 3dpIR zebrafish, the optimised *in situ* hybridisation protocol and ranking analysis was carried out following 5 or 12Gy irradiation. A clear dose-dependent increase in *p21* staining following irradiation was seen compared to unirradiated controls, whilst the negative control *p21* sense probe showed no staining whatsoever (Figure 3.9). This purple staining was particularly localised to the pharyngeal arches, brain, and intestinal regions of the zebrafish, depicted by the red arrows. It did also seem that there was some expression in the unirradiated control group, compared to the sense probe, most notably in the regions where the pharyngeal arches are located, which corroborates with previous qPCR data that there is an irradiation-independent component to *p21 mRNA* regulation.


A
p21, 5dpf, 0Gy


B
p21, 5dpf, 5Gy

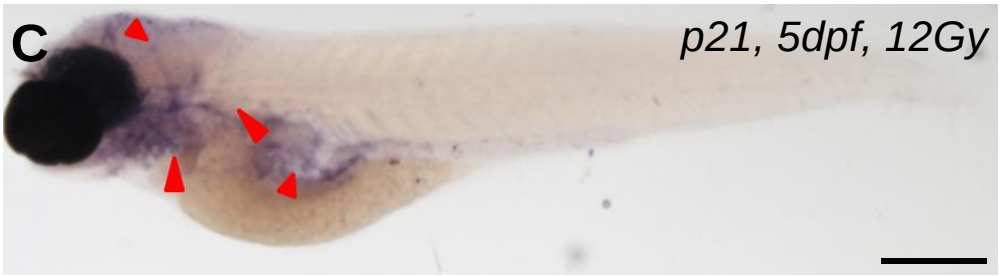
C
p21, 5dpf, 12Gy

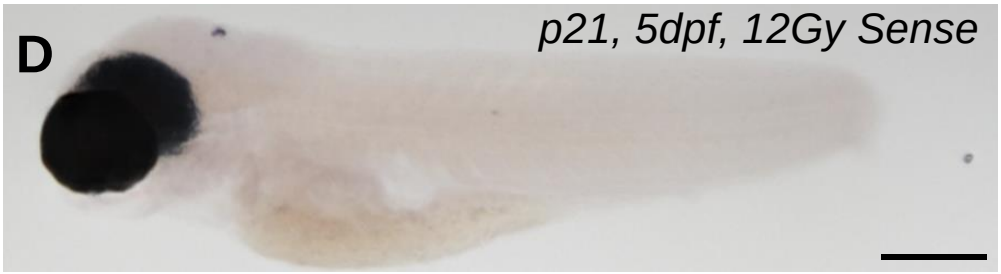
D
p21, 5dpf, 12Gy Sense

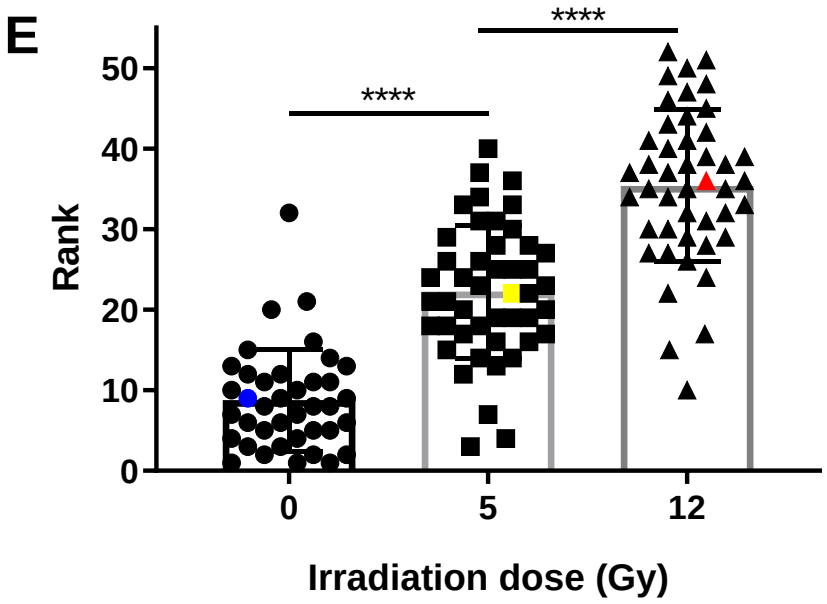
E
****
****
Rank
50
40
30
20
10
0
0
5
12
Irradiation dose (Gy)

Figure 3.9. Whole-mount in situ hybridisation (WISH) of 5dpf zebrafish larvae shows dose-dependent *p21* mRNA induction by irradiation. Zebrafish with irradiated at 2 days post-fertilisation with 5 (B) or 12Gy (C) irradiation, unirradiated zebrafish werre used for comparison**.** A DIG-labelled antisense RNA probe was used to detect *p21* expression, with sense probes used as a negative control. A-D)Transmitted light photomicropraphs of an *in situ* hybridisation, representative images of each group are shown and coloured on graph. Red arrows depict areas of increased staining. E) Analysis of zebrafish images (4.5x magnification) was carried out through blind ranking according strength of purple staining, such that the fish with the strongest staining correlated with the highest rank. Data was examined by Kruskal Wallace test with Dunn's mutiple comparisons. ****P ⩽0.0001. 15 fish were used for each of the three independent experiments. Scale 250μm. Error bars standard deviation.

3.4.4. An *in situ* hybridisation probe was unable to detect changes in *p16-like* expression in 3dpIR zebrafish larvae

To assess spatial expression of *p16-like* mRNA expression, an *in situ* hybridisation probe was developed (Figure 2.5, 2.6). Interestingly, unlike *p21*, the *p16*-like probe did not show specific increases in expression following irradiation, with the sense probe consistently showing a similar pattern to the antisense probe (Figure 3.10). Ranking of the images showed insignificant differences following irradiation in one independent experiment, but then less staining in another. I believe this is an artefact due to there being such small differences in staining between the groups, and as such, the analysis method is less reliable than with *p21* staining. The spread of the data is such that there was not clear separation between the two groups, despite knowing that by qPCR, expression was expected to increase. This indicates that *p16-like* may not be as useful as *p21* in detecting *in vivo* senescent cells in irradiated zebrafish larvae at 5 days post-fertilisation.

A

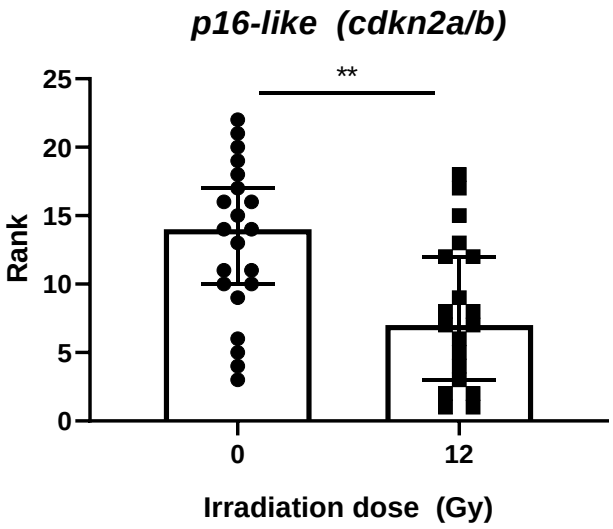
p16-like (cdkn2a/b)
**
Rank
25
20
15
10
5
0
0
12
Irradiation dose (Gy)

B

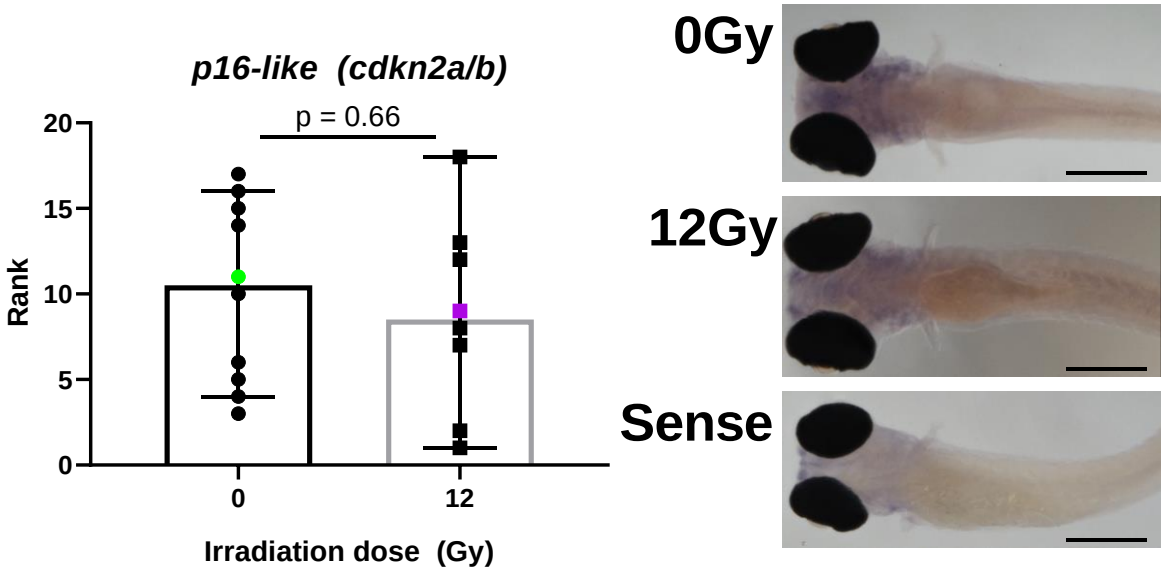
p16-like (cdkn2a/b)
p = 0.66
Rank
20
15
10
5
0
0
12
Irradiation dose (Gy)
0Gy
12Gy
Sense

C

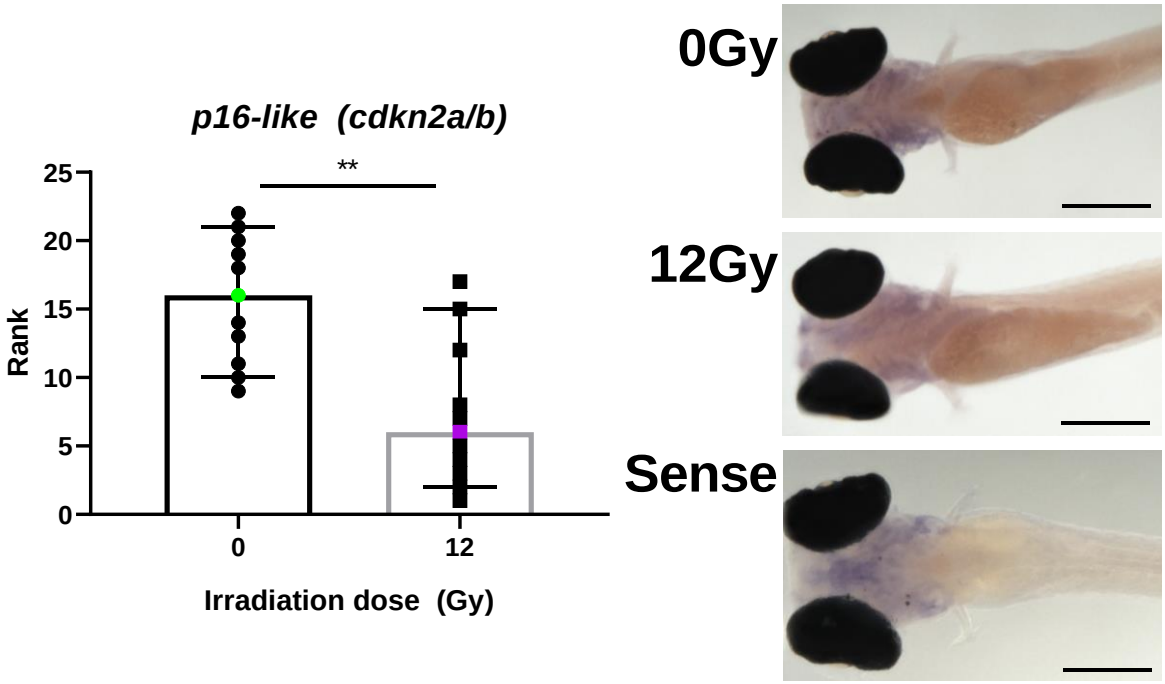
p16-like (cdkn2a/b)
**
Rank
25
20
15
10
5
0
0
12
Irradiation dose (Gy)
0Gy
12Gy
Sense

Figure 3.10. Blind ranking of *in situ* hybridisation for *p16-like* did not show reliable changes in spatial expression following irradiation. *p16-like* mRNA expression was detected through a DIG-labelled antisense mRNA probe, with sense probes used as a negative control. Analysis of ventral zebrafish head images (4.5x magnification) was carried out through blind ranking according strength of purple staining, such that the fish with the strongest staining correlated with the highest rank. A) Quantification of 20 zebrafish stained for *p16-like* expression either irradiated (12Gy) or not (0Gy) over two independent repeats. B) Quantication of zebrafish from the Irst independent experiment, with images that represent mean rank and coloured on graph. C) Quantication of zebrafish from the second independent experiment, with images that represent median rank and coloured on graph. Error bars represent median rank and 95% confidence intervals. Data was examined by Mann-Whitney test. ** $p<0.01$. Scale 250μm. Error bars standard deviation.

3.5. Irradiated zebrafish larvae show increased senescence-associated β galactosidase activity in comparable regions to p21 mRNA expression

To provide further evidence of irradiation-induced senescence in 3dpIR zebrafish larvae, a whole-mount senescence-associated β-Galactosidase (SA-β-Gal) assay was carried out to determine whether this senescence-associated marker is also up regulated in regions of high *p21* mRNA expression. Blind ranking of the images showed a significant increase for SA-β-Gal staining in the head region of the 3dpIR zebrafish (Figure 3.11 A-D). Looking at the median ranked fish (Figure 3.11A, B), there is a clear increase in the amount of blue staining in the brain regions, and a few blue cells around the pharyngeal arches, areas previous shown to have high *p21* mRNA levels. Interestingly, when looking at images of the whole zebrafish there seemed to be irradiation-independent expression in the intestine and the caudal haematopoietic tract (CHT) of 5dpf zebrafish (Figure 3.11 E, F). To confirm the ranking method is applicable for SA-β-Gal staining, the head regions of these zebrafish were also quantified for mean grey value (Figure 3.12A, B). A sample of 35 fish were analysed for both their rank and mean grey value, which allowed a correlation to be drawn between the two analysis methods (Figure 3.12C). This information to assess correlation for *in situ* hybridisation techniques was not available (Figure 3.8C, D). This correlation suggested that both methods could be used to draw the same conclusion.

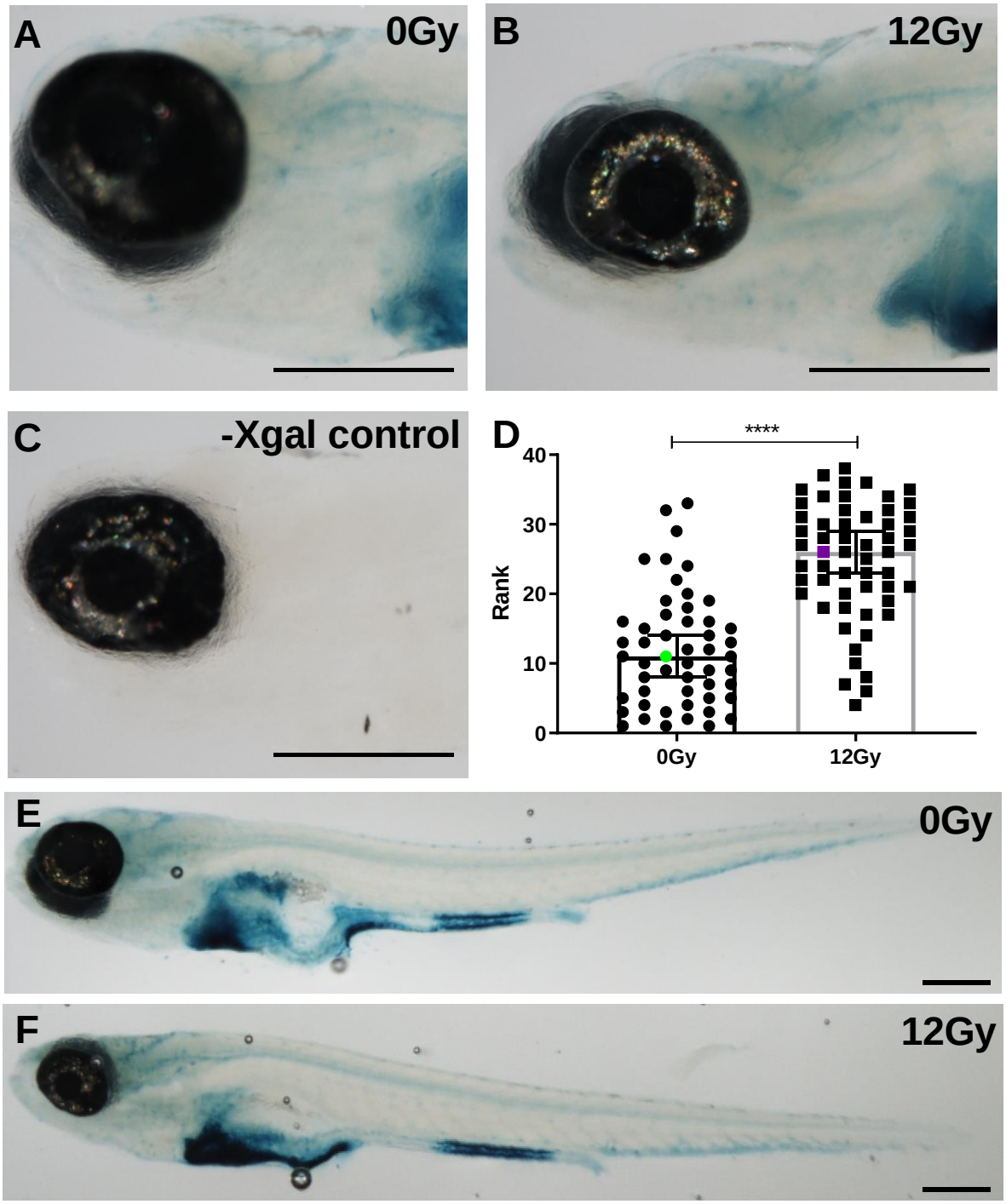

Figure 3.11. Senescence-associated β-galactosidase activity in regions of p21-positivity. Transmitted light photomicrographs of irradiated zebrafish stained for senescence-associated β-Galactosidase activity, A-C) Representative images of 3dpIR zebrafish, 0Gy (A) or 12Gy (B) irradiation at 2dpf, 12Gy fish without X-gal substrate added as negative control (C). D) Analysis of zebrafish images (11x magnification) was carried out by blinded ranking according strength of blue staining, such that the fish with the strongest staining correlated with the highest rank. E, F) Representative whole-body images (4x magnification) of 3dpIR zebrafish, 0Gy (E), or 12Gy (F) irradiation at 2dpf. Data examined with Mann-Whitney test of ranks. 15-20 fish were used for each of the three independent experiments. **** $p < 0.0001$. Scale 200μm. Error bars standard deviation.

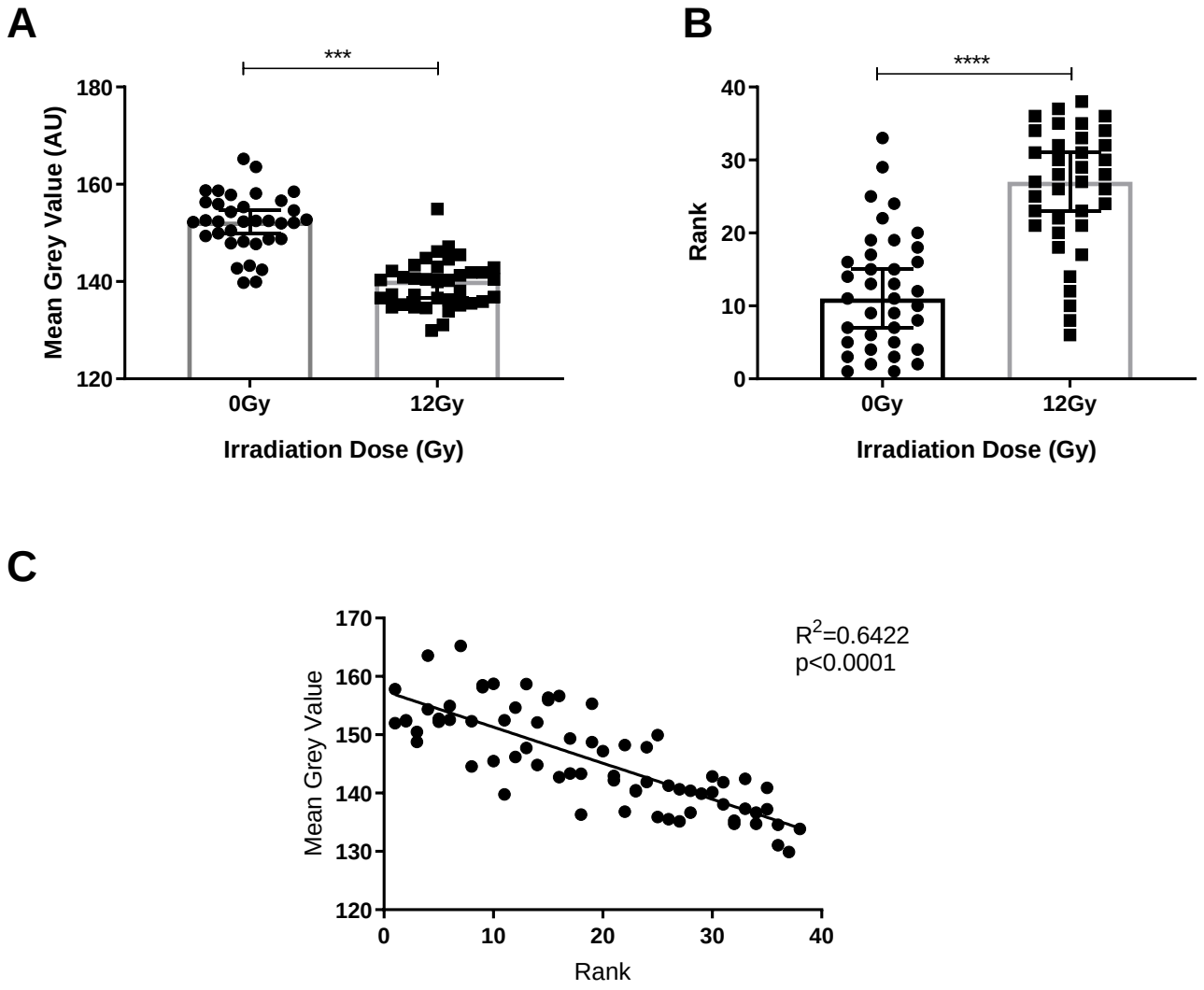

Figure 3.12. Blind ranking of SA-β-Gal staining correlataes with pixel intensity. A) Quantification of zebrafish head region by pixel intensity, whereby the darker the pixel, the lower the mean grey value. B) Quantification of by blinded ranking according strength of blue staining, such that the fish with the strongest staining correlated with the highest rank. C) Correlation of mean grey value with rank for each fish. Data examined with Mann-Whitney test, 15-20 fish were used over two independent experiments. *** $p < 0.001$; **** $p < 0.0001$. Error bars standard deviation.

3.6. Irradiated zebrafish larvae have an activated DNA damage response pathway at 3dpIR

The canonical stress-induced senescence pathway following irradiation occurs through the DNA-damage response (DDR) pathway. To provide further evidence as to whether 3dpIR zebrafish contain stress-induced senescent cells, I analysed expression of a key component of the DDR, phosphorylated γH2AX foci in the nuclei through immunofluorescence.

3.6.1. Detecting activation of γH2AX in whole mount zebrafish larvae

To first optimise detection of the DNA damage foci, I imaged the tail fin of 3dpIR zebrafish (Figure 3.13). Being the thinnest tissue in the zebrafish, it is the clearest to image, and I previously showed increased *p21* and *p16*-like mRNA expression in the tail region (Figure 3.13B). There was a dose dependent increase in the number of γH2AX positive cells in the tails of 3dIR zebrafish, but due to the number of cells imaged, maximum intensity projections proved difficult to count foci, which is a commonly used technique for determining γH2AX positive cells. Mean fluorescence intensity was instead examined (Figure 3.13C). Further, a pilot experiment was used to assess whether imaging of the head region of the zebrafish, where *p21* expression was highest could show γH2AX foci (Figure 3.14). As was seen in the tail regions, irradiated zebrafish had higher expression of γH2AX foci and quantification of single slices permitted foci counting. Now that imaging and analysis have been optimised to detect γH2AX foci in regions of irradiated zebrafish larvae that are positive for *p21* expression, an experiment using more zebrafish can be used to more robustly assess this senescence-associated protein.

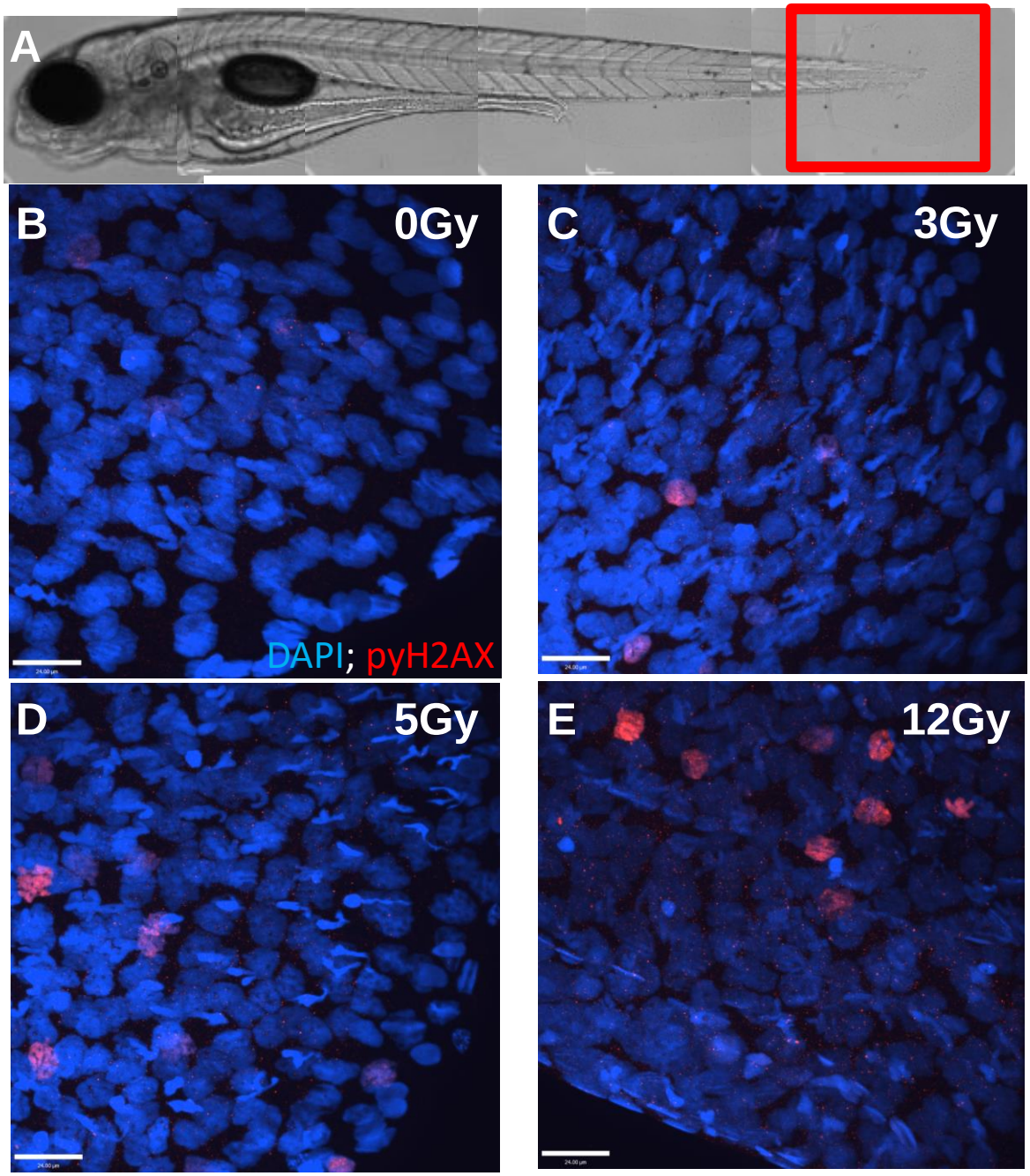
A
B
0Gy
DAPI; pyH2AX
C
3Gy
D
5Gy
E
12Gy

F

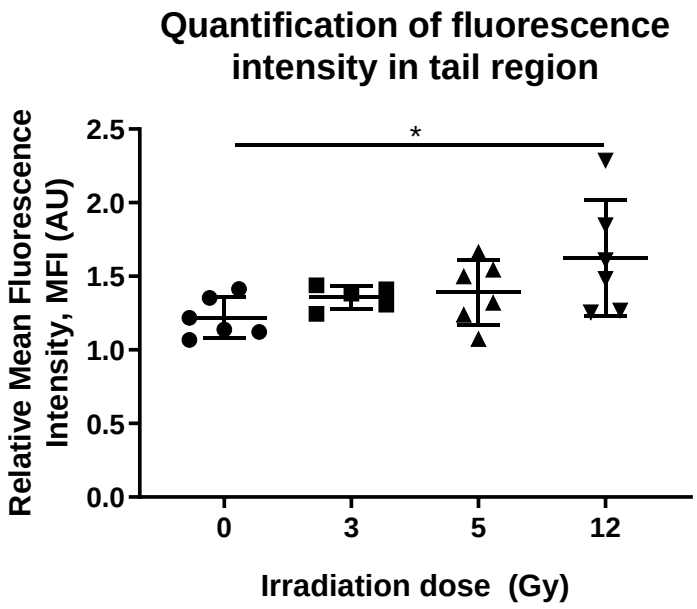
Quantification of fluorescence intensity in tail region
Relative Mean Fluorescence Intensity, MFI (AU)
2.5
2.0
1.5
1.0
0.5
0.0
*
0
3
5
12
Irradiation dose (Gy)

Figure 3.13. Pilot experiment shows imaging & quantification of zebrafish tail regions allows for detection of γH2AX positive foci in 3dpIR zebrafish larave. A) Reflected light photomicrograph of a 5 days post-fertilisation zebrafish larvae to demonstrate where imaging was first optimised in the tail fin, highlighted in red. B-D) Confocal fluorescence photomicrographs of antibody staining to detect γH2AX protein expression (red), DAPI was used to stain nuclei (blue). Example maximum intensity projections of zebrafish following 0Gy (B), 3Gy (C), 5Gy (D), 12Gy (E). Scale bar 24μM. F) quantification γH2AX expression by mean fluorescence intensity relative to secondary alone. Six fish were examined over two independent experiments. Two 3μM substacks were imaged, 10μM apart, to quantify expression. Data were examined by the Kruskal Wallace with Dunn's test for multiple comparisons, * $p < 0.05$. Scale 24μm. Error bars standard deviation.

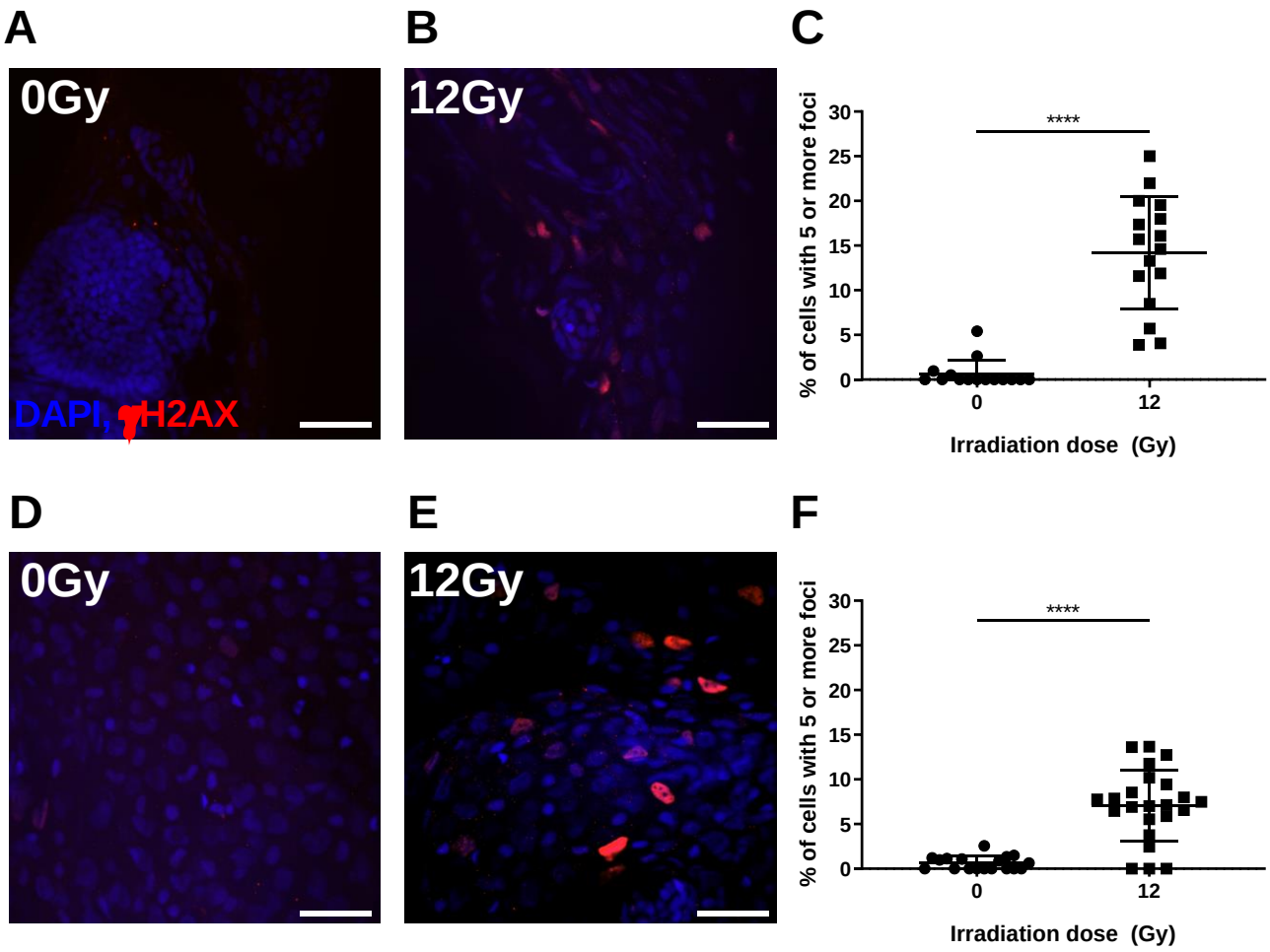

Figure 3.14. Pilot experiment shows imaging & quantification of zebrafish head regions allows for detection of γH2AX foci in 3dpIR zebrafish larave. Confocal fluorescence photomicrographs of antibody staining to detect γH2AX protein expression (red), DAPI was used to stain nuclei (blue). A - C) Analysis of lateral images of the zebrafish head. A) Example unirradiated, 0Gy, control. B) Example 12Gy image. C) percentage of cells with 5 or more foci quantified. D-F) Analysis of ventral images of the zebrafish head. D) 0Gy example E) 12Gy example F) percentage of cells with 5 or more foci quantified. Two 3μM substacks were imaged, 10μM apart, to quantify expression in four distinct regions of the zebrafish head. Data examined by unpaired t test. 18 images from two fish were used. **** $p < 0.0001$. Scale 24μm. Error bars standard deviation.

3.6.2. Irradiation activates the DNA-damage response marker γH2AX in *p21*-positive regions of 3dpIR zebrafish

To assess whether DNA damage response foci was present in regions of high *p21* mRNA expression in 3dpIR nacre-strain zebrafish, I carried out whole-mount γH2AX immunofluorescence and imaged and quantified the ventral head region of the zebrafish, where p21 expression was previously described (Figure 3.9). An increase in γH2AX positive cells following 12Gy irradiation was demonstrated (Figure 3.15). 3dpIR zebrafish showed 6.27% (SD 2.369) positive cells, whereas unirradiated fish had 0.53% (SD 0.50) at the same time point (Figure 3.15D). As the 5dpf zebrafish head is a thick tissue and contains many cells, I would envisage that confocal imaging of this region would prove difficult to pick up DNA-damage foci themselves, as well as brightly positive cells, and so the true percentage of positive cells is likely under-represented through this whole mount imaging method.

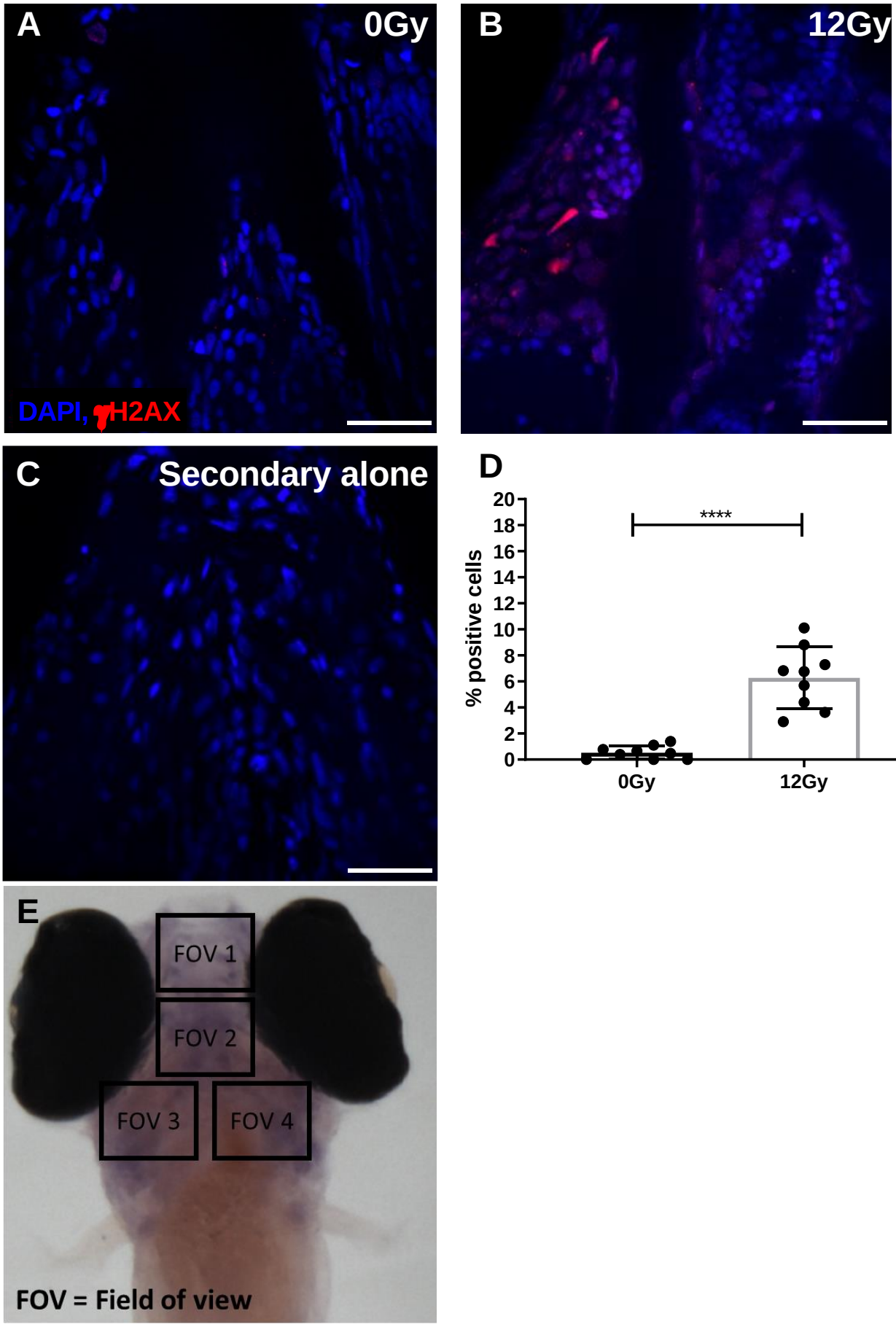
A
0Gy
DAPI, γH2AX
B
12Gy
C
Secondary alone
D
% positive cells
20
18
16
14
12
10
8
6
4
2
0
****
0Gy
12Gy
E
FOV 1
FOV 2
FOV 3
FOV 4
FOV = Field of view

Figure 3.15. Upregulation of γH2AX DNA damage-associated foci in irradiated zebrafish larvae. Confocal fluorescent photomicrographs of antibody staining to detect γH2AX protein expression (red), DAPI was used to stain nuclei (blue). Representative images of pγH2AX antibody staining (red) in the ventral zebrafish head regions (40x magnification). A) 0Gy, B) 12Gy, C) Control in 12Gy irradiated zebrafish with only the secondary antibody. E) Quantification of pγH2AX immunofluorescence. The % of positive (red) cells were plotted for each image. 4 Fields of view (FOV), and 3 substacks were quantified within each FOV were quantified. 3 fish were examined for each of the three independent experiments. E) Diagram of areas imaged per fish. Data was examined by Mann-Whitney test. **** $p < 0.0001$. Scale 24μm. Error bars standard deviation.

3.7.2. RNA from whole irradiated zebrafish larvae shows up-regulation of some but not all SASP factors

By assessing genes that are both up-regulated following irradiation-induced senescence and present in zebrafish, I was able to better assess the senescence profile of 3dpIR zebrafish larvae, including the SASP (Appendix table 3.9.1). Primers were optimised to detect mRNA expression of SASP factors *il1b, il6, il8a, mmp2, mmp9, mmp13,* as well as *p53*, a central regulator of the DDR and senescence induction, and *cyclin g1*, an indicator of reduced proliferation that is associated with senescence. In whole zebrafish mRNA, the SASP factor *mmp2* showed a significant increase, more than doubling following irradiation. Significant increases in p53 and cyclin G1 were also seen following irradiation, further evidencing activation of the DNA damage response, and that less cells are proliferating and instead in G1 phase of the cell cycle (Figure 3.16). The other SASP factors examined however showed no detectable change in mRNA expression (Figure 3.16 A, B, D, E). Interestingly, one independent experiment showed increased expression of *il1, mmp9,* and *mmp13* (Figure 12H). The reason for this pool of 50 3dpIR zebrafish larvae to have high expression is not known, but as this effect is specific to some genes and not others, there may have been a compounding factor that induced inflammation in some fish within this group.

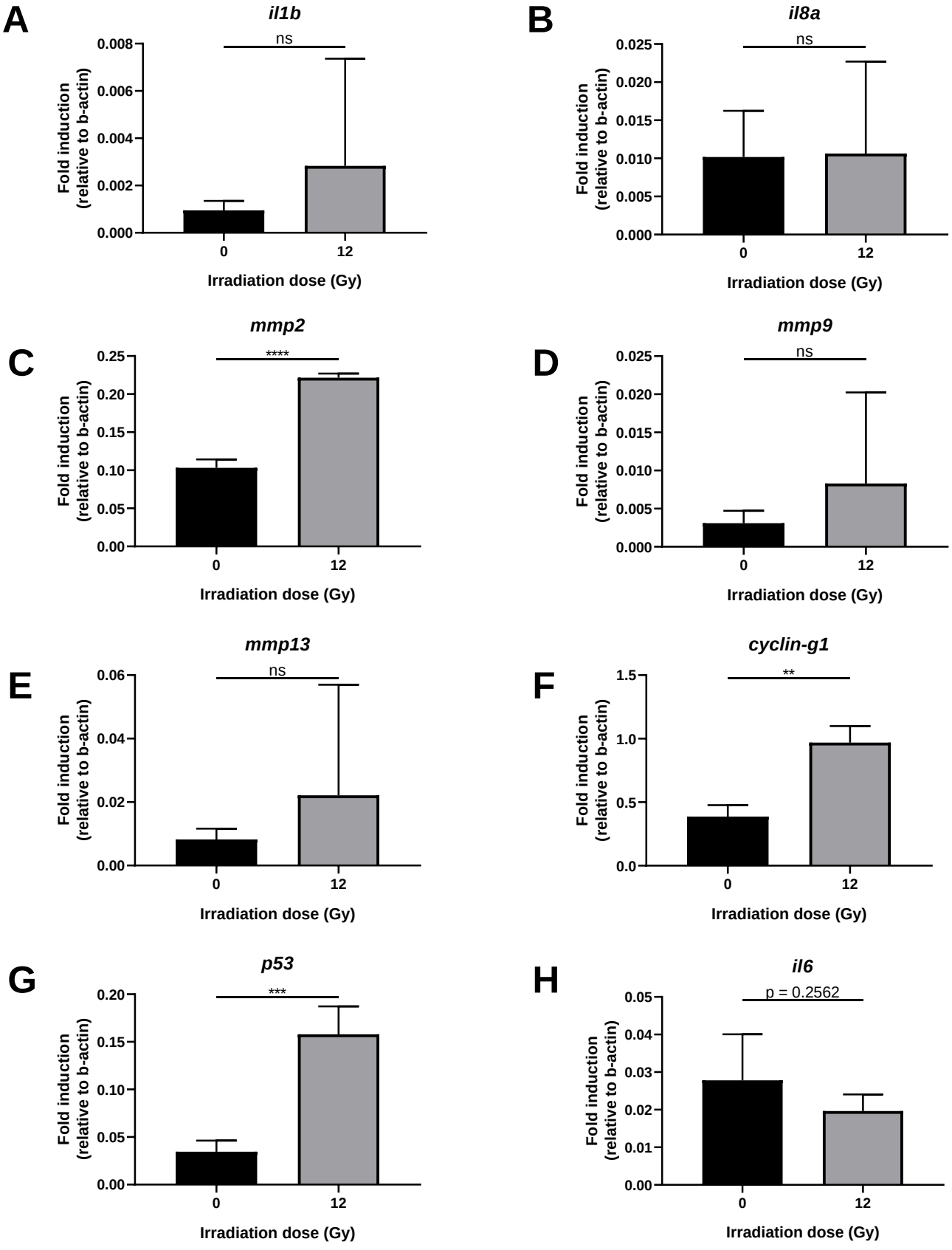
A
il1b
ns
0.008
0.006
0.004
0.002
0.000
Fold induction (relative to b-actin)
0
12
Irradiation dose (Gy)
B
il8a
ns
0.025
0.020
0.015
0.010
0.005
0.000
Fold induction (relative to b-actin)
0
12
Irradiation dose (Gy)
C
mmp2
****
0.25
0.20
0.15
0.10
0.05
0.00
Fold induction (relative to b-actin)
0
12
Irradiation dose (Gy)
D
mmp9
ns
0.025
0.020
0.015
0.010
0.005
0.000
Fold induction (relative to b-actin)
0
12
Irradiation dose (Gy)
E
mmp13
ns
0.06
0.04
0.02
0.00
Fold induction (relative to b-actin)
0
12
Irradiation dose (Gy)
F
cyclin-g1
**
1.5
1.0
0.5
0.0
Fold induction (relative to b-actin)
0
12
Irradiation dose (Gy)
G
p53
***
0.20
0.15
0.10
0.05
0.00
Fold induction (relative to b-actin)
0
12
Irradiation dose (Gy)
H
il6
p = 0.2562
0.05
0.04
0.03
0.02
0.01
0.00
Fold induction (relative to b-actin)
0
12
Irradiation dose (Gy)

Figure 3.16. mRNA expression of alternative senescence-associated genes by qRT-PCR. Zebrafish were irradiated at 2 days post-fertilisation (2dpf) and assessed for the senescence markers *il1b* (A), *il8* (B), mmp2 (C), *mmp9* (D), *mmp13* (E), *cyclin g1* (F), *p53* (G) *il6.* Absolute expression change calculated by 2^-ΔCt. RNA was collected from 50 pooled zebrafish for each of the 4 independent experiments that were carried out. Data was examined by Mann-Whitney test (A,B,D,E) or unpaired T test (C,F,G). ** $p < 0.01$; **** $p < 0.0001$. Error bars represent standard deviation.

3.8. Conclusion and chapter discussion

In this chapter, I have established a method for ectopically inducing markers of senescence in early development zebrafish without causing significant toxicity or lethality. By studying expression of key senescence genes and proteins following γ-irradiation, I have characterised for the first time that 12Gy irradiation can activate numerous markers of senescence in 5dpf zebrafish larvae. I demonstrated that irradiation of zebrafish larvae shows a dose-dependent increase in cyclin-dependent kinases *p21* and *p16-like* within 24 hours and remains elevated until the latest time-point examined*,* 5dpf (3dpIR). In the case of *p21,* mRNA is predominantly located in the head and intestinal regions. Most notably, my work has begun to dissect a novel model to rapidly induce and assess an *in vivo* hallmark of ageing and age-associated disease, the accumulation of senescent cells. As this assay only takes 5 days to see these senescence markers, this system could be amenable to *in vivo* drug screening for novel senolytics. I have identified that within this timeframe, there is activation of the canonical senescence-induction signalling pathway, the DNA damage response, cell cycle inhibitors are increased, as well as SA-β-Gal activity, and some but not much SASP activation. I now have significant evidence to support the development of a transgenic reporter for cellular senescence, which could allow unprecedented access to this phenotype that is causal to age-associated multimorbidity.

The assay to induce rapid *in vivo* senescence accumulation uses 12Gy of Cs^{137} γ-Irradiation on 2dpf zebrafish, before assessing the onset of senescence markers at 5dpf. The timing and dose was optimised based on a balance between being a high enough dose and early enough time point such that it can be tolerated by the zebrafish without severely disrupting off-target developmental mechanisms that could reduce the reliability of the assay. The dose and times assessed were based on previous evidence of zebrafish embryo survival following irradiation. For example, zebrafish embryos between 2 and 8hpf show significant sensitivity to radiation doses between 2 and 10Gy (McAleer *et al.,* 2005). Irradiation at 24hpf showed a reduction in survival at 10Gy only, suggesting that the zebrafish become more resistant to radiation with age. Additionally, 1dpf zebrafish embryos irradiated with 20Gy showed a significant reduction in survival by 5dpf, which is demonstrated in this study (Daroczi *et al.*, 2009). A dose of 8Gy of total body irradiation dose is typically used to induce senescence in mice (Demaria *et al.,* 2014). A reason for the higher dose of 12Gy being tolerated in zebrafish larvae may be because only a shorter time after irradiation was examined, though this was important to make the senescence-induction assay rapid and therefore more amenable to *in vivo* compound screens for senolytics. Additionally, zebrafish have been extensively studied in the context of regenerative medicine as they are better than mammals at recovering from injuries such as heart transections (Poss, Wilson and Keating, 2002). In the context of irradiation, it is not clear whether zebrafish have improved DNA repair mechanisms compared to mammals. Though, a study comparing the ability of zebrafish to repair UV-induced DNA lesions with humans suggested they were able to tolerate a higher dose (Sussman, 2007). However, this data was obtained by comparing an assay to assess DNA repair capacity human peripheral blood cells with an assay using whole zebrafish embryos (Athas *et al.,* 1991). The comparison therefore is strenuous, statistical analysis could not be performed and there was no matching of cell type and age, which are both contributing factors to the DNA damage response and repair capacity (Song *et al.,* 2005; Probin *et al.,* 2006; Gorbunova *et al.,* 2007). More in-depth comparisons between zebrafish and mammalian DNA repair capacity would prove useful for understanding the similarities of the DNA damage response between the two organisms. Importantly for this study, the dose optimised for senescence induction in irradiated zebrafish larvae

does not reduce survival in the time-points examined, and are relatively comparable with previously published evidence.

Senescence can be a difficult phenotype to identify *in vivo,* as there is no marker that will always identify the phenotype specifically. Following irradiation of zebrafish larvae, I identified markers that indicated activation of central DNA-damage response, the pathway known to prompt stress-induced senescence (γH2AX, p53). Though it is associated with senescence, an important limitation of γH2AX is that it can also be present during DNA replication (Sedelnikova *et al.*, 2004; Gagou, Zuazua-Villar and Meuth, 2010). To overcome this in mammals, researchers often use another marker of the DNA damage response such as 53BP1 in combination with γH2AX (Ward *et al.,* 2003). However, the antibodies for both of these markers for zebrafish are raised in the same species, and so cannot be used together without difficulty (Henriques *et al.*, 2013; Percival *et al.*, 2015). Further, both p53 and γH2AX can play a role in cell death mechanisms, and so in future it would be useful to carry out assays for markers of apoptosis like caspase 3 or TUNEL alongside senescence markers to discount these cells when quantifying senescence burden in irradiated zebrafish (Rogakou *et al.*, 2000; Haupt *et al.*, 2003; Sorrells *et al.*, 2013). Importantly though, irradiated zebrafish larvae also show up-regulated cyclin-dependent kinase inhibitors $p21^{Waf1}$ and $p16^{Ink4a}$, both of which have been described as negative regulators of apoptosis (Bissonnette and Hunting, 1998; Sviderskaya *et al.*, 2003). These genes inhibit cyclin-dependent kinases and alongside cyclin g1 can help arrest the cell cycle, a key component of senescence (Kimura *et al.*, 2001; Suzuki *et al.*, 2001). Regardless, even if senescent cells were induced in irradiated zebrafish larvae, the evidence does not show whether apoptosis is also present. $P16^{Ink4a}$, though a well described and commonly used senescence marker, is also part of a reversible response in macrophages that does not seem related to senescence, but instead class switching to M2-type macrophages in response to nearby senescent cells (Hall *et al.,* 2017, Liu *et al.,* 2019). Additionally, *p21* has shown regulation by the circadian clock, which I also demonstrated (Figures 3.5 & 3.6), and may be up regulated in quiescent cells that do not become senescent (Laranjeiro *et al.,* 2013; Sang *et al.,* 2008). To tackle this, I intend to examine senescence marker expression at a later time point following irradiation to validate whether *p21* cells persist and are therefore more likely senescent (Sang *et al.,* 2008). This would also be useful in the context of the SASP, as the majority of work published around irradiation-induced senescence in mice suggests that a 6-10 day period post-irradiation are required for strong expression of SASP markers such as IL6 and IL8 (Demaria *et al.,* 2014; Laberge *et al.,* 2015; Freund *et al.,* 2011; Acosta *et al.,* 2008). This would likely explain why only *mmp2* up-regulation at 3-days post-irradiation in zebrafish larvae (Figure 3.15). One could argue that if the SASP were greater at a later time-point in irradiated zebrafish larvae, then this would validate the model organism, because the temporal regulation of senescence marker induction would be comparable with mammalian systems. Moreover, with more time a more in-depth assessment of the SASP profile would bolster the current evidence of senescence in irradiated zebrafish larvae (Table 3.1). Antibody arrays and RNAseq that are comparable to data from mammalian systems would describe in greater detail the similarities and differences in irradiated zebrafish larvae (Coppé *et al.,* 2008; Coppé *et al.,* 2011; Demaria *et al.,* 2014; Purcell *et al.,* 2014; Wiley *et al.,* 2017). The limitations of *in vivo* markers of senescence mean that assessing a panel of them provides the most confidence that senescence is truly present. A strength of the

current evidence is that multiple of the aforementioned markers of senescence (γH2AX, SA-β-gal, *p21*) were present within the same regions of the fish. Further, previous evidence assessing senescence induction in zebrafish larvae was limited to SA-β-Gal, which is not required for senescence (Lee *et al.,* 2006; Koshimizu *et al.,* 2011; Kishi *et al.,* 2008). The markers identified in irradiated zebrafish larvae are comparable with mammalian systems, with the exception of IL6 (Demaria *et al.,* 2014; Fuhrmann-Stroissnigg *et al.,* 2017). Now, there is enough evidence to support the development of a transgenic reporter of senescence, which would allow assessment of multiple senescence markers at the cellular level through cell sorting.

Irradiated zebrafish larvae show senescence in some regions that have been highlighted in irradiated murine systems, providing evidence to support the notion that this model system can be used to understand mammalian senescence. The regions of the 3dpIR zebrafish larvae with the greatest up-regulation of *p21* mRNA following irradiation were the intestinal and head regions, particularly the pharyngeal arches and brain regions, which are highly proliferative regions during early development (Wallace *et al.*, 2005; Hall and Tropepe, 2018). Highly proliferative cells would be more likely to have encountered irradiation-induced DNA damage through reaching the relevant cell cycle checkpoints (Weinert and Hartwell, 1988). Zebrafish with mutated telomerase also showed up-regulated *p21* expression in the intestine faster than wild-type siblings (Henriques *et al.,* 2013). Increases in SA-β-Gal activity were also described in the intestine, head kidney and testes of these mutant zebrafish. The testes are not present in 5dpf zebrafish larvae, and though there are functioning pronephros, the head kidney is also not fully developed and so neither can be examined at these stages (Orban, Sreenivasan and Olsson, 2009; Gerlach and Wingert, 2013). Irradiated mice also show senescent cells in the brain and small intestine, as was described in irradiated zebrafish larvae (Oanh N.L. Le *et al.*, 2010; Demaria *et al.*, 2014; Zhao *et al.*, 2019). Expression of DNA damage markers were present in the liver, kidney, brain and lungs as early as 24 hours after irradiation and persisted for 45 weeks, which was the latest time point examined. However, p16 expression was not reliably detected until 12 weeks after irradiation (Oanh N.L. Le *et al.*, 2010). It is worth noting that these murine studies were carried out at adult stages, and a much longer period after irradiation (10 months for small intestine) was used before assessing senescence marker onset in these organs, which is a possible reason for the differences described. Additionally, as irradiated zebrafish larvae are in early development, they are rapidly proliferating and as such could alter the sensitivity of different tissues to irradiation (Sugiyama *et al.*, 2009). Increased SA-β-Gal activity was detected in the skin of irradiated adult zebrafish (Tsai *et al.,* 2007). This was not directly examined in zebrafish larvae, though as a similar induction of *p21* mRNA by qPCR in their tail fin compared to mRNA of the whole zebrafish, this may be due to expression in the skin (Figure 3.4B). A comparison of where senescent cells are seen in irradiated zebrafish larvae, irradiated adult zebrafish, and old wild-type aged zebrafish would provide important evidence about organ-sensitivities to stress-induced senescence. However, the initial similarities in the sensitivity of the brain and intestine to irradiation in zebrafish larvae compared adult zebrafish and mice are promising and provoke more in-depth studies.

An important difference between irradiated zebrafish larvae and adult mammalian systems is that *p16-like* was not a very reliable reporter of senescence. The zebrafish orthologue for P16 (*CDKN2A)*, *p16*-like *(cdkn2ab)*, showed significant transcriptional activation by qPCR, but there was not reliable spatial expression by *in situ* hybridisation. This may be due to resolution of the technique compared to qPCR, which would be able detect smaller changes in expression. Indeed, relative mRNA expression at 3 days post-irradiation (dpIR) for *p21* was 0.07 (Figure 3.5C), whereas *p16*-like was approximately 0.002 (Figure 3.5D). This low level of expression would probably be difficult to detect by *in situ* hybridisation. An alternative explanation for low transcript levels aside from low expression is low transcript stability; however, a recent study on mammalian *P16* showed that the mRNA had a half-life of over 24 hours (Liu *et al.,* 2019). This is unusually long, longer than >95% of mRNA transcripts, and further emphasises that expression of zebrafish *p16-like* is very low in 3dpIR, and perhaps *p21* may prove a more reliable reporter in this context. This disparity in *p16*-like expression may be due to a lack in our understanding of the zebrafish orthologue of *P16*. In mammals, there are separate loci for $p16^{INK4A}$ (*CDKN2A*) and p15 (CDKN2B), as well as a splice variant in the *CDKN2A* locus for the protein $p19^{ARF}$ (ZFIN, 2019; Zerbino *et al.*, 2018). However, in zebrafish, there is seemingly no splice variant in the *cdkn2a* locus for *p16*, and no identified *cdkn2b* locus. Therefore, it is feasible that the zebrafish orthologue may be carrying out roles that the mammalian p15 and p19 genes are doing. Both of these genes are involved in cell cycle arrest in mammals, much like p16, but it has been shown that inactivation of p19 can exacerbate senescence in a BUBR1 mutant mouse (Baker *et al.*, 2008). It is not clear currently how zebrafish *p16-like* gene functions in comparison to mammalian *p16,* and requires further characterisation. Though, a CRISPR knockdown of the zebrafish gene does result in tumour formation, one could infer that the gene could therefore play a role in the anti-tumour function of senescence, as is known in mammals, but it was not directly examined (Ablain *et al.,* 2018). As I have described increased expression following irradiation of larvae, this further shows that the gene may have a conserved role in senescence. Timing may also be a factor, as mentioned, irradiated mice are often left for much longer until increases in P16 are described (Oanh N L Le *et al.*, 2010; Demaria *et al.*, 2014). Therefore, examining this gene at a later time point could help discern whether this is an important factor. Due to these factors, *p21* is our best senescence-associated gene to develop a transgenic reporter for live detection of potentially senescent cells in zebrafish larvae. Certainly, single-cell RNA sequencing on serum-starved quiescent human cells versus bleomycin-induced senescent cells, identifying the genes most reliably activated in senescence (Wiley *et al.,* 2017). *CDKN1A* (P21) was one of the best, predicting senescence over quiescence 89% of the time. As *p21* is not unique to senescence, like all other senescence-associated genes, an assessment of how reliable *p21* is as a reporter of senescence at the cellular level is vital in this system, and can be carried out once the transgenic reporter is developed.

Whilst identifying markers of senescence that are up-regulated following irradiation in zebrafish larvae, I also identified that some of these genes showed expression in normally developing unirradiated controls. For example, irradiation-independent activity of SA-β-Gal was observed in the intestine and caudal hematopoietic tract (CHT), in a pattern that matched previous evidence in a wild-type 4.5dpf zebrafish (Kishi *et al.,* 2008). SA-β-Gal Intestinal expression could be due to detecting a different type of beta-galactosidase activity, with it also being a digestive enzyme, and expression in the gastrointestinal tract of SA-β-Gal has been identified in humans (Gray and Santiago, 1969; Going *et al.*, 2002). The SA-β-Gal assay is not run at the optimal pH to detect this type of galactosidase activity, however that does not necessarily mean it will not be detected at all. The CHT is where innate immune cells, such as neutrophils and macrophages are formed and reside during early zebrafish development (Murayama *et al.*, 2006). There has been recent evidence suggesting that SA-β-Gal can be present in some macrophages that are likely not senescent, so this may be what is shown in these zebrafish larvae (Hall *et al.,* 2016; Hall *et al.,* 2017; Liu *et al.,* 2019). However, the a-specificity of SA-β-Gal is well described and should be considered when inferring this evidence (Lee *et al.,* 2006; Untergasser *et al.,* 2003). Additionally, p*21* also showed some irradiation-independent expression in developing zebrafish larvae. There is evidence of circadian clock-regulation of *p21* (Laranjeiro *et al.,* 2013). This may be an evolutionary response to slowing the cell cycle to avoid DNA-damage from UV radiation following sunrise, as a temporary quiescence (Dakup and Gaddameedhi, 2017). Importantly for our assay, I needed to choose a time-point to assess senescence such that the fold increase of *p21* is the true increase following irradiation and not an over-representation by altered background levels. There may be a case for *p21* expression due to embryonic senescence being present at these stages of development also. For example, SA-b-Gal expression was demonstrated in the developing chick embryo pharyngeal arches and gut endoderm (Storer *et al.,* 2013), which are regions where I also see expression, particularly *p21* (Figure 3.9). The development of a transgenic reporter for *p21* would allow for assessment of the differences between those *p21*-positive cells from irradiation and those present in irrespective of radiation. If there are brighter cells with more *p21* expression following irradiation, which the *in situ* hybridisation would suggest (Figure 3.9), then one could use unirradiated transgenic zebrafish to set a threshold upon which irradiated transgenic zebrafish are imaged, to only include those most likely associated with stress-induced senescence. If there are actually developmental senescent cells in the zebrafish, and I could distinguish between developmental and irradiation-induced senescence by sorting *p21* positive cells from irradiated and non-irradiated zebrafish, this could also provide a unique opportunity to identify differences between the two contexts. Due to this, it is still worthwhile using *p21* as a transgenic reporter for potentially senescent cells.

3.8.5 Future work and conclusions

I have identified that, as is described in mammals, irradiation can up-regulate multiple markers of senescence in zebrafish larvae. This evidence permits the development of a transgenic reporter for senescence, like the p16-3MR mouse model (Demaria *et al.,* 2014), but with the advantage of being in a transparent organism. This will allow us to identify potentially senescent cells live and *in vivo,* sort them by flow cytometry, and validate several of these markers in the same cell to give a true representation of the number of senescent cells in irradiated zebrafish larvae. This will give us a better understanding of how good *p21* is as a marker of senescence in our system, and perhaps the kinetics of its promoter activation *in vivo* following senescence induction. This method of assessing senescence will have much greater resolution than simply extracting RNA from a whole zebrafish for example, which will dampen the signal of senescent cells by also including RNA from non-senescent cells. This is particularly important when looking relatively early after irradiation, to assess small changes in genes such as those associated with the SASP. Further, because of the technical difficulties of quantifying H2AX staining in thick tissues, this method will give a more accurate read of the proportion of cells are truly senescent, and allow us to combine immuno-fluorescent antibodies more accurately, such as PCNA as a marker for proliferation. Once validated, this zebrafish reporter for senescence could allow for live identification of potentially senescent cells at the cellular level *in vivo* within a 5-day period, something that has not been previously possible. Potential benefits of this include a novel system for identification of senescence-modulating compounds that show efficacy *in vivo* in the first instance, something that would likely streamline the drug development process and help speed up the identification of drugs that could reduce the prevalence of ill health in our rapidly growing elderly population. As I have demonstrated that it is feasible to increase the amount of senescence in zebrafish through irradiation, it does not seem far-fetched to assume that drugs that are effective at removing senescent cells can be assessed within this system. This level of resolution could also allow depicting the kinetics of senescence genes following irradiation, examining tissues and cell types that they interact with, tackling questions in the field such as mechanisms for immune cell senescence clearance.

3.9. Appendix

3.9.1. Table of SASP factors induced by irradiation

SASP Factor	Induction method	Dose/method	Model used[reference]	Analysis technique	Change in expression (fold)
IL6	Irradiation	10Gy (X-ray) 12Gy Xray[22]	MEFs [1/22]	qRT-PCR / Antibody array / secreted protein level	Increase (>4 fold) 32 fold (secreted protein level)
			HCA2 [2, 3] HCA2, IMR90 [20], WI38 [7/8/9/12/16]		
		7Gy TBI (X-ray)	Mouse [1]	qRT-PCR	Increase
	Tissue injury	Full-thickness punch biopsy	Mouse [1]	qRT-PCR	No change
	Replicative exhaustion	*In vitro* population doubling	HCA2/IMR90/WI38 [2,3] Primary mouse lung fibroblasts [6] Various cell lines [7/8/9/12]	ELISA	Increase (>4 fold)
	Oncogene-induced	Lentiviral RASV12/MKK6EE overexpression RAS/MEK overexpression	HCA2 [2, 3] Various cell lines [7/8/9/12]	ELISA	*Assumed* increase (decrease following rapamycin)
	Oxidative stress	50uM Bleomycin 40uM Bleomyci	IMR90[5] BJ & HCA2[21]	Single cell qPCR ELISA	Increase
		250nM Doxorubicin, 24h	HCA2 [2]	ELISA / cytokine array	Assumed increase (decrease following rapamycin)
		75uM H2O2	CD1 mouse lung fibroblasts [6]	Cytokine array	Increase
IL1A	Irradiation	10Gy (Xray)	HCA2[2, 3] Various cell types [7/8/9/11] IMR90[20]	qPCR/antibody array/secreted cytokine levels	Increase (>4 fold)
	Oxidative stress	50uM Bleomycin 40uM Bleomycin	IMR90[5] BJ & HCA2[21]	Single cell qPCR Western blotting	Increase
		75uM H2O2	Primary mouse lung fibroblasts [6]	Cytokine array	Increase
	Replicative exhaustion	*In vitro* population doubling	Primary mouse lung fibroblasts [6]	Cytokine Array	Increase
	OIS	RAS/MEK	IMR-90, HCA2, PrECs, BPH1, RWPE1, PC3 [7/8/9/11]	Secreted protein level	Increase (>4 fold)

SASP Factor	Induction method	Dose/method	Model used[reference]	Analysis technique	Change in expression (fold)
IL1B	Irradiation	10Gy (Xray)	HCA2[2] IMR-90, HCA2, WI-38, BJ, PrECs, BPH1, RWPE1, PC3 [8/9/11] IMR90[20]	qPCR Secreted protein level	Increase (4 fold)
	Oncogene-induced	Lentiviral RASV12 RAS	HCA2 [3] IMR-90, HCA2, WI-38, BJ, PrECs, BPH1, RWPE1, PC3 [8/9/11] Mouse hepatocytes (*in vivo*)[24]	Antibody array	Increase
	Oxidative stress	50uM Bleomycin	IMR90[5] IMR-90, HCA2, WI-38, BJ, PrECs, BPH1, RWPE1, PC3 [8/9/11]	Single cell qPCR	Decrease
		75uM H2O2	Primary mouse lung fibroblasts [6]	Cytokine array	Increase (4x greater than replicative)
	Replicative exhaustion	*In vitro* population doubling	Primary mouse lung fibroblasts [6]	Cytokine Array	Increase
IL8	Irradiation	10Gy (Xray)	HCA2 [2, 3] IMR90, WI38, HCA2 [16]	Antibody array ELISA qPCR	Increase (>4 fold)
	Oncogene-induced	Lentiviral RASV12	HCA2 [3]	Antibody array	Increase
	Oxidative stress	50uM Bleomycin	IMR90[5]	Single cell qPCR	Increase
IL7	Irradiation	10Gy (Xray)	IMR-90, HCA2, WI-38, BJ [7/8/16]	Antibody array	Increase (>4 fold)
	Oncogene-induced	RAS			
	Replicative exhaustion				

SASP Factor	Induction method	Dose/method	Model used[reference]	Analysis technique	Change in expression (fold)
IL12	Replicative exhaustion	*In vitro* population doubling	Primary mouse lung fibroblasts [6]	Cytokine Array	Increase (10x more than oxidative stress)
	Oxidative stress	75uM H2O2	Primary mouse lung fibroblasts [6]	Cytokine array	Increase
IL13	Irradiation	10Gy Xray	HCA2, WI38 [7/8/16]	Antibody array	Increase (>4 fold)
	Oncogene-induced	RAS			
	Replicative exhaustion				
MMP3	Irradiation	10Gy (X-ray)	MEFs [1] IMR-90, HCA2, WI-38, BJ [8/9/11/13]	qRT-PCR	Increase (7 fold)
		7Gy TBI (X-ray)	Mouse [1]	qRT-PCR	Increase (4 fold)
	OIS	RAS/MEK	WI-38, BJ [8/9/11/13]	Secreted protein level	Increase (>4 fold)
	Replicative exhaustion	*In vitro* population doubling	WI-38, BJ [8/9/11/13]	Secreted protein level	Increase (>4 fold)
	Ageing	Age-associated human IPF	Human IPF biosections[20]	Microarray	Increase
MMP2	Irradiation	10Gy (X-ray)	IMR-90[20]	Secreted protein level	Increase (8 fold)
	Oxidative stress	50uM Bleomycin	IMR90[5] (PSC27, PSC31, and PSC32)[10]	Single cell qPCR	Increase
				Secreted protein level	Increase (>4 fold)
	Replicative exhaustion	*In vitro* population doubling	(PSC27, PSC31, and PSC32)[10]	Secreted protein level	Increase (>4 fold)
	Ageing	Age-associated human IPF	Human IPF biosections[20]	Microarray	Increase

SASP Factor	Induction method	Dose/method	Model used[reference]	Analysis technique	Change in expression (fold)
MMP12	Irradiation	10Gy (Xray)	HCA2 [2] IMR-90, HCA2, WI-38, BJ, hepati c myo broblasts [8/9/14] IMR90[20]	ELISA / Secreted protein level	Increase (4-8 fold)
	Oxidative stress	Etoposide	IMR-90, HCA2, WI-38, BJ, hepati c myo broblasts [8/9/14]	Secreted protein level	Increase (>4 fold)
		Bleomycin 2 U /kg (Aerosolized intratracheal instillation)	Fibroblasts, epithelial, and endothelial cells from whole mouse lung (*in vivo*)[20]	Flow & RT-PCR	Increase (500 fold)
	Ageing	Age-associated human IPF	Human IPF biosections[20]	Microarray	Increase
MMP13	Irradiation	10Gy (Xray)	IMR-90, HCA2, WI-38, BJ, hepati c myo broblasts [8/9/14]	ELISA / Secreted protein level	Increase (>4 fold)
	Oxidative stress	Etoposide	IMR-90, HCA2, WI-38, BJ, hepati c myo broblasts [8/9/14]	Secreted protein level	Increase (>4 fold)
	Ageing	Age-associated human IPF	Human IPF biosections[20]	Microarray	Increase
Lamin B1	Irradiation	10Gy X-ray 12Gy X-ray	MEFs [1, 22] HCA2, BJ [18] WI38[18]	qRT-PCR / Western blotting	Decrease (10 fold)
	Tissue injury	Full-thickness punch biopsy	Mouse [1]	qRT-PCR	Decrease (2 fold)
	Oxidative stress	50uM Bleomycin	IMR90s[5]	Single cell qPCR	Decrease
	Replicative exhaustion	>70 population doublings	HCA2[18]	Western blotting	Decrease
	Oncogene-induced senescence	MKK6EE overexpression	HCA2[18]	Western blotting	Decrease
HMGB1	Irradiation	8Gy	BJ & MEFs[19]	Flow	Decrease
	Oxidative stress	50uM Bleomycin Etoposide (20/50uM	IMR90s[5] BJ & MEFs [19]	Single cell qPCR Flow	Decrease (leaving nucleus)
	Oncogene-induced senescence	RAS	MEF injected to NUDE mice [19]	Flow	Decrease
	Replicative senescence	*In vitro* population doubling	Aged mice [19]	Flow	Decrease

SASP Factor	Induction method	Dose/method	Model used[reference]	Analysis technique	Change in expression (fold)
TNF-alpha	Irradiation	10Gy (Xray)	HCA2 [3]	Antibody Array	Increase
	Oxidative stress	75uM H2O2	Primary mouse lung fibroblasts [6]	Cytokine array	Increase (4x greater than replicative)
		Bleomycin 2 U /kg (Aerosolized intratracheal instillation)	Fibroblasts, epithelial, and endothelial cells from whole mouse lung (*in vivo*)[20]	Flow & RT-PCR	Increase (between 2-5 fold)
	Replicative exhaustion	*In vitro* population doubling	Primary mouse lung fibroblasts [6]	Cytokine Array	Increase
pNF-kappaB	Irradiation	10Gy (Xray)	HCA2 [2]	qPCR	Increase
		6Gy (Xray)	MDA-MB-231-2A cells [17]	Western blot	Increase
PDGF-A	Irradiation	10Gy (X-ray)	MSFs/MECs [1]	qRT-PCR/ELISA	Increase (2/3 fold)
	Tissue injury	Full-thickness punch biopsy	Mouse [1]	qRT-PCR	Increase (12 fold)
	Ageing	Age-associated human IPF	Human IPF biosections[20]	Microarray	Increase
PAI-1	Tissue injury	Full-thickness punch biopsy	Mouse [1]	qRT-PCR	Increase (2 fold)
	Replicative Exhaustion	*In vitro* population doubling	IMR-90, BJ, JAS-3, HUVEC [15]	Secreted protein level	Increase (>4 fold)
	Oxidative stress	Bleomycin 2 U /kg (Aerosolized intratracheal instillation)	Fibroblasts, epithelial, and endothelial cells from whole mouse lung (*in vivo*)[20]	Flow & RT-PCR	Increase (between 2-5 fold)
	Irradiation	10Gy Xray	IMR90[20]	Secreted protein level	Increase (60 fold)
CCL5	Tissue injury	Full-thickness punch biopsy	Mouse [1]	qRT-PCR	Increase (2 fold)
CCL2	Tissue injury	Full-thickness punch biopsy	Mouse [1]	qRT-PCR	Increase (2 fold)
	Irradiation	10Gy (Xray)	HCA2 [2]	qPCR	Increase
	Oxidative stress	50uM Bleomycin	IMR90 [5]	Single cell qPCR	Increase
CCL7	Irradiation	10Gy (Xray)	HCA2 [2]	Antibody array	Increase
CCL8	Irradiation	10Gy (Xray)	HCA2 [2]	Antibody array	Increase
				ELISA	
CSF2	Irradiation	10Gy (Xray)	HCA2 [2]	Antibody array	Increase

SASP Factor	Induction method	Dose/method	Model used[(reference)]	Analysis technique	Change in expression (fold)
GM-CSF	Irradiation	10Gy (Xray)	HCA2 [3] IMR-90, HCA2, WI-38, BJ, PrECs, BPH1, RWPE1, PC3 [7/8/9/16]	Antibody Array	Increase (>4 fold)
	Oxidative stress	75uM H2O2	Primary mouse lung fibroblasts [6]	Cytokine array	Increase (4x greater than replicative)
	Replicative exhaustion	*In vitro* population doubling	Primary mouse lung fibroblasts [6] IMR-90, HCA2, WI-38, BJ, PrECs, BPH1, RWPE1, PC3 [7/8/9]	Cytokine Array	Increase
	OIS	RAS/MEK	IMR-90, HCA2, WI-38, BJ, PrECs, BPH1, RWPE1, PC3 [7/8/9]	Secreted protein level	Increase (>4 fold)
CXCL3	Oxidative stress	50uM Bleomycin	IMR90 [5]	Single cell qPCR	Increase
GRO-alpha, beta & gamma	Irradiation	10Gy (Xray)	HCA2 [3] IMR-90, HCA2, WI-38, BJ, PrECs, BPH1, RWPE1, PC3, prostate broblasts [8/9/10/16]	Antibody array	Increase (>4 fold)
	Oxidative stress	Bleomycin	IMR-90, HCA2, WI-38, BJ, PrECs, BPH1, RWPE1, PC3, prostate broblasts [7/8/9/10]	Secreted protein level	Increase (>4 fold)
	Oncogene-induced	Lentiviral RASV12 / RAS /MEK	HCA2 [3]IMR-90, HCA2, WI-38, BJ, PrECs, BPH1, RWPE1, PC3, prostate broblasts [7/8/9/10]	Antibody array	Increase (>4 fold)
	Replicative exhaustion	*In vitro* population doubling	IMR-90, HCA2, WI-38, BJ, PrECs, BPH1, RWPE1, PC3, prostate broblasts [7/8/9/10]	Secreted protein level	Increase (>4 fold)
TRAILR3 (or TNFRSF10C)	Oxidative stress	50uM Bleomycin	IMR90[5]	Single cell qPCR	Increase
	Irradiation	X-ray	IMR-90, HCA2, WI-38, BJ [8/9/12]	Secreted protein level	Increase (>4 fold)
	Replicative exhaution	*In vitro* population doubling	IMR-90, HCA2, WI-38, BJ [8/9/12]	Secreted protein level	Increase (>4 fold)

SASP Factor	Induction method	Dose/method	Model used(reference)	Analysis technique	Change in expression (fold)
MCP-2	Irradiation	10Gy (Xray)	HCA2 [3] IMR-90, HCA2, WI-38, BJ [8/9] IMR-90, HCA2, WI-38 [16]	Antibody Array Secreted protein level	Increase (>4 fold)
	Replicative exhaustion	*In vitro* population doubling	IMR-90, HCA2, WI-38, BJ [8/9]	Secreted protein level	Increase (>4 fold)
	Oncogene-induced	RAS /MEK overexpression	IMR-90, HCA2, WI-38, BJ [8/9]	Secreted protein level	Increase (>4 fold)
MCP-3 (CCL7)	Irradiation	10Gy (Xray) 12Gy Xray	HCA2 [3] MEFs[22]	Antibody Array	Increase
MCP-5	Oxidative stress	75uM H2O2	Primary mouse lung fibroblasts [6]	Cytokine array	Increase
	Replicative exhaustion	*In vitro* population doubling	Primary mouse lung fibroblasts [6]	Cytokine Array	No change
VCAM1	Irradiation	10Gy (Xray) 12Gy Xray	IMR90[20] MEFs[22]	Secreted protein levels	Increase (16 fold)
	Oxidative stress	75uM H2O2	Primary mouse lung fibroblasts [6]	Cytokine array	Increase (10x more than replicative)
	Ageing	Age-associated human IPF	Human IPF biosections[20]	Microarray	Increase
TGF-beta	Irradiation	10Gy (Xray)	HCA2 [3] IMR90[20]	Antibody Array Secreted protein level	Increase (200 fold)
		20Gy (Cs137)	HFF, MRC5 [4]	RNAseq	
	Oxidative stress	Bleomycin 2 U /kg (Aerosolized intratracheal instillation)	Fibroblasts, epithelial, and endothelial cells from whole mouse lung (*in vivo*)[20]	Flow & RT-PCR	Increase (between 2-4 fold)
	Ageing	Age-associated human IPF	Human IPF biosections[20]	Microarray	Increase

SASP Factor	Induction method	Dose/method	Model used[(reference)]	Analysis technique	Change in expression (fold)
IGFB1/2/3/4/7	Irradiation	10Gy Xray 12Gy Xray [22]	HCA2 [3/8/9/10/12] IMR-90, HCA2, WI-38, BJ, PrECs, BPH1, RWPE1, PC3 [16] MEFs[22]	Antibody Array Secreted protein levels	Increase (>4 fold)
	Oxidative stress	Bleomycin	HCA2 [8/9/10/12] IMR90[5]	Secreted protein levels Single cell qPCR	Increase (>4 fold)
	Replicative exhaustion	*In vitro* population doubling	HCA2 [8/9/10/12]	Secreted protein levels	Increase (>4 fold)
	Ageing	Age-associated human IPF	Human IPF biosections[20]	Microarray	Increase
VEGF	Replicative exhaustion	*In vitro* population doubling	HCA2, BJ, WI-38, IMR-90 [17]	mRNA & protein expression	Increase (2-3fold mRNA, 6fold protein)
	Oxidative stress	Bleomycin Anthracycline-based Chemotherapy (human in vivo)	IMR90[5] Human breast cancer patients[23]	Single cell qPCR Blood plasma expression	Increase (>4 fold)
	Ageing	Age-associated human IPF	Human IPF biosections[20]	Microarray	Decrease (2fold mRNA) (VEGFA)

Table 3.1. List of SASP factors up-regulated following irradiation. References are numbered as follows: 1) Demaria *et al.,* 2014; 2) Laberge *et al.,* 2015; 3) Freund *et al.,* 2011; 4) Marthandan *et al.,* 2016; 5) Wiley et al., 2017; 6) Maciel-Barón *et al.,* 2016; 7) Acosta JC*, et al.,* 2008; 8) Coppé, *et al.*, 2008; 9) Coppé, *et al.*, 2010; 10) Bavik C, *et al.,* 2006; 11) Liu *et al.,* 2007; 12) Rodier F *et al.,* 2009; 13) Parrinello S *et al.,* 2005; 14)(Krizhanovsky *et al.*, 2008)Krizhanovsky V, *et al.,* 2008; 16) Coppé, *et al.*, 2011; 17) Liao *et al.,* 2014 18)Laberge *et al.*, 2012; 19) Biran *et al.,* 2017; 20) Schafer *et al.,* 2017; 21) Bhaumik *et al.,* 2009; 22) Gluck *et al.,* 2017; 23) Sanoff *et al.,* 2014; 24) Kang *et al.,* 2011.

Chapter 4 – Development of transgenic larval zebrafish reporter for *p21*

4.1.1. Introduction

Having a method for inducing early senescence accumulation in optically transparent zebrafish larvae provides a more amenable system for studying *in vivo* senescent cells within a whole organism context. To better identify and track senescent cells in irradiated zebrafish larvae, a transgenic system whereby cells expressing a marker of senescence fluoresce was developed. Due to the genetic malleability of this model organism, a technique called Bacterial Artificial Chromosome (BAC) transgenesis can be utilised to report promoter activation of a gene of interest (Suster *et al.*, 2011). This is particularly useful since zebrafish are transparent during early development, which means that fluorescently-labelled cells can be tracked over time, to allow visualisation of cellular life-span and the tissues they are located in and interact with (Renshaw and Loynes, 2006). Live visualisation of senescent cells can allow a deeper understanding about senescence and their roles in age-associated disease. This includes an appreciation for what and where these cells are, how long they live for *in vivo,* how they interact with surrounding tissues, and whether drugs can efficiently remove them in a systemic context with translatability to age-associated multimorbidity. The SASP is highly interactive, and different cell types have different rates of senescence induction (Song, Lee and Hwang, 2005; Probin *et al.*, 2006; Hernandez-Segura *et al.*, 2017). Therefore, by looking in a whole organism context, it would better recapitulate these complicated aspects of *in vivo* senescence over typical *in vitro* systems and provide novel insight into a causal mechanism underlying age-associated multimorbidity.

To develop a transgenic reporter for senescence, I chose to report the *p21 (cdkn1a)* promoter. This is the best-characterised reporter of senescence in zebrafish currently. In support of this, there has been recent evidence highlighting the ability of *p21* in mammalian systems to identify bleomycin-induced senescent cells (Wiley *et al.,* 2017). This induction method in mammalian cells, which also acts through the DNA damage response, showed that *p21* expression could distinguish senescent from quiescent cells at the single cellular level. I have also previously demonstrated the spatial expression within irradiated zebrafish, which I can use to assess whether GFP expression faithfully reports the endogenous expression pattern. Another commonly used senescence marker in mammalian systems is $P16^{INK4A}$ (*CDKN2A*), however in zebrafish the orthologous locus is described as $p16\text{-}like^{INK4A/B}$ *(cdkn2ab)* (ZFIN, 2019). The locus in zebrafish is a combined form of mammalian p15 and 16, and they do not have the splice variant $p19^{ARF}$. An alginate bead injection into the murine peritoneum lead to the recruitment of immune cells, predominantly macrophages, to senescent beads via the SASP (Hall *et al.*, 2016). What was interesting is that it seemed that these macrophages themselves used P16 and SA-β-Gal to switch to an M2-like phenotype (Hall *et al.*, 2017). I have therefore made the decision to use *p21* as the transgenic reporter for senescence, due to the similarity between zebrafish and mammalian orthologues and better characterisation of this gene in zebrafish over *p16-like*.

4.1.2. Aims

To be able to study live senescent cells in irradiated zebrafish larvae, a transgenic reporter that fluoresces under *p21* promoter regulation is required. An optimised assay for irradiation-induced senescence accumulation provides a method for determining whether the fluorescent reporter being developed fluoresces under the correct regulation, for example in the same spatial and temporal kinetics as previously demonstrated by assessment of *p21* mRNA expression. I hypothesise that fluorescence from a transgenic reporter for *p21* promoter activation using BAC transgenesis will mimic spatial and temporal kinetics of *p21* mRNA expression. The aims of this chapter are:

- To develop a novel transgenic zebrafish that reports *p21* promoter regulation.
- To characterise the fluorescence seen in the novel transgenic zebrafish to confirm the fluorescence increases following irradiation and matches *p21* mRNA expression.
- To confirm that the transgenic reporter activates *p21* mRNA following irradiation in the same manner as wild-type strain zebrafish.

4.2. BAC transgenesis

To develop a transgenic zebrafish that reports the gene of interest's expression pattern, a technique called Bacterial Artificial Chromosome (BAC) transgenesis was used. This involves firstly identifying a BAC, which is a large (100-150kbp) segment of genomic DNA, that encompasses the locus of *p21*. It must then be modified such that, once randomly inserted into the zebrafish genome through tol2-mediated transgenesis, the extra p21 locus will now express GFP under *p21* promoter (summarised in Figure 2.7).

4.2.1. BAC identification

First, the gene sequence that encodes for human p21 (*CDKN1A)* was acquired on Ensembl and used to acquire the *danio rerio* (zebrafish) orthologue (*cdkn1a)* (ZFIN, 2019; Zerbino *et al.*, 2018). Three BACs containing the *cdkn1a* zebrafish locus and the two associated splice variants (*cdkn1a-001; cdkn1a-002*) were identified using Ensembl blast feature (Figure 4.1). Two were shotgun clones sequences from the Daniokey library, from partially digested genomic DNA (HindIII) from Tübingen zebrafish strain male testis (prefix: DKEY) (ZFIN, 2019c). The other being from the Chori-211 library, also from Tübingen zebrafish strain male testis DNA, but instead cut with EcoR1 (prefix CH211) (ZFIN, 2019). Once acquired, the BACs were transformed into electroporation-competent E-coli cells and then grown up in appropriate antibiotic resistance (Chloramphenicol) medium, to allow for modification steps that allow *p21*-regulated GFP expression from the BAC.

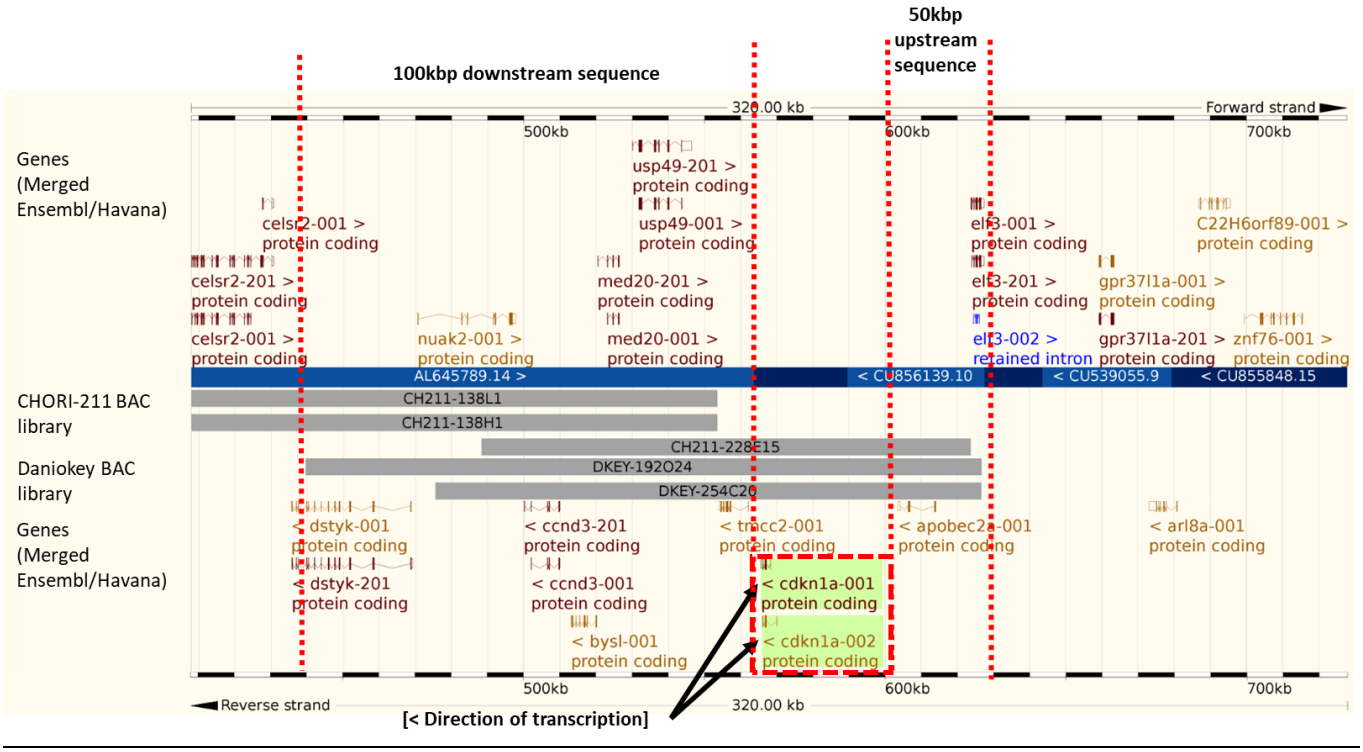

Figure 4.1. Identification of BAC sequences at *cdkn1a (p21)* zebrafish locus. Examined Ensembl *danio rerio* version 82.10 (GRCz10) at Chromosome 22: bases 407,874 – 727,875. Three BACs were identified that overlapped with *cdkn1a* locus and contained at least 100kbp downstream and 590kbp upstream of the start codon (arrow, also indicates direction of transcription).

4.2.2. Inserting GFP sequence after BAC *p21* start codon.

Once I had identified BACs of interest, I next had to modify them such that GFP was under *p21*-promoter regulation and that the BAC itself did not express an extra copy of *p21* when inserted into the zebrafish genome. Ultramer primers were designed to modify the GFP-targeting sequence such that there were overhanging single-strand DNA sequences that matched the BAC (Figure 4.2A). For example, the forward primer was designed such that the first 50 base pairs complimented with the BAC sequence, with the last three bases being the start codon of the *p21* locus, followed by 24 more bases that overlap with the end of the target cassette (Figure 4.2A). Once the GFP sequence with homology arms to the BAC was designed and purified (figure 4.2B), it was electroporated into BAC-containing cells. This allows for the GFP sequence to be incorporated into the BACs after the initial start codon (ATG sequence) of the *p21*-encoding region, so that the GFP is placed under *p21*-promoter regulation, and disrupts the BAC's copy of *p21* (Figure 4.2C). Using Ensembl and ZFIN, I checked that both *p21* splice variants contained the same first exon, which is where the GFP was targeted and so it should represent both splice variants' expression (ZFIN, 2019). To check that these sequences contained the *p21* promoter region, I aligned them against primers for *cdkn1a* published in Henriques *et al.,* 2013 and showed a 100% match. I also blasted the version of *cdkn1a* that were used to design primers against a published *p21* sequence (Laranjeiro *et al.,* 2013). As the GFP-targeting sequence contained a kanamycin-resistance cassette, the cells were then grown on kanamycin antibiotic medium to identify cells that have incorporated the GFP cassette, as only those that have would survive in the presence of this antibiotic. Cells containing the modified back that have grown on the antibiotic-containing medium were extracted and the BAC purified. The purified BAC was then sequenced to confirm the GFP coding sequence was fully incorporated. As the BAC no longer requires this antibiotic resistance cassette, the FLP/FRT system was used to remove it (Figure 4.2D). FRT recognition sites were contained within the GFP-targeting sequence, flanking the kanamycin resistance cassette. These are recognised and excised once the enzyme L-arabinose is added to BAC-containing cells (Schlake and Bode, 1994).

A

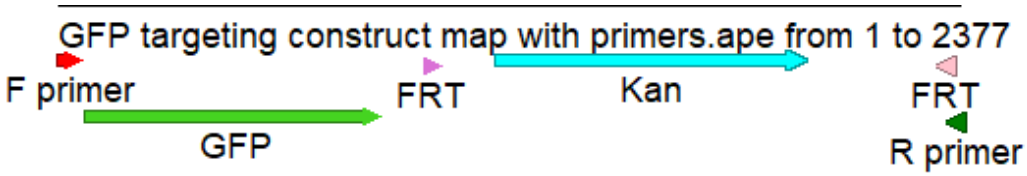
GFP targeting construct map with primers.ape from 1 to 2377
F primer
FRT
Kan
FRT
GFP
R primer

B

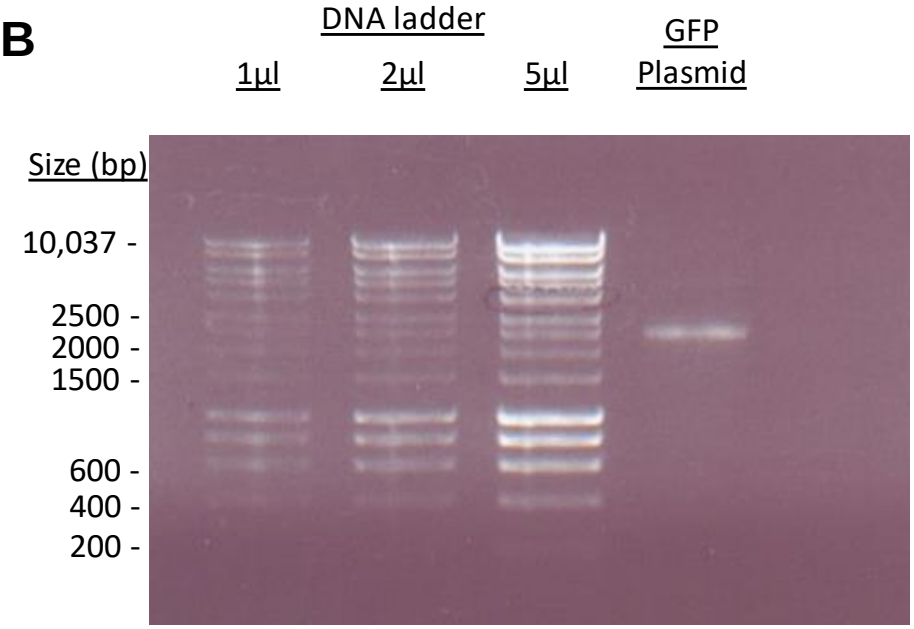
DNA ladder
1µl
2µl
5µl
GFP
Plasmid
Size (bp)
10,037 -
2500 -
2000 -
1500 -
600 -
400 -
200 -

C

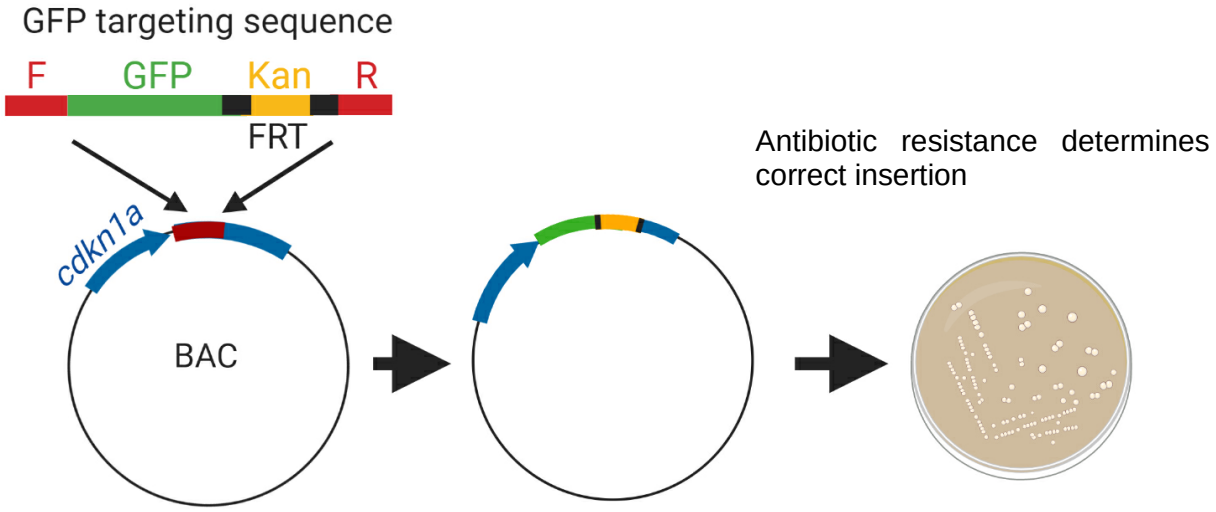
GFP targeting sequence
F
GFP
Kan
R
FRT
cdkn1a
BAC
Antibiotic resistance determines correct insertion

D

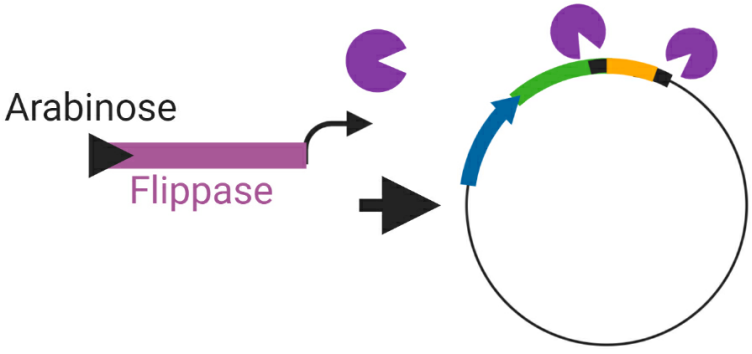
Arabinose
Flippase

Figure 4.2. Development of GFP targeting construct for TgBAC(p21:GFP) transgenic zebrafish. A) ApE plasmid map for GFP targeting construct, 2.4kbp in size. **B**) Visualisation of modified, linearised and purified GFP plasmid with primers for insertion into cdkn1a BACs. C) Diagram depicting targeting of the GFP sequence after the promoter for the *p21* locus (*cdkn1a)*. The kanmycin resistance sequence (Kan) is introduced to the BAC such that once successfully targeted, they can be grown on agar plates containing the antibiotic kanamycin. D) Diagram depicting how the Kanamycin sequence is removed from the GFP-BAC. In the presence of arabinose, the recombinase flippase is expressed in BAC-containing E.coli, which recognises the FRT sites surrounding the Kanamycin sequence and removes it from the BAC. Diagrams created on BioRender.com.

4.2.3. Modification of GFP-BAC for tol2-mediated transgenesis in single cell-stage zebrafish embryos

To improve the likelihood that the modified BAC will be fully incorporated into the zebrafish genome, a transposon-mediated system was utilised. As the BAC is a large plasmid, it is therefore prone to breakage and partial insertions (Suster *et al.,* 2011). Introducing the tol2-mediated system involves modifying the GFP-BAC plasmid with inverted cis-sequence tol2-recognition sites, such that the tol2 transposase can recognise and insert randomly into the zebrafish genome by homologous recombination. This sequence also contained a Chloramphenicol resistance sequence within the two recognition sites as was seen in the GFP-targeting cassette. Once the tol2 sequence is electroporated into the GFP-BAC, it will provide selective resistance to identify those competent cells with the tol2 sites incorporated. Cells containing the newly modified BAC were again purified and sequenced to confirm correct insertion of the tol2-regonition sequence. The FLP/FRT system was not required to then remove this antibiotic resistance sequence, because this was located outside of the sequence that the tol2-recognition sites will incorporate into the zebrafish genome, as depicted in Figure 2.7. For a successful tol2-mediated transgenesis, tol2 mRNA was synthesised and purified (Figure 4.3A). The BAC was then injected alongside tol2 mRNA, which in turn will be translated into transposase protein that recognises the cis sites within the BAC, and incorporate the plasmid as a whole randomly into the zebrafish genome. The exception to this is the kanamycin-resistance cassette, which are located outside of the tol2 recognition sites. Once the BACs were modified and tol2 transgenesis system established, injected single-stage zebrafish were allowed to develop before screening for GFP expression at 4 or 5dpf before the onset of independent feeding. Compared to zebrafish injected with BAC alone, tol2 mRNA concurrent injection did not show a significant increase in the number of GFP-positive zebrafish (Figure 4.3B). However, within those fish positive for GFP, tol2 concurrent injection increased the number of GFP-positive cells in these fish (Figure 4.3C), possibly indicating improved incorporation of the BAC into the genome but due to only being a pilot experiment this cannot be confirmed statistically. Figure 4.4 further demonstrates example images of BAC & tol2 mRNA-injected zebrafish with larger numbers of GFP positive cells in the head and tail regions at 4dpf, areas previously demonstrated to express *p21* mRNA.

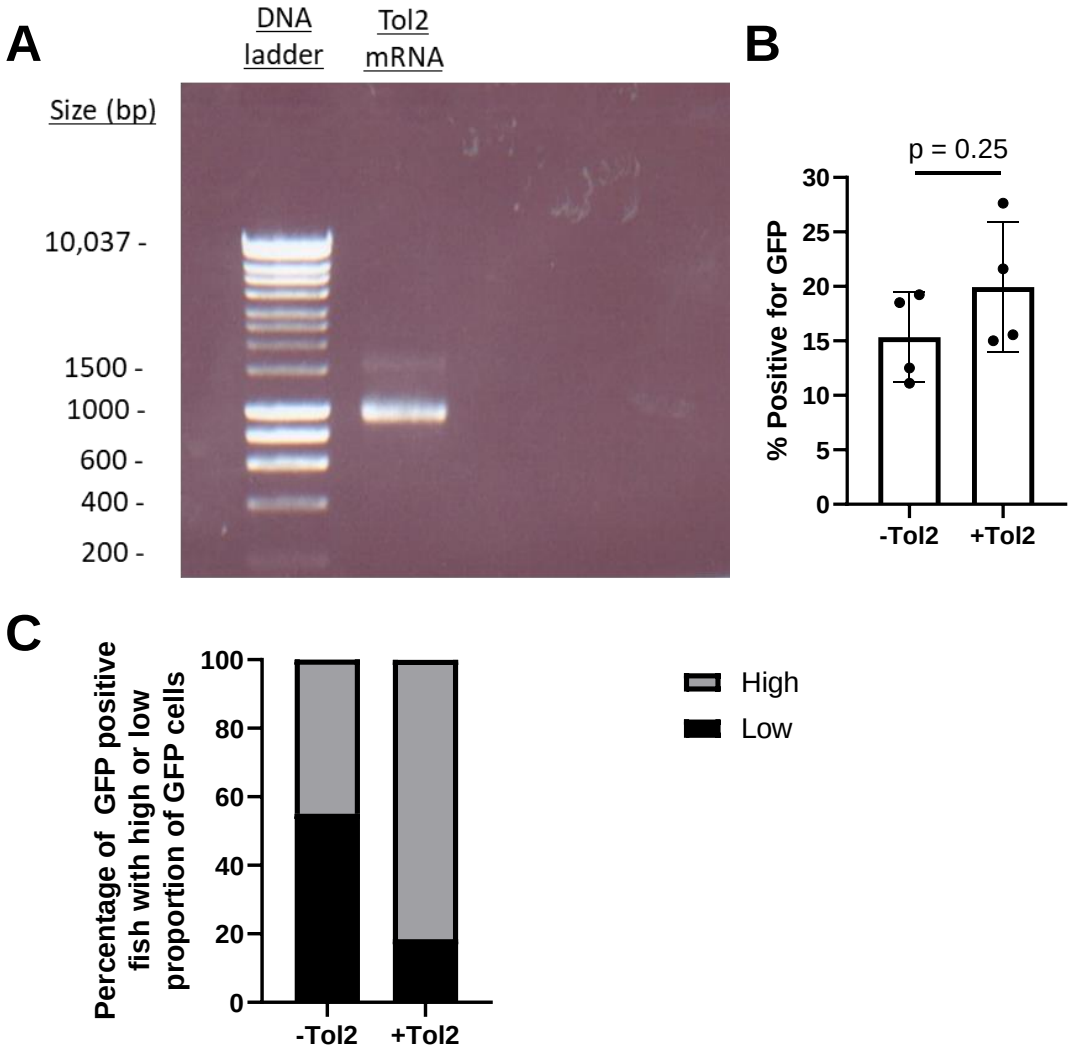

Figure 4.3 Tol2 transposase mRNA synthesis. A) Gel electrophoresis showing synthesised tol2 mRNA, with predicted sequence length of 1000bp. B) Analysis of GFP positive fish 4-5 days after injection of TgBAC(*p21:GFP*) with or without tol2 mRNA. 261 to 451 fish analysed over 4 independent experiments, no statistical significance observed using unpaired t-test. C) Proportion of GFP positive fish 4 or 5 days after injection with low (5 or fewer) or high (more than 5) numbers of GFP positive cells. 20-38 fish examined in a single pilot experiment.

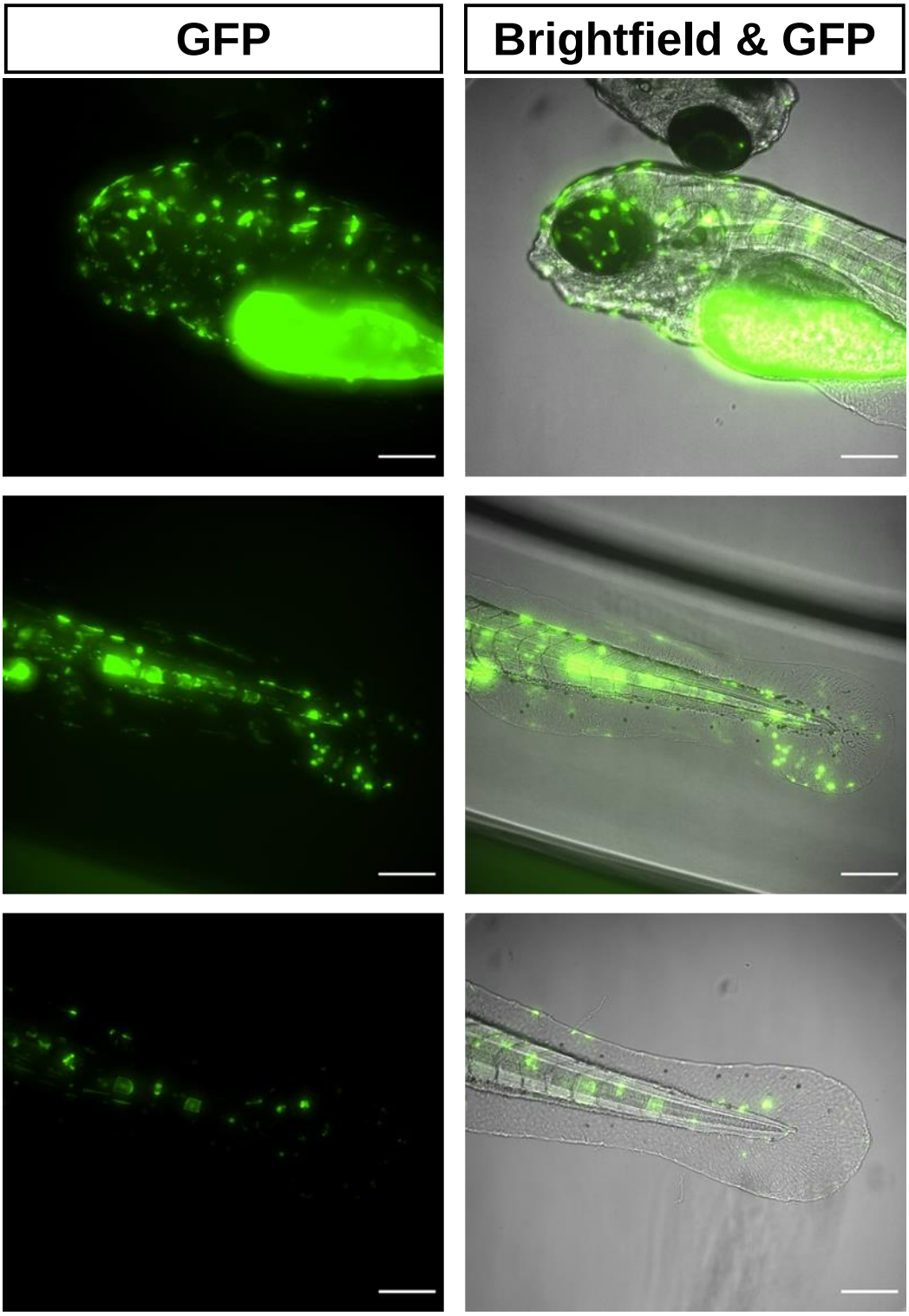

Figure 4.4. Example images of zebrafish injected with the p21:GFP BAC at 4dpf. Regions with high (more than 5) GFP positive cells that are known to express p21 mRNA at these timepoints. 100μm scale bar.

4.2.4. Identification of stable founders of the TgBAC(p21:GFP) zebrafish line

To identify whether any of the BAC-injected zebrafish had incorporated the transgene into their germline, the injected GFP-positive fish were grown to sexual maturity. At 3-4 months of age, the next generation of zebrafish larvae were assessed for *p21* promoter-regulation of GFP expression. The adult fish were placed into individual tanks during screening of the next generation, such that the parent fish could be identified from different groups of offspring. Two adult zebrafish (Allele numbers SH506, SH507 respecitvely) were identified that were able to produce GFP-positive offspring (Figure 4.5A). These offspring were grown up to adulthood to have stocks of fish with stable incorporation of the p21:GFP BAC into their genome. Quantification of the unirradiated transgenic fish showed increased fluorescence compared to their siblings that did not express the transgene, notably in the head, intestine and trunk regions (Figure 4.5B-E). The largest region for transgene-specific expression compared to wild-type siblings was the intestine, which was previously highlighted as a region of interest with endogenous *p21* expression (Figure 4.5C). The expression of GFP-positive zebrafish from these crosses were approximately 50%, which is evidence towards a single insertion of the transgene into the genome.

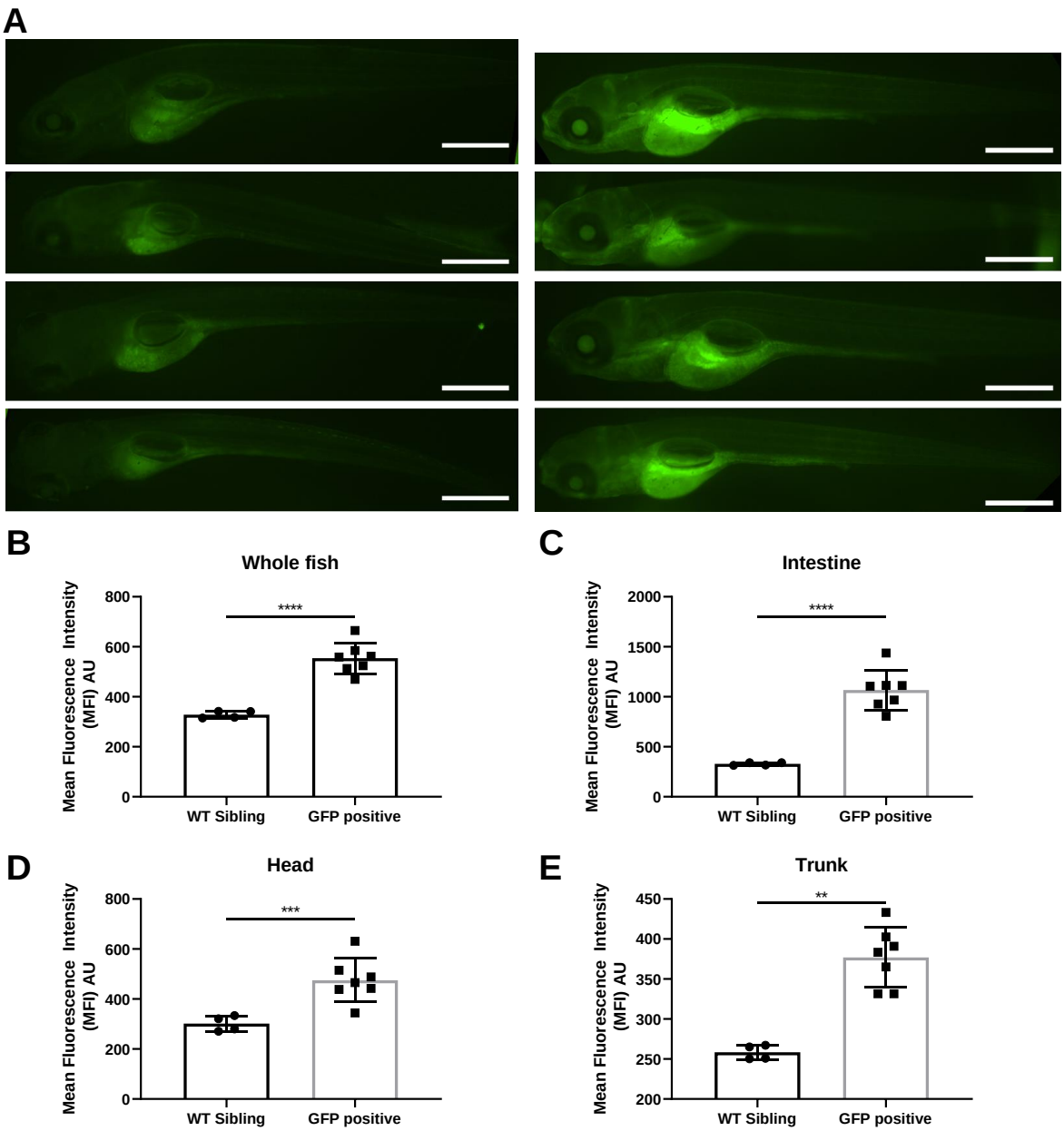

Figure 4.5. Confirming germline transmission of *TgBAC(p21:GFP)sh506*. A) Outcross of *TgBAC(p21:GFP)sh506* with wild-type zebrafish resulted in 50% of the next generation were GFP negative (left) and 50% GFP positive (right). 1mm scale bar. B-E) Quantification of different regions of the zebrafish. B) Whole fish. C) Intestine. D) Head region. E) Trunk. Statistical significance determined by unpaired T test, 4-7 fish analysed.

4.3. Characterisation of *TgBAC(p21:GFP)sh506*

4.3.1. Fluorescence imaging of *TgBAC(p21:GFP)sh506* after irradiation showed increased fluorescence that matches endogenous p21 mRNA patterns.

Following identification of injected zebrafish with germ-cell incorporation of the BAC, characterisation using the developed irradiation assay was carried out to confirm that the GFP is under *p21*-promoter regulation (Figure 4.6.). For example, it is possible that partial incorporation of the BAC into the zebrafish genome has occurred, which would result in GFP expression that is not *p21* promoter regulated. This would mean that the GFP expression might not be specific to *p21*-promoter activation. Expression of *p21* mRNA is increased following 12Gy of Cs^{137} γ-irradiation at 2dpf, and predominantly located in the head and intestinal regions at 3 days post-irradiation (dpIR) (Figure 3.9.). Following 12Gy of Cs^{137} γ-irradiation of an in-cross between *TgBAC(p21:GFP)sh506* zebrafish at 2 days post-fertilisation (dpf), increased fluorescence was detected 3dpIR (Figure 4.6). This increase in GFP expression is consistent with previous qPCR and *in situ* hybridisation expression data for *p21* mRNA levels, indicating that the fluorescence is associated with *p21*-promoter activation, with the intestine and head regions, such as pharyngeal arches, being most obviously increased. The unirradiated fish had more GFP expression compared to wild-type siblings, albeit much less than irradiated transgenic fish. This was also demonstrated in my previous work showing some *p21*-promoter activation independent of irradiation.

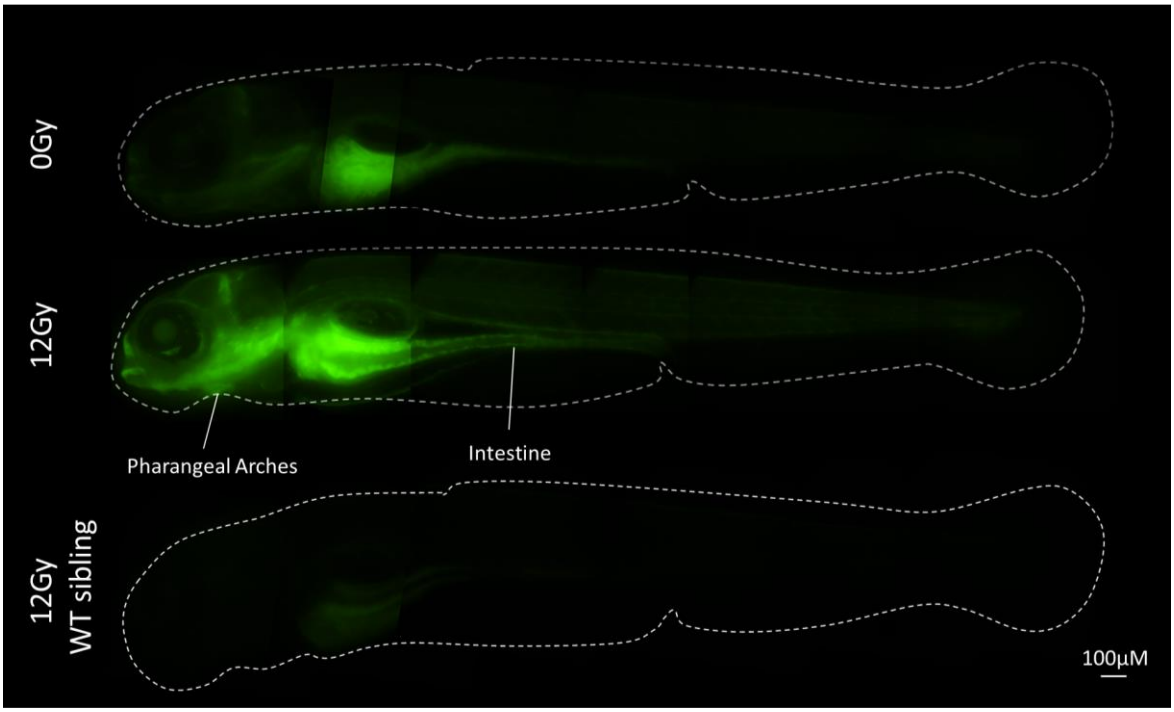

Figure 4.6. Representative images of *TgBAC(p21:GFP)sh506* zebrafish. GFP expression pattern of whole 5dpf zebrafish. Increased fluorescence seen following 12Gy 3pdIR, particularly in the head regions, including the pharangeal arches, and intestinal regions.

To quantify this increased fluorescence, I chose the head region of the zebrafish, which, alongside the intestine, is the region of highest irradiation-induced *p21* mRNA expression (Figure 4.7). The head was chosen over the intestine because this area contains less fluorescence in unirradiated zebrafish compared to the intestinal region (Figure 4.5C, D). A quantitative increase in GFP fluorescence following irradiation was demonstrated, being on average 2.86x brighter (SD 0.759) than wild-type siblings, compared to unirradiated zebrafish that were 1.67x brighter than wild-type siblings (SD 0.409) Thus the fluorescence from *TgBAC(p21:GFP)sh506* zebrafish compliments evidence describing *p21* mRNA increase in the head region of 3dpIR zebrafish

(Figure 3.9.).

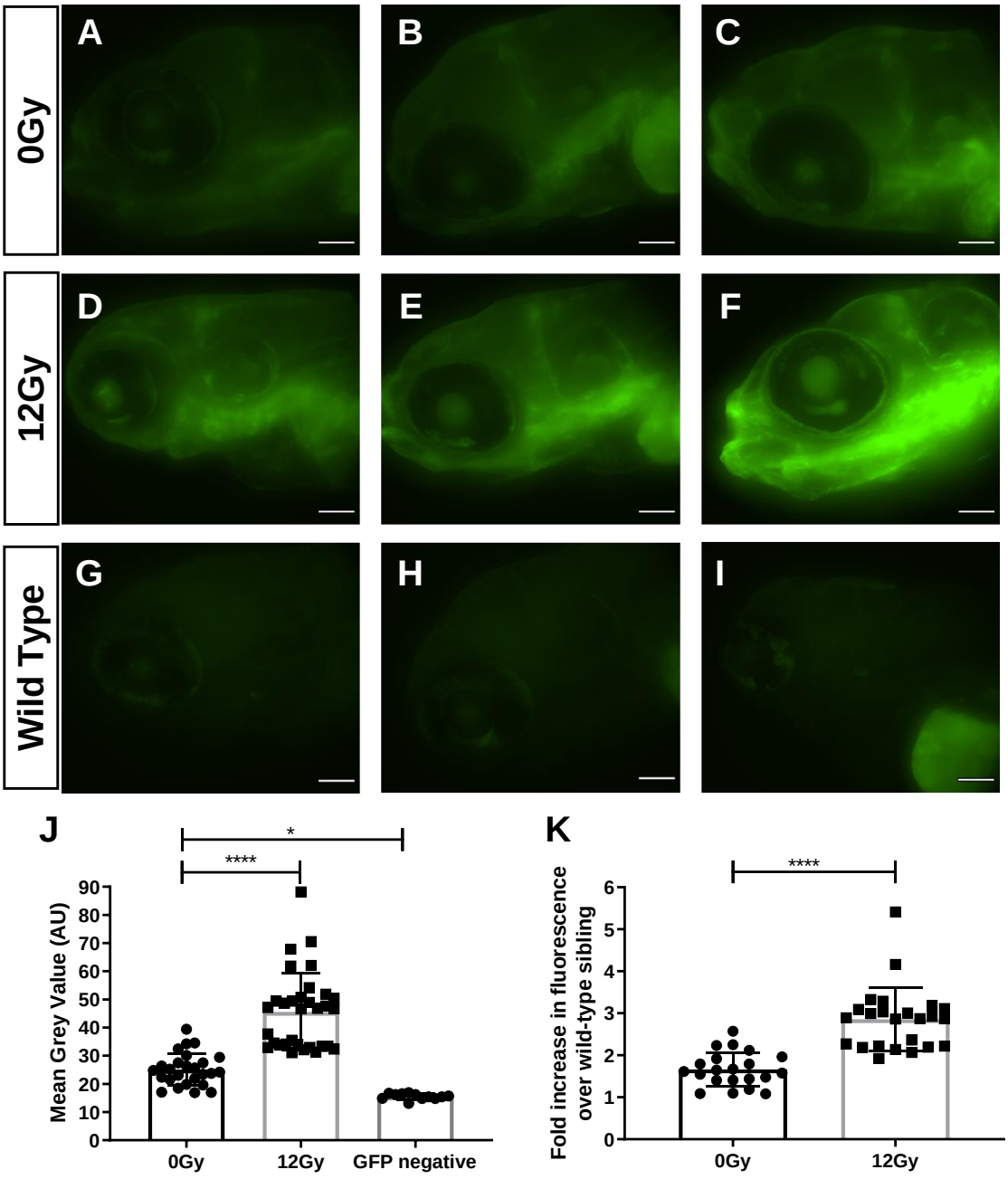

Figure 4.7. Quantification of head region fluorescence of 5dpf *TgBAC(p21:GFP)sh506*. A-C) Unirradiated examples. A) Example with lower expression. B) Mean expression. C) High expression. D-F) 12Gy 3dpIR examples. D) Example with low expression. E) Mean expression. F) High expression. G-I) Wild type sibling examples. J & K) Quantification of head region of 5dpf zebrafish. J) Pixel intensity of fluorescent fish analysed. K) Fold increase in expression compared to wild-type siblings. Data was examined by Kruskal Wallace test with Dunn;s multiple comparisons, as wild type sibling data is non-parametric (J) or relative (K). 24 fish analysed over 3 independent experiments. Error bars represent standard deviation.

To assess whether GFP fluorescence from *TgBAC(p21:GFP)sh506* zebrafish has the same spatial regulation as *p21* mRNA expression detected by *in situ* hybridisation, I compared the patterns of these two techniques (Figure 4.9.). The transgene faithfully recapitulates endogenous *p21* mRNA expression patterns. Lateral and ventral images of the head region show that both *p21* mRNA and GFP following irradiation are located predominantly in the pharyngeal arches and specific brain regions at 3dpIR. Additionally, *p21* mRNA is also increased in the intestine of zebrafish, which is shown clearly in the previous figure of whole zebrafish fluorescence.

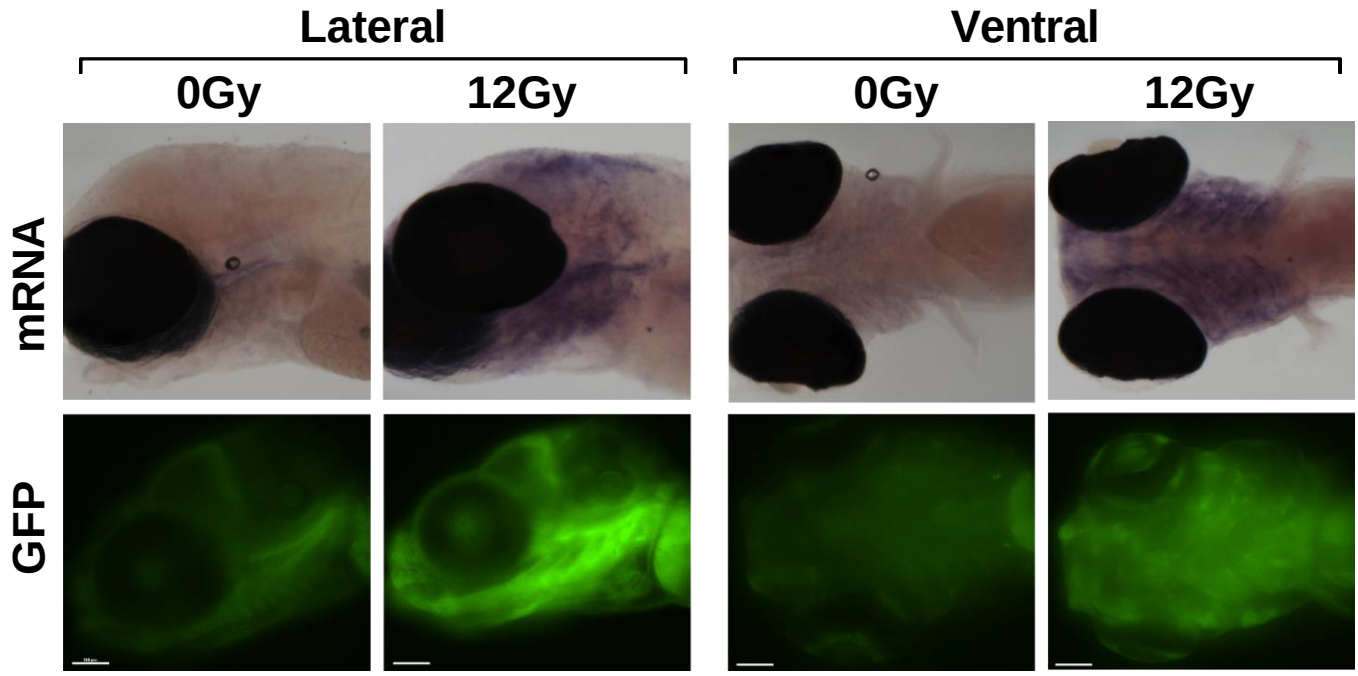

Figure 4.8. Comparison of *p21* mRNA expression and *TgBAC(p21:GFP)sh506* fluorescence at 5dpf in zebrafish head region. 12Gy irradiation 3dpIR and unirradiated controls, taken laterally and ventrally showing transgenic fish recapitulates endogenous expression patterns. Scale bar 100μM.

4.3.2. *TgBAC(p21:GFP)sh506* zebrafish show endogenous levels of *p21* mRNA expression

To further characterise the new transgenic reporter for *p21*, quantitative assessment for mRNA expression levels of *p21* and GFP using qPCR in *TgBAC(p21:GFP)sh506* zebrafish was used. It is important to compare this with expression levels in wild-type strain zebrafish to ensure that the transgenic reporter has a comparable endogenous *p21* mRNA response without any contribution from the BAC. Following irradiation, *p21* mRNA expression was increased in RNA extracted from whole *TgBAC(p21:GFP)sh506* 3dpIR zebrafish compared to unirradiated controls, and this 5-fold increase was matched in Nacre (wild type) 3dpIR zebrafish not containing the BAC transgene (Figure 4.9A & B). Expression levels of GFP mRNA were increased following irradiation in only the transgenic zebrafish and not wild-type strains (Figure 4.9C). The level of increase was approximately half that of *p21* mRNA (Figure 4.9A), which may support the notion that there is only a single insertion of the GFP-BAC in these transgenic fish, whereas there are two copies of endogenous *p21*, though this evidence is not definitive as RNA stability may differ between the two genes for example. Importantly, this shows that the endogenous *p21* expression levels, both with and without irradiation, are comparable between *TgBAC(p21:GFP)sh506* and the Nacre-strain zebrafish used to optimise the irradiation assay.

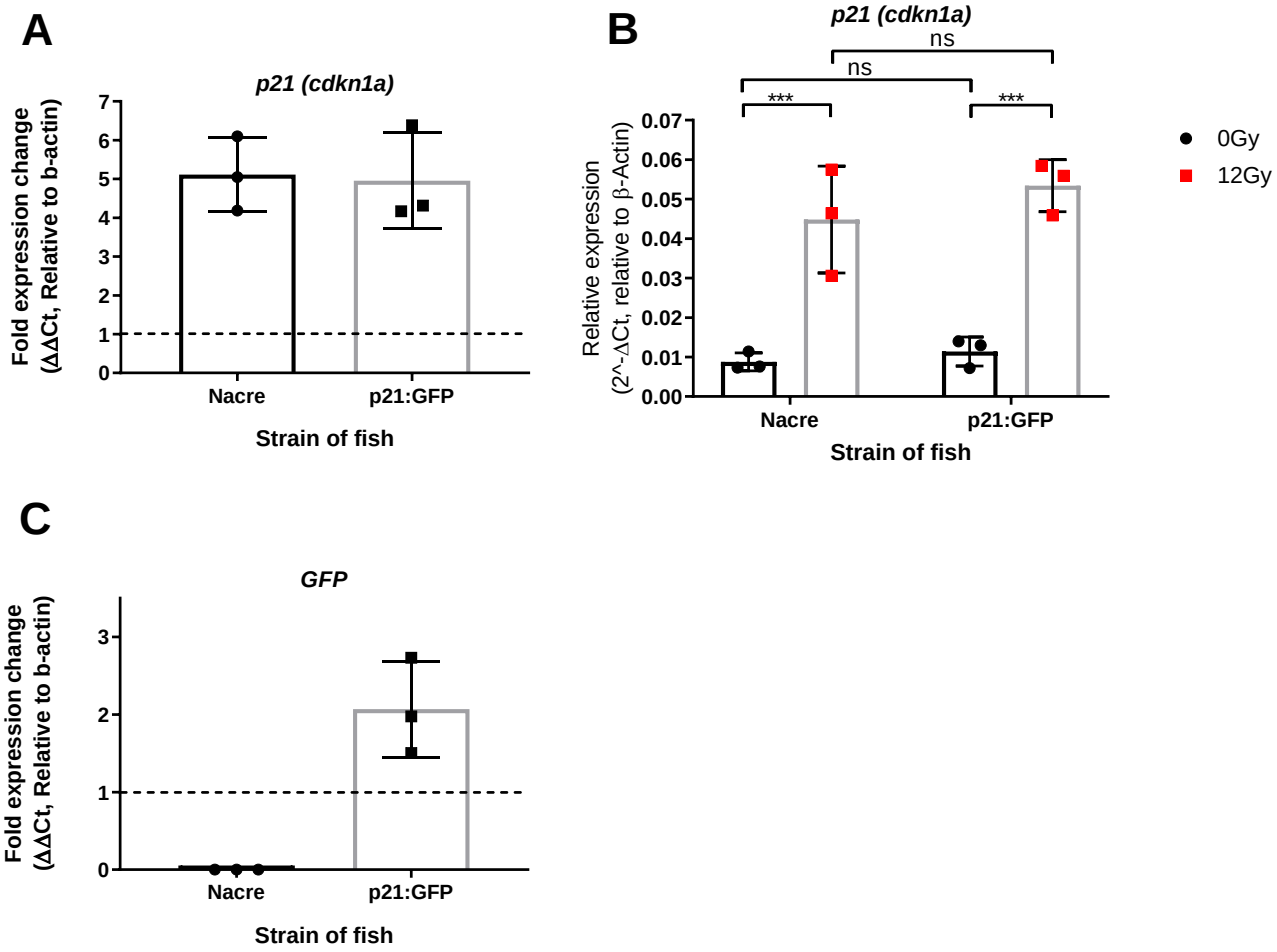

Figure 4.9. mRNA expression of *p21* and *GFP* in *TgBAC(p21:GFP)sh506* zebrafish by qPCR. Zebrafish were irradiated at 2 days post-fertilisation (2dpf) and assessed for the senescence marker *p21* in *TgBAC(p21:GFP)sh506 and Nacre-strain zebrafish.* A) Fold expression change 3 days post-irradiation (dpIR) in transgenic and wild-type strain zebrafish, calculated by ΔΔCt, relative to β-actin expression and unirradiated controls. B) p21 fold induction in transgenic and wildtype strains, relative to β-actin (2^-ΔCt). Data examined by 2way ANOVA with Sidak's multiple comparison test. C) GFP fold expression change 3dpIR in transgenic and wild-type strain zebrafish. *** $p < 0.001$. RNA from 50 zebrafish were pooled for each of the three independent repeats. Error bars represent standard deviation.

4.4. Conclusion and chapter discussion

To assess *in vivo* senescent cells live in irradiated zebrafish larvae, development and characterisation of a novel transgenic zebrafish reporting *p21* promoter activation by GFP fluorescence was carried out. As zebrafish larvae are transparent, new insights into *in vivo* senescent cells are now possible at cellular resolution. By comparing GFP fluorescence with *p21* mRNA expression following irradiation in zebrafish larvae, I was able to ascertain with confidence that the GFP fluorescence seen in the transgenic zebrafish reporter does indeed match *p21* expression patterns spatially, suggesting I was successful in placing GFP under *p21* promoter regulation in this transgenic zebrafish. Here I demonstrated that the endogenous *p21* mRNA expression levels, both with and without irradiation, are unchanged in the transgenic zebrafish compared to wild-type counterparts. This retains physiological relevance and allows me to make comparisons with previous data on senescence in irradiated wild-type fish.

4.4.1. Development of *TgBAC(p21:GFP)sh506*

Transgenic zebrafish reporters for gene activation can be made through a variety of methods (Meyes, 2018). GFP-fusion proteins can be developed to assess subcellular protein localisation, but this tag can affect translational modifications and protein function (Burket *et al.*, 2008). Similarly, targeting GFP to an endogenous p21-locus would disrupt an allele of the gene, therefore possibly altering endogenous signalling. Additionally, the BACs used encompassed 50kbp of upstream and 100kbp downstream of DNA sequence around the gene of interest. This is important because not only the proximal promoter region can regulate gene transcription, but also nearby regulatory elements and enhancers that are not always proximal to the gene of interest (Suster *et al.*, 2011; Gallegos and Rose, 2017). By considering this, it increases the likelihood that the fluorescence from the BAC is as closely related to endogenous *p21* transcriptional regulation as possible.

I chose to use Nacre-strain zebrafish as the background for the transgenic because they do not produce melanophores and have a reduced number of pigmented cells (Lister *et al.*, 1999). Having a transgenic reporter for senescence with reduced pigmented cells will improve my ability to track, image, and prospectively isolate potentially senescent cells based on GFP expression (Renshaw *et al.,* 2006). Further, I previously showed that the induction of *p21* following irradiation in nacre fish is comparable to the AB wild-type zebrafish, so the lack of pigmented cells due to the *nac(w2)* mutation has not caused any confounding factors that affect the senescence response (Lister *et al.,* 1999). This was important because different zebrafish strains may exhibit different sensitivities to irradiation or patterning of senescence. For example, different zebrafish strains can have differing telomere lengths (Anchellin *et al.,* 2011). Additionally, zebrafish have a high degree of genetic diversity between genomes (Guryev *et al.*, 2006).

4.4.2. *TgBAC(p21:GFP)sh506* faithfully reports *in vivo p21* promoter activation

My previous evidence showed that *p21* expression could be induced following 12Gy irradiation of 2dpf zebrafish larvae without significant developmental abnormalities. Using this assay, I was able to demonstrate that the fluorescence from *TgBAC(p21:GFP)sh506* was comparable with the spatial and temporal kinetics of *p21* mRNA, as detected by *in situ* hybridisation. It was important to compare the spatial location of GFP fluorescence with *p21* mRNA expression as it is possible that the irradiation induces auto-fluorescence due to cell death and so could give false positives (Schaue, Ratikan and Iwamoto, 2012). The fluorescence was located in regions where highest *p21* mRNA expression. These are

typically areas of high proliferation such as the intestine, pharyngeal arches, and hindbrain. Additionally, irradiation of wild-type siblings did not increase the number of fluorescent cells by flow cytometry. Looking at the transcriptional level, GFP induction following irradiation was approximately half that was seen with *p21*, which correlates with a single copy of the transgene being inserted. Whenever these fish were crossed with a wild-type zebrafish, 50% of offspring would be fluorescent and so further indicates a single insertion of the transgene. To strengthen this evidence in hindsight, I would also use zebrafish that have two copies of the transgene following an in-cross to show that GFP mRNA induction is the same as p21 mRNA induction following irradiation.

Though the presented evidence suggests that fluorescence recapitulates patterns of *p21* transcriptional expression, this has not been described at the cellular level. For example, GFP has a 26-hour half-life, compared to 4.1-hour half-life of *p21* mRNA and even shorter half-life of p21 protein (Corish and Tyler-Smith, 1999; Jascur *et al.*, 2005; Scoumanne *et al.*, 2011). It is worth noting however that it was demonstrated that HSP90 can stabilise p21 expression, and the inhibition of HSP90 has been identified as a senolytic pathway (Jascur *et al.,* 2005; Fuhrmann-Stroissnigg *et al.,* 2017). Therefore, it is possible that any senescent cells may have an extended p21-protein half-life due to HSP90 expression, and that the GFP reporter may coincide with this more than expected in senescent cells specifically. Regardless, this may mean that by 3dpIR, some cells with early *p21* promoter activation could have repaired their DNA, returned into the cell cycle, and switched of *p21* transcription, whilst still expressing GFP signal (Sang *et al.,* 2008). This further emphasises the importance of using flow cytometry to assess the true proportion of senescent cells in this system.

4.4.5. Future work and conclusions

This study provides the first example of a transgenic reporter in a translucent organism that can track potentially senescent cells live and *in vivo,* providing new insights into where these cells are located and which tissues are most sensitive to irradiation-induced senescence. Assessment of GFP positive cells that are truly senescent in irradiated *TgBAC(p21:GFP)sh506* is still required, by reviewing a combination of markers within specific GFP populations at the cellular level. I will additionally examine whether senescent cell phenotype changes according to length of time after irradiation. I would expect there to be temporal changes in these senescence markers, such as later SASP induction, as has been published in mammalian systems (Demaria *et al.,* 2014; Laberge *et al.,* 2015; Freund *et al.,* 2011; Acosta *et al.,* 2008). I will also assess zebrafish behaviour for changes in phenotype of movement & heart function, as you would expect in an aged animal with high burden of senescence, providing evidence to support the idea that irradiation-induced senescence is acting as a proxy for ageing-induced senescence. These in combination would validate the zebrafish system, and allow us to begin to tackle the current gaps in knowledge within the senescence field.

Chapter 5. Validation of zebrafish larval irradiation-induced senescence model.

5.1.1. Introduction

Having a method for identifying *p21* positive cells in a translucent model organism will allow assessment of *in vivo* senescent cells in a whole organism context. Irradiation of zebrafish larvae up-regulates multiple markers of senescence described in the context of mammalian ageing, such as *p21, p16-like, mmp2, p53 and* γH2AX. As these zebrafish develop rapidly and have high fecundity, then compounds that modulate the amount of senescence following irradiation, can be screened by monitoring fluorescence intensity in *TgBAC(p21:GFP)sh506* zebrafish. To be able to fully establish a new model of stress-induced senescence in irradiated zebrafish larvae, comparisons between senescent cells in an aged mammalian context with the fluorescent cells seen in irradiated *TgBAC(p21:GFP)sh506* zebrafish are required. One major component is the assessment and presence of a multitude of senescence-associated markers within the same cell. Demonstrating comparable markers in 3 days post-irradiation (dpIR) *TgBAC(p21:GFP)sh506* zebrafish would greatly support the theory that the GFP positive cells were truly senescent. Using the transgenic fluorescent reporter established in the previous chapter, I have used techniques such as flow cytometry and fluorescent activate cell sorting (FACS) to assess alternative markers of senescence in GFP positive cells.

A further feature of senescent cells is that they are long lasting *in vivo,* with levels of p16 still being present in chemotherapy-treated breast cancer patients 12 months after chemotoxic therapy (Sanoff *et al.*, 2014). Additionally, it can take up to 8 days after irradiation of cells for later SASP factors to be induced (Demaria *et al.,* 2014; Laberge *et al.,* 2015; Freund *et al.,* 2011; Acosta *et al.,* 2008). Therefore, it would be a useful validation of the model to determine whether the GFP cells in irradiated *TgBAC(p21:GFP)sh506* zebrafish were persistent for longer after irradiation and have the same temporal SASP regulation.

In an irradiated zebrafish with a significant portion of senescent cells, I would expect to see changes in organismal health status that would mimic common signs of ageing. A typical example is reduced mobility, a common sign of age-associated frailty (Goodpaster *et al.*, 2006; Bergland *et al.*, 2017). The benefit of being able to study whole organism health in our senescent model is so to establish whether senolytics, which were supposed to reduce age-associated disease, can improve changes in our irradiated zebrafish's health status. Altogether, this would permit screening for senolytics *in vivo* in the first instance, therefore taking into account off-target toxicities and changes in organism health. This would likely improve the success rate of senolytics going through preclinical and clinical trials that identified through this method.

5.1.2. Aims

This chapter aims to validate the new transgenic reporter for *p21* promoter activation, *TgBAC(p21:GFP)sh506*. It is important to assess how well the GFP reports live *in vivo* senescence, by examining multiple senescence markers and whether they correlate with GFP fluorescence. Further validation is required to strengthen the evidence that irradiation-induced senescence in zebrafish larvae is comparable to phenotypes described in age-associated senescence accumulation in mammals.

The aims of this chapter are:

1. To develop an assay for assessing multiple markers of senescence within the same cell through Fluorescent Activated Cell Sorting (FACS) and immunofluorescence.
2. To determine the proportion of fluorescent cells from *TgBAC(p21:GFP)sh506* that also express markers for the DNA damage response, SASP, and lack of proliferation.
3. To assess whether *TgBAC(p21:GFP)sh506* fluorescence is persistent after 3dpIR.
4. To identify changes in health status that were relevant in age-associated pathology following irradiation of zebrafish larvae.

5.2.1. Optimisation of flow cytometry for assessment of cells from *TgBAC(p21:GFP)sh506*

Alongside live imaging of senescent cells, a useful feature of having a fluorescent transgenic reporter zebrafish for *p21* is the ability to analyse cell morphology and protein expression by flow cytometry and cell sorting. First, optimisation of the dissociation process was required to retrieve live cells from whole 3dpIR zebrafish larvae. 30 minutes of dissociation using the collagenase liberase (40µg/ml) was the minimum amount of time required for zebrafish tissue to disintegrate into a dissociated cell suspension. Cells were then assessed on a haemocytometer, where it was confirmed that the majority of cells were in single cell suspension (Figures 5.1, 5.2). Fluorescent microscopy of these cells showed a much higher proportion of GFP positive cells in transgenic fish compared to wild-type siblings, and even more so in cells from irradiated fish compared to unirradiated controls, corroborating results from live fluorescence imaging at the same time-point.

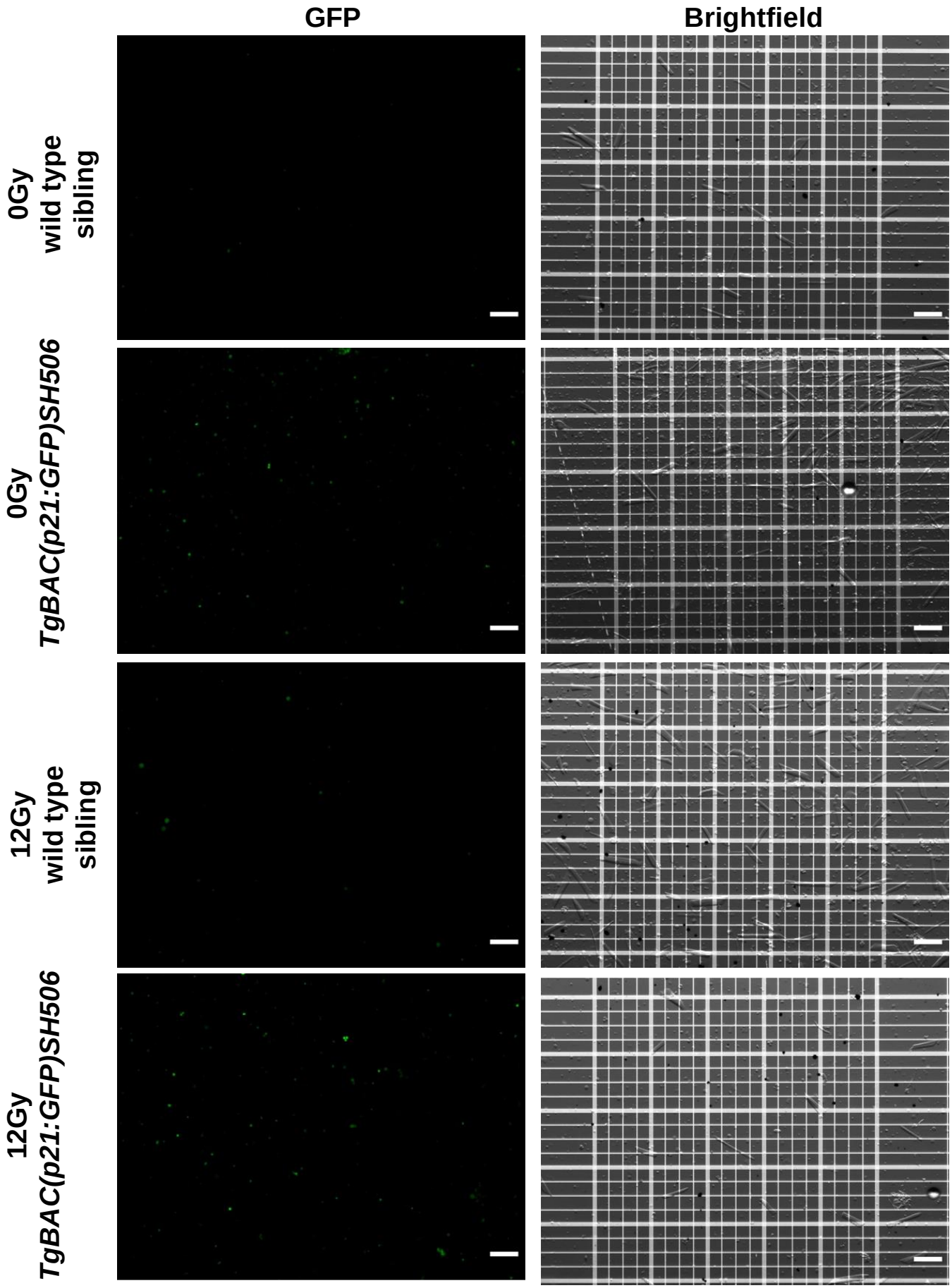
GFP
Brightfield
0Gy wild type sibling
0Gy TgBAC(p21:GFP)SH506
12Gy wild type sibling
12Gy TgBAC(p21:GFP)SH506

Figure 5.1. Live cells dissociated from 5dpf *TgBAC(p21:GFP)sh506* zebrafish (example 1). 10ul of dissociated cells were added to a haemocytometer, before being imaged for GFP fluorescence. Wild type siblings and unirradiated fish were used to compare with cells from 12Gy 3dpIR zebrafish. Scale bar 25μM.

GFP
Brightfield
0Gy wild type sibling
0Gy TgBAC(p21:GFP)SH506
12Gy wild type sibling
12Gy TgBAC(p21:GFP)SH506

Figure 5.2. Live cells dissociated from 5dpf *TgBAC(p21:GFP)sh506* zebrafish (example 2). 10ul of dissociated cells were added to a haemocytometer, before being imaged for GFP fluorescence. Wild type siblings and unirradiated fish were used to compare with cells from 12Gy 3dpIR zebrafish. Scale bar 25μM

To assess GFP intensity of single cells dissociated from *TgBAC(p21:GFP)sh506* zebrafish, flow cytometry of single cell suspensions were carried out (Figure 5.3). I then determined a suitable gating strategy such that only live cells are assessed. Debris was removed from analysis by gating out regions that were too small to be cells and were present in a control sample of live cell media alone. Secondly, a gate was used to remove non-spherical objects, which were usually clumped cells, by removing data that did not have a 1:1 ratio of forward scatter height to area. The viability dye 7AAD allowed removal of dead cells from later analyses. A 7AAD negative sample determined the amount of fluorescence required for a cell to be deemed live or dead in this system. The same was then carried out for GFP fluorescence, using both irradiated and unirradiated wild-type siblings to assess whether the treatment may induce auto-fluorescence or non-specific signal, which was not the case under these conditions. During the gating for GFP, I was able to assess not only GFP positive or negative groups, but also split the positive cells into dim and bright, with the bright cells having high GFP intensities that were only seen in transgenic zebrafish following irradiation (Figure 5.3E).

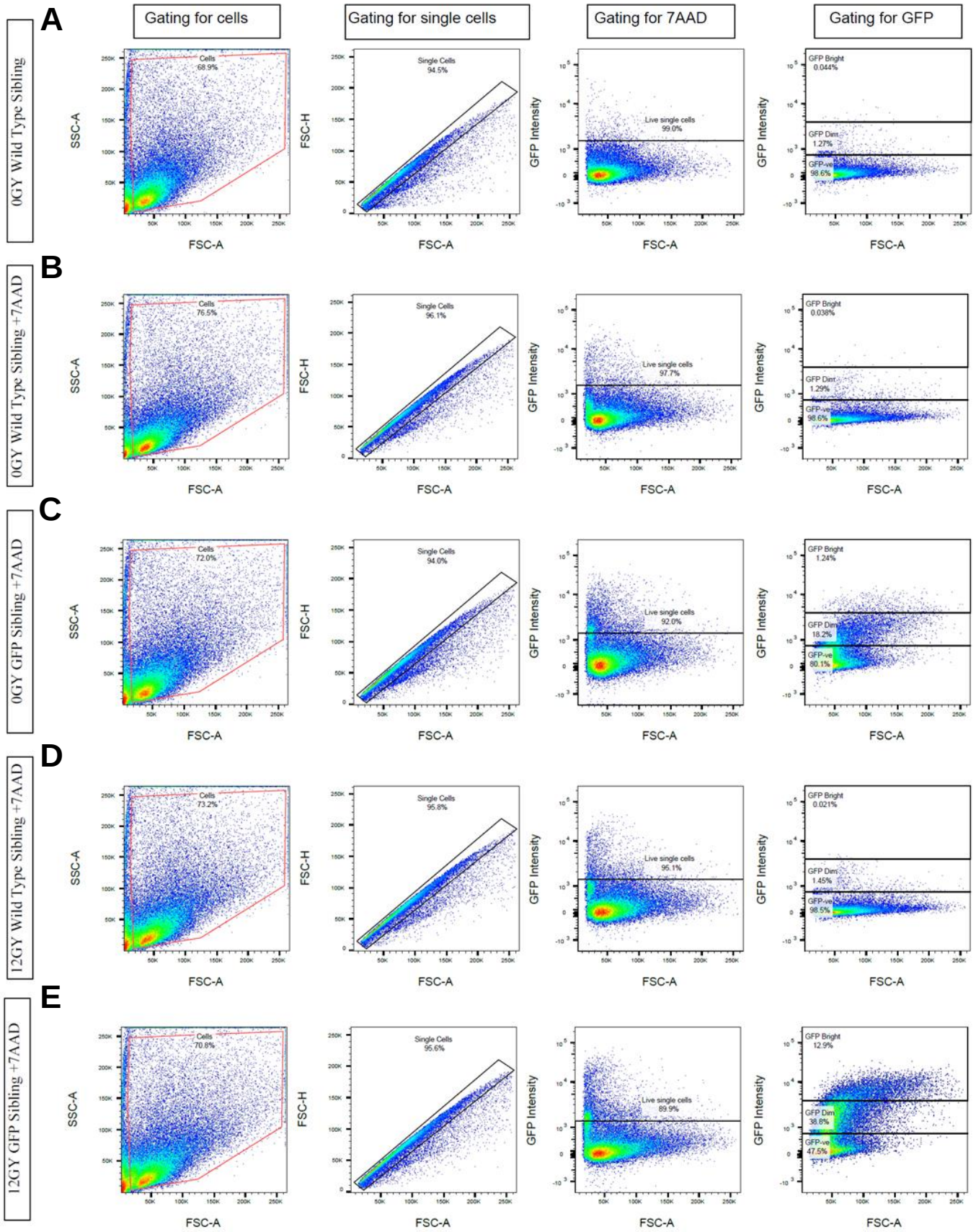
A
Gating for cells
Gating for single cells
Gating for 7AAD
Gating for GFP
0GY Wild Type Sibling
Cells
68.9%
Single Cells
94.5%
Live single cells
99.0%
GFP Bright
0.044%
GFP Dim
1.27%
GFP-ve
98.6%
B
0GY Wild Type Sibling +7AAD
Cells
76.5%
Single Cells
96.1%
Live single cells
97.7%
GFP Bright
0.038%
GFP Dim
1.29%
GFP-ve
98.6%
C
0GY GFP Sibling +7AAD
Cells
72.0%
Single Cells
94.0%
Live single cells
92.0%
GFP Bright
1.24%
GFP Dim
18.2%
GFP-ve
80.1%
D
12GY Wild Type Sibling +7AAD
Cells
73.2%
Single Cells
95.8%
Live single cells
95.1%
GFP Bright
0.021%
GFP Dim
1.45%
GFP-ve
98.5%
E
12GY GFP Sibling +7AAD
Cells
70.8%
Single Cells
95.6%
Live single cells
89.9%
GFP Bright
12.9%
GFP Dim
38.6%
GFP-ve
47.5%
SSC-A
FSC-A
FSC-H
GFP Intensity

Figure 5.3. Flow cytometry gating strategy to assess GFP intensity of live cells dissociated from 5dpf *TgBAC(p21:GFP)sh506* zebrafish. Dissociated cells were gated to remove debris using forward and side scatter (column 1). The population was then gated to remove doublets using forward scatter height and area (column 2). Dead cells were then removed from analysis using 7-Aminoactinomycin D (7AAD) viability dye (column 3), live cells were gated using a 7AAD negative control (A). Live cells were then assessed for GFP intensity (column 4), using cells from wild type siblings as negative controls (B,D) to determine the gate for positive cells (column 4). A further gate was established to determine a population of cells specific to irradiation according to GFP intensity, using unirradiated transgenic fish (C) as a negative control.

5.2.2. Quantifying live GFP positive cells in *TgBAC(p21:GFP)sh506* fish after irradiation by flow cytometry

Following dissociation of live fluorescent cells from irradiated zebrafish larvae, GFP intensity at the single-cell level was determined by flow cytometry (Figure 5.4). Not only were there more GFP positive cells overall following irradiation, 14% (SD 1.762) of GFP positive cells from irradiated *TgBAC(p21:GFP)sh506* zebrafish had a higher intensity that was ever seen in their unirradiated counterparts, I defined these as 'GFP-bright' (Figure 5.4A). The proportion of cells positive for GFP in unirradiated fish [23% (SD 5.696)], classified as GFP-dim, was also increased to 39.9% (SD 7.802) following irradiation. The mean fluorescence intensity of all live cells also increased both with the transgene compared to wild-type siblings, being on average 3x brighter, and with the irradiated vs. unirradiated transgenic fish being 2.5x brighter still (Figure 5.4B). Verifying this, histograms for GFP intensity of cells with or without irradiation also displayed higher fluorescence intensity following irradiation of *TgBAC(p21:GFP)sh506* (Figure 5.4C). This suggested that, as was seen by fluorescence microscopy (Figure 4.7), GFP intensity was higher in *TgBAC(p21:GFP)sh506* compared to wild-type siblings. Further, GFP intensity increased following irradiation of *TgBAC(p21:GFP)sh506* zebrafish compared to unirradiated *TgBAC(p21:GFP)sh506* siblings. The proportion of cells positive for GFP when quantified in this manner was 38.96% (SD 1.509) at 3dpIR, and 8.35% (SD 3.063) without irradiation. Importantly, fluorescence intensity and number of positive cells did not change following irradiation in live cells from wild-type siblings (Figure 5.4B-D). All of these data show comparable results to previous microscopy data (Figure 4.7), strengthening the conclusions from both of these techniques.

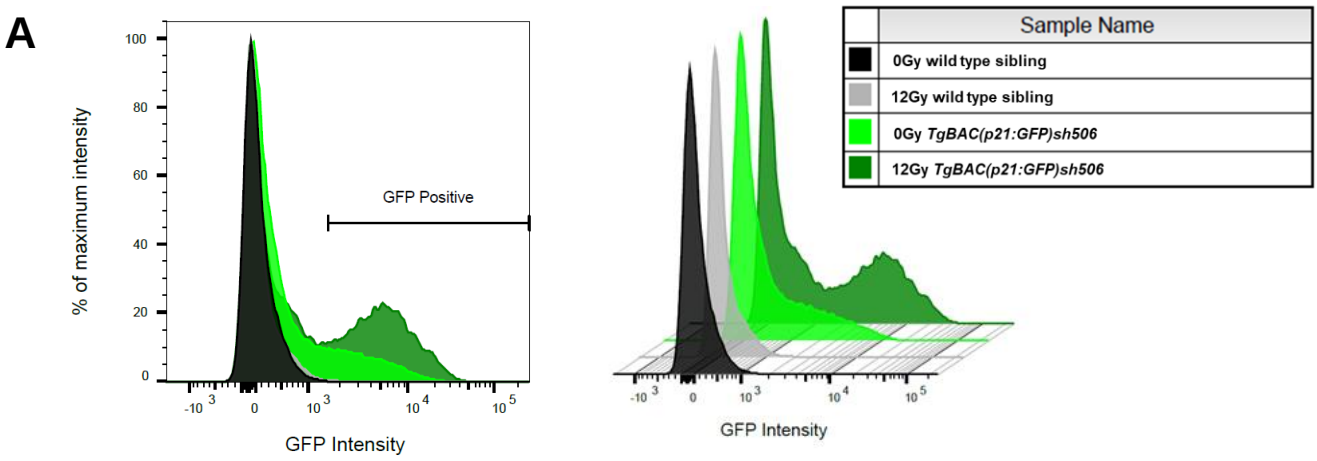
A
% of maximum intensity
GFP Positive
GFP Intensity
Sample Name
0Gy wild type sibling
12Gy wild type sibling
0Gy TgBAC(p21:GFP)sh506
12Gy TgBAC(p21:GFP)sh506
GFP Intensity

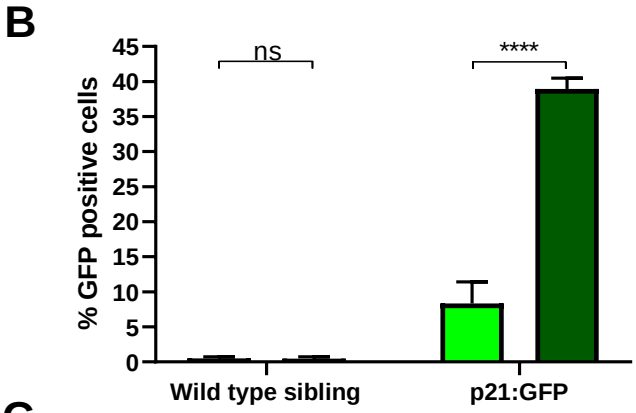
B
% GFP positive cells
ns
****
Wild type sibling
p21:GFP

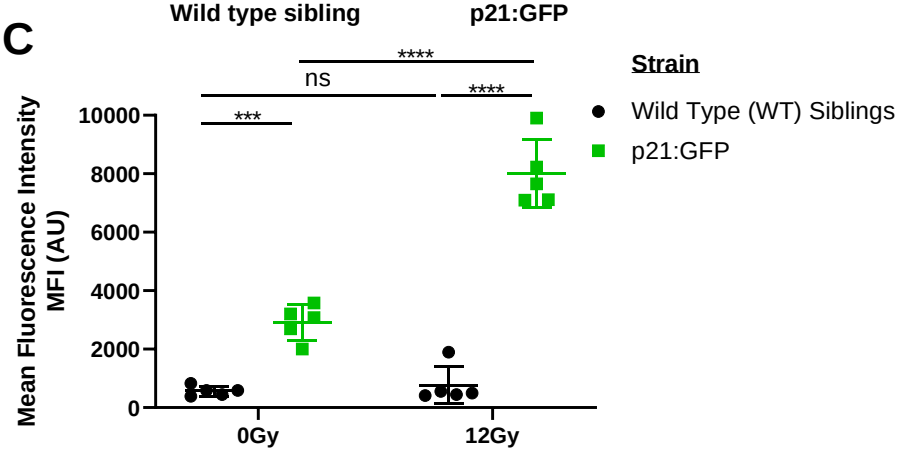
C
Mean Fluorescence Intensity
MFI (AU)
****
ns
****
***
Strain
Wild Type (WT) Siblings
p21:GFP
0Gy
12Gy

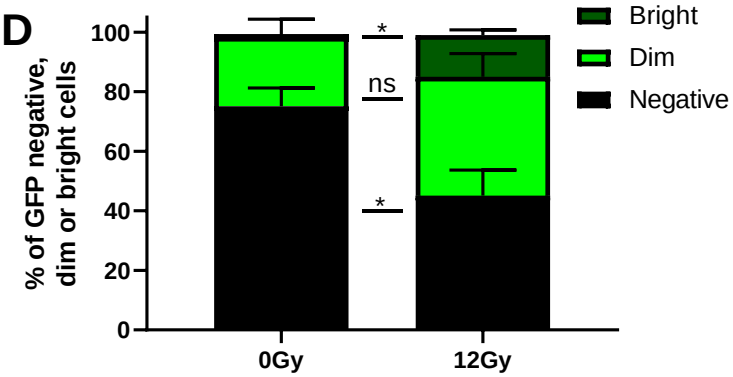
D
% of GFP negative,
dim or bright cells
*
ns
*
Bright
Dim
Negative
0Gy
12Gy

Figure 5.4. Quantification of live cells dissociated from 3dpIR *TgBAC(p21:GFP)sh506*. A) Histogram of GFP intensity of live cells, each group is plotted as a % of maximum intensity. Gate for cells deemed as GFP positive is demonstrated. Staggered overlay is also shown for visualisation purposes. B) Percentage of live GFP positive cells, using wild type siblings to determine intensity that is GFP negative, as anotated by GFP positive gate in (A). C) Mean GFP fluorescence intensity of live cells. D) The proportion of live cells that are GFP negative, dim, or bright in 3dpIR *TgBAC(p21:GFP)506*, determined by aforementioned gating strategy. Wild type siblings and unirradiated fish were used for comparison. Data was examined by 2way ANOVA with Tukey's (B,C) or Sidak's (D) multiple comparison test. At least 50 fish were examined in three-five indepenent experiments. * $p < 0.05$; *** $p < 0.001$; **** $p < 0.0001$. Error bars represent standard deviation.

Cells dissociated from *TgBAC(p21:GFP)sh506* zebrafish had a larger cell size (forward scatter) and granularity (side scatter) at higher GFP intensities (Figure 5.5). This change in size is a phenotype well associated with *in vitro* senescence and so could support the notion that GFP fluorescence is marking senescent cells in our irradiated zebrafish (Parrinello *et al.*, 2003a).

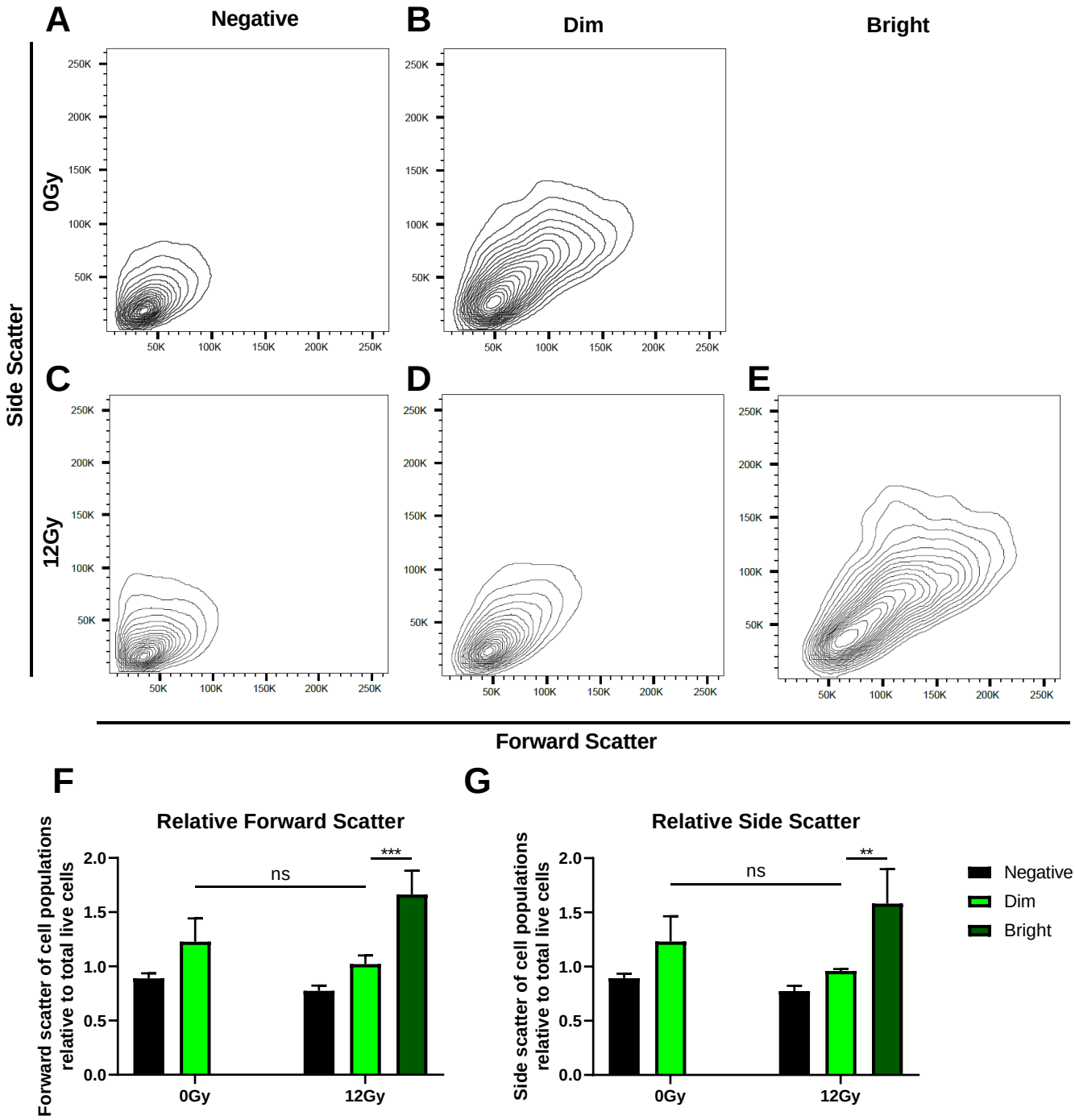

Figure 5.5. Assessment of cell size and granularity according to GFP intensity in 3dpIR *TgBAC(p21:GFP)sh506.* Live cells were dissociated from 3dpIR TgBAC(p21:GFP)506, forward scatter was used to assess cell size, side scatter was used to assess granularity. A-E) Representative contour plots of live cells. A-B) Unirradiated controls, with either negative (A) and Dim (B) GFP expression. C-E) 12Gy 3dpIR cells, with either negative (C), Dim (D) and bright (E) GFP expression. F) relative cell size determined by forward scatter values in different GFP populations relative to forward scatter of all live cells regardless of GFP intensity. G) relative cell granularity determined by side scatter values in different GFP populations relative to side scatter of all live cells. Three independent repeats were carried out. Data was examined by 2way ANOVA with Tukey's multiple comparisons. ** $p < 0.01$; *** $p < 0.001$. Error bars represent standard deviation.

5.2.3. Optimisation of FACS for separating dissociated zebrafish cells based on GFP intensity in *TgBAC(p21:GFP)sh506*

To be able to assess numerous alternative senescence markers in these different cell populations of GFP intensity, by FACS for 3dpIR zebrafish cells, I first assessed the efficiency of the sorting process itself in our system. Using optimised flow cytometry gating strategies (Figure 5.3.), cells were sorted according to GFP-negative, dim and bright populations in 5dpf *TgBAC(p21:GFP)sh506* zebrafish (Figure 5.6). Unirradiated controls were sorted into negative and dim populations, and 12Gy 3dpIR zebrafish were sorted into negative, dim and bright. Following this, the sorted cells were placed back into the flow cytometer to assess fluorescence intensity of each population. The resulting populations were between 86 and 99% specific to their sorted groups, which I deemed efficient enough for later experiments.

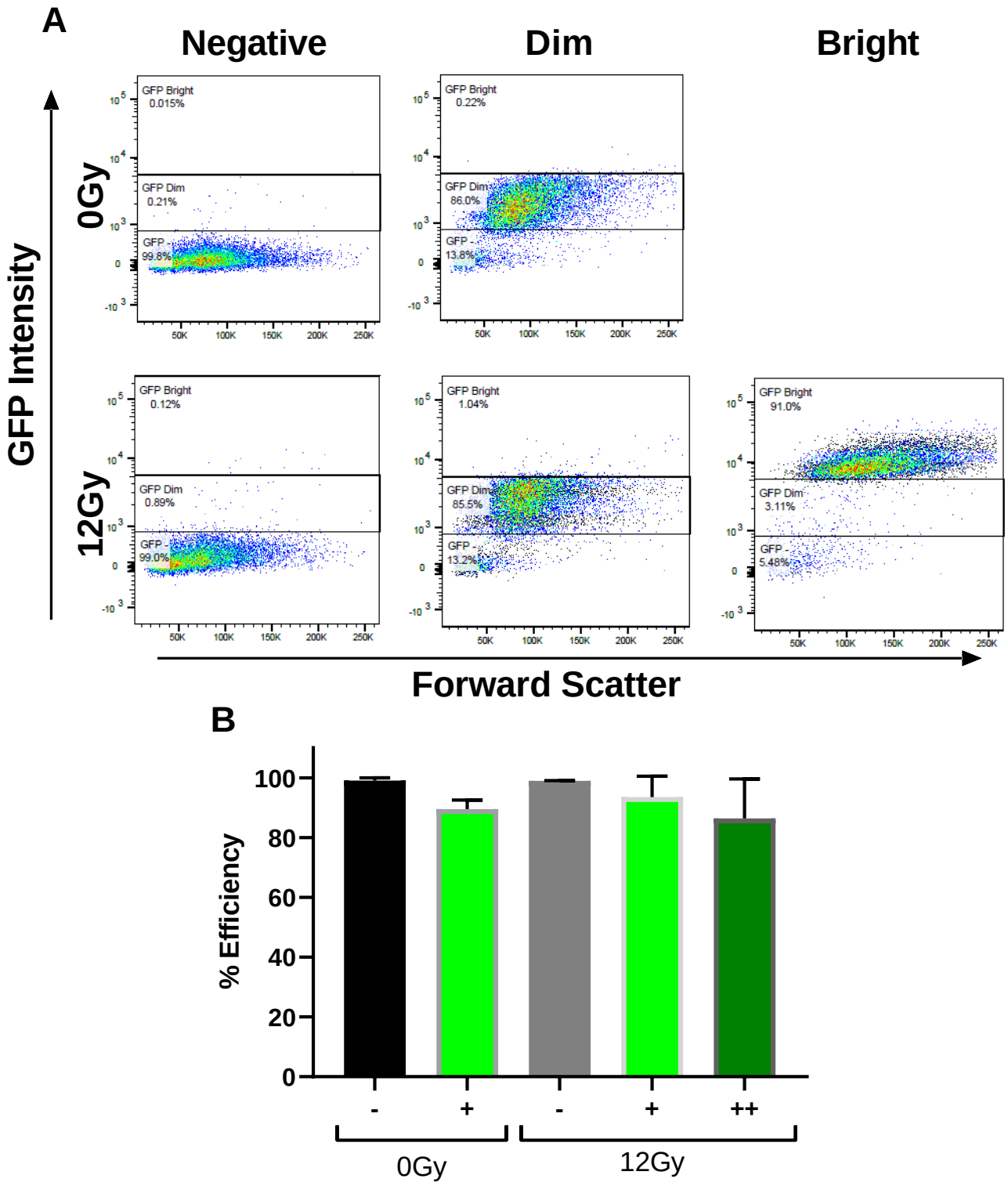

Figure 5.6. FACS of *TgBAC(p21:GFP)sh506* zebrafish is between 86 and 99% efficient. A) Representative images of flow cytometry profile of cells sorted by FACS Aira II flow cytometer. B) Efficiency of cell sorting was calculated in each of the sorted groups according to percentage of cells that are within the correct groups of GFP intensity that they were originally sorted for. Assessed over three independent experiments. Data was analysed by one-way ANOVA and Tukey's test for multiple comparisons, P values were between 0.23 and 0.99. Error bars standard deviation.

I next developed a protocol to cytospin these cell populations onto individual slides for immunofluorescence analysis. A pilot experiment whereby cells were fixed and cytospun at different speeds and cell densities, before Haematoxylin and Eosin (H&E) staining to look at cell morphology post-cytospin (Figure 5.7). 500rpm was found to be the best protocol to cytospin cells at densities typically seen following sorting the zebrafish previously (50,000-250,000), they were spaced out enough to identify individual cells whilst remaining intact.

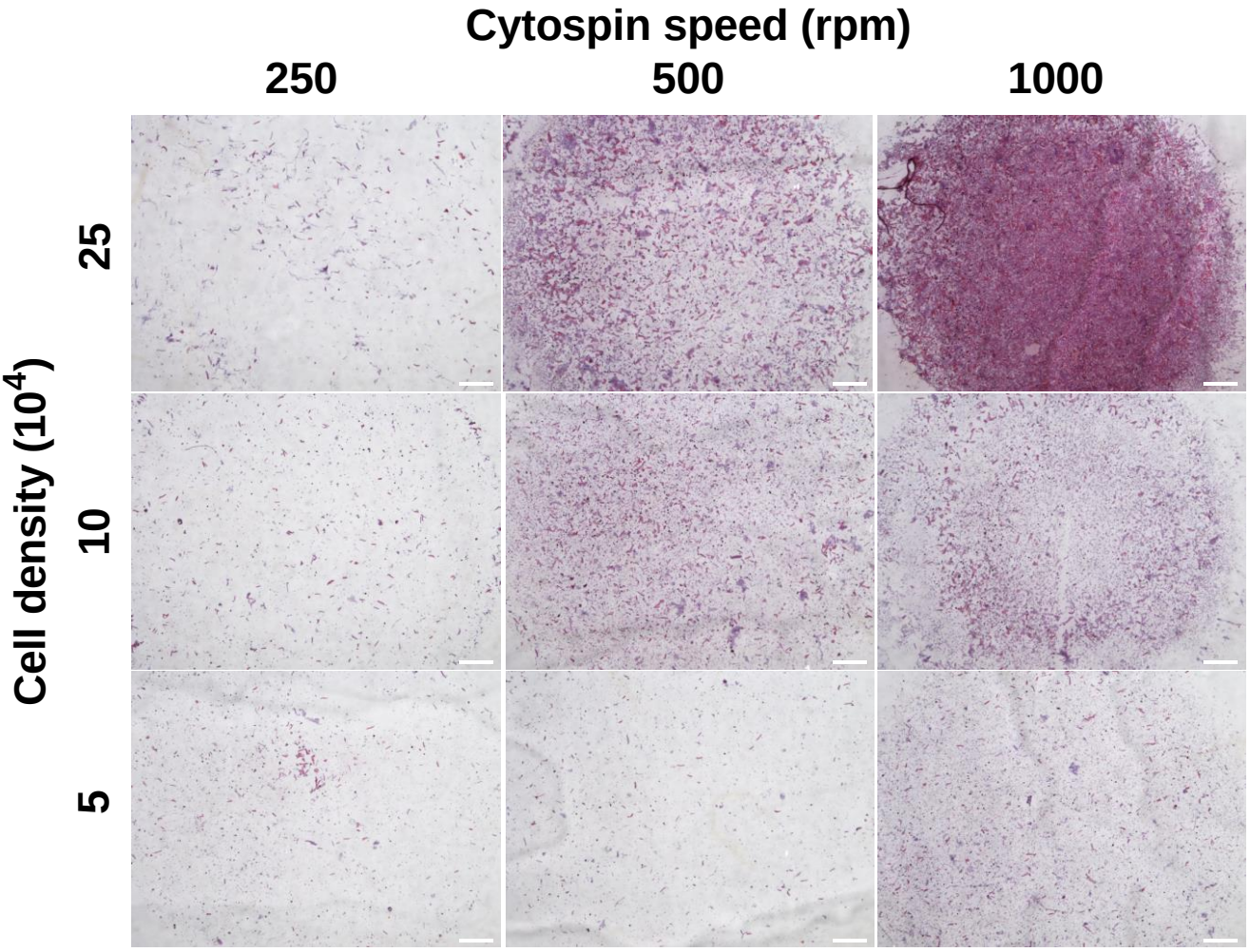

Figure 5.7. Cytospin at 500rpm of dissociated 5dpf zebrafish cells allowed single cells to be distinguished and maintain morphology. Transmitted light photomicropraphs of Haemotoxylin and Eosin staining of cytospun cells at different densities that are typically seen from sorting *TgBAC(p21:GFP)sh506* zebrafish (50,000 in GFP bright; 100,000-250,000 in GFP negative and dim populations). Representative images (2x magnification) shown. Different cytospin speeds were assessed to determine optimal conditions required to get a single layer of dissociated zebrafish cells adhering to a microscope slide. Scale 500μm.

To confirm that the sorted cells did in-fact have differing proportions of GFP intensity, the cytospun cells were stained by immunofluorescence using an anti-GFP antibody (Figure 5.8). Similar to the flow cytometry profile of these post-sorted cells, there was a clear association with anti-GFP staining and GFP intensity used to sort the cells. Cells sorted as GFP-negative has practically no staining, whilst the majority of cells sorted as dim were majority positive for anti-GFP staining, but were not as high in intensity as the GFP-bright group. Together, these confirmed that I could now sort fluorescent cells from my zebrafish model, cytospin them onto microscope slides, and carry out an immunofluorescence procedure such that enough cells remain adherent to assess protein expression in these different populations.

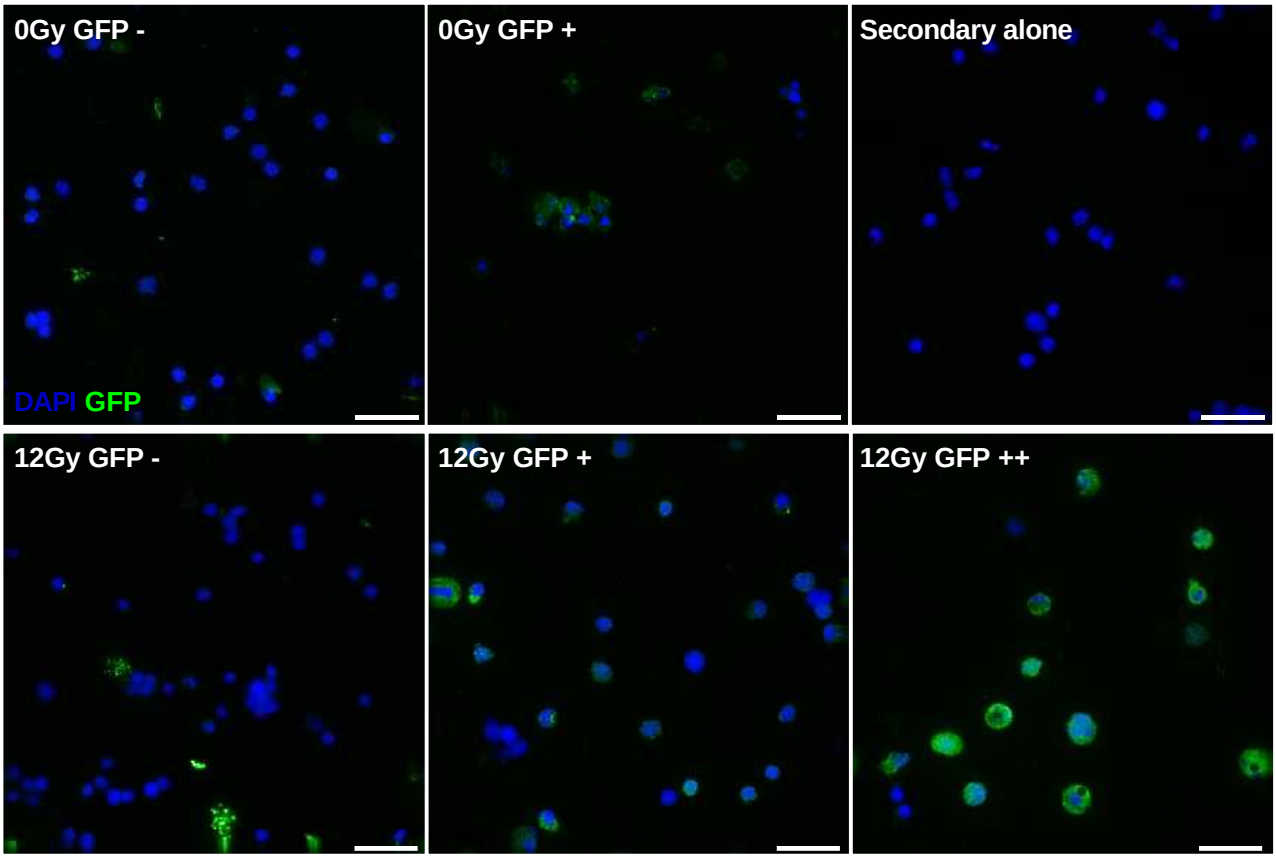

Figure 5.8. GFP immunofluorescence on sorted cells from 3dpIR *TgBAC(p21:GFP)sh506* zebrafish. Confocal fluorescent photomicrographs of immunofluorescence images to assess GFP fluorescence in sorted and cytospun cells. Representative images shown. DAPI was used to stain nuclei. Cells sorted as Negative (-), Dim (+), and Bright (++) populations. Scale bar 25μM.

5.2.4. Markers for DNA damage response and lack of proliferation associated with GFP intensity in cells sorted from irradiated *TgBAC(p21:GFP)sh506*

To assess the proportion of alternative markers of senescence in cells sorted from *TgBAC(p21:GFP)sh506* zebrafish, immunofluorescence for γH2AX, a marker of DNA-damage response and PCNA, a marker of proliferation, was carried out (strategy depicted in Figure 2.8). GFP-bright cells had the highest proportion of H2AX positive, PCNA negative cells at 52.16% (SD 8.15), and the GFP-dim populations had more than the GFP-negative group (Figure 5.9). The GFP-dim population from 3dpIR zebrafish had more senescent cells (29.60%, SD 11.39) compared to their unirradiated counterparts (9.54%; SD 3.80). This confirms that the fluorescence from irradiated *TgBAC(p21:GFP)sh506* zebrafish is able enrich for markers of senescent cells in the brightest groups.

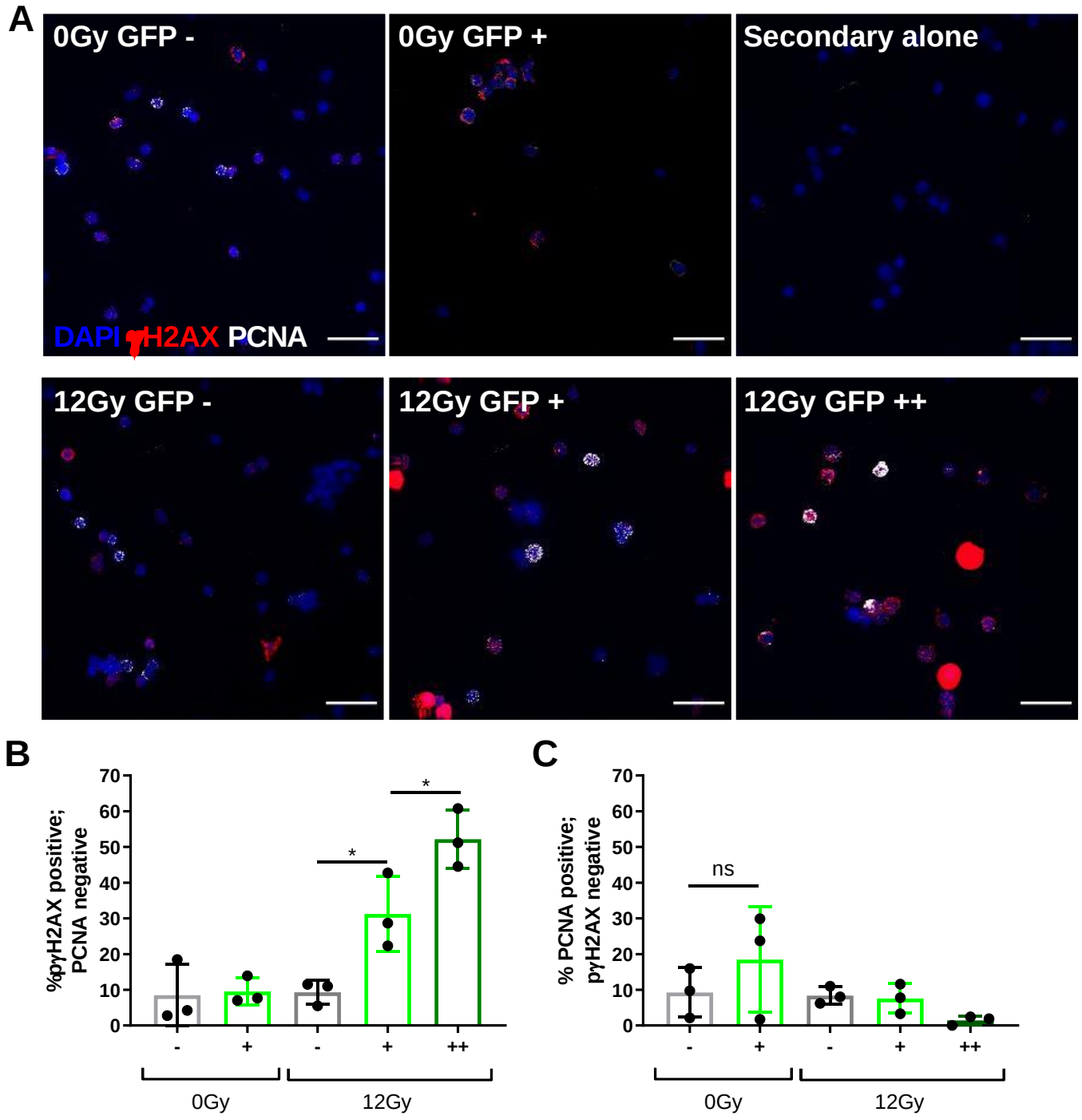
A
0Gy GFP -
0Gy GFP +
Secondary alone
DAPI γH2AX PCNA
12Gy GFP -
12Gy GFP +
12Gy GFP ++
B
%pγH2AX positive; PCNA negative
70
60
50
40
30
20
10
0
*
*
-
+
-
+
++
0Gy
12Gy
C
% PCNA positive; pγH2AX negative
70
60
50
40
30
20
10
0
ns
-
+
-
+
++
0Gy
12Gy

Figure 5.9. GFP intensity positively correlates with γH2AX positive, PCNA negative cells following irradiation in 3dpIR *TgBAC(p21:GFP)sh506 ze*brafish. A) Confocal fluorescent photomicrographs of double immunofluorescence for γH2AX (red) and PCNA (white) in cells sorted by GFP intensity (- negative; + dim; ++ bright) and cytospun onto microscope slides. Representative images shown. A sample without the primary antibody (secondary alone) was used as a negative control. Scale bar 25μM. B) Quantification of the proportion of γH2AX positive, PCNA negative cells within each group. C) Quantification of γH2AX negative, PCNA positive cells within the same groups. Data examined by one-way ANOVA with Sidak's multiple comparisons test. 300 cells quantified for each group over 3 independent experiments. * $p < 0.05$. Error bars represent standard deviation.

5.2.5. IL6 expression correlates with GFP intensity in 5dpf *TgBAC(p21:GFP)sh506* regardless of irradiation

To examine the presence of late senescence markers in these sorted populations, a dual immunofluorescence for IL6 and PCNA was carried out. Due to limited availability of zebrafish-compatible antibodies, γH2AX could not be used in combination with IL6 as they shared the same species of secondary antibody. As with γH2AX expression, there was a significant proportion of IL6 positive and PCNA negative cells in the GFP-bright population (Figure 5.10). Importantly, the levels of IL6 positive and PCNA negative GFP-bright cells was 20.3% (SD 5.332), was less than half the amount of γH2AX positive and PCNA negative GFP-bright cells at the same time-point (52.16%, SD 8.15). Additionally, there was 14.7% (SD 3.549) of IL6 positive, PCNA negative cells in unirradiated GFP-dim cells, which is comparable to that which was demonstrated following irradiation in the GFP-bright group. This suggests that following irradiation in zebrafish larvae, it may take longer for the onset of the SASP compared to DNA damage response and *p21* expression.

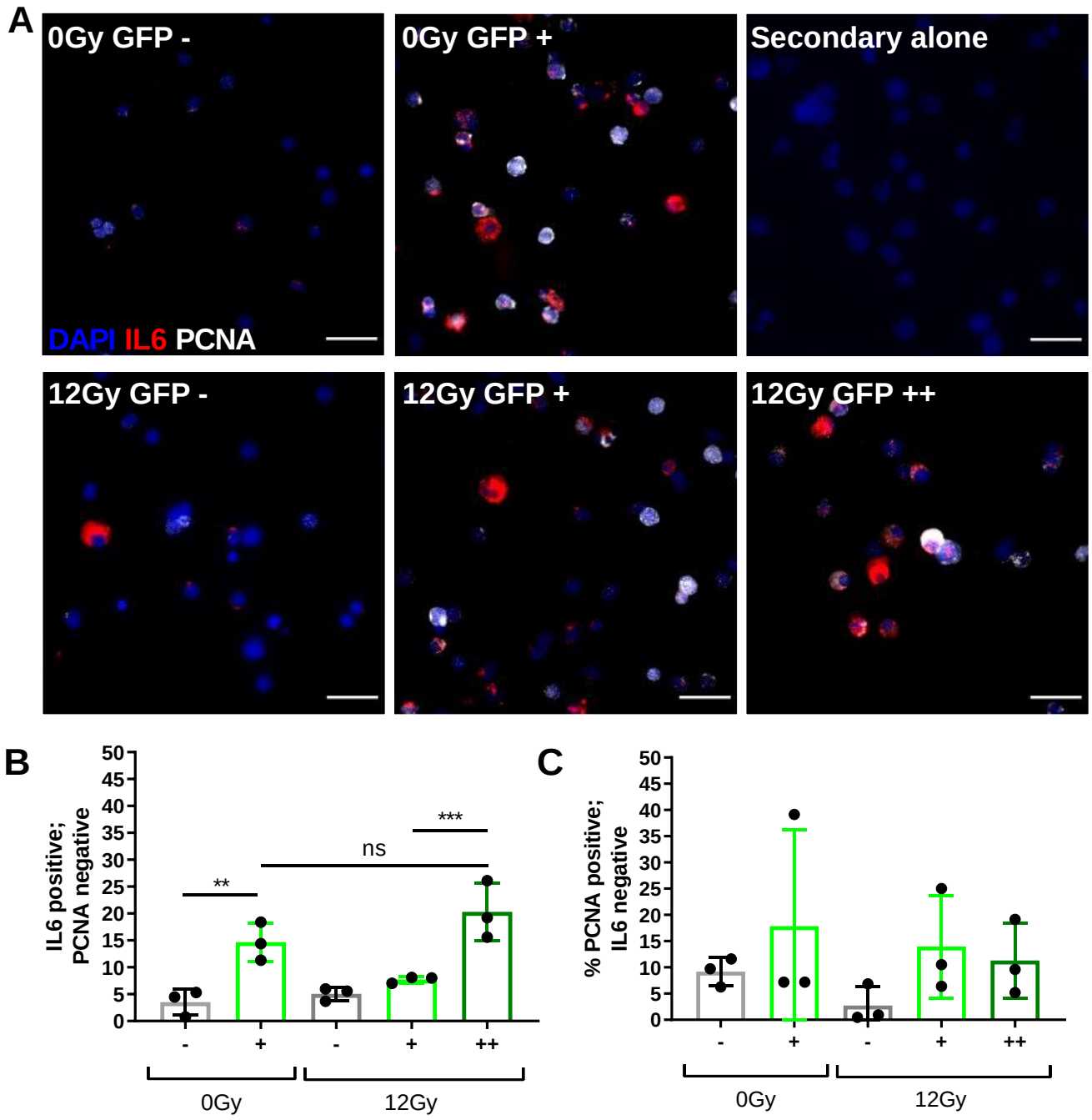

Figure 5.10. A portion of GFP positive cells are IL6 positive, PCNA negative irrespective of irradiation in 3dpIR *TgBAC(p21:GFP)sh506* zebrafish. A) Transmitted fluorescent photomicrographs of double immunofluorescence for IL6 (red) and PCNA (white) in cells sorted by GFP intensity (- negative; + dim; ++ bright) and cytospun onto microscope slides. Representative images shown. A sample without the primary antibody (secondary alone) was used as a negative control. Scale bar 25μM. B) Quantification of the proportion of IL6 positive, PCNA negative cells within each group. C) Quantification of IL6 negative, PCNA positive cells within the same groups. Data examined by one-way ANOVA with Sidak's multiple comparisons test. 300 cells quantified for each group over 3 independent experiments. **p < 0.01; *** p < 0.001. Error bars represent standard deviation.

5.3.1 - Irradiated zebrafish show no reduction in survival by 10dpIR

To address whether expression of markers of senescence changes at later time-points in irradiated zebrafish larvae, I next assessed survival and irradiation-induced toxicity of these animals at 10dpIR. It is important to emphasise at these time-points, zebrafish become protected animals and as such, I first received approval from the UK Home Office to allow me to carry out these experiments. Zebrafish were irradiated at 2dpf and assessed for signs of toxicity at 5dpf, those that looked healthy and did not present with signs of toxicity described in Figure 3.2 were allowed to grow until 12dpf. No reduction in survival was seen between 5 and 12dpf in irradiated zebrafish compared to unirradiated counterparts (Table 5.1). 12dpf zebrafish were smaller in overall size compared to unirradiated counterparts (Figure 5.11), despite displaying no obvious signs of ill health and irradiation-induced toxicity. 12dpf zebrafish were irradiated 10 days prior, in mammalian models the same timeframe was enough to show SASP factors like IL6 to be up regulated compared to unirradiated controls (Coppé *et al.,* 2008).

	0Gy Survival at 12dpf (%)	12Gy Survival at 12dpf (%)
Experiment 1	96	94
Experiment 2	94	92
Experiment 3	90	90

Table 5.1. % survival of zebrafish from 5 to 12dpf. Zebrafish were irradiated at 2dpf and were assessed daily between 5 and 12dpf for signs of ill-health such as abnormal swimming behaviour. % survival was calculated between 5 and 12dpf. 50 fish used per independent experiment. Data examined by unpaired T test, p = 0.5614.

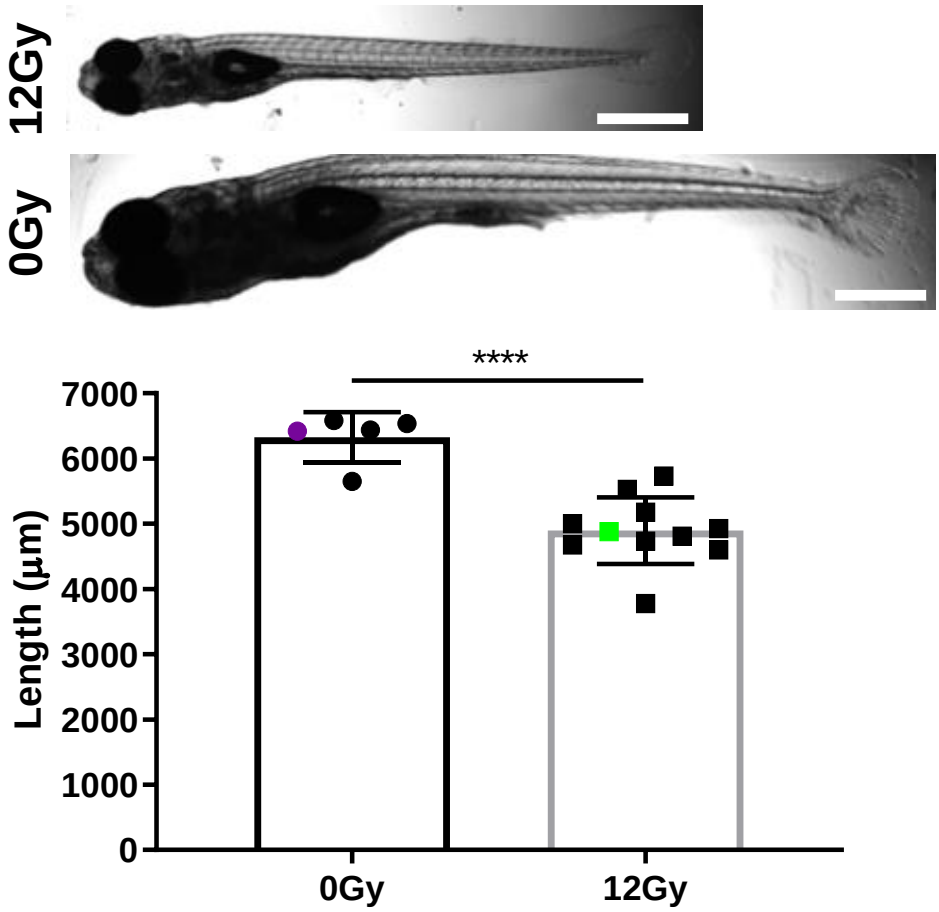

Figure 5.11. 10dpIR zebrafish are smaller than unirradiated counterparts. 12dpf zebrafish, either irradiated at 2dpf or not, were imaged to assess morphology. A) Reflected light photomicrographs are representative 4x magnification images that refer to averagely sized fish from each group (coloured in graph, arrow in image). B) Quantification of whole body length from mouth to end of tail fin. Statistical significance determined by unpaired T-test with Welch's correction. n = 5 (0Gy), 11 (12Gy). Scale 500µm. Error bars standard deviation.

5.3.2 – GFP-dim and bright populations were persistent in 10dpIR *TgBAC(p21:GFP)sh506* zebrafish

To examine whether *p21* promoter activation and GFP fluorescence is persistent following irradiation of zebrafish larvae, cells from 10dpIR *p21*:GFP zebrafish were sorted and examined for GFP expression. Live dissociated cells from 10dpIR zebrafish showed an increased proportion of GFP positive cells when compared to their unirradiated counterparts (Figure 5.12). There remained a 'GFP-bright' population, which most likely suggests that there were cells with sustained *p21*-promoter activation. Compared to 3dpIR, the number of cells classified as GFP-bright was reduced from 14.07% (SD 1.76) of the total cell population to 6.33% (SD 0.69) (Figure 5.12B). There were a greater proportion of GFP-dim cells in unirradiated *TgBAC(p21:GFP)sh506* zebrafish (54%, SD 10.96) compared to the earlier 5dpf time-point (23.27% SD 5.97). The proportion of GFP-dim cells following irradiation, 48.33% (SD 5.599) is much more comparable to unirradiated zebrafish at this time-point. However, the mean fluorescence intensity of all live cells remained around twice as bright following irradiation (5.12C). These data suggest that some of the irradiation-induced GFP expression in *TgBAC(p21:GFP)sh506* zebrafish is persistent at later time-points.

A

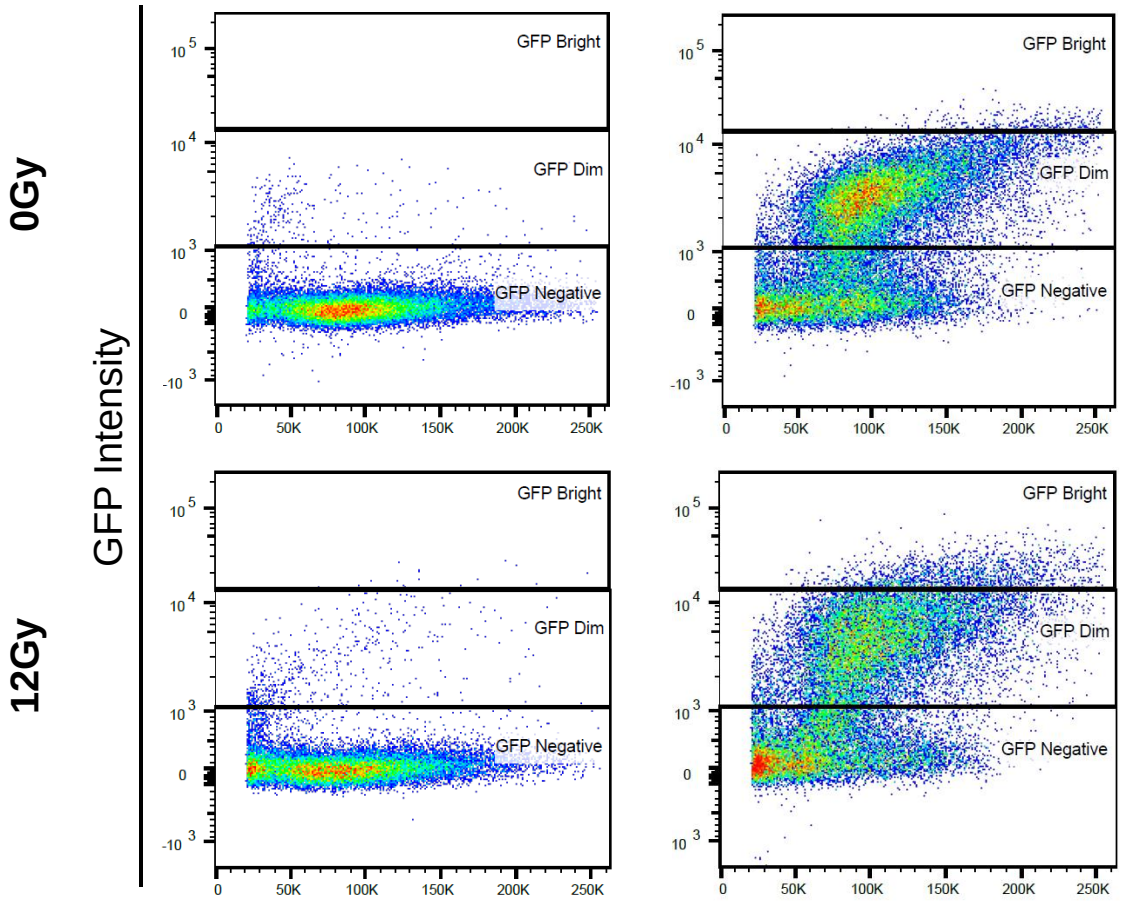

B

Irradiation dose (Gy)	% GFP - (SD)		% GFP + (SD)		% GFP ++ (SD)	
	3dpIR	10dpIR	3dpIR	10dpIR	3dpIR	10dpIR
0Gy	**75.13** (6.099)	**44.37** (11.48)	**23.27** (5.97)	**54** (10.96)	**0.95** (0.02)	**0.98** (0.03)
12Gy	**45.07** (8.656)	**44.63** (5.52)	**39.9** (7.8)	**48.33** (5.599)	**14.07** (1.76)	**6.33** (0.69)

C

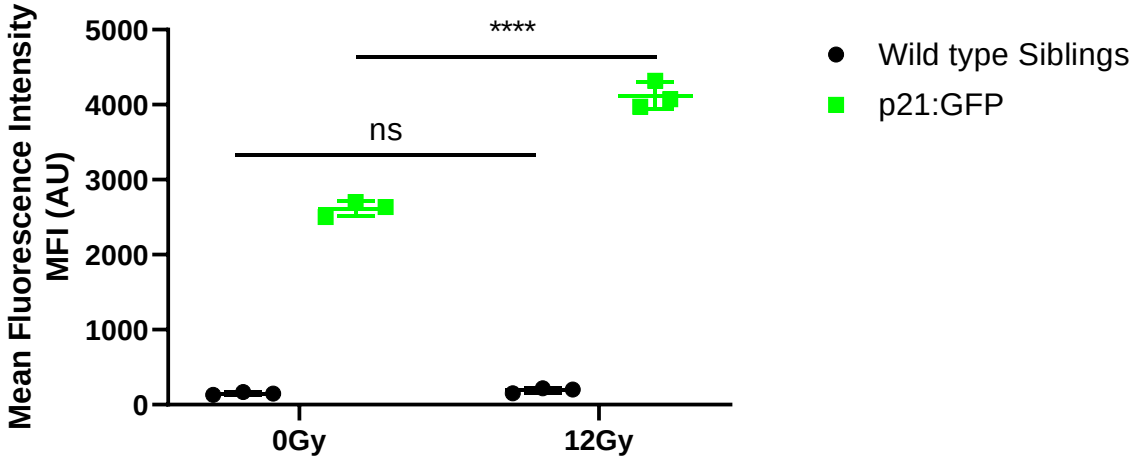

Figure 5.12. GFP bright cells are still present in 10dpIR *TgBAC(p21:GFP)sh506* zebrafish. A) Representative flow cytometry profile of 10dpIR *TgBAC(p21:GFP)506* zebrafish compared to wild-type siblings and unirradiated counterparts. B) Summary table of the average proportions of negative, dim and bright cells that make up the transgenic zebrafish at 10dpIR compared to 3dpIR . C) Mean fluorescence intensity of live cells of 10dpIR *TgBAC(p21:GFP)506* zebrafish compared to wild type siblings and unirradiated counterparts. Data examined by 2way ANOVA with Tukey's multiple comparisons. 3 independent experiments. **** $p < 0.0001$. Error bars represent standard deviation.

5.3.3. GFP-bright cells from 10dpIR *TgBAC(p21:GFP)sh506* zebrafish show persistent DNA damage response and increased IL6 expression

To test whether the persistent GFP positive cells from 10dpIR *TgBAC(p21:GFP)sh506* zebrafish had changes in the proportions of aforementioned markers of senescence, FACS, cytospin and immunofluorescence was carried out. There were fewer GFP-bright cells that remained positive for the DNA damage response and negative for proliferation, with 38.49% (SD 4.50) being positive compared to 52.16% (SD 8.15) at 3dpIR (Figure 5.13). 29.35% (SD 0.55) of GFP-dim cells remained positive for DNA damage response and negative for proliferation, which was comparable to that which was seen at 3dpIR [29.60% (SD 11.39)]. At the later time-point, the p value was 0.16 between the irradiated GFP-dim and bright groups, which may suggest they are more variable compared to 3dpIR. When examining proliferating cells (PCNA positive, γH2AX negative cells), there was an increase in GFP-dim cells compared to negative in the unirradiated population, but this was not seen in the irradiated groups. Though there are consistent GFP positive cells at later time-points, the exact proportion of senescence markers does change over time suggesting a dynamic temporal regulation in the onset of these markers of senescence following irradiation in zebrafish larvae.

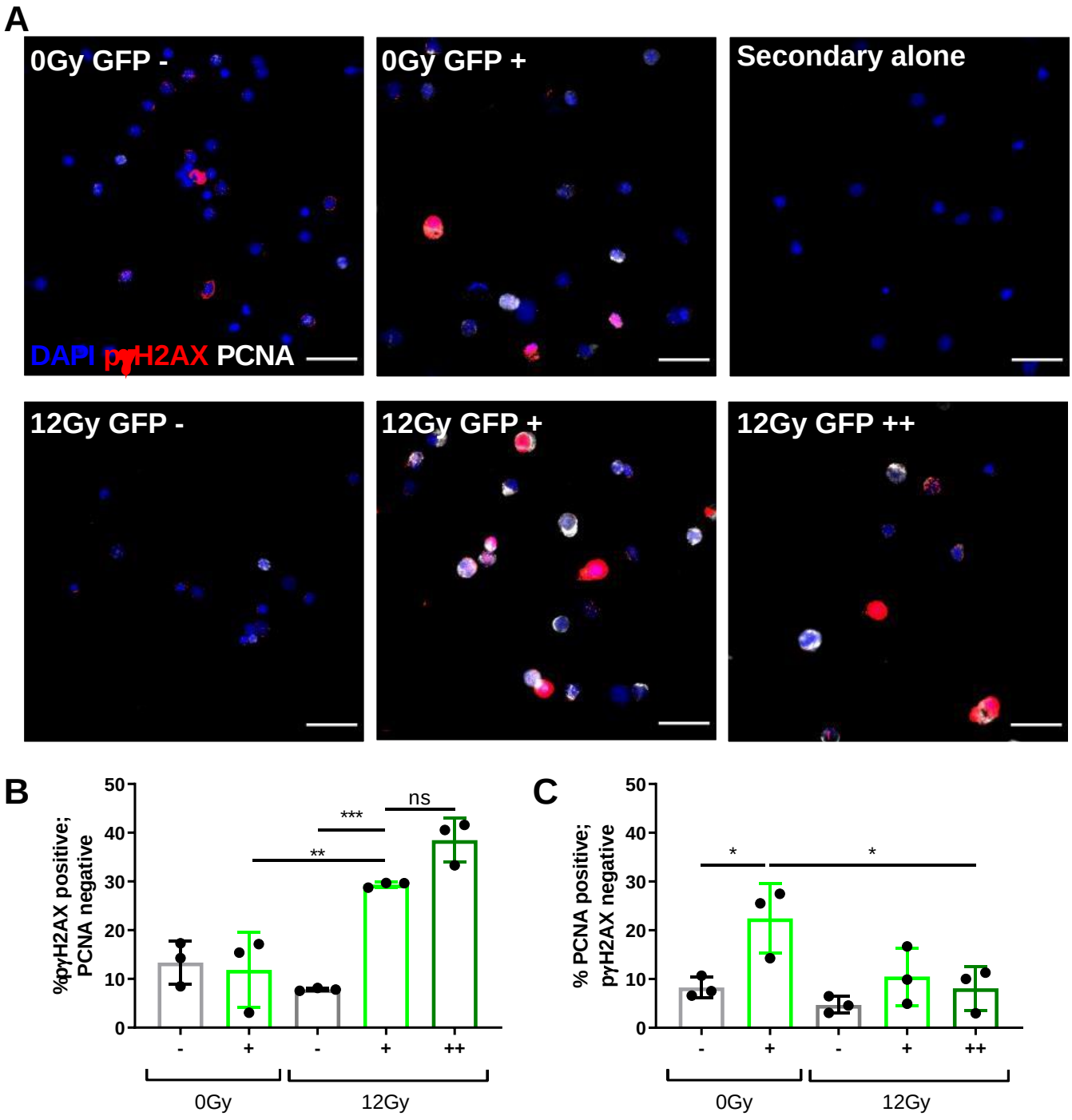

Figure 5.13. GFP positive cells following irradiation have a persistent proportion of γH2AX positive, PCNA negative cells in 10dpIR TgBAC(p21:GFP)sh506 zebrafish. A) Conforcal fluorescent photomicrographs of double immunofluorescence for γH2AX (red) and PCNA (white) in cells sorted by GFP intensity (- negative; + dim; ++ bright) and cytospun onto microscope slides. Representative images shown. A sample without the primary antibody (secondary alone) was used as a negative control. Scale bar 25μM. B) Quantification of the proportion of γH2AX positive, PCNA negative cells within each group. C) Quantification of γH2AX negative, PCNA positive cells within the same groups. Data examined by one-way ANOVA with Sidak's multiple comparisons test. 300 cells quantified for each group over 3 independent experiments. * $p < 0.05$; ** $p < 0.01$; *** $p < 0.001$. Error bars represent standard deviation.

The presence of the SASP-associated marker IL6 did not associate with irradiation at 3dpIR (Figure 5.10.). However, a much greater association of IL6 positive, and PCNA negative cells with GFP fluorescence was seen at 10dpIR (Figure 5.14). 48.09% (SD 6.67) of GFP-bright cells are IL6 positive PCNA negative. This is much greater than the 12.72% (SD 5.70) and 14.87% (SD 0.88) seen in unirradiated and irradiated GFP-dim populations. The proportion of PCNA positive, IL6 negative cells were comparable in GFP-dim populations regardless of irradiation, but was lower in GFP-negative ($p = 0.037$) and bright ($p = 0.065$) cells. Therefore, at 10dpIR, IL6 much more strongly correlates with strong GFP fluorescence compared to 3dpIR.

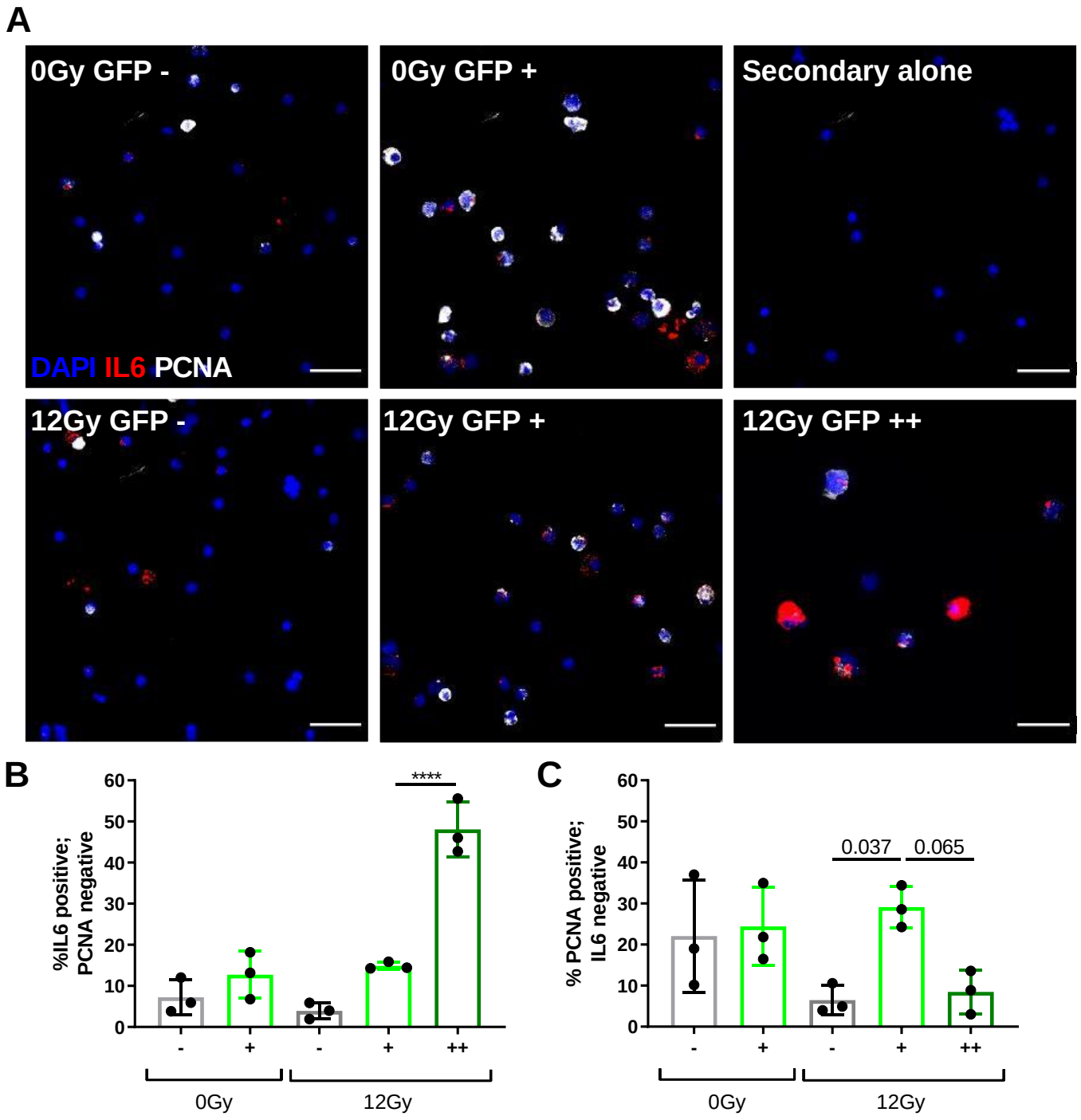

Figure 5.14. GFP bright cells from *TgBAC(p21:GFP)sh506* zebrafish 10 days after irradiation have a specific population of IL6 positive PCNA negative cells. A) Confocal fluorescent photmicrographs showing double immunofluorescence for IL6 (red) and PCNA (white) in cells sorted by GFP intensity (- negative; + dim; ++ bright) and cytospun onto microscope slides. Representative images shown. A sample without the primary antibody (secondary alone) was used as a negative control. Scale bar 25μM. B) Quantification of the proportion of IL6 positive, PCNA negative cells within each group. C) Quantification of IL6 negative, PCNA positive cells within the same groups. Data examined by one-way ANOVA with Sidak's multiple comparisons test. 300 cells quantified for each group over 3 independent experiments. * $p < 0.05$; **** $p < 0.0001$. Error bars represent standard deviation.

5.4. Irradiated zebrafish show persistently reduced motility

To test whether irradiated zebrafish larvae show behavioural changes seen with age, I tested for altered swimming ability by tracking irradiated zebrafish movement at different times post irradiation (Figure 5.15). Mobility was persistently reduced over a 30-minute period at 2, 3 and 10dpIR compared to unirradiated counterparts. The zebrafish were able to move more over time regardless of irradiation. with the average distance moved in a 30 minute period being 1583mm (SD 1588) and 2923mm (SD 1602) at 2dpIR for irradiated and non-irradiated fish, whilst at 10dpIR irradiated and non-irradiated zebrafish moved 7008mm (SD 1930) and 10484mm (SD 2827) respectively. This demonstrates that irradiation induces reduced swimming ability in zebrafish larvae at multiple time-points.

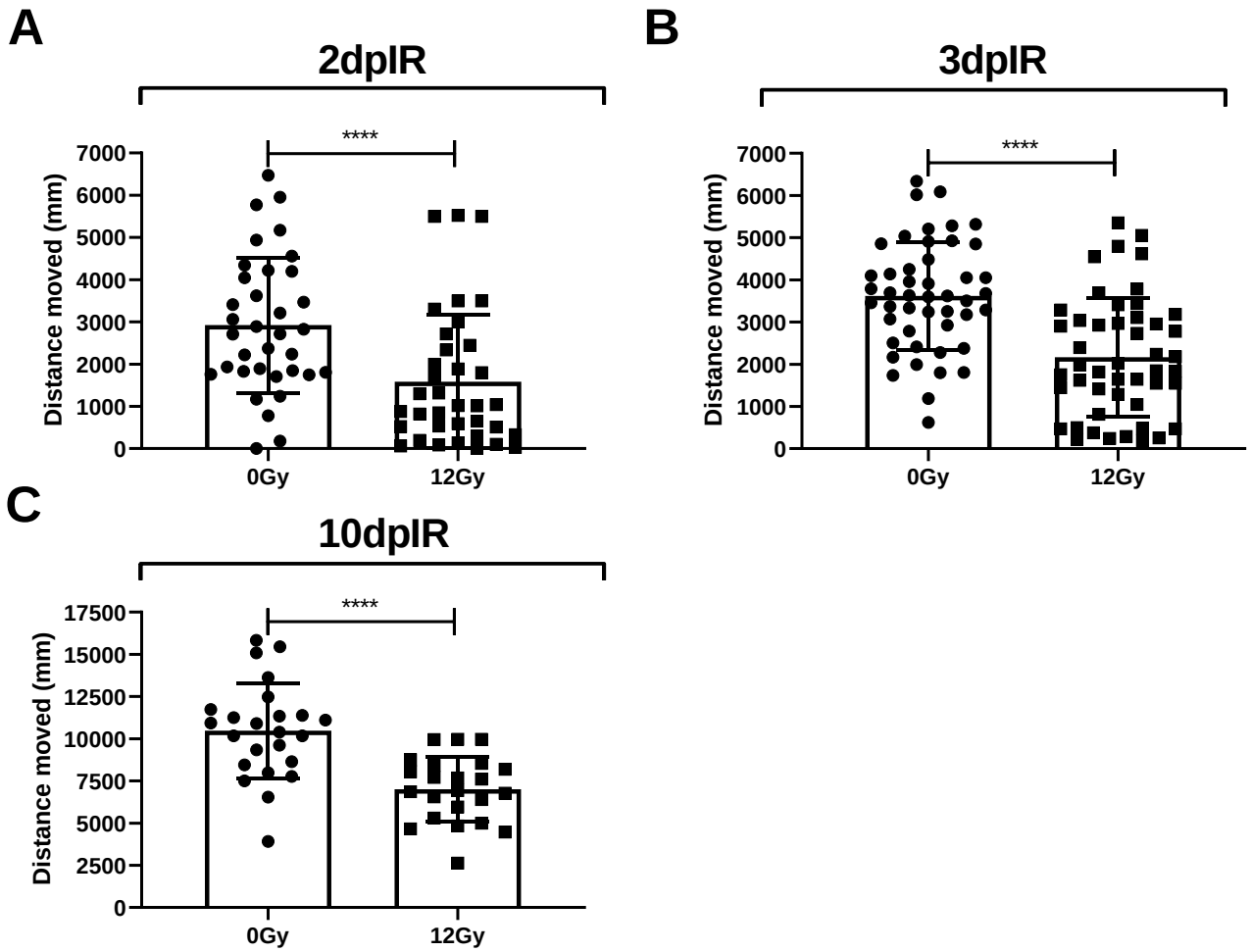

Figure 5.15. Irradiated zebrafish show persistently reduced mobility. Zebrafish larvae were placed individually in a 24-well plate and their movement assessed over a 30-minute period at 2, 3, and 10dpIR. A) A significant reduction in the distance moved over a 30min period was observed in 2dpIR zebrafish exposed to 12Gy irradiation at 2dpf, compared to non-irradiated fish (n = 50/group over four independent experiments). This is a persistent change that is also seen at 3dpIR (B) and 10dpIR (C). n = 24 - 50 per group over three independent experiments. Data was examined by unpaired T-test. **** $p < 0.0001$. Error bars represent standard deviation.

5.5. Conclusion and chapter discussion

In this chapter, I have characterised the ability of this novel transgenic reporter for *p21* to identify live senescent cells *in vivo*. By using the aforementioned gating strategy, I was able to sort live cells from *TgBAC(p21:GFP)sh506* and cytospin the different populations to study the relationship of GFP intensity with other markers of senescence, the presence of γH2AX and IL6, and the absence of PCNA. I have provided evidence to support the idea that irradiated zebrafish larvae can act as a model for mammalian ageing-induced senescence by comparing how the phenotype changes over time and demonstrating that these fish show a persistently reduced mobility, a common symptom of mammalian frailty. I have shown that a portion of GFP-bright cells were present at 10dpIR, and that these cells had a larger proportion of IL6 positive, PCNA negative cells compared to 3dpIR. This recapitulated the kinetics of this late senescence marker described in mammalian systems. In summary, I have now evidenced that using the irradiated zebrafish can model numerous aspects of mammalian age-induced senescence. I can now begin to explore the applications for this model system by taking advantage of the optical transparency and rapid development of zebrafish larvae. Being able to study *in vivo* senescent cells accumulation and assess off-target toxicities and changes in health status in a 5-day test will compliment already-established mammalian models of senescence and hopefully streamline the drug development process to identify novel compounds that can remove these cells effectively.

A unique feature of this study is that two p21-positive cell populations were examined, deemed dim and bright that seemed to show important differences in senescence marker expression. In mammalian transgenic reporters for P16, only positive and negative cells were examined both in the context of irradiation and ageing (Baker *et al.,* 2011; Baker *et al.,* 2016; Demaria *et al.,* 2014; Liu *et al.,* 2019). Importantly, I demonstrated that there were differences in dim and bright cells. For example, at 3 days post-irradiation (dpIR), 52.16% (SD 8.15%) GFP-bright cells but only 29.5% (SD 3.80) of 12Gy GFP-dim cells were positive for γH2AX and negative for PCNA. However, at 10dpIR, γH2AX positive PCNA negative cells are still much higher in the irradiated GFP-dim and bright groups compared to unirradiated cells, but the irradiated GFP-bright cells do not show much more than the irradiated GFP-dim cells. Further, at 10dpIR, IL6 positive and PCNA negative cells were only identified in the 12Gy GFP-bright population and not the dim population. This may have relevance in terms of senescence subtypes, where expression of IL6 was demonstrate in p16-positive cells in mice following irradiation but not wound healing (Demaria *et al.,* 2014). Very little is known about the differences between physiological senescence such as those involved in wound healing and present during development, compared to stress-induced senescence more commonly associated with age-associated pathology. This model could provide a unique means to identify differences between these groups, but more work is required to assess this effectively. For example, if GFP dim, IL6 negative cells were identified following in a zebrafish wound healing model, as was shown in mice, comparisons could be made to distinguish this type of senescence from irradiation-induced senescence (Demaria *et al.,* 2014). Similarly, developmentally senescent cells were deemed to be negative for IL6 (Storer, Mas, Robert-Moreno, *et al.*, 2013). As the majority of GFP dim cells were IL6 negative, there may be some developmentally senescent cells present in this population, which prompts further study. For example, if a portion of the GFP dim cells were identified as developmentally senescent and comparable with previous evidence in chick and mouse embryos, then zebrafish could uniquely assess differences between GFP dim and bright cells within the same

organism (Muñoz-Espín *et al.,* 2013; Storer *et al.,* 2013). To do this, one could demonstrate that GFP dim are still present in a p53-null zebrafish, as was described in mice (Muñoz-Espín *et al.,* 2013). Further evidence to show that this is not a senescence-independent effect of *p21* and *il6,* sorting the GFP dim cells and showing they have SA-β-Gal activity would prove useful. As some macrophages have been shown to be p16 and SA-β-Gal positive, a dual transgenic zebrafish for *p21* and the macrophage reporter *mpeg1:mCherry* could be utilized, and only mCherry-negative cells could be sorted (Ellett *et al.,* 2011). Understanding these differences in senescence subtypes would have great implications in terms of senolytic development, as once differences are identified, drugs could be developed to specifically remove stress-induced senescent cells and not those present from wounding or development. As senolytics currently have problems with toxicity, this would likely improve their therapeutic window and make it more feasible for senolytics to be administered systemically to treat multiple age-associated diseases at once.

Zebrafish larvae only demonstrate an irradiation-specific induction of the SASP marker, IL6, at the later 10 days post-irradiation (10dpIR) time-point. This indicates that the SASP is a later marker of senescence compared to *p21* and γH2AX, corroborating the limited SASP-marker expression shown previously at the whole-organism RNA level at 3dpIR (Figure 3.15). This is well described in mammalian systems and provides validation that the zebrafish respond to irradiation in a comparable manner (Laberge *et al.,* 2015; Freund *et al.,* 2011). An important consideration is that as IL6 was the only SASP-associated marker examined at 10dpIR, a panel of markers by microarray or RNAseq on sorted populations would greatly strengthen this conclusion (Baker *et al.,* 2011; Coppé *et al.,* 2008; Coppé *et al.,* 2011; Demaria *et al.,* 2014; Purcell *et al.,* 2014; Wiley *et al.,* 2017). This also provides evidence to support my hypothesis that the population of cells with the highest GFP intensity would be more likely senescent. This could be due to some DNA repair occurring over time, with dim cells having less extensive DNA damage that is repairable, whilst the bright cells have a more serious damage load, which induces senescence and IL6 expression. This would imply that a portion of the 3dpIR p21-positive cells may have instead been quiescent (Sang *et al.,* 2008). Complimenting this idea, single cell RNAseq of human bleomycin-treated cells showed *p21* expression was highly related to senescence 10 days after treatment (Wiley *et al.,* 2017). Additionally, cells that were positive for p21 for more than 4 days were shown to no longer return to the cell cycle (Sang *et al.,* 2008). The idea that the reporter is more specific to senescence at 10dpIR would have implications for the use of the zebrafish model as a senolytic screening tool. To assess this, a future intention is to test already-available senolytics such as Dasatinib & Quercetin, ABT-263 (Navitoclax), and Fisetin for their ability to modulate GFP fluorescence in 3 and 10dpIR zebrafish (Zhu *et al.,* 2015; Zhu *et al.,* 2016; Yousefzadeh *et al.,* 2018). Unirradiated zebrafish would be used to threshold the quantification such that only changes in bright cells, those with IL6 at 10dpIR, would be assessed to reduce background noise.

Though there was an enrichment for senescence-associated markers with increasing GFP intensity, some expression was present irrespective of radiation. For example, I have described a population of IL6 positive cells in GFP dim populations at 3dpIR independent of irradiation. One possible reason for this is that IL6 is induced following mechanical stress of smooth muscle, independently of senescence (Zampetaki *et al.*, 2005). In 4-day-old zebrafish larvae, there is smooth muscle in the intestine, which is a region that I had demonstrate GFP expression without irradiation (Seiler, Abrams and Pack, 2010) (Figure 4.6). Additionally, IL6 is expressed in macrophages in zebrafish larvae (Nguyen-Chi *et*

al., 2015). This expression was more prominent following caudal tailfin amputation or infection, however their data did not demonstrate that there was no expression in uninfected or uninjured zebrafish. Indeed, macrophages can be activated in normally developing zebrafish through clearing apoptotic bodies that appear as a part of development (Herbomel, Thisse and Thisse, 1999; Yabu *et al.*, 2001). IL6 is also known to play a role in neurogenesis, both directly on neurons as a neurotrophic-like factors, and in non-stimulated human microglia, a macrophage subtype typically associated with the central nervous system (Satoh *et al.*, 1988; Kim and de Vellis, 2005). These microglia were present in the brain of zebrafish around the same time that I have examined unirradiated *p21*:GFP fluorescence, and I have demonstrated GFP fluorescence in the head regions of these fish (Casano, Albert and Peri, 2016) (Figure 4.6). In all examples, we do not know whether any of these macrophages are also positive for *p21,* but as macrophages only make up a small population of total cell number, then they could only ever account for a small proportion of these IL6 & *p21* positive cells (Nguyen-Chi *et al.,* 2015). This could be examined in future by utilising the macrophage reporter *mpeg1:mCherry* alongside the p21 reporter (Ellett *et al.,* 2011). Further, this emphasises that the specificity of the reporter could potentially be improved in the future. An additional reporter for IL6 in the *TgBAC(p21:GFP)sh506* zebrafish would allow live sorting of cells according to IL6 expression as well as p21 expression for example. This could potentially prove more specific than the current murine reporters that rely on p16 alone, with the added benefit of being in a transparent organism (Demaria *et al.,* 2014; Baker *et al.,* 2011; Liu *et al.,* 2019). A more in-depth assessment of the dual reporter, looking at a larger panel of senescence-associated genes and proteins would be required before this is clear. Further, assessment of transcript expression by qPCR in cells sorted by *p21* and *il6* expression could provide novel insights into the reliability of these markers of senescence. Even without the dual reporter however, single-cell RNAseq of cells sorted by GFP fluorescence of the p21 reporter could provide these insights by possibly distinguishing the GFP bright cells that are negative for markers of senescence (Wiley *et al.,* 2017). Though there are cells detected by the *TgBAC(p21:GFP)sh506* that may not be senescent, there is a clear enrichment of these markers according to GFP intensity making it a useable senescence reporter.

An important advantage of studying senescence in zebrafish is that it is a whole organism, and therefore assessments of health status could be used to determine whether senolytics actually reduce signs of pathology. I have described that irradiated zebrafish show reduced mobility compared unirradiated counterparts. In humans, mobility is classified as one of the greatest predictors all-cause mortality (Bergland *et al.*, 2017). The 'Timed Up and Go' test is one of the most suitable performance measures for older people and clearly decreases with age-associated muscle loss (Samson *et al.*, 2000; Lin *et al.*, 2004). In this sense, irradiated zebrafish larvae phenocopy this age-associated predictor of pathology, however a limitation of this evidence is that it is not yet known whether the effect is due to increased senescence or another effect of irradiation. To assess this, if senolytics such show efficacy in irradiated zebrafish larvae, they will be assessed to see whether mobility is improved in their presence. In humans, Dasatinib and Quercetin improve mobility in Ideopathic Pulmonary Fibrosis patients (Justice *et al.,* 2019). Walk distance and gait speed were assessed in this case, but it is worth noting that this phase 1 clinical trial did not have a placebo control, and only used a limited number of patients. Further, as 10dpIR zebrafish are clearly smaller in overall size, more in-depth assessment of muscle loss would bolster this data to demonstrate that it is not just their smaller size that contributes to their

reduced movement. Histology staining of sections of 10dpIR zebrafish larvae could be able to demonstrate changes in muscle that are correlated with sarcopenia in aged mice, as can phalloidin staining of actin filaments (Snow *et al.*, 2008; Lin *et al.*, 2018). Assessment of other health parameters are also possible in zebrafish larvae. Heart failure is an age-associated pathology for example, and removal of senescent cells in mice shows improved recovery after heart attacks, as well as alleviates age-associated cardiac dysfunction (Strait and Lakatta, 2012; Lewis-McDougall *et al.*, 2019; Walaszczyk *et al.*, 2019). Heart rate and blood flow can be assessed in zebrafish larvae, and so may prove a useful health parameter to assess following irradiation (Zakaria *et al.*, 2018). Additionally, senescent cells contribute to anxiety-like phenotypes in obese mice (Ogrodnik *et al.*, 2019). Parameters to assess stress and anxiety have been established in zebrafish larvae, and shock responses could be incorporated to test these measures in irradiated zebrafish also (Alsop and Vijayan, 2008). Together, these relatively simple assessments of whole organism health status that are associated to senescence and ageing can be employed in zebrafish and provide a great advantage in the development of senolytics.

Currently in the field of senescence and ageing, it is not well understood how well irradiation acts as a proxy ageing. I have demonstrated reduced mobility and increases in multiple senescence markers that are associated with ageing in irradiated zebrafish larvae. Increases in *p16*, SA-β-Gal, γH2AX, IL6 expression are all associated with mammalian ageing and indicate an age associated accumulation of senescent cells. For example, IL6 protein levels in the blood serum strongly correlates with frailty in the elderly (Van Epps *et al.*, 2016). Now with the development of the transgenic reporter and ability to sort potentially senescent cells, their abundance can be quantified and compared with mammalian ageing. At 3dpIR, 19.64% of all cells were positive for *p21*, γH2AX, and negative for PCNA, as 11.77% and 7.87% of all cells were γH2AX positive and PCNA negative cells in the 12Gy GFP-dim and bright populations respectively. At 10dpIR, 16.62% of all cells were positive for *p21*, γH2AX, and negative for PCNA, with 14.18% and 2.44% being γH2AX positive and PCNA negative in the 12Gy GFP-dim and bright populations respectively. In the skin of aged primates, 15% of cells were positive for three markers of senescence, including activation of the DNA damage response (Herbig *et al.,* 2006). The majority of 24-month old mice had increased SA-β-Gal activity compared to 2-month old mice (Biran *et al.*, 2017b), however the actual levels varied from 2% in the lymph node to 15% in subcutaneous stroma indicating there is tissue-specific variation in the prevalence of senescence. Additionally, more than 20% of cells were positive for senescence markers SA-β-Gal and senescence-associated heterochromatic foci (SAHF) in 22-month murine liver hepatocytes (Panda, Isbatan and Adami, 2008). These old mice also have 20% of hepatocytes with an activated DNA damage response (53BP1 positive; phosphorylated ATM positive), but these markers were not used in combination with SA-β-Gal and SAHF so may not all be specific to senescence. The amount of DNA damage response activation in the aged mouse liver was comparable with the amount seen 1 week after the addition of the DNA damaging agent Aminoazotoluene (AAT) in juvenile mice, which was used to induce ectopic senescence accumulation. The percentage of cells that were senescent in my larval zebrafish irradiation model were therefore comparable with the prevalence senescence in the skin of aged primates and the liver of mice. The limitation to this is that all cells positive for *p21*, γH2AX, and negative for PCNA are senescent, which may not be the case. If instead cells positive for p21, IL6, and negative for PCNA were considered 'senescent', only 3.03% of all cells would fit

this category at 10dpIR. Regardless, this method of inducing *in vivo* senescence is a much more cost and time-effective method with multiple similarities to mammalian age-induced senescence, as well as reducing the number of ASPA-regulated animals required for this type of research (Home Office, 2014). In the future, a more in-depth assessment comparing the GFP positive cells seen following irradiation in *TgBAC(p21:GFP)sh506* compared to those seen in aged *TgBAC(p21:GFP)sh506* would provide novel insights into similarities and differences between irradiation-induced and age-induced senescence. Paraffin sections of old versus young *TgBAC(p21:GFP)sh506* zebrafish would demonstrate whether fluorescence is increased with age and whether the tissues with the highest burden of senescent are similar or different to those seen in irradiated larvae. Expression of p21 has not been studied in old wild-type aged zebrafish, but the head kidney, gut and testes express high levels of *cdkn1a* (p21) in telomerase mutant zebrafish (Henriques *et al.,* 2013). Moreover, actually sorting the tissues from aged transgenic zebrafish to assess whether there is again a GFP bright population that is more specific to IL6 expression compared to GFP dim cells would elucidate whether this is an irradiation-specific effect or one directly relevant to ageing.

Another factor to consider in the context of whole organism ageing is immune-system clearance of senescent cells (Kang *et al.,* 2012). Until 4-6 weeks of age, zebrafish do not have a functional adaptive immune system and so T-cell mediated clearance of senescence would not be possible in 5-12dpf zebrafish (Lam *et al.*, 2004). However, macrophages have also been implicated as senescence-clearing cells and were present at these time-points and so may have played a role in clearing GFP-bright cells (Herbomel, Thisse and Thisse, 1999; Kang *et al.*, 2011a). In the context of the irradiated zebrafish larvae, it is possible that these macrophages may have altered functional capacity as they themselves have also been irradiated. This is well established in radiotherapy-treated cancer patients, who present with reduced lymphocyte numbers following treatment (Belka *et al.*, 1999). If this was the case then one could argue that this irradiated zebrafish larval model is actually even more comparable with an ageing context in that both contexts show compromised immune cell function. This could be explored in the future through already established techniques for studying immune cell function in zebrafish, to see how well they handle infection for example (Renshaw and Trede, 2012). Alternatively, transplanting *mpeg1:mCherry* macrophages sorted from non-irradiated zebrafish could potentially show whether any change in function is due to irradiation of the macrophages or increased senescence burden. As zebrafish are transparent at these stages, one could dissect whether immune cell clearance of senescent cells does take place in real time. Further, one could modulate the amount of macrophages present with Liposome encapsulated clodronate (L-clodronate), and show whether the senescence burden is increased and signs of pathology such as mobility are worsened (Bernut *et al.*, 2014).

6. Final discussion and future work

Lifelong exposure to endogenous and exogenous sources of stress, and a time-dependent decline in our immune system's ability to clear damaged tissue and mediate inflammation causes a chronically inflamed and pathogenic environment (Figure 1.1) (Solana, Alonso and Peña, 1999; Solana and Mariani, 2000; d'Adda di Fagagna *et al.*, 2003a; Deng *et al.*, 2004a; Czesnikiewicz-Guzik *et al.*, 2008; Baker *et al.*, 2011). It is now well established that the amount of senescent cells present in many of our tissues, increases with age (Martin and Buckwalter, 2002; Kang *et al.*, 2011a, 2015; Bhat *et al.*, 2012). Not only this, they are directly causal to the onset and pathology of a multitude of age-associated diseases (Childs *et al.,* 2016; Baker *et al.,* 2016; Jeon *et al.,* 2017; Bussian *et al.,* 2018; Chinta *et al.,* 2018). As our population is ageing rapidly, thereby increasing the prevalence of age-associated diseases, there is an unmanageable strain on our health and social care services that cannot be sustained. Therefore, it is imperative that we understand the mechanisms that lead to age-dependent increases in disease incidence, including senescent cell accumulation, with great urgency. Drugs called senolytics are being developed to remove senescent cells and are starting to show promise in early clinical trials (Justice *et al.,* 2019; Spark, 2019; Hickson *et al.,* 2019). However, these trials are focusing on individual age-associated diseases, and some of the senolytics interact with cytochrome p450 that is causing issues of polypharmacy with other common medications in older people (Doan *et al.,* 2013; Elbarbry *et al.,* 2014; Jung & Lee *et al.,* 2014). To be able to use senolytics to tackle age-associated multimorbidity, more work is required to understand senescent cells *in vivo.* This is because i*n vitro* studies do not take into account the paracrine nature and complex tissue interactions that senescent cells are involved in *in vivo.* Additionally, as senolytics currently have a small therapeutic window; identifying efficacy *in vivo* in the first instance would likely improve the translatability of these compounds (Fuhrmann-Stroissnigg *et al.,* 2017; Zhu *et al.,* 2015; Zhu *et al.,* 2016; Baar *et al.,* 2017). Currently, it is difficult to study senescent cells *in vivo* due to multiple markers being required to identify them, and the resulting phenotype is dynamic and contextually dependent (Maciel-Barón *et al.,* 2016; Basisty *et al.,* 2019). Additionally, age-associated accumulation of senescent cells is a laborious process as it is costly in terms of both time and money to study old animals. Further, mouse models to identify senescence do not allow live tracking of these cells in a mixed population and at the cellular level (Baker *et al.,* 2011; Demaria *et al.,* 2014; Liu *et al.,* 2019). Here, I have investigated the potential of zebrafish larvae to compliment already established systems and provide novel information about senescent cells *in vivo*. Irradiation is a well-described means of inducing senescence, both *in vitro* and *in vivo,* but a dose and time had not been optimised to induce rapid senescent cell accumulation without causing significant lethality or toxicity in zebrafish larvae (Coppé *et al.,* 2008; Demaria *et al.,* 2014). Once optimised, I was able to study senescent cells and show that irradiation of zebrafish larvae, much like is seen in mammalian systems, can induce accumulation of multiple senescence markers. The predominant reasons for developing this model is that zebrafish larvae are optically transparent, genetically malleable, and develop rapidly. This allowed the development of a tool that could track *in vivo* senescent cells, live and at the cellular level, which was not possible previously. The *TgBAC(p21:GFP)SH506* zebrafish, once irradiated, shows multiple similarities with the senescent cell phenotype in mammals, and therefore

provides a means to study these cells in a much more timely and cost-effective manner, whilst also reducing the number of ASPA-protected animals required for this type of research.

6.1. Developing an assay for *in vivo* senescence accumulation with the potential for senolytic screens.

I have demonstrated that irradiated zebrafish larvae accumulate multiple senescence markers that have been demonstrated in the context of stress and age-induced mammalian senescence. Expression of markers identified include *p21, p16-like, mmp2,* γH2AX, il6, SA-β-Gal and reduced proliferation were all present following irradiation. Complimentary to this, irradiation of human fibroblasts also showed increased expression of $P21^{WAF1}$, γH2AX, $P16^{INK4A}$, IL6 and MMP2 (Schafer *et al.,* 2017). MMP2 was additionally implicated as a central SASP marker by unbiased analysis of two human cell lines induced to senescence by five different methods (Özcan *et al.*, 2016). Further, in the skin and brain of aged non-diseased primates, there is an increase in SA-β-Gal, $P16^{INK4A}$ and γH2AX foci (G P Dimri *et al.*, 1995; Martin and Buckwalter, 2002; Herbig *et al.*, 2006b; Jeyapalan *et al.*, 2007; Bhat *et al.*, 2012; Kang *et al.*, 2015). Additionally, combinations of $P16^{INK4A}$, IL6, SA-β-Gal, MMP2, γH2AX, and reduced proliferation are seen in tissues from human patients with age-associated diseases such as Alzheimer's Disease, Ideopathic Pulmonary Fibrosis and Osteoarthritis (Chinta *et al.,* 2018; Schafer *et al.,* 2017; Jeon *et al.,* 2017). As is demonstrated in the context of mammalian ageing, the irradiated zebrafish also demonstrated reduced mobility, a common pathology of ageing and predictor of mortality (Goodpaster *et al.,* 2006; Bergland *et al.,* 2017). Using BAC transgenesis, I have developed a method of imaging fluorescent cells in irradiated zebrafish that correlate with multiple senescence markers within the same cell. With more time, I would change the inducer of senescence to see how well this reporter can detect senescence in different contexts, particularly in aged zebrafish. Comparing the location of fluorescent cells in older fish and the expression of SASP factors with irradiated zebrafish larvae would provide important validation about the use of irradiation as a model for age-associated senescent cell accumulation. Further, I would expand the SASP markers assessed, principally in sorted cell populations, and identify whether the SASP changes according to the inducer as is suggested in mammalian systems (Demaria *et al.,* 2014; Maciel-Barón *et al.,* 2016). Finally, I would test known senolytics to determine whether they show efficacy and are able to both reduce the amount of fluorescence seen following irradiation and rescue the loss in mobility, this would emphasise the unique ability to identify senolytics with the ability to improve health status in a rapid and reliable manner. The current evidence does describe multiple similarities in the phenotype of irradiated zebrafish with human ageing and age-associated disease, at the transcript, proteomic and behavioural level, and therefore it is now feasible to study aspects of *in vivo* senescent cell accumulation within a live organism in a 5-day test.

A vital use of this zebrafish system is to for an *in vivo* drug screen for modulators of senescence. Drugs are being developed to remove the age-associated burden of senescence and extend the healthspan of our ageing population. Currently, these drugs are identified through *in vitro* approaches that do not take into account the paracrine effects of the SASP, and the complex interactions between cell types that result *in vivo* (Fuhrmann-Stroissnigg *et al.,* 2017; Zhu *et al.,* 2015; Zhu *et al.,* 2016). Additionally, these drugs have a limited therapeutic index, meaning the dose required for an effect is close to the dose required to see side effects. As these side effects are only seen once tested in mice, this wastes animals, time and money if the compounds are not effective *in vivo*. Further, as current senolytics such as Quercetin and Fisetin are cleared by cytochrome p450, this interferes with other drugs commonly used in older people (Doan *et al.,* 2013; Elbarbry *et al.,* 2014; Jung & Lee *et al.,* 2014). The result of these drawbacks is that only one age-associated disease can be tackled at a time, which is not tackling the urgent issue of multimorbidity and polypharmacy (Justice *et al.,* 2019; Spark, 2019). Systemic administration of senescence-modifying drugs has the potential to tackle multiple diseases at once and overcome the current issues of polypharmacy (Bellantuono, 2018). To achieve systemic treatment of senescence-modifying compounds, a method for screening senescence modifying drugs in a whole organism context, in a timely manner, is required. In this regard, compounds would be identified as hits if they were able to remove senescent cells, have limited off-target toxicities, and actually improve the health status of an organism. This approach would more likely identify compounds that would go through pre-clinical and clinical trials successfully, as the compounds would be identified in a more physiologically relevant manner. Here, I have described how irradiation of zebrafish larvae induces senescent cell accumulation within a 5-day test. Zebrafish are amenable to high throughput drug screening approaches (Robertson *et al.*, 2014; Wang, Rajpurohit, Delaspre, Walker, White, Ceasrine, Kuruvilla, R. Li, *et al.*, 2015). They develop rapidly, and by 5dpf have multiple other organ systems that would better recapitulate the context of senescence in an aged individual compared to *in vitro* screening (Vaz *et al.,* 2018). Zebrafish larvae are considered a replacement for mice since they are not protected by the Animals (Scientific Procedures) Act (ASPA) also, reducing the number of animals required for *in vivo* screening (Home Office, 2014). Therefore, this system could be used to rapidly identify novel compounds that modulate the amount of *in vivo* senescence seen following irradiation, as well as monitoring for off-target toxicities and changes in mobility in the first instance.

To develop an *in vivo* compound screen for modulating senescence using irradiated *TgBAC(p21:GFP)SH506* zebrafish, a pipeline for the drug development process must first be established. Initially, the amount of fluorescence after irradiation without the presence of any compounds must be assessed in greater detail to assess signal variability compared to unirradiated controls. Z-scores, inter- and intra-plate variability would permit effective experimental design to appropriately power the screen (Fuhrmann-Stroissnigg *et al.,* 2017). Secondly, drugs with already established efficacy at killing senescent cells *in vivo* would be assessed in irradiated zebrafish larvae to identify whether they reduce the amount of fluorescence seen following irradiation (Figure 6.1.). Dasatinib & Quercetin (DQ), ABT-263 (Navitoclax) and Fisetin would be amongst the first to be tested (Zhu *et al.,* 2015; Zhu *et al.,* 2016; Yousefzadeh *et al.,* 2018). The timing of this treatment would also be important, as it would affect the translation of the compound. For

example, drugs that can remove senescence after they are established would probably prove more beneficial for patients that come to the clinic with symptoms already present. Whereas, drugs that can prevent senescence may prove more useful in the context of preventing senescence accumulation in response to surgery or chemotherapy (Sanoff *et al.*, 2014; Collins *et al.*, 2017). To confirm that compounds are effectively reducing senescent cell burden and able to improve organism health, a secondary screen to assess for changes in IL6 following FACS of treated and irradiated zebrafish, as well as monitoring for mobility as I have previously described (Fuhrmann-Stroissnigg *et al.,* 2017). Additional behavioural screens for health status would be established to strengthen the model, such as assessment of heart function and anxiety, both of which are senescence-associated pathologies (Lewis-McDougall *et al.*, 2019; Ogrodnik *et al.*, 2019; Walaszczyk *et al.*, 2019). Once validated with positive control senolytics, screening a library of compounds to compare their efficacy to the already-established drugs would be carried out (Figure 6.1.). Once hit compounds are identified, then the mechanism for how they can induce cell death selectively in senescence would be investigated. Additionally, if an assay to assess physiological senescence in zebrafish, such as from a wound healing perspective, hit compounds would be tested in this context also (Demaria *et al.,* 2014). The benefit of this would be that one could take hit compounds forward if they selectively remove stress-induced pathological senescence and not physiological senescent cells. Once elucidated, the compounds would be tested in a mammalian system, ideally an aged mouse with signs of multimorbidity. This method will hopefully provide a more streamlined pipeline for the development of senescence modifying drugs to tackle multiple age-associated pathologies.

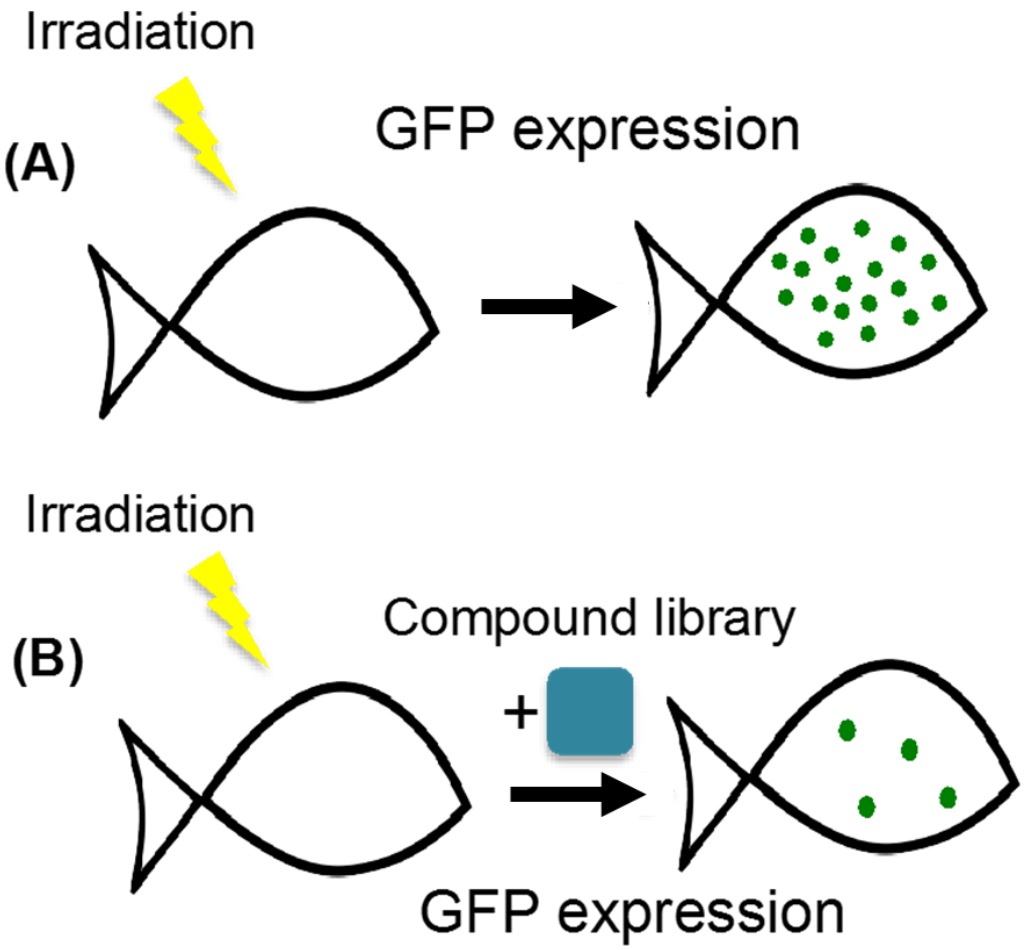

Figure 6.1. An *in vivo* compound screen to identify modulators of senescence in irradiated *TgBAC(p21:GFP)SH506* zebrafish. Diagram depicting an approach for an initial screen to identify modulators of *in vivo* senescence. A) Careful assessment of the amount of fluorescence seen following irraidation of *TgBAC(p21:GFP)SH506* zebrafish will allow assessment of the robustness of the assay, through Z-scores and understanding inter and intra-plate variability. B) A compound library will then be added to irradiated zebrafish before assessment of fluorescence to identify those that are able to reduce the amount of senescent cells in the zebrafish without causing obvious toxicity.

6.2. Prospective isolation of cells with p21 promoter activation could provide novel insight into the senescence phenotype

As the irradiation assay causes a rapid accumulation of multiple senescent cell markers in a developing and transparent organism, one could propose that the system provides a unique opportunity to study physiological and pathological senescence to identify features that distinguish them from one another. For example, I have also demonstrated the presence of senescence markers such as *p21* and SA-β-Gal in unirradiated zebrafish larvae that could be a form of developmental senescence, though more work is required to confirm this (Kishi *et al.,* 2008). The intestine and pharyngeal arches are areas highlighted as SA-β-Gal positive and potentially a form of developmental senescence in the mouse and chick embryo (Munoz Espin *et al.,* 2013; Storer *et al.,* 2013). The same regions showed expression in unirradiated developing zebrafish larvae showed some expression of these markers and so it is possible that the same process is being identified here. As the process of developmental senescence is p21-dependent (Munoz Espin *et al.,* 2013), then it could be possible to study these cells in comparison to the stress-induced senescent cells in *TgBAC(p21:GFP)SH506* zebrafish. Being able to study both types of senescence within the same organism could prove extremely useful in understanding whether there are distinguishable features between the two types of senescence.
I have begun to describe a possible example of this, where at 10dpIR only the GFP bright cells from irradiated *TgBAC(p21:GFP)SH506* zebrafish have IL6. One study has shown that IL6 is only up regulated in senescent cells following irradiation and not following wound healing, potentially defining an example difference between physiological and pathological senescence (Demaria *et al.,* 2014). Though the evidence is limited to IL6 currently in these zebrafish, it highlights the ability to identify p21-positive cells that may have different phenotypes. This could be examined further with single cell RNAseq to determine whether there are more distinguishable features about the two types of p21-positive cell (Wiley *et al.,* 2017). Though it is not well understood currently, SASP-expressing senescent cells are thought to contribute to their pathogenicity and without the SASP the tumour promoting effects of senescence are abrogated (Georgilis *et al.,* 2018). It is worth noting that work is required to determine whether the expression of p21 and SA-β-Gal in these zebrafish larvae does have a component of developmental senescence, and is not just a senescence-independent role of these markers (Untergasser *et al.,* 2003; Laranjeiro *et al.,* 2013; Hall *et al.,* 2017). If this is the case however, it would have relevance and provide further insight into precautions for reliably detecting senescent cells *in vivo* (line Cudejko *et al.*, 2011; Hall *et al.*, 2017). The zebrafish would be a uniquely useful tool for assessing the kinetics of senescence markers such as *p21* with the development of the transgenic reporters such as *TgBAC(p21:GFP)SH506*. This is because the transparency of the zebrafish allows tracking of different reporters of senescence over time after taking into account potential differences in fluorescent protein and p21 protein half-life (Corish and Tyler-Smith, 1999; Jascur *et al.*, 2005). It would further emphasise the need for analysis of senescence at the single-cellular level to help determine an effective gold standard that can detect senescence reliably. I do not believe that this disregards *p21* as a good marker currently, single cell RNAseq has shown this in other comparable contexts for example, and our transgenic reporter is able to enrich cells that are more likely senescent by cell sorting (Wiley et al., 2017). It would be useful in this regard to also make transgenic reporters for *il6*, and *p16-like* promoter regulation to other well-used reporters in detail. As I have demonstrated that the expression of *p16-like* is lower than

p21 in 3dpIR zebrafish, and it the half-life of *p16-like* mRNA is unusually long, including enhancer elements and brighter fluorescent proteins may be essential to report expression effectively in zebrafish (Liu et al., 2019). This work would also ideally involve characterisation of the zebrafish *p16-like* orthologue as a senescence marker in comparison to human & mouse $P16^{INK4A}$.

As well as being present in development, literature suggests interactions between senescent cells and the innate and active immune system, predominantly through Natural Killer T cells and macrophages (Munoz Espin *et al.,* 2013; Storer *et al.,* 2013; Kang *et al.,* 2011; Krizhanovsky *et al.,* 2008; Antonangeli *et al.,* 2016). I have demonstrated a novel ability to track senescent cells in transparent zebrafish larval tissues, in the same stages of development whereby there is only an innate immune system (Lam *et al.,* 2004). These in combination provide a powerful opportunity to study macrophage interactions with senescent cells by making a dual transgenic reporter from *TgBAC(p21:GFP)SH506* and *TgBAC(mpeg1:mCherry-CAAX)SH378*. Time-lapse LightSheet imaging of this dual transgenic reporter could elucidate whether macrophages do indeed interact with irradiation-induced senescent cells, as no one is yet to demonstrate this directly in real time. To ensure that the macrophages are functional and not themselves hindered by irradiation, transplanting *mpeg1:mCherry* positive cells that are sorted from non-irradiated zebrafish would prove useful. Alternatively, as senescent cells are induced in response to wounding and have a direct role in tissue repair, developing an assay to induce senescence from tissue injury in zebrafish larvae could also prove useful (Demaria *et al.,* 2014). Zebrafish larvae have well-established methods for monitoring wounding, macrophage recruitment, and tissue repair, and as such could be examined in *TgBAC(p21:GFP)SH506* also (Ellet *et al.,* 2011). If senescent cells were present at the site of injury, then experimental manipulation of the wound environment by removing senescent cells by senolytics could demonstrate modified tissue regeneration (Demaria *et al.,* 2014). Further, mechanisms of the interaction between senescent cells and immune cells could be examined in greater detail compared to mouse models due to transparency of the organism. For example, if macrophages transplanted into larvae from older fish are not as able to interact with senescent cells compared to macrophages from younger fish, then it would provide direct evidence for the first time that the age-dependent decline in the immune system could be a mechanism for senescent cell accumulation with age.

6.3. Final conclusions and closing remarks

In summary, I have described the development, characterisation and validation of a unique tool to study *in vivo* senescent cell accumulation in zebrafish larvae. The in-depth characterisation of irradiation-induced senescent cells in early-development zebrafish has identified that there are multiple similarities with the context of mammalian ageing-induced senescence. I have identified common features that include expression of the cyclin-dependent kinase inhibitors *p21* and *p16-like*, senescence-associated β-galactosidase activity, reduced proliferation and SASP markers such as *mmp2* and Il6. Development of a novel transgenic reporter for p21 promoter activation permitted prospective isolation of fluorescent cells that recapitulate endogenous *p21* mRNA expression patterns. FACS of these fluorescent cells demonstrated that a majority of those with high fluorescence intensity present with multiple senescent markers within the same cell, and that these cells can persist for at least 10 days following irradiation. The persistent highly fluorescent cells contained a greater proportion of IL6-positive cells within them compared to earlier time-points, replicating the kinetics of this senescence marker in mammalian senescence models. Together, these findings implicate zebrafish larvae as a new model to gain further insight into the senescence phenotype, in a much more timely and cost-effective manner.

Expanding our knowledge on senescent cells is essential, and may help to identify novel targets to drive the removal of senescent cells in the context of age-associated pathology. Much work is still required to confirm whether pharmacologically removing senescent cells can actually improve the healthspan of our ageing population, thereby reducing the strain on health and social services and increasing the quality of life in our later years. Though, this study provides evidence that *TgBAC(p21:GFP)SH506* zebrafish can complement alternative model systems with the unique advantages of amenability to *in vivo* drug screening and optical transparency to study senescent cells in a whole organism context at high resolution.

References

Abel, J. *et al.* (2018) 'Reducing emergency hospital admissions: A population health complex intervention of an enhanced model of primary care and compassionate communities', *British Journal of General Practice*. Royal College of General Practitioners, 68(676), pp. e803–e810. doi: 10.3399/bjgp18X699437.

Ablain, J. *et al.* (2018) 'Human tumor genomics and zebrafish modeling identify SPRED1 loss as a driver of mucosal melanoma HHS Public Access', *Science*, 362(6418), pp. 1055–1060. doi: 10.1126/science.aau6509.

Acosta, J. C. *et al.* (2008) 'Chemokine Signaling via the CXCR2 Receptor Reinforces Senescence', *Cell*, 133(6), pp. 1006–1018. doi: 10.1016/j.cell.2008.03.038.

Acosta, J. C. *et al.* (2013) 'A complex secretory program orchestrated by the inflammasome controls paracrine senescence', *Nature Cell Biology*, 15(8), pp. 978–990. doi: 10.1038/ncb2784.

Alcorta, D. A. *et al.* (1996) 'Involvement of the cyclin-dependent kinase inhibitor p16 (INK4a) in replicative senescence of normal human fibroblasts', *Proceedings of the National Academy of Sciences of the United States of America*. National Academy of Sciences, 93(24), pp. 13742–13747. doi: 10.1073/pnas.93.24.13742.

Almaida-Pagán, P. F., Lucas-Sánchez, A. and Tocher, D. R. (2014) 'Changes in mitochondrial membrane composition and oxidative status during rapid growth, maturation and aging in zebrafish, Danio rerio', *Biochimica et Biophysica Acta - Molecular and Cell Biology of Lipids*. Elsevier, 1841(7), pp. 1003–1011. doi: 10.1016/j.bbalip.2014.04.004.

Alsop, D. and Vijayan, M. M. (2008) 'Development of the corticosteroid stress axis and receptor expression in zebrafish.', *American journal of physiology. Regulatory, integrative and comparative physiology*, 294(3), pp. R711-9. doi: 10.1152/ajpregu.00671.2007.

Alyodawi, K. *et al.* (2019) 'Compression of morbidity in a progeroid mouse model through the attenuation of myostatin/activin signalling', *Journal of Cachexia, Sarcopenia and Muscle*. Wiley Blackwell, 10(3), pp. 662–686. doi: 10.1002/jcsm.12404.

Anchelin, M. *et al.* (2011) 'Behaviour of telomere and telomerase during aging and regeneration in zebrafish', *PLoS ONE*, 6(2). doi: 10.1371/journal.pone.0016955.

Antonangeli, F. *et al.* (2016) 'Natural killer cell recognition of in vivo drug-induced senescent multiple myeloma cells', *OncoImmunology*, 5. doi: 10.1080/2162402X.2016.1218105.

Aoshiba, K., Tsuji, T. and Nagai, A. (2003) 'Bleomycin induces cellular senescence in alveolar epithelial cells', *European Respiratory Journal*, 22(3), pp. 436–443. doi: 10.1183/09031936.03.00011903.

Baar, M. P. *et al.* (2017) 'Targeted Apoptosis of Senescent Cells Restores Tissue Homeostasis in Response to Chemotoxicity and Aging', *Cell*, 169(1), pp. 132–147. doi: 10.1016/j.cell.2017.02.031.

Baker, D. J. *et al.* (2008) 'Opposing roles for p16Ink4a and p19Arf in senescence and ageing caused by BubR1

insufficiency.', *Nature cell biology*, 10(7), pp. 825–36. doi: 10.1038/ncb1744.

Baker, D. J. *et al.* (2011) 'Clearance of p16Ink4a-positive senescent cells delays ageing-associated disorders', *Nature*. Nature Publishing Group, 479(7372), pp. 232–236. doi: 10.1038/nature10600.

Baker, D. J. *et al.* (2016) 'Naturally occurring p16 Ink4a -positive cells shorten healthy lifespan', *Nature*. Nature Publishing Group, pp. 1–20. doi: 10.1038/nature16932.

Basisty, N. *et al.* (2019) 'A Proteomic Atlas of Senescence-Associated Secretomes for Aging Biomarker Development', *bioRxiv*. Cold Spring Harbor Laboratory, p. 604306. doi: 10.1101/604306.

Bavik, C. (2006) 'The Gene Expression Program of Prostate Fibroblast Senescence Modulates Neoplastic Epithelial Cell Proliferation through Paracrine Mechanisms', *Cancer Research*, 66(2), pp. 794–802. doi: 10.1158/0008-5472.CAN-05-1716.

Baxendale, S. *et al.* (2012) 'Identification of compounds with anti-convulsant properties in a zebrafish model of epileptic seizures', *DMM Disease Models and Mechanisms*, 5(6), pp. 773–784. doi: 10.1242/dmm.010090.

Beerman, I. *et al.* (no date) 'Functionally distinct hematopoietic stem cells modulate hematopoietic lineage potential during aging by a mechanism of clonal expansion'. doi: 10.1073/pnas.1000834107.

Belka, C. *et al.* (1999) 'Impact of localized radiotherapy on blood immune cells counts and function in humans', *Radiotherapy and Oncology*, 50(2), pp. 199–204. doi: 10.1016/S0167-8140(98)00130-3.

Bellantuono, I. (2018) 'Find drugs that delay many diseases of old age.', *Nature*, 554(7692), pp. 293–295. doi: 10.1038/d41586-018-01668-0.

Bellantuono, I. and Potter, P. K. (2016) 'Modelling ageing and age-related disease', *Drug Discovery Today: Disease Models*. Elsevier Ltd, pp. 27–32. doi: 10.1016/j.ddmod.2017.07.005.

Berghmans, S. *et al.* (2005) 'tp53 mutant zebrafish develop malignant peripheral nerve sheath tumors', *Proceedings of the National Academy of Sciences of the United States of America*, 102(2), pp. 407–412. doi: 10.1073/pnas.0406252102.

Bergland, A. *et al.* (2017) 'Mobility as a predictor of all-cause mortality in older men and women: 11.8 year follow-up in the Tromsø study', *BMC Health Services Research*. BioMed Central Ltd., 17(1). doi: 10.1186/s12913-016-1950-0.

Bernardes de Jesus, B. *et al.* (2012) 'Telomerase gene therapy in adult and old mice delays aging and increases longevity without increasing cancer', *EMBO Molecular Medicine*, 4(8), pp. 691–704. doi: 10.1002/emmm.201200245.

Bernut, A. *et al.* (2014) 'Mycobacterium abscessus cording prevents phagocytosis and promotes abscess formation.', *Proceedings of the National Academy of Sciences of the United States of America*, 111(10), pp. E943-52. doi: 10.1073/pnas.1321390111.

Bhat, R. *et al.* (2012) 'Astrocyte senescence as a component of Alzheimer's disease', *PloS one*, 7(9), p. e45069. doi:

10.1371/journal.pone.0045069.

Biran, A. *et al.* (2017) 'Quantitative identification of senescent cells in aging and disease', *Aging Cell*. doi: 10.1111/acel.12592.

Bissonnette, N. and Hunting, D. J. (1998) 'p21-induced cycle arrest in G1 protects cells from apoptosis induced by UV-irradiation or RNA polymerase II blockage.', *Oncogene*, 16(26), pp. 3461–9. Available at: http://www.ncbi.nlm.nih.gov/pubmed/9692554 (Accessed: 21 September 2019).

Bitto, A. *et al.* (2016) 'Transient rapamycin treatment can increase lifespan and healthspan in middle-aged mice.', *eLife*, 5. doi: 10.7554/eLife.16351.

Blais, A. *et al.* (2007) 'Retinoblastoma tumor suppressor protein-dependent methylation of histone H3 lysine 27 is associated with irreversible cell cycle exit.', *The Journal of cell biology*, 179(7), pp. 1399–412. doi: 10.1083/jcb.200705051.

Bracken, A. P. *et al.* (2007) 'The Polycomb group proteins bind throughout the INK4A-ARF locus and are disassociated in senescent cells', *Genes and Development*, 21(5), pp. 525–530. doi: 10.1101/gad.415507.

Bryant, H. E. *et al.* (2005) 'Specific killing of BRCA2-deficient tumours with inhibitors of poly(ADP-ribose) polymerase.[erratum appears in Nature. 2007 May 17;447(7142):346]', *Nature*, 434(7035), pp. 913–917. Available at: www.nature.com/nature (Accessed: 2 September 2019).

Buettner, D. and Skemp, S. (2016) 'Blue Zones: Lessons From the World's Longest Lived', *American Journal of Lifestyle Medicine*. SAGE Publications Inc., pp. 318–321. doi: 10.1177/1559827616637066.

Bulman, M. (2017) *Demand for care home places will soar by more than three quarters in less than 20 years, study shows*. Available at: https://www.independent.co.uk/news/uk/home-news/care-home-demand-soars-86-two-decades-elderly-lancet-a7895046.html.

Bulua, A. C. *et al.* (2011) 'Mitochondrial reactive oxygen species promote production of proinflammatory cytokines and are elevated in TNFR1-associated periodic syndrome (TRAPS)', *Journal of Experimental Medicine*, 208(3), pp. 519–533. doi: 10.1084/jem.20102049.

Bunz, F. *et al.* (1998) 'Requirement for p53 and p21 to sustain G2 arrest after DNA damage', *Science*. American Association for the Advancement of Science, 282(5393), pp. 1497–1501. doi: 10.1126/science.282.5393.1497.

Burket, C. T. *et al.* (2008) 'Generation and characterization of transgenic zebrafish lines using different ubiquitous promoters', *Transgenic Research*, 17(2), pp. 265–279. doi: 10.1007/s11248-007-9152-5.

Burma, S. *et al.* (2001) 'ATM Phosphorylates Histone H2AX in Response to DNA Double-strand Breaks', *Journal of Biological Chemistry*, 276(45), pp. 42462–42467. doi: 10.1074/jbc.C100466200.

Bussian, T. J. *et al.* (2018) 'Clearance of senescent glial cells prevents tau-dependent pathology and cognitive decline', *Nature*. Nature Publishing Group, pp. 578–582. doi: 10.1038/s41586-018-0543-y.

Buttitta, L. A. and Edgar, B. A. (2007) 'Mechanisms controlling cell cycle exit upon terminal differentiation', *Current Opinion in Cell Biology*, pp. 697–704. doi: 10.1016/j.ceb.2007.10.004.

Carneiro, M. C., Castro, I. P. De and Ferreira, M. G. (2016) 'Telomeres in aging and disease : lessons from zebrafish', pp. 737–748. doi: 10.1242/dmm.025130.

Casano, A. M., Albert, M. and Peri, F. (2016) 'Developmental Apoptosis Mediates Entry and Positioning of Microglia in the Zebrafish Brain.', *Cell reports*, 16(4), pp. 897–906. doi: 10.1016/j.celrep.2016.06.033.

Centre for Ageing Better (2019) *The State of ageing in 2019*. Available at: https://www.ageing-better.org.uk/publications/state-of-ageing-2019.

Chan, G. K. and Duque, G. (no date) 'Age-related bone loss: old bone, new facts.', *Gerontology*, 48(2), pp. 62–71. doi: 10.1159/000048929.

Chance, B., Sies, H. and Boveris, A. (1979) 'Hydroperoxide metabolism in mammalian organs', *Physiological Reviews*, 59(3), pp. 527–605. doi: 10.1152/physrev.1979.59.3.527.

Chen, L. *et al.* (2003) 'WRN, the protein deficient in Werner syndrome, plays a critical structural role in optimizing DNA repair.', *Aging cell*, 2(4), pp. 191–9. doi: 10.1046/j.1474-9728.2003.00052.x.

Chen, Q. M. *et al.* (1998) 'Molecular analysis of H2O2-induced senescent-like growth arrest in normal human fibroblasts: p53 and Rb control G1 arrest but not cell replication', *Biochemical Journal*. Portland Press Ltd, 332(1), pp. 43–50. doi: 10.1042/bj3320043.

Chen, X. I. *et al.* (2002) 'Senescence-like changes induced by expression of p21 Waf1 / Cip1 in NIH3T3 cell line', 12, pp. 229–233.

Chen, Z. *et al.* (2005) 'Crucial role of p53-dependent cellular senescence in suppression of Pten-deficient tumorigenesis.', *Nature*, 436(7051), pp. 725–730. doi: 10.1038/nature03918.

Chien, W. W. *et al.* (2011) 'Cyclin-dependent kinase 1 expression is inhibited by p16(INK4a) at the post-transcriptional level through the microRNA pathway.', *Oncogene*. Nature Publishing Group, 30(16), pp. 1880–91. doi: 10.1038/onc.2010.570.

Childs, B. G. *et al.* (2014) 'Senescence and apoptosis: dueling or complementary cell fates?', *EMBO Reports*, 15(11), pp. 1139–1153. doi: 10.15252/embr.201439245.

Childs, B. G. *et al.* (2016) 'Senescent intimal foam cells are deleterious at all stages of atherosclerosis', 354(6311), pp. 472–477. doi: 10.1126/science.aaf6659.Senescent.

Chinta, S. J., Woods, G., Demaria, M., Rane, A., *et al.* (2018) 'Cellular Senescence Is Induced by the Environmental Neurotoxin Paraquat and Contributes to Neuropathology Linked to Parkinson's Disease.', *Cell reports*, 22(4), pp. 930–940. doi: 10.1016/j.celrep.2017.12.092.

Chinta, S. J., Woods, G., Demaria, M., Madden, D. T., *et al.* (2018) 'Cellular Senescence Is Induced by the Environmental Neurotoxin Paraquat and Contributes to Neuropathology Linked to Parkinson's Disease'. doi: 10.1016/j.celrep.2017.12.092.

Choudhury, A. R. *et al.* (2007) 'Cdkn1a deletion improves stem cell function and lifespan of mice with dysfunctional telomeres without accelerating cancer formation.', *Nature genetics*, 39(1), pp. 99–105. doi: 10.1038/ng1937.

Christensen, K. *et al.* (2009) 'Ageing populations: the challenges ahead', *The Lancet*, pp. 1196–1208. doi: 10.1016/S0140-6736(09)61460-4.

Clements, P. *et al.* (1995) 'Inter and intraobserver variability of total skin thickness score (modified Rodnan TSS) in systemic sclerosis.', *The Journal of rheumatology*, 22(7), pp. 1281–5. Available at: http://www.ncbi.nlm.nih.gov/pubmed/7562759 (Accessed: 30 September 2019).

Collins, C. J. and Sedivy, J. M. (2003) 'Involvement of the INK4a/Arf gene locus in senescence.', *Aging cell*. England, 2(3), pp. 145–150.

Collins, K. *et al.* (2017) 'Bridging the age gap in breast cancer: evaluation of decision support interventions for older women with operable breast cancer: protocol for a cluster randomised controlled trial', *BMJ Open*, 7, p. 15133. doi: 10.1136/bmjopen-2016-015133.

Colman, R. J. *et al.* (2009) 'Caloric restriction delays disease onset and mortality in rhesus monkeys.', *Science (New York, N.Y.)*, 325(5937), pp. 201–4. doi: 10.1126/science.1173635.

Coppé, J.-P. *et al.* (2006) 'Secretion of vascular endothelial growth factor by primary human fibroblasts at senescence.', *The Journal of biological chemistry*, 281(40), pp. 29568–29574. doi: 10.1074/jbc.M603307200.

Coppé, J.-P. *et al.* (2008) 'Senescence-Associated Secretory Phenotypes Reveal Cell-Nonautonomous Functions of Oncogenic RAS and the p53 Tumor Suppressor', *PLoS Biology*, 6(12), p. e301. doi: 10.1371/journal.pbio.0060301.

Corish, P. and Tyler-Smith, C. (1999) 'Attenuation of green fluorescent protein half-life in mammalian cells.', *Protein engineering*, 12(12), pp. 1035–40. Available at: http://www.ncbi.nlm.nih.gov/pubmed/10611396 (Accessed: 29 August 2019).

Correia-Melo, C. *et al.* (2019) 'Rapamycin improves healthspan but not inflammaging in nfκb1-/- mice.', *Aging cell*, 18(1), p. e12882. doi: 10.1111/acel.12882.

Cutler, C. *et al.* (2013) 'Prostaglandin-modulated Umbilical cord blood hematopoietic stem cell transplantation', *Blood*, 122(17), pp. 3074–3081. doi: 10.1182/blood-2013-05-503177.

Czesnikiewicz-Guzik, M. *et al.* (2008) 'T cell subset-specific susceptibility to aging.', *Clinical immunology (Orlando, Fla.)*, 127(1), pp. 107–18. doi: 10.1016/j.clim.2007.12.002.

d'Adda di Fagagna, F. *et al.* (2003) 'A DNA damage checkpoint response in telomere-initiated senescence.', *Nature*, 426(6963), pp. 194–8. doi: 10.1038/nature02118.

Dakup, P. and Gaddameedhi, S. (2017) 'Impact of the Circadian Clock on UV-Induced DNA Damage Response and Photocarcinogenesis', *Photochemistry and Photobiology*. Blackwell Publishing Inc., pp. 296–303. doi: 10.1111/php.12662.

Daroczi, B. *et al.* (2006) 'In vivo radioprotection by the fullerene nanoparticle DF-1 as assessed in a zebrafish model', *Clinical Cancer Research*, 12(23), pp. 7086–7091. doi: 10.1158/1078-0432.CCR-06-0514.

Daroczi, B. *et al.* (2009) 'Nuclear factor κB inhibitors alleviate and the proteasome inhibitor PS-341 exacerbates radiation toxicity in zebrafish embryos', *Molecular Cancer Therapeutics*, 8(9), pp. 2625–2634. doi: 10.1158/1535-7163.MCT-09-0198.

Daróczi, B. (2006) 'Evaluation of agents that can modify the radiation response'.

Davies, M. R. Q. *et al.* (1980) 'Colouring the damaged tissues on the burn wound surface', *Burns*, 6(3), pp. 156–159. doi: 10.1016/0305-4179(80)90059-5.

Debacq-Chainiaux, F. *et al.* (2005) 'Repeated exposure of human skin fibroblasts to UVB at subcytotoxic level triggers premature senescence through the TGF-β1 signaling pathway', *Journal of Cell Science*, 118(4), pp. 743–758. doi: 10.1242/jcs.01651.

Demaria, M. *et al.* (2014) 'An Essential Role for Senescent Cells in Optimal Wound Healing through Secretion of PDGF-AA', *Developmental Cell*, 31(6), pp. 722–733. doi: 10.1016/j.devcel.2014.11.012.

Demaria, M. *et al.* (2017) 'Cellular senescence promotes adverse effects of chemotherapy and cancer relapse', *Cancer Discovery*. American Association for Cancer Research Inc., 7(2), pp. 165–176. doi: 10.1158/2159-8290.CD-16-0241.

Deng, C. *et al.* (1995) 'Mice lacking p21CIP1/WAF1 undergo normal development, but are defective in G1 checkpoint control.', *Cell*, 82(4), pp. 675–84. doi: 10.1016/0092-8674(95)90039-x.

Deng, Y. *et al.* (2004) 'Age-related impaired type 1 T cell responses to influenza: reduced activation ex vivo, decreased expansion in CTL culture in vitro, and blunted response to influenza vaccination in vivo in the elderly.', *Journal of immunology (Baltimore, Md. : 1950)*, 172(6), pp. 3437–46. doi: 10.4049/jimmunol.172.6.3437.

van Deursen, J. M. (2014) 'The role of senescent cells in ageing', *Nature*. Nature Publishing Group, 509(7501), pp. 439–446. doi: 10.1038/nature13193.

Dimri, G P *et al.* (1995) 'A biomarker that identifies senescent human cells in culture and in aging skin in vivo.', *Proceedings of the National Academy of Sciences of the United States of America*, 92(20), pp. 9363–9367. doi: 10.1073/pnas.92.20.9363.

Dimri, Goberdhan P. *et al.* (1995) 'A biomarker that identifies senescent human cells in culture and in aging skin in vivo', *Proceedings of the National Academy of Sciences of the United States of America*, 92(20), pp. 9363–9367. doi: 10.1073/pnas.92.20.9363.

Ding, Z. *et al.* (2012) 'Telomerase reactivation following telomere dysfunction yields murine prostate tumors with bone metastases', *Cell*, 148(5), pp. 896–907. doi: 10.1016/j.cell.2012.01.039.

Doan, J. *et al.* (2013) 'Prevalence and Risk of Potential Cytochrome P450–Mediated Drug-Drug Interactions in Older Hospitalized Patients with Polypharmacy', *Annals of Pharmacotherapy*. SAGE Publications, 47(3), pp. 324–332. doi: 10.1345/aph.1r621.

Driessens, N. *et al.* (2009) 'Hydrogen peroxide induces DNA single- and double-strand breaks in thyroid cells and is therefore a potential mutagen for this organ.', *Endocrine-related cancer*, 16(3), pp. 845–56. doi: 10.1677/ERC-09-0020.

Efeyan, A. *et al.* (2009) 'Limited role of murine ATM in oncogene-induced senescence and p53-dependent tumor suppression', *PLoS ONE*, 4(5). doi: 10.1371/journal.pone.0005475.

Elbarbry, F., Ung, A. and Abdelkawy, K. (2017) 'Studying the Inhibitory Effect of Quercetin and Thymoquinone on Human Cytochrome P450 Enzyme Activities', *Pharmacognosy Magazine*. Medknow Publications, 13(52), pp. S895–S899. doi: 10.4103/0973-1296.224342.

Elks, P. M. *et al.* (2013) 'Hypoxia Inducible Factor Signaling Modulates Susceptibility to Mycobacterial Infection via a Nitric Oxide Dependent Mechanism', *PLoS Pathogens*. Public Library of Science, 9(12), pp. 1–16. doi: 10.1371/journal.ppat.1003789.

Ellett, F. *et al.* (2011) 'mpeg1 promoter transgenes direct macrophage-lineage expression in zebrafish', *Blood*, 117(4). doi: 10.1182/blood-2010-10-314120.

Van Epps, P. *et al.* (no date) 'Frailty has a stronger association with inflammation than age in older veterans'. doi: 10.1186/s12979-016-0082-z.

EPSTKIN, C. J. *et al.* (1966) 'A Review of its Symptomatology, Natural History, Pathologic Features, Genetics And Relationship to the Natural Aging Process', *Medicine*, 45(3). Available at: https://journals.lww.com/md-journal/Fulltext/1966/05000/A_Review_of_its_Symptomatology,_Natural_History,.1.aspx.

Eriksson, M. *et al.* (2003) 'Recurrent de novo point mutations in lamin A cause Hutchinson-Gilford progeria syndrome', *Nature*, 423(6937), pp. 293–298. doi: 10.1038/nature01629.

Fabian, D. & Flatt, T. (2011) 'The Evolution of Aging.', *Nature Education Knowledge* , 3(10), p. 9.

Fali, T. *et al.* (2018) 'Elderly human hematopoietic progenitor cells express cellular senescence markers and are more susceptible to pyroptosis', *JCI insight*. NLM (Medline), 3(13). doi: 10.1172/jci.insight.95319.

Farr, J. N. *et al.* (2017) 'Targeting cellular senescence prevents age-related bone loss in mice', *Nature Medicine*. Nature Publishing Group, 23(9), pp. 1072–1079. doi: 10.1038/nm.4385.

Feng, Y. *et al.* (2010) 'Live imaging of innate immune cell sensing of transformed cells in zebrafish larvae: Parallels between tumor initiation and wound inflammation', *PLoS Biology*, 8(12). doi: 10.1371/journal.pbio.1000562.

Feng, Z. *et al.* (2007) 'Declining p53 function in the aging process: a possible mechanism for the increased tumor incidence in older populations.', *Proceedings of the National Academy of Sciences of the United States of America*, 104(42), pp. 16633–16638. doi: 10.1073/pnas.0708043104.

Finkel, T., Serrano, M. and Blasco, M. a (2007) 'The common biology of cancer and ageing.', *Nature*, 448(7155), pp. 767–74. doi: 10.1038/nature05985.

Freund, A. *et al.* (2010) 'Inflammatory networks during cellular senescence: causes and consequences.', *Trends in molecular medicine*, 16(5), pp. 238–46. doi: 10.1016/j.molmed.2010.03.003.

Fries, J. F. (1980) 'Aging, natural death, and the compression of morbidity.', *The New England journal of medicine*, 303(3), pp. 130–5. doi: 10.1056/NEJM198007173030304.

Fuhrmann-Stroissnigg, H. *et al.* (2017) 'Identification of HSP90 inhibitors as a novel class of senolytics', *Nature Communications*. Nature Publishing Group, 8(1), p. 422. doi: 10.1038/s41467-017-00314-z.

Futosi, K. *et al.* (2012) 'Dasatinib inhibits proinflammatory functions of mature human neutrophils.', *Blood*, 119(21), pp. 4981–91. doi: 10.1182/blood-2011-07-369041.

Gagou, M. E., Zuazua-Villar, P. and Meuth, M. (2010) 'Enhanced H2AX phosphorylation, DNA replication fork arrest, and cell death in the absence of Chk1', *Molecular Biology of the Cell*, 21(5), pp. 739–752. doi: 10.1091/mbc.E09-07-0618.

Gallegos, J. E. and Rose, A. B. (2017) 'Intron DNA Sequences Can Be More Important Than the Proximal Promoter in Determining the Site of Transcript Initiation.', *The Plant cell*, 29(4), pp. 843–853. doi: 10.1105/tpc.17.00020.

García-Cao, I. *et al.* (2002) '"Super p53" mice exhibit enhanced DNA damage response, are tumor resistant and age normally.', *The EMBO journal*, 21(22), pp. 6225–35. doi: 10.1093/emboj/cdf595.

García-Prat, L. *et al.* (2016) 'Autophagy maintains stemness by preventing senescence.', *Nature*, 529(7584), pp. 37–42. doi: 10.1038/nature16187.

Gasser, S. *et al.* (2005) 'The DNA damage pathway regulates innate immune system ligands of the NKG2D receptor.', *Nature*, 436(7054), pp. 1186–90. doi: 10.1038/nature03884.

Georgakopoulou, E. A. *et al.* (2013) 'Specific lipofuscin staining as a novel biomarker to detect replicative and stress-induced senescence. A method applicable in cryo-preserved and archival tissues.', *Aging*, 5(1), pp. 37–50. doi: 10.18632/aging.100527.

Georgilis, A. *et al.* (2018) 'PTBP1-Mediated Alternative Splicing Regulates the Inflammatory Secretome and the Pro-tumorigenic Effects of Senescent Cells', *Cancer Cell*, 34, pp. 85–102. doi: 10.1016/j.ccell.2018.06.007.

Gerhard, G. S. *et al.* (2002) 'Life spans and senescent phenotypes in two strains of Zebrafish (Danio rerio)', *Experimental Gerontology*, 37(8–9), pp. 1055–1068. doi: 10.1016/S0531-5565(02)00088-8.

Gerlach, G. F. and Wingert, R. A. (2013) 'Kidney organogenesis in the zebrafish: insights into vertebrate nephrogenesis and regeneration', *Wiley interdisciplinary reviews. Developmental biology*, pp. 559–585. doi: 10.1002/wdev.92.

Gilbert, M. J. H., Zerulla, T. C. and Tierney, K. B. (2013) 'Zebrafish (Danio rerio) as a model for the study of aging and exercise: Physical ability and trainability decrease with age', *Experimental Gerontology*, 50(1), pp. 106–113. doi: 10.1016/j.exger.2013.11.013.

Gizard, F. *et al.* (2005) 'PPAR α inhibits vascular smooth muscle cell proliferation underlying intimal hyperplasia by inducing the tumor suppressor p16 INK4a', 115(11). doi: 10.1172/JCI22756DS1.

Going, J. J. *et al.* (2002) '"Senescence-associated" beta-galactosidase activity in the upper gastrointestinal tract.', *The Journal of pathology*, 196(4), pp. 394–400. doi: 10.1002/path.1059.

Goldman, D. P. *et al.* (2013) 'Substantial health and economic returns from delayed aging may warrant a new focus for medical research', *Health Affairs*, 32(10), pp. 1698–1705. doi: 10.1377/hlthaff.2013.0052.

Goodpaster, B. H. *et al.* (2006) *The Loss of Skeletal Muscle Strength, Mass, and Quality in Older Adults: The Health, Aging and Body Composition Study*. Available at: https://academic.oup.com/biomedgerontology/article-abstract/61/10/1059/600461.

Gottlieb, S. and Ruvkun, G. (1994) *daf-2, daf-16 and daf-23: Genetically Interacting Genes Controlling Dauer Formation i n Caenorhabditis elegans*, *Genetics*.

Granados, J. A. T. and Roux, A. V. D. (no date) *Life and death during the Great Depression*. Available at: www.pnas.orgcgidoi10.1073pnas.0904491106.

Gray, G. M. and Santiago, N. A. (1969) 'Intestinal β-galactosidases', *Journal of Clinical Investigation*, 48(4), pp. 716–728. doi: 10.1172/JCI106029.

Griffin, A. *et al.* (2017) 'Clemizole and modulators of serotonin signalling suppress seizures in Dravet syndrome', *Brain*. Oxford University Press, 140(3), pp. 669–683. doi: 10.1093/brain/aww342.

Guryev, V. *et al.* (2006) 'Genetic variation in the zebrafish', *Genome Research*, 16(4), pp. 491–497. doi: 10.1101/gr.4791006.

Halazonetis, T. D., Gorgoulis, V. G. and Bartek, J. (2008) 'An Oncogene-Induced DNA Damage Model for Cancer Development', 319(March), pp. 1352–1356.

Hall, B. M. *et al.* (2016) 'Aging of mice is associated with p16 (Ink4a) - and β - galactosidase - positive macrophage accumulation that can be induced in young mice by senescent cells', 8(7).

Hall, B. M. *et al.* (2017) 'p16(Ink4a) and senescence-associated β-galactosidase can be induced in macrophages as part of a reversible response to physiological stimuli', *Aging*, 9(8), pp. 1867–1884. doi: 10.18632/aging.101268.

Hall, Z. J. and Tropepe, V. (2018) 'Movement maintains forebrain neurogenesis via peripheral neural feedback in larval zebrafish.', *eLife*, 7. doi: 10.7554/eLife.31045.

HAMILTON, J. B. (1951) 'Patterned loss of hair in man; types and incidence.', *Annals of the New York Academy of Sciences*, 53(3), pp. 708–28. doi: 10.1111/j.1749-6632.1951.tb31971.x.

Harley, C B, Futcher, A. B. and Greider, C. W. (1990) 'Telomeres shorten during ageing of human fibroblasts.', *Nature*, 345(6274), pp. 458–60. doi: 10.1038/345458a0.

Harrison, D. E. *et al.* (2009) 'Rapamycin fed late in life extends lifespan in genetically heterogeneous mice', *Nature*, 460(7253), pp. 392–395. doi: 10.1038/nature08221.

Haupt, S. *et al.* (2003) 'Apoptosis - The p53 network', *Journal of Cell Science*, pp. 4077–4085. doi: 10.1242/jcs.00739.

Hayes, A. J. *et al.* (2013) 'Spinal deformity in aged zebrafish is accompanied by degenerative changes to their vertebrae that resemble osteoarthritis.', *PloS one*, 8(9), p. e75787. doi: 10.1371/journal.pone.0075787.

Hayflick, L. (1965) 'The limited in vitro lifetime of human diploid cell strains', *Experimental Cell Research*, 37(3), pp. 614–636. doi: 10.1016/0014-4827(65)90211-9.

Hayflick, L. and Moorhead, P. S. (1961) 'Hayflick and Moorhead Characterize Cellular Senescence in Primary Human Cells', *Experimental cell research*, 1(25), pp. 585–621. Available at: https://www.science-of-aging.com/timelines/hayflick-moorhead-senescence-telomeres.php (Accessed: 31 August 2019).

He, S. and Sharpless, N. E. (2017) 'Senescence in Health and Disease', *Cell*. Elsevier Inc., 169(6), pp. 1000–1011. doi: 10.1016/j.cell.2017.05.015.

Hebert, L. E. *et al.* (2001) 'Annual incidence of Alzheimer disease in the United States projected to the years 2000 through 2050.', *Alzheimer disease and associated disorders*, 15(4), pp. 169–173. doi: 10.1097/00002093-200110000-00002.

Henriques, C. M. *et al.* (2013) 'Telomerase Is Required for Zebrafish Lifespan', *PLoS Genetics*, 9(1), p. e1003214. doi: 10.1371/journal.pgen.1003214.

Herbig, U. *et al.* (2004) 'Telomere shortening triggers senescence of Human Cells through a Pathway Involving ATM , p53 , and p21 CIP1 , but Not p16 INK4a', *Molecular cell*, 14, pp. 501–513. doi: 10.1016/S1097-2765(04)00256-4.

Herbig, U. *et al.* (2006) 'Cellular senescence in aging primates.', *Science (New York, N.Y.)*, 311(5765), p. 1257. doi: 10.1126/science.1122446.

Herbomel, P., Thisse, B. and Thisse, C. (1999) 'Ontogeny and behaviour of early macrophages in the zebrafish embryo.', *Development (Cambridge, England)*, 126(17), pp. 3735–45. Available at: http://www.ncbi.nlm.nih.gov/pubmed/10433904 (Accessed: 30 September 2019).

Hernandez-Segura, A. *et al.* (2017) 'Unmasking Transcriptional Heterogeneity in Senescent Cells.', *Current biology :*

CB, 27(17), pp. 2652-2660.e4. doi: 10.1016/j.cub.2017.07.033.

Herranz, N. *et al.* (2015) 'mTOR regulates MAPKAPK2 translation to control the senescence-associated secretory phenotype.', *Nature cell biology*, 17(9), pp. 1205–17. doi: 10.1038/ncb3225.

Hickson, L. J. *et al.* (2019) 'Senolytics decrease senescent cells in humans: Preliminary report from a clinical trial of Dasatinib plus Quercetin in individuals with diabetic kidney disease', *EBioMedicine*, 47, pp. 446–456. doi: 10.1016/j.ebiom.2019.08.069.

Hodi, F. S. *et al.* (2013) 'NIH Public Access', 363(8), pp. 711–723. doi: 10.1056/NEJMoa1003466.Improved.

Hoffman, J. M. *et al.* (2018) 'The companion dog as a model for human aging and mortality.', *Aging cell*, 17(3), p. e12737. doi: 10.1111/acel.12737.

Holmes, W. R. and Joseph, J. (2011) 'Social participation and healthy ageing: A neglected, significant protective factor for chronic non communicable conditions', *Globalization and Health*, 7. doi: 10.1186/1744-8603-7-43.

Home Office (2014) *Guidance on the Operation of the Animals (Scientific Procedures) Act 1986*.

Van houcke, J. *et al.* (2015) 'The zebrafish as a gerontology model in nervous system aging, disease, and repair', *Ageing Research Reviews*. Elsevier Ireland Ltd, pp. 358–368. doi: 10.1016/j.arr.2015.10.004.

Howe, K. *et al.* (2013) 'The zebrafish reference genome sequence and its relationship to the human genome.', *Nature*, 496(7446), pp. 498–503. doi: 10.1038/nature12111.

Huffman, K. E. *et al.* (2000) 'Telomere shortening is proportional to the size of the G-rich telomeric 3'-overhang.', *The Journal of biological chemistry*, 275(26), pp. 19719–22. doi: 10.1074/jbc.M002843200.

Huisman, M. *et al.* (2013) 'Socioeconomic inequalities in mortality rates in old age in the world health organization Europe region', *Epidemiologic Reviews*, 35(1), pp. 84–97. doi: 10.1093/epirev/mxs010.

Hutchinson, J. (1886) 'Congenital Absence of Hair and Mammary Glands with Atrophic Condition of the Skin and its Appendages, in a Boy whose Mother had been almost wholly Bald from Alopecia Areata from the age of Six', *Medico-chirurgical transactions*, 69, pp. 473–477. doi: 10.1177/095952878606900127.

Hwang, H. T. V. *et al.* (2018) 'Investigation of quercetin and hyperoside as senolytics in adult human endothelial cells', *PLoS ONE*. Public Library of Science, 13(1). doi: 10.1371/journal.pone.0190374.

Jacks, T. *et al.* (1994) 'Tumor spectrum analysis in p53-mutant mice.', *Current biology : CB*, 4(1), pp. 1–7. doi: 10.1016/s0960-9822(00)00002-6.

Jascur, T. *et al.* (2005) 'Regulation of p21 WAF1/CIP1 Stability by WISp39, a Hsp90 Binding TPR Protein', *Molecular Cell*. Maki and Howley, 17, pp. 237–249. doi: 10.1016/j.molcel.2004.11.049.

Jeon, O. H. *et al.* (2017) 'Local clearance of senescent cells attenuates the development of post-traumatic osteoarthritis and creates a pro-regenerative environment', *Nature Medicine*. Nature Publishing Group, 23(6), pp.

775–781. doi: 10.1038/nm.4324.

Jeyapalan, J. C. *et al.* (2007) 'Accumulation of senescent cells in mitotic tissue of aging primates', *Mechanisms of Ageing and Development*, 128(1), pp. 36–44. doi: 10.1016/j.mad.2006.11.008.

Jones, O. R. *et al.* (2014) 'Diversity of ageing across the tree of life', *Nature*, 505(7482), pp. 169–173. doi: 10.1038/nature12789.

Jun, J.-I. and Lau, L. F. (2010) 'The matricellular protein CCN1 induces fibroblast senescence and restricts fibrosis in cutaneous wound healing.', *Nature cell biology*, 12(7), pp. 676–85. doi: 10.1038/ncb2070.

Jurk, D. *et al.* (2012) 'Postmitotic neurons develop a p21-dependent senescence-like phenotype driven by a DNA damage response', *Aging Cell*, 11(6), pp. 996–1004. doi: 10.1111/j.1474-9726.2012.00870.x.

Justice, J. N. *et al.* (2019) 'Senolytics in idiopathic pulmonary fibrosis: Results from a first-in-human, open-label, pilot study'. doi: 10.1016/j.ebiom.2018.12.052.

Kang, C. *et al.* (2015) 'The DNA damage response induces inflammation and senescence by inhibiting autophagy of GATA4'. doi: 10.1126/science.aaa5612.

Kang, T.-W. *et al.* (2011) 'Senescence surveillance of pre-malignant hepatocytes limits liver cancer development', *Nature*. Nature Publishing Group, 479(7374), pp. 547–551. doi: 10.1038/nature10599.

Kao, T.-T. *et al.* (2014) 'Folate deficiency-induced oxidative stress contributes to neuropathy in young and aged zebrafish--implication in neural tube defects and Alzheimer's diseases.', *Neurobiology of disease*, 71, pp. 234–44. doi: 10.1016/j.nbd.2014.08.004.

Katzman, W. B. *et al.* (2010) 'Age-related hyperkyphosis: Its causes, consequences, and management', *Journal of Orthopaedic and Sports Physical Therapy*. Movement Science Media, pp. 352–360. doi: 10.2519/jospt.2010.3099.

Kawabata, K. *et al.* (no date) 'Flavonols enhanced production of anti-inflammatory substance(s) by Bifidobacterium adolescentis: prebiotic actions of galangin, quercetin, and fisetin.', *BioFactors (Oxford, England)*, 39(4), pp. 422–9. doi: 10.1002/biof.1081.

Kenyon, C. *et al.* (1993) 'A C. elegans mutant that lives twice as long as wild type', *Nature*, 366(6454), pp. 461–464. doi: 10.1038/366461a0.

Kheirbek, R. E. *et al.* (2017) 'Characteristics and Incidence of Chronic Illness in Community-Dwelling Predominantly Male U.S. Veteran Centenarians', *Journal of the American Geriatrics Society*. Blackwell Publishing Inc., 65(9), pp. 2100–2106. doi: 10.1111/jgs.14900.

Kierdorf, K. *et al.* (2013) 'Microglia emerge from erythromyeloid precursors via Pu.1- and Irf8-dependent pathways.', *Nature neuroscience*, 16(3), pp. 273–80. doi: 10.1038/nn.3318.

Kim, Jun Ho *et al.* (2015) 'Fisetin suppresses macrophage-mediated inflammatory responses by blockade of Src and

Syk', *Biomolecules and Therapeutics*. Korean Society of Applied Pharmacology, 23(5), pp. 414–420. doi: 10.4062/biomolther.2015.036.

Kim, N. W. *et al.* (1994) 'Specific Association of Human Telomerase Activity with Immortal Cells and Cancer', *Science*, 266(5193), pp. 2011–2015. doi: 10/ff9vwh.

Kim, S. U. and de Vellis, J. (2005) 'Microglia in health and disease.', *Journal of neuroscience research*, 81(3), pp. 302–13. doi: 10.1002/jnr.20562.

Kimura, S. H. *et al.* (2001) 'Cyclin G1 is involved in G2/M arrest in response to DNA damage and in growth control after damage recovery', *Oncogene*. Nature Publishing Group, 20(25), pp. 3290–3300. doi: 10.1038/sj.onc.1204270.

Kirkland, J. L. *et al.* (2017) 'The Clinical Potential of Senolytic Drugs', *Journal of the American Geriatrics Society*. Blackwell Publishing Inc., 65(10), pp. 2297–2301. doi: 10.1111/jgs.14969.

Kishi, S. *et al.* (2003) 'The zebrafish as a vertebrate model of functional aging and very gradual senescence.', *Experimental gerontology*, 38(7), pp. 777–86. doi: 10.1016/S0531-5565(03)00108-6.

Kishi, S. *et al.* (2008) 'The Identification of Zebrafish Mutants Showing Alterations in Senescence-Associated Biomarkers', *PLoS Genetics*, 4(8), p. e1000152. doi: 10.1371/journal.pgen.1000152.

Klass, M. R. (1983) 'A method for the isolation of longevity mutants in the nematode Caenorhabditis elegans and initial results', *Mechanisms of Ageing and Development*, 22(3–4), pp. 279–286. doi: 10.1016/0047-6374(83)90082-9.

Knights, C. D. *et al.* (2006) 'Distinct p53 acetylation cassettes differentially influence gene-expression patterns and cell fate', *Journal of Cell Biology*, 173(4), pp. 533–544. doi: 10.1083/jcb.200512059.

Kobayashi, S. *et al.* (2005) 'EGFR mutation and resistance of non-small-cell lung cancer to gefitinib', *New England Journal of Medicine*, 352(8), pp. 786–792. doi: 10.1056/NEJMoa044238.

Koshimizu, E. *et al.* (2011) 'Embryonic Senescence and Laminopathies in a Progeroid Zebrafish Model', *PLoS ONE*, 6(3), p. e17688. doi: 10.1371/journal.pone.0017688.

Kovacovicova, K. *et al.* (2018) 'Senolytic cocktail dasatinib+quercetin (D+Q) does not enhance the efficacy of senescence-inducing chemotherapy in liver cancer', *Frontiers in Oncology*. Frontiers Media S.A., 8(OCT). doi: 10.3389/fonc.2018.00459.

Krishna, D. R. *et al.* (1999) 'Does pH 6 β-galactosidase activity indicate cell senescence?', *Mechanisms of Ageing and Development*, 109(2), pp. 113–123. doi: 10.1016/S0047-6374(99)00031-7.

Krizhanovsky, V. *et al.* (2008) 'Implications of cellular senescence in tissue damage response, tumor suppression, and stem cell biology', in *Cold Spring Harbor Symposia on Quantitative Biology*. doi: 10.1101/sqb.2008.73.048.

Krtolica, A. *et al.* (2011) 'GROα regulates human embryonic stem cell self-renewal or adoption of a neuronal fate.', *Differentiation; research in biological diversity*, 81(4), pp. 222–32. doi: 10.1016/j.diff.2011.01.001.

Kuilman, T. and Peeper, D. S. (2009) 'SMS-ing cellular stress', 9(FEBRUARy). doi: 10.1038/nrc2560.

Kumar, S. and Hedges, S. B. (1998) 'A molecular timescale for vertebrate evolution.', *Nature*, 392(6679), pp. 917–20. doi: 10.1038/31927.

Kuo, C.-L. *et al.* (2011) 'Cdkn2a is an atherosclerosis modifier locus that regulates monocyte/macrophage proliferation.', *Arteriosclerosis, thrombosis, and vascular biology*, 31(11), pp. 2483–92. doi: 10.1161/ATVBAHA.111.234492.

Laberge, R.-M. *et al.* (2012) 'Glucocorticoids suppress selected components of the senescence-associated secretory phenotype.', *Aging cell*, 11(4), pp. 569–78. doi: 10.1111/j.1474-9726.2012.00818.x.

Laberge, R.-M. *et al.* (2015) 'MTOR regulates the pro-tumorigenic senescence-associated secretory phenotype by promoting IL1A translation', *Nat Cell Biol*. 17(8), pp. 1049–1061. doi: 10.1038/ncb3195.

Lam, S. H. *et al.* (2004) 'Development and maturation of the immune system in zebrafish, Danio rerio: a gene expression profiling, in situ hybridization and immunological study.', *Developmental and comparative immunology*, 28(1), pp. 9–28. doi: 10.1016/s0145-305x(03)00103-4.

Laranjeiro, R. *et al.* (2013) 'Cyclin-dependent kinase inhibitor p20 controls circadian cell-cycle timing.', *Proceedings of the National Academy of Sciences of the United States of America*, 110(17), pp. 6835–40. doi: 10.1073/pnas.1217912110.

Larsson, L. *et al.* (2019) 'Sarcopenia: Aging-related loss of muscle mass and function', *Physiological Reviews*. American Physiological Society, 99(1), pp. 427–511. doi: 10.1152/physrev.00061.2017.

Lawless, C. *et al.* (2010) 'Quantitative assessment of markers for cell senescence', *Experimental Gerontology*. Elsevier Inc., 45(10), pp. 772–778. doi: 10.1016/j.exger.2010.01.018.

Le, Oanh N L *et al.* (2010) 'Ionizing radiation-induced long-term expression of senescence markers in mice is independent of p53 and immune status.', *Aging cell*, 9(3), pp. 398–409. doi: 10.1111/j.1474-9726.2010.00567.x.

Lee, B. Y. *et al.* (2006) 'Senescence-associated β-galactosidase is lysosomal β-galactosidase', *Aging Cell*, 5(2), pp. 187–195. doi: 10.1111/j.1474-9726.2006.00199.x.

Lee, E.-C. *et al.* (2001) 'A Highly Efficient Escherichia coli-Based Chromosome Engineering System Adapted for Recombinogenic Targeting and Subcloning of BAC DNA', *Genomics*, 73(1), pp. 56–65. doi: 10.1006/geno.2000.6451.

Lee, G. T. *et al.* (2014) 'Prostate cancer bone metastases acquire resistance to androgen deprivation via WNT5A-mediated BMP-6 induction.', *British journal of cancer*, 110(6), pp. 1634–44. doi: 10.1038/bjc.2014.23.

Leng, S., Chen, X. and Mao, G. (2014) 'Frailty syndrome: an overview', *Clinical Interventions in Aging*. Dove Medical Press Ltd., p. 433. doi: 10.2147/cia.s45300.

Di Leonardo, A. *et al.* (1994) 'DNA damage triggers a prolonged p53-dependent G1 arrest and long-term induction of

Cip1 in normal human fibroblasts.', *Genes & development*, 8(21), pp. 2540–51. doi: 10.1101/gad.8.21.2540.

Lewis-McDougall, F. C. *et al.* (2019) 'Aged-senescent cells contribute to impaired heart regeneration', *Aging Cell*. Blackwell Publishing Ltd, 18(3). doi: 10.1111/acel.12931.

Lieschke, G. J. and Currie, P. D. (2007) 'Animal models of human disease: zebrafish swim into view.', *Nature reviews. Genetics*, 8(5), pp. 353–67. doi: 10.1038/nrg2091.

Lin, A. W. *et al.* (1998) 'Premature senescence involving p53 and p16 is activated in response to constitutive MEK/MAPK mitogenic signaling', *Genes and Development*, 12(19), pp. 3008–3019. doi: 10.1101/gad.12.19.3008.

Lin, I. H. *et al.* (2018) 'Skeletal muscle in aged mice reveals extensive transformation of muscle gene expression', *BMC Genetics*. BioMed Central Ltd., 19(1). doi: 10.1186/s12863-018-0660-5.

Lin, M.-R. *et al.* (2004) 'Psychometric comparisons of the timed up and go, one-leg stand, functional reach, and Tinetti balance measures in community-dwelling older people.', *Journal of the American Geriatrics Society*, 52(8), pp. 1343–8. doi: 10.1111/j.1532-5415.2004.52366.x.

Lindsten, T. *et al.* (2000) 'The combined functions of proapoptotic Bcl-2 family members Bak and Bax are essential for normal development of multiple tissues', *Molecular Cell*. doi: 10.1016/S1097-2765(00)00136-2.

Cudejko, C. *et al.* (2011) 'p16 INK4a deficiency promotes IL-4-induced polarization and inhibits proinflammatory signaling in macrophages', *Blood*. doi: 10.1182/blood-2010-10-313106.

Lister, J. a *et al.* (1999) 'Nacre Encodes a Zebrafish Microphthalmia-Related Protein That Regulates Neural-Crest-Derived Pigment Cell Fate.', *Development (Cambridge, England)*, 126(17), pp. 3757–67. Available at: http://www.ncbi.nlm.nih.gov/pubmed/10433906.

Liu, J. Y. *et al.* (2019) 'Cells exhibiting strong p16 INK4a promoter activation in vivo display features of senescence', *Proceedings of the National Academy of Sciences of the United States of America*, 116(7), pp. 2603–2611. doi: 10.1073/pnas.1818313116.

Liu, Y. *et al.* (2009) 'Expression of p16(INK4a) in peripheral blood T-cells is a biomarker of human aging.', *Aging cell*, 8(4), pp. 439–48. doi: 10.1111/j.1474-9726.2009.00489.x.

Livak, K. J. and Schmittgen, T. D. (2001) 'Analysis of relative gene expression data using real-time quantitative PCR and the 2-ΔΔCT method', *Methods*. Academic Press Inc., 25(4), pp. 402–408. doi: 10.1006/meth.2001.1262.

Loeser, R. F. (2017) 'The Role of Aging in the Development of Osteoarthritis.', *Transactions of the American Clinical and Climatological Association*, 128, pp. 44–54. Available at: http://www.ncbi.nlm.nih.gov/pubmed/28790486 (Accessed: 29 September 2019).

López-Otín, C. *et al.* (2013) 'The hallmarks of aging.', *Cell*, 153(6), pp. 1194–217. doi: 10.1016/j.cell.2013.05.039.

Maciel-Barón, L. A. *et al.* (2016) 'Senescence associated secretory phenotype profile from primary lung mice

fibroblasts depends on the senescence induction stimuli', *Age*, 38(1), pp. 1–14. doi: 10.1007/s11357-016-9886-1.

Makrantonaki, E. and Zouboulis, C. C. (2007) 'Molecular mechanisms of skin aging: state of the art.', *Annals of the New York Academy of Sciences*, 1119, pp. 40–50. doi: 10.1196/annals.1404.027.

Mantovani, A. *et al.* (2010) 'The chemokine system in cancer biology and therapy.', *Cytokine & growth factor reviews*. Elsevier Ltd, 21(1), pp. 27–39. doi: 10.1016/j.cytogfr.2009.11.007.

Marešová, P., Mohelská, H. and Kuča, K. (2015) 'Economics Aspects of Ageing Population', *Procedia Economics and Finance*. Elsevier BV, 23, pp. 534–538. doi: 10.1016/s2212-5671(15)00492-x.

Martín-Caballero, J. *et al.* (2001) 'Tumor susceptibility of p21(Waf1/Cip1)-deficient mice.', *Cancer research*, 61(16), pp. 6234–8. Available at: http://www.ncbi.nlm.nih.gov/pubmed/11507077 (Accessed: 31 August 2019).

Martin-Montalvo, A. *et al.* (2013) 'Metformin improves healthspan and lifespan in mice', *Nature Communications*, 4. doi: 10.1038/ncomms3192.

Martin, J. A. and Buckwalter, J. A. (2002) 'Human chondrocyte senescence and osteoarthritis.', *Biorheology*, 39(1–2), pp. 145–52. Available at: http://www.ncbi.nlm.nih.gov/pubmed/12082277 (Accessed: 27 August 2019).

Martyanov, V., Whitfield, M. L. and Varga, J. (2019) 'Senescence signature in skin biopsies from systemic sclerosis patients treated with senolytic therapy: potential predictor of clinical response?', *Arthritis & Rheumatology*. Wiley. doi: 10.1002/art.40934.

Matheu, A. *et al.* (2004) 'Increased gene dosage of Ink4a/Arf results in cancer resistance and normal aging.', *Genes & development*, 18(22), pp. 2736–46. doi: 10.1101/gad.310304.

Mathias, J. R. *et al.* (2008) 'Development | Supplementary Material Development | Supplementary Material', *Journal of leukocyte biology*. Society for Leukocyte Biology, 3(C), pp. 1–4. doi: 10.1189/jlb.0506346.

Mattison, J. A. *et al.* (2012) 'Impact of caloric restriction on health and survival in rhesus monkeys from the NIA study', *Nature*, 489(7415), pp. 318–321. doi: 10.1038/nature11432.

Maures, T. J. *et al.* (2011) 'The H3K27 demethylase UTX-1 regulates C. elegans lifespan in a germline-independent, insulin-dependent manner.', *Aging cell*, 10(6), pp. 980–90. doi: 10.1111/j.1474-9726.2011.00738.x.

McCay, C. M., Crowell, M. F. and Maynard, L. A. (1935) 'The Effect of Retarded Growth Upon the Length of Life Span and Upon the Ultimate Body Size', *The Journal of Nutrition*, 10(1), pp. 63–79. doi: 10.1093/jn/10.1.63.

McHugh, D. and Gil, J. (2018) 'Senescence and aging: Causes, consequences, and therapeutic avenues.', *The Journal of cell biology*. Rockefeller University Press, 217(1), pp. 65–77. doi: 10.1083/jcb.201708092.

McKercher, S. R. *et al.* (1996) 'Targeted disruption of the PU.1 gene results in multiple hematopoietic abnormalities.', *The EMBO journal*, 15(20), pp. 5647–58. Available at: http://www.ncbi.nlm.nih.gov/pubmed/8896458 (Accessed: 25 September 2019).

McPhee, J. S. *et al.* (2016) 'Physical activity in older age: perspectives for healthy ageing and frailty', *Biogerontology*. Springer Netherlands, pp. 567–580. doi: 10.1007/s10522-016-9641-0.

Meyers, J. R. (2018) 'Zebrafish: Development of a Vertebrate Model Organism', *Current Protocols in Essential Laboratory Techniques*. Blackwell Publishing Inc., 16(1). doi: 10.1002/cpet.19.

Michaloglou, C. *et al.* (2005) 'BRAFE600-associated senescence-like cell cycle arrest of human naevi.', *Nature*, 436(7051), pp. 720–4. doi: 10.1038/nature03890.

Moiseeva, O. *et al.* (2013) 'Metformin inhibits the senescence-associated secretory phenotype by interfering with IKK/NF-κB activation', *Aging Cell*, 12(3), pp. 489–498. doi: 10.1111/acel.12075.

Molofsky, A. V. *et al.* (2006) 'Increasing p16INK4a expression decreases forebrain progenitors and neurogenesis during ageing', *Nature*. Nature Publishing Group, 443(7110), pp. 448–452. doi: 10.1038/nature05091.

Moriwaki, S. *et al.* (1996) 'The effect of donor age on the processing of UV-damaged DNA by cultured human cells: reduced DNA repair capacity and increased DNA mutability.', *Mutation research*, 364(2), pp. 117–23. doi: 10.1016/0921-8777(96)00029-8.

Moskalev, A. A. *et al.* (2013) 'The role of DNA damage and repair in aging through the prism of Koch-like criteria.', *Ageing research reviews*, 12(2), pp. 661–84. doi: 10.1016/j.arr.2012.02.001.

Muñoz-Espín, D. *et al.* (2013) 'Programmed Cell Senescence during Mammalian Embryonic Development', *Cell*, 155(5), pp. 1104–1118. doi: 10.1016/j.cell.2013.10.019.

Münzel, E. J. *et al.* (2014) 'Zebrafish regenerate full thickness optic nerve myelin after demyelination, but this fails with increasing age.', *Acta neuropathologica communications*, 2, p. 77. doi: 10.1186/s40478-014-0077-y.

Murayama, E. *et al.* (2006) 'Tracing hematopoietic precursor migration to successive hematopoietic organs during zebrafish development.', *Immunity*, 25(6), pp. 963–75. doi: 10.1016/j.immuni.2006.10.015.

Murtha, J. M. and Keller, E. T. (2003) 'Characterization of the heat shock response in mature zebrafish (Danio rerio).', *Experimental gerontology*, 38(6), pp. 683–91. Available at: http://www.ncbi.nlm.nih.gov/pubmed/12814804 (Accessed: 3 September 2019).

Narita, Masako *et al.* (2011) 'Spatial coupling of mTOR and autophagy augments secretory phenotypes', *Science*. doi: 10.1126/science.1205407.

Narita, Masashi *et al.* (2003) 'Rb-mediated heterochromatin formation and silencing of E2F target genes during cellular senescence', *Cell*. Cell Press, 113(6), pp. 703–716. doi: 10.1016/S0092-8674(03)00401-X.

Nelson, G. *et al.* (2012) 'A senescent cell bystander effect: senescence-induced senescence.', *Aging cell*, 11(2), pp. 345–9. doi: 10.1111/j.1474-9726.2012.00795.x.

Neustadt, J. and Pieczenik, S. (2008) *Organ Reserve and Healthy Aging*.

Nguyen-Chi, M. *et al.* (2015) 'Identification of polarized macrophage subsets in zebrafish', *eLife*. eLife Sciences Publications Ltd, 4(JULY 2015). doi: 10.7554/eLife.07288.

North, T. E. *et al.* (2007) 'Prostaglandin E2 regulates vertebrate haematopoietic stem cell homeostasis', *Nature*. Nature Publishing Group, 447(7147), pp. 1007–1011. doi: 10.1038/nature05883.

Nüsslein-Volhard, C. and Dahm, R. (2002) 'Zebrafish: a practical approach.', *New York: Oxford University Press*, 303p.

O'Sullivan, R. J. and Karlseder, J. (2010) 'Telomeres: protecting chromosomes against genome instability.', *Nature reviews. Molecular cell biology*, 11(3), pp. 171–81. doi: 10.1038/nrm2848.

Office for National Statistics (2015) *National population projections for the UK, 2014-based*. Available at: https://www.ons.gov.uk/peoplepopulationandcommunity/populationandmigration/populationprojections/bulletins/nationalpopulationprojections/2015-10-29.

Ogrodnik, M. *et al.* (2019) 'Obesity-Induced Cellular Senescence Drives Anxiety and Impairs Neurogenesis.', *Cell metabolism*, 29(5), pp. 1061-1077.e8. doi: 10.1016/j.cmet.2018.12.008.

Olovnikov, A. M. (1971) '[Principle of marginotomy in template synthesis of polynucleotides].', *Doklady Akademii nauk SSSR*, 201(6), pp. 1496–9. Available at: http://www.ncbi.nlm.nih.gov/pubmed/5158754 (Accessed: 31 August 2019).

Olsen, C. L. *et al.* (2002) 'Raf-1-induced growth arrest in human mammary epithelial cells is p16-independent and is overcome in immortal cells during conversion.', *Oncogene*, 21(41), pp. 6328–39. doi: 10.1038/sj.onc.1205780.

Orban, L., Sreenivasan, R. and Olsson, P.-E. (2009) 'Long and winding roads: testis differentiation in zebrafish.', *Molecular and cellular endocrinology*, 312(1–2), pp. 35–41. doi: 10.1016/j.mce.2009.04.014.

Özcan, S. *et al.* (2016) 'Unbiased analysis of senescence associated secretory phenotype (SASP) to identify common components following different genotoxic stresses.', *Aging*, 8(7), pp. 1316–29. doi: 10.18632/aging.100971.

Panda, S., Isbatan, A. and Adami, G. R. (2008) 'Modification of the ATM/ATR directed DNA damage response state with aging and long after hepatocyte senescence induction in vivo', *Mechanisms of Ageing and Development*, 129(6), pp. 332–340. doi: 10.1016/j.mad.2008.02.014.

Parrinello, S. *et al.* (2003) 'Oxygen sensitivity severely limits the replicative lifespan of murine fibroblasts.', *Nature cell biology*, 5(8), pp. 741–7. doi: 10.1038/ncb1024.

Partridge, L. (2010) 'The new biology of ageing', *Philosophical Transactions of the Royal Society B: Biological Sciences*. Royal Society, pp. 147–154. doi: 10.1098/rstb.2009.0222.

Pensions, D. for W. and (2018) *No Title Households below average income time series, 1994-95 to 2016/17*. Available at: https://www.gov.uk/government/statistics/households-below-average-income-199495-to-201617.

Percival, S. M. *et al.* (2015) 'Variations in dysfunction of sister chromatid cohesion in esco2 mutant zebrafish reflect

the phenotypic diversity of Roberts syndrome', *DMM Disease Models and Mechanisms*. Company of Biologists Ltd, 8(8), pp. 941–955. doi: 10.1242/dmm.019059.

Perls, T. T. (1997) 'Centenarians prove the compression of morbidity hypothesis, but what about the rest of us who are genetically less fortunate?', *Medical Hypotheses*. Churchill Livingstone, 49(5), pp. 405–407. doi: 10.1016/S0306-9877(97)90086-4.

Pes, G. M. *et al.* (2013) 'Lifestyle and nutrition related to male longevity in Sardinia: An ecological study', *Nutrition, Metabolism and Cardiovascular Diseases*, 23(3), pp. 212–219. doi: 10.1016/j.numecd.2011.05.004.

Poleo, G. *et al.* (2001) 'Cell proliferation and movement during early fin regeneration in zebrafish.', *Developmental dynamics : an official publication of the American Association of Anatomists*, 221(4), pp. 380–90. doi: 10.1002/dvdy.1152.

Poss, K. D., Wilson, L. G. and Keating, M. T. (2002) 'Heart regeneration in zebrafish', *Science*, 298(5601), pp. 2188–2190. doi: 10.1126/science.1077857.

Povedano, J. M. *et al.* (2018) 'Therapeutic effects of telomerase in mice with pulmonary fibrosis induced by damage to the lungs and short telomeres', *eLife*. eLife Sciences Publications Ltd, 7. doi: 10.7554/eLife.31299.

Prajsnar, T. K. *et al.* (2012) 'A privileged intraphagocyte niche is responsible for disseminated infection of *Staphylococcus aureus* in a zebrafish model', *Cellular Microbiology*, 14(10), pp. 1600–1619. doi: 10.1111/j.1462-5822.2012.01826.x.

Price, J. S. *et al.* (2002) 'The role of chondrocyte senescence in osteoarthritis.', *Aging cell*, 1(1), pp. 57–65. doi: 10.1046/j.1474-9728.2002.00008.x.

Probin, V. *et al.* (2006) 'Busulfan selectively induces cellular senescence but not apoptosis in WI38 fibroblasts via a p53-independent but extracellular signal-regulated kinase-p38 mitogen-activated protein kinase-dependent mechanism.', *The Journal of pharmacology and experimental therapeutics*, 319(2), pp. 551–560. doi: 10.1124/jpet.106.107771.

Public Health England (2019) *Death in people aged 75 years and older in England in 2017*. Available at: https://www.gov.uk/government/publications/death-in-people-aged-75-years-and-older-in-england-in-2017/death-in-people-aged-75-years-and-older-in-england-in-2017 (Accessed: 24 June 2019).

Purvis, J. E. *et al.* (2012) 'p53 dynamics control cell fate', 336(6087), pp. 1440–1444. doi: 10.1126/science.1218351.p53.

Rajagopalan, S. and Long, E. O. (2012) 'Cellular senescence induced by CD158d reprograms natural killer cells to promote vascular remodeling.', *Proceedings of the National Academy of Sciences of the United States of America*, 109(50), pp. 20596–601. doi: 10.1073/pnas.1208248109.

Renshaw, S. A. and Trede, N. S. (2012) 'A model 450 million years in the making: Zebrafish and vertebrate immunity',

DMM Disease Models and Mechanisms, pp. 38–47. doi: 10.1242/dmm.007138.

Renshaw, S. and Loynes, C. (2006) 'A transgenic zebrafish model of neutrophilic inflammation', *Blood…*, 108(13), pp. 3976–3978. doi: 10.1182/blood-2006-05-024075.The.

Riddle, D. L., Swanson, M. M. and Albert, P. S. (1981) 'Interacting genes in nematode dauer larva formation.', *Nature*, 290(5808), pp. 668–71. doi: 10.1038/290668a0.

Robertson, A. L. *et al.* (2014) 'A zebrafish compound screen reveals modulation of neutrophil reverse migration as an anti-inflammatory mechanism.', *Science translational medicine*, 6(225), p. 225ra29. doi: 10.1126/scitranslmed.3007672.

Robinson, S. M. (2018) 'Improving nutrition to support healthy ageing: What are the opportunities for intervention?', in *Proceedings of the Nutrition Society*. Cambridge University Press, pp. 257–264. doi: 10.1017/S0029665117004037.

Rodier, F. *et al.* (2009) 'Persistent DNA damage signalling triggers senescence-associated inflammatory cytokine secretion', *Nature Cell Biology*, 11(8), pp. 973–979. doi: 10.1038/ncb1909.

Rodier, F. *et al.* (2011) 'DNA-SCARS: Distinct nuclear structures that sustain damage-induced senescence growth arrest and inflammatory cytokine secretion', *Journal of Cell Science*. Company of Biologists Ltd, 124(1), pp. 68–81. doi: 10.1242/jcs.071340.

Rodriguez, R. and Meuth, M. (2006) 'Chk1 and p21 Cooperate to Prevent Apoptosis during DNA Replication Fork Stress', *Molecular biology of the cell*, 17(2), pp. 1018–1032. doi: 10.1091/mbc.E05.

Rogakou, E. P. *et al.* (2000) 'Initiation of DNA fragmentation during apoptosis induces phosphorylation of H2AX histone at serine 139.', *The Journal of biological chemistry*, 275(13), pp. 9390–5. doi: 10.1074/jbc.275.13.9390.

Roos, C. M. *et al.* (2016) 'Chronic senolytic treatment alleviates established vasomotor dysfunction in aged or atherosclerotic mice.', *Aging cell*, 15(5), pp. 973–7. doi: 10.1111/acel.12458.

Rosa, C. E. da *et al.* (2010) 'GH overexpression modifies muscle expression of anti-oxidant enzymes and increases spinal curvature of old zebrafish.', *Experimental gerontology*, 45(6), pp. 449–56. doi: 10.1016/j.exger.2010.03.012.

Ruhl, T. *et al.* (2015) 'Oxidation and Cognitive Impairment in the Aging Zebrafish.', *Gerontology*, 62(1), pp. 47–57. doi: 10.1159/000433534.

Sagiv, A. *et al.* (2016) 'NKG2D ligands mediate immunosurveillance of senescent cells.', *Aging*, 8(2), pp. 328–44. doi: 10.18632/aging.100897.

Salaris, L. (2015) 'Examining mortality differentials between a long-living community in Sardinia and the Italian population: a longitudinal analysis', *Longitudinal and Life Course Studies*, 6, pp. 43–58. doi: 10.14301/llcs.v6i1.304.

Samson, M. M. *et al.* (2000) 'Relationships between physical performance measures, age, height and body weight in healthy adults.', *Age and ageing*, 29(3), pp. 235–42. doi: 10.1093/ageing/29.3.235.

Sandrini, J. Z. *et al.* (2009) 'Time-course expression of DNA repair-related genes in hepatocytes of zebrafish (Danio rerio) after UV-B exposure', *Photochemistry and Photobiology*, 85(1), pp. 220–226. doi: 10.1111/j.1751-1097.2008.00422.x.

Sang, L., Coller, H. A. and Roberts, J. M. (2008) 'Control of the reversibility of cellular quiescence by the transcriptional repressor HES1.', *Science (New York, N.Y.)*, 321(5892), pp. 1095–100. doi: 10.1126/science.1155998.

Sanoff, H. K. *et al.* (2014) 'Article effect of cytotoxic chemotherapy on Markers of Molecular Age in Patients With Breast cancer', 106. doi: 10.1093/jnci/dju057.

Santhakumar, K. *et al.* (2012) 'A zebrafish model to study and therapeutically manipulate hypoxia signaling in tumorigenesis', *Cancer Research*, 72(16), pp. 4017–4027. doi: 10.1158/0008-5472.CAN-11-3148.

Sasaki, M. *et al.* (2001) 'Senescent cells are resistant to death despite low Bcl-2 level.', *Mechanisms of ageing and development*, 122(15), pp. 1695–706. doi: 10.1016/s0047-6374(01)00281-0.

Satoh, T. *et al.* (1988) 'Induction of neuronal differentiation in PC12 cells by B-cell stimulatory factor 2/interleukin 6.', *Molecular and Cellular Biology*. American Society for Microbiology, 8(8), pp. 3546–3549. doi: 10.1128/mcb.8.8.3546.

Schafer, M. J. *et al.* (2017) 'ARTICLE Cellular senescence mediates fibrotic pulmonary disease', *Nature Communications*, 8. doi: 10.1038/ncomms14532.

Schaue, D., Ratikan, J. A. and Iwamoto, K. S. (2012) 'Cellular autofluorescence following ionizing radiation', *PLoS ONE*, 7(2). doi: 10.1371/journal.pone.0032062.

Schlake, T. and Bode, J. (1994) 'Use of Mutated FLP Recognition Target (FRT) Sites for the Exchange of Expression Cassettes at Defined Chromosomal Loci', *Biochemistry*, 33(43), pp. 12746–12751. doi: 10.1021/bi00209a003.

Schuler, M. *et al.* (2000) 'p53 induces apoptosis by caspase activation through mitochondrial cytochrome c release.', *The Journal of biological chemistry*, 275(10), pp. 7337–42. doi: 10.1074/jbc.275.10.7337.

Scoumanne, A. *et al.* (2011) 'The cyclin-dependent kinase inhibitor p21 is regulated by RNA-binding protein PCBP4 via mRNA stability', *Nucleic Acids Research*, 39(1), pp. 213–224. doi: 10.1093/nar/gkq778.

Scudellari, M. (2017) 'To stay young,kill zombies', *Nature*. Nature Publishing Group, 550(7677), pp. 448–450. doi: 10.1038/550448a.

Sedelnikova, O. A. *et al.* (2004) 'Senescing human cells and ageing mice accumulate DNA lesions with unrepairable double-strand breaks.', *Nature cell biology*, 6(2), pp. 168–70. doi: 10.1038/ncb1095.

Seiler, C., Abrams, J. and Pack, M. (2010) 'Characterization of zebrafish intestinal smooth muscle development using a novel sm22α-b promoter', *Developmental Dynamics*, 239(11), pp. 2806–2812. doi: 10.1002/dvdy.22420.

Seluanov, A. *et al.* (2001) 'Change of the Death Pathway in Senescent Human Fibroblasts in Response to DNA Damage Is Caused by an Inability To Change of the Death Pathway in Senescent Human Fibroblasts in Response to

DNA Damage Is Caused by an Inability To Stabilize p53', 21(5), pp. 1552–1564. doi: 10.1128/MCB.21.5.1552.

Serrano, M. *et al.* (1996) 'Role of the INK4a locus in tumor suppression and cell mortality', *Cell*. Cell Press, 85(1), pp. 27–37. doi: 10.1016/S0092-8674(00)81079-X.

Serrano, Manuel *et al.* (1997) 'Oncogenic ras provokes premature cell senescence associated with accumulation of p53 and p16(INK4a)', *Cell*, 88(5), pp. 593–602. doi: 10.1016/S0092-8674(00)81902-9.

Serrano, M., Hannon, G. J. and Beach, D. (1993) 'A new regulatory motif in cell-cycle control causing specific inhibition of cyclin D/CDK4.', *Nature*, 366(6456), pp. 704–7. doi: 10.1038/366704a0.

Serwer, L. *et al.* (2010) 'Systemic and local drug delivery for treating diseases of the central nervous system in rodent models', *Journal of Visualized Experiments*. Journal of Visualized Experiments, (42). doi: 10.3791/1992.

Severino, J. *et al.* (2000) 'Is beta-galactosidase staining a marker of senescence in vitro and in vivo?', *Experimental cell research*, 257(1), pp. 162–71. doi: 10.1006/excr.2000.4875.

Shah, a C. *et al.* (2007) 'Enhanced antiglioma activity of chimeric HCMV/HSV-1 oncolytic viruses.', *Gene therapy*, 14(13), pp. 1045–54. doi: 10.1038/sj.gt.3302942.

Shane Anderson, A. and Loeser, R. F. (2010) 'Why is osteoarthritis an age-related disease?', *Best Practice and Research: Clinical Rheumatology*. doi: 10.1016/j.berh.2009.08.006.

Sharpless, N. E. and Sherr, C. J. (2015) 'Forging a signature of in vivo senescence', *Nature Reviews Cancer*. Nature Publishing Group, pp. 397–408. doi: 10.1038/nrc3960.

Shay, J. W. and Bacchetti, S. (1997) 'A survey of telomerase activity in human cancer', *European Journal of Cancer Part A*. doi: 10.1016/S0959-8049(97)00062-2.

Shay, J. W., Pereira-Smith, O. M. and Wright, W. E. (1991) 'A role for both RB and p53 in the regulation of human cellular senescence.', *Experimental cell research*, 196(1), pp. 33–9. doi: 10.1016/0014-4827(91)90453-2.

Shelton, D. N. *et al.* (1999) 'Microarray analysis of replicative senescence.', *Current biology : CB*, 9(17), pp. 939–45. doi: 10.1016/s0960-9822(99)80420-5.

Shimoda, N. *et al.* (2014) 'Decrease in cytosine methylation at CpG island shores and increase in DNA fragmentation during zebrafish aging.', *Age (Dordrecht, Netherlands)*, 36(1), pp. 103–15. doi: 10.1007/s11357-013-9548-5.

da Silva, P. F. L. *et al.* (2019) 'The bystander effect contributes to the accumulation of senescent cells in vivo', *Aging Cell*. Blackwell Publishing Ltd, 18(1). doi: 10.1111/acel.12848.

Silverstein, M. (2008) 'Meeting the challenges of an aging workforce.', *American journal of industrial medicine*, 51(4), pp. 269–80. doi: 10.1002/ajim.20569.

Sliwinska, M. A. *et al.* (2009) 'Induction of senescence with doxorubicin leads to increased genomic instability of HCT116 cells', *Mechanisms of Ageing and Development*, 130(1–2), pp. 24–32. doi: 10.1016/j.mad.2008.04.011.

Snow, C. J. *et al.* (2008) 'Muscle development is disrupted in zebrafish embryos deficient for fibronectin', *Developmental Dynamics*, 237(9), pp. 2542–2553. doi: 10.1002/dvdy.21670.

Solana, R. *et al.* (2012) 'Innate immunosenescence: effect of aging on cells and receptors of the innate immune system in humans.', *Seminars in immunology*, 24(5), pp. 331–41. doi: 10.1016/j.smim.2012.04.008.

Solana, R., Alonso, M. C. and Peña, J. (1999) 'Natural killer cells in healthy aging.', *Experimental gerontology*, 34(3), pp. 435–43. Available at: http://www.ncbi.nlm.nih.gov/pubmed/10433398 (Accessed: 1 September 2019).

Solana, R. and Mariani, E. (2000) 'NK and NK/T cells in human senescence.', *Vaccine*, 18(16), pp. 1613–20. doi: 10.1016/s0264-410x(99)00495-8.

Song, Y. S., Lee, B. Y. and Hwang, E. S. (2005) 'Dinstinct ROS and biochemical profiles in cells undergoing DNA damage-induced senescence and apoptosis', *Mechanisms of Ageing and Development*, 126(5), pp. 580–590. doi: 10.1016/j.mad.2004.11.008.

Sorrells, S. *et al.* (2013) 'Analysis of apoptosis in zebrafish embryos by whole-mount immunofluorescence to detect activated caspase 3', *Journal of Visualized Experiments*. Journal of Visualized Experiments, (82). doi: 10.3791/51060.

Sozen, T., Ozisik, L. and Calik Basaran, N. (2017) 'An overview and management of osteoporosis', *European Journal of Rheumatology*. AVES Publishing Co., 4(1), pp. 46–56. doi: 10.5152/eurjrheum.2016.048.

Spark, J. (Unity B. (2019) *UNITY Biotechnology Reports Promising Topline Data from Phase 1 First-in-human Study of UBX0101 in Patients with Osteoarthritis of the Knee*. Available at: https://www.globenewswire.com/news-release/2019/06/18/1870153/0/en/UNITY-Biotechnology-Reports-Promising-Topline-Data-from-Phase-1-First-in-human-Study-of-UBX0101-in-Patients-with-Osteoarthritis-of-the-Knee.html (Accessed: 27 August 2019).

Statistics, O. of N. (2017) 'Principal projection - UK population in age groups, mid-2017 based', pp. 1–10. Available at: https://www.ons.gov.uk/peoplepopulationandcommunity/populationandmigration/populationestimates/articles/overviewoftheukpopulation/november2018.

Stein, G. H. *et al.* (1999) 'Differential roles for cyclin-dependent kinase inhibitors p21 and p16 in the mechanisms of senescence and differentiation in human fibroblasts.', *Molecular and cellular biology*, 19(3), pp. 2109–17. doi: 10.1128/MCB.19.3.2109.

Stiff, T. *et al.* (2004) 'ATM and DNA-PK function redundantly to phosphorylate H2AX after exposure to ionizing radiation.', *Cancer research*, 64(7), pp. 2390–6. Available at: http://www.ncbi.nlm.nih.gov/pubmed/15059890 (Accessed: 21 September 2019).

Storer, M., Mas, A., Robert-moreno, A., *et al.* (2013) 'Senescence Is a Developmental Mechanism that Contributes to Embryonic Growth and Patterning', *Cell*. Elsevier Inc., 155(5), pp. 1119–1130. doi: 10.1016/j.cell.2013.10.041.

Strait, J. B. and Lakatta, E. G. (2012) 'Aging-Associated Cardiovascular Changes and Their Relationship to Heart Failure', *Heart Failure Clinics*, pp. 143–164. doi: 10.1016/j.hfc.2011.08.011.

Streisinger, G. *et al.* (1981) 'Production of clones of homozygous diploid zebra fish (Brachydanio rerio)', *Nature*, 291(5813), pp. 293–296. doi: 10.1038/291293a0.

Studenski, S. (2008) 'Challenges in clinical aging research: Building the evidence base for care of the older adult', *Journal of the American Geriatrics Society*, December, pp. 2351–2352. doi: 10.1111/j.1532-5415.2008.02028.x.

Sugiyama, M. *et al.* (2009) 'Illuminating cell-cycle progression in the developing zebrafish embryo', *Proceedings of the National Academy of Sciences of the United States of America*, 106(49), pp. 20812–20817. doi: 10.1073/pnas.0906464106.

Sulston, J. E. *et al.* (1983) 'The embryonic cell lineage of the nematode Caenorhabditis elegans', *Developmental Biology*, pp. 64–119. doi: 10.1016/0012-1606(83)90201-4.

Sun, N. *et al.* (2015) 'Measuring In Vivo Mitophagy.', *Molecular cell*, 60(4), pp. 685–96. doi: 10.1016/j.molcel.2015.10.009.

Sussman, R. (2007) 'DNA repair capacity of zebrafish', *Proceedings of the National Academy of Sciences of the United States of America*, 104(33), pp. 13379–13383. doi: 10.1073/pnas.0706157104.

Suster, M. L. *et al.* (2011) 'Transposon-mediated BAC transgenesis in zebrafish', *Nature Protocols*. Nature Publishing Group, 6(12), pp. 1998–2021. doi: 10.1038/nprot.2011.416.

Suzuki, K. *et al.* (2001) 'Radiation-induced senescence-like growth arrest requires TP53 function but not telomere shortening.', *Radiation research*, 155(1 Pt 2), pp. 248–253. doi: 10.1667/0033-7587(2001)155[0248:rislga]2.0.co;2.

Sviderskaya, E. V *et al.* (2003) 'p16/cyclin-dependent kinase inhibitor 2A deficiency in human melanocyte senescence, apoptosis, and immortalization: possible implications for melanoma progression.', *Journal of the National Cancer Institute*, 95(10), pp. 723–32. doi: 10.1093/jnci/95.10.723.

Szilard, L. (1959) 'ON THE NATURE OF THE AGING PROCESS', *Proceedings of the National Academy of Sciences*. Proceedings of the National Academy of Sciences, 45(1), pp. 30–45. doi: 10.1073/pnas.45.1.30.

Thompson, A. A. R. *et al.* (2014) 'Hypoxia-inducible factor 2α regulates key neutrophil functions in humans, mice, and zebrafish.', *Blood*, 123(3), pp. 366–76. doi: 10.1182/blood-2013-05-500207.

Thompson, J. J., Ritenbaugh, C. and Nichter, M. (2009) 'Reconsidering the placebo response from a broad anthropological perspective.', *Culture, medicine and psychiatry*, 33(1), pp. 112–52. doi: 10.1007/s11013-008-9122-2.

Tian, X. *et al.* (2019) 'SIRT6 Is Responsible for More Efficient DNA Double-Strand Break Repair in Long-Lived Species.', *Cell*, 177(3), pp. 622-638.e22. doi: 10.1016/j.cell.2019.03.043.

Toussaint, O. *et al.* (2002) 'Stress-induced premature senescence and tissue ageing.', *Biochemical pharmacology*, 64(5–6), pp. 1007–9. doi: 10.1016/s0006-2952(02)01170-x.

Tsai, S. B. *et al.* (2007) 'Differential effects of genotoxic stress on both concurrent body growth and gradual

senescence in the adult zebrafish.', *Aging cell*, 6(2), pp. 209–24. doi: 10.1111/j.1474-9726.2007.00278.x.

Tse, C. *et al.* (2008) 'ABT-263: a potent and orally bioavailable Bcl-2 family inhibitor.', *Cancer research*, 68(9), pp. 3421–8. doi: 10.1158/0008-5472.CAN-07-5836.

UNITY Biotechnology (2019) *Pipeline*. Available at: https://unitybiotechnology.com/pipeline/ (Accessed: 26 September 2019).

Untergasser, G. *et al.* (2003) 'TGF-beta cytokines increase senescence-associated beta-galactosidase activity in human prostate basal cells by supporting differentiation processes, but not cellular senescence.', *Experimental gerontology*, 38(10), pp. 1179–88. doi: 10.1016/j.exger.2003.08.008.

Vakifahmetoglu, H. *et al.* (2006) 'Functional connection between p53 and caspase-2 is essential for apoptosis induced by DNA damage.', *Oncogene*, 25(41), pp. 5683–92. doi: 10.1038/sj.onc.1209569.

Varela, M. *et al.* (2012) 'Characterisation, expression and ontogeny of interleukin-6 and its receptors in zebrafish (Danio rerio)', *Developmental & Comparative Immunology*, 37(1), pp. 97–106. doi: 10.1016/j.dci.2011.11.004.

Vaz, R. L., Outeiro, T. F. and Ferreira, J. J. (2018) 'Zebrafish as an animal model for drug discovery in Parkinson's disease and other movement disorders: A systematic review', *Frontiers in Neurology*. Frontiers Media S.A. doi: 10.3389/fneur.2018.00347.

Ventura, A. *et al.* (2007) 'Restoration of p53 function leads to tumour regression in vivo.', *Nature*, 445(7128), pp. 661–5. doi: 10.1038/nature05541.

Vogeli, C. *et al.* (2007) 'Multiple Chronic Conditions: Prevalence, Health Consequences, and Implications for Quality, Care Management, and Costs', *J Gen Intern Med*, 22(3), pp. 391–396. doi: 10.1007/s11606-007-0322-1.

Wade Harper, J. *et al.* (1993) 'The p21 Cdk-interacting protein Cip1 is a potent inhibitor of G1 cyclin-dependent kinases', *Cell*. doi: 10.1016/0092-8674(93)90499-G.

Walaszczyk, A. *et al.* (2019) 'Pharmacological clearance of senescent cells improves survival and recovery in aged mice following acute myocardial infarction', *Aging Cell*. Blackwell Publishing Ltd, 18(3). doi: 10.1111/acel.12945.

Wallace, K. N. *et al.* (2005) 'Intestinal growth and differentiation in zebrafish.', *Mechanisms of development*, 122(2), pp. 157–73. doi: 10.1016/j.mod.2004.10.009.

Wang, G., Rajpurohit, S. K., Delaspre, F., Walker, S. L., White, D. T., Ceasrine, A., Kuruvilla, R., Li, R.-J., *et al.* (2015) 'First quantitative high-throughput screen in zebrafish identifies novel pathways for increasing pancreatic β-cell mass.', *eLife*, 4. doi: 10.7554/eLife.08261.

Wang, J. C. and Bennett, M. (2012) 'Aging and Atherosclerosis Mechanisms , Functional Consequences , and Potential Therapeutics for Cellular Senescence'. doi: 10.1161/CIRCRESAHA.111.261388.

Wang, L. *et al.* (2017) 'High-Throughput Functional Genetic and Compound Screens Identify Targets for Senescence

Induction in Cancer', *Cell Reports*. Elsevier B.V., 21(3), pp. 773–783. doi: 10.1016/j.celrep.2017.09.085.

Wang, N. *et al.* (2019) 'Exploration of age-related mitochondrial dysfunction and the anti-aging effects of resveratrol in zebrafish retina', *Aging*. Impact Journals LLC, 11(10), pp. 3117–3137. doi: 10.18632/aging.101966.

Watson, J. D. (1972) 'Origin of concatemeric T7 DNA', *Nature New Biology*, 239(94), pp. 197–201. doi: 10.1038/newbio239197a0.

Wei, Q. *et al.* (1993) 'DNA repair and aging in basal cell carcinoma: a molecular epidemiology study.', *Proceedings of the National Academy of Sciences of the United States of America*, 90(4), pp. 1614–8. doi: 10.1073/pnas.90.4.1614.

Wei, S., Wei, S. and Sedivy, J. M. (1999) 'Expression of catalytically active telomerase does not prevent premature senescence caused by overexpression of oncogenic Ha-Ras in normal human fibroblasts.', *Cancer research*, 59(7), pp. 1539–43. Available at: http://www.ncbi.nlm.nih.gov/pubmed/10197626 (Accessed: 24 September 2019).

Weinberger, B. *et al.* (2008) 'Biology of Immune Responses to Vaccines in Elderly Persons', *Clinical Infectious Diseases*. Oxford University Press (OUP), 46(7), pp. 1078–1084. doi: 10.1086/529197.

Weindruch, R. *et al.* (1986) 'The retardation of aging in mice by dietary restriction: Longevity, cancer, immunity and lifetime energy intake', *Journal of Nutrition*, 116(4), pp. 641–654. doi: 10.1093/jn/116.4.641.

Weinert, T. A. and Hartwell, L. H. (1988) 'The RAD9 gene controls the cell cycle response to DNA damage in Saccharomyces cerevisiae.', *Science (New York, N.Y.)*, 241(4863), pp. 317–22. doi: 10.1126/science.3291120.

Whittemore, K. *et al.* (2019) 'Telomere shortening rate predicts species life span', *Proceedings of the National Academy of Sciences*. Proceedings of the National Academy of Sciences, 116(30), pp. 15122–15127. doi: 10.1073/pnas.1902452116.

Wiley, C. D. *et al.* (2017) 'Analysis of individual cells identifies cell-to-cell variability following induction of cellular senescence', (May), pp. 1–8. doi: 10.1111/acel.12632.

Williams, G. C. (1957) 'Pleiotropy, Natural Selection, and the Evolution of Senescence', *Evolution*. JSTOR, 11(4), p. 398. doi: 10.2307/2406060.

Wilmoth, J. R. (2000) 'Demography of longevity: Past, present, and future trends', in *Experimental Gerontology*, pp. 1111–1129. doi: 10.1016/S0531-5565(00)00194-7.

Xiong, Y. *et al.* (1993) 'p21 is a universal inhibitor of cyclin kinases.', *Nature*, 366(6456), pp. 701–4. doi: 10.1038/366701a0.

Xu, M. *et al.* (2015) 'Targeting Senescent Cells Enhances Adipogenesis and Metabolic Function in Old Age Robert and Arlene Kogod Center on Aging , Mayo Clinic , Rochester , MN These authors contributed equally to this work . * To whom correspondence should be addressed at : Jam', (December).

Xu, M. *et al.* (2018) 'Senolytics improve physical function and increase lifespan in old age.', *Nature medicine*, 24(8),

pp. 1246–1256. doi: 10.1038/s41591-018-0092-9.

Xue, W. *et al.* (2007) 'Senescence and tumour clearance is triggered by p53 restoration in murine liver carcinomas.', *Nature*, 445(7128), pp. 656–60. doi: 10.1038/nature05529.

Yabu, T. *et al.* (2001) 'Characterization of zebrafish caspase-3 and induction of apoptosis through ceramide generation in fish fathead minnow tailbud cells and zebrafish embryo.', *The Biochemical journal*, 360(Pt 1), pp. 39–47. doi: 10.1042/0264-6021:3600039.

Yang, N.-C. and Hu, M.-L. (2005) 'The limitations and validities of senescence associated-beta-galactosidase activity as an aging marker for human foreskin fibroblast Hs68 cells.', *Experimental gerontology*, 40(10), pp. 813–9. doi: 10.1016/j.exger.2005.07.011.

Yoo, S. K. and Huttenlocher, A. (2011) 'Spatiotemporal photolabeling of neutrophil trafficking during inflammation in live zebrafish', *Journal of Leukocyte Biology*. Wiley-Blackwell, 89(5), pp. 661–667. doi: 10.1189/jlb.1010567.

Yousefzadeh, M. J. *et al.* (2018) 'Fisetin is a senotherapeutic that extends health and lifespan', *EBioMedicine*. Elsevier B.V., 36, pp. 18–28. doi: 10.1016/j.ebiom.2018.09.015.

Yu, L. *et al.* (2006) 'Cognitive aging in zebrafish', *PLoS ONE*, 1(1). doi: 10.1371/journal.pone.0000014.

Zakaria, Z. Z. *et al.* (2018) 'Using Zebrafish for Investigating the Molecular Mechanisms of Drug-Induced Cardiotoxicity', *BioMed research international*. NLM (Medline), p. 1642684. doi: 10.1155/2018/1642684.

Zampetaki, A. *et al.* (2005) 'Biomechanical stress induces IL-6 expression in smooth muscle cells via Ras/Rac1-p38 MAPK-NF-kappaB signaling pathways.', *American journal of physiology. Heart and circulatory physiology*, 288(6), pp. H2946-54. doi: 10.1152/ajpheart.00919.2004.

Zarbock, A. (2012) 'The shady side of dasatinib', *Blood*, pp. 4817–4818. doi: 10.1182/blood-2012-03-418582.

Zerbino, D. R. *et al.* (2018) 'Ensembl 2018 (Release 92)', *Nucleic Acids Research*, 46(D1), pp. D754–D761. doi: 10.1093/nar/gkx1098.

ZFIN (2019a) *cdkn1a*, *Zebrafish Information Network (ZFIN), University of Oregon, Eugene*. Available at: https://zfin.org/ZDB-GENE-070705-7 (Accessed: 7 June 2019).

ZFIN (2019b) *cdkn2a/b*, *Zebrafish Information Network (ZFIN), University of Oregon, Eugene*. Available at: https://zfin.org/ZDB-GENE-081104-306 (Accessed: 9 June 2019).

ZFIN (2019c) *Molecular probes for zebrafish*. Available at: https://zfin.org/zf_info/zfprbs.html.

Zhang, C. and Cuervo, A. M. (2008) 'Restoration of chaperone-mediated autophagy in aging liver improves cellular maintenance and hepatic function.', *Nature medicine*, 14(9), pp. 959–65. doi: 10.1038/nm.1851.

Zhang, X.-J. and Jia, S.-S. (2016) 'Fisetin inhibits laryngeal carcinoma through regulation of AKT/NF-κB/mTOR and ERK1/2 signaling pathways.', *Biomedicine & pharmacotherapy = Biomedecine & pharmacotherapie*, 83, pp. 1164–

1174. doi: 10.1016/j.biopha.2016.08.035.

Zhao, Y. *et al.* (2019) 'Total body irradiation induced mouse small intestine senescence as a late effect.', *Journal of radiation research*, 60(4), pp. 442–450. doi: 10.1093/jrr/rrz026.

Zhu, Y. *et al.* (2015) 'The Achilles' Heel of Senescent Cells: From Transcriptome to Senolytic Drugs', *Aging Cell*, (March), p. n/a--n/a. doi: 10.1111/acel.12344.

Zhu, Y. *et al.* (2016) 'Identification of a novel senolytic agent, navitoclax, targeting the Bcl-2 family of anti-apoptotic factors'. doi: 10.1111/acel.12445.

Zou, H. *et al.* (1999) 'An APAf-1·cytochrome C multimeric complex is a functional apoptosome that activates procaspase-9', *Journal of Biological Chemistry*, 274(17), pp. 11549–11556. doi: 10.1074/jbc.274.17.11549.

Zou, H. and Niswander, L. (1996) 'Requirement for BMP signaling in interdigital apoptosis and scale formation.', *Science (New York, N.Y.)*, 272(5262), pp. 738–41. doi: 10.1126/science.272.5262.738.